GFDセミナー@休暇村支笏湖
（R7. 3/15-16）

太陽内部のプラズマの流れ：診断・モデル化・推定

政田洋平（福岡大学）

共同研究者
横井喜充（東大生産研），滝脇知也（NAOJ），原田了（茨城高専），
仲田資季（駒澤大学），本武陽一（一橋大学），佐野孝好（大阪大学）

太陽内部のプラズマの流れ:
診断・モデル化・推定

①診断：太陽内部のプラズマの流れの観測

- 太陽の内部構造モデルと日震学
- 標準太陽モデルと熱対流の物理
- 太陽磁場の観測と太陽MHDを考える上で知っておくべきこと

②モデル化：太陽内部MHDモデリング

- 太陽ダイナモモデル（ダイナモの基礎・標準シナリオ）
- グローバルモデルと過去20年の研究の進展
- セミグローバルモデルとダイナモのロスビー数依存性

③推定：太陽熱対流の難問:計算・データサイエンス手法を使った対流駆動機構の検討と推定

- Convection conundrum と 非局所駆動型熱対流
- Topological Data Analysis (TDA)の基礎
- 太陽熱対流のトポロジカルな特徴（モデル vs. 観測）

太陽内部のプラズマの流れ：
診断・モデル化・推定

①診断：太陽内部のプラズマの流れの観測

- 太陽の内部構造モデルと日震学
- 標準太陽モデルと熱対流の物理
- 太陽磁場の観測＋太陽MHDを考える上で知っておくべきこと

②モデル化：太陽内部MHDモデリング

- 太陽ダイナモモデル（ダイナモの基礎・標準シナリオ）
- グローバルモデルと過去20年の研究の進展
- セミグローバルモデルとダイナモのロスビー数依存性

③推定：太陽熱対流の難問：計算・データサイエンス手法を使った対流駆動機構の検討と推定

- Convection conundrum と 非局所駆動型熱対流
- Topological Data Analysis (TDA)の基礎
- 太陽熱対流のトポロジカルな特徴（モデル vs. 観測）

太陽の内部構造

太陽の内部構造①

標準太陽モデル（Standard Solar Model）：

（中心核：0 ≦ r ≦0.3R_s）

・放射層：0 ≦ r ≦0.7R_s

・対流層：0.7 ≦ r ≦1R_s　　Re > 10^{12}

→ 激しい乱流状態

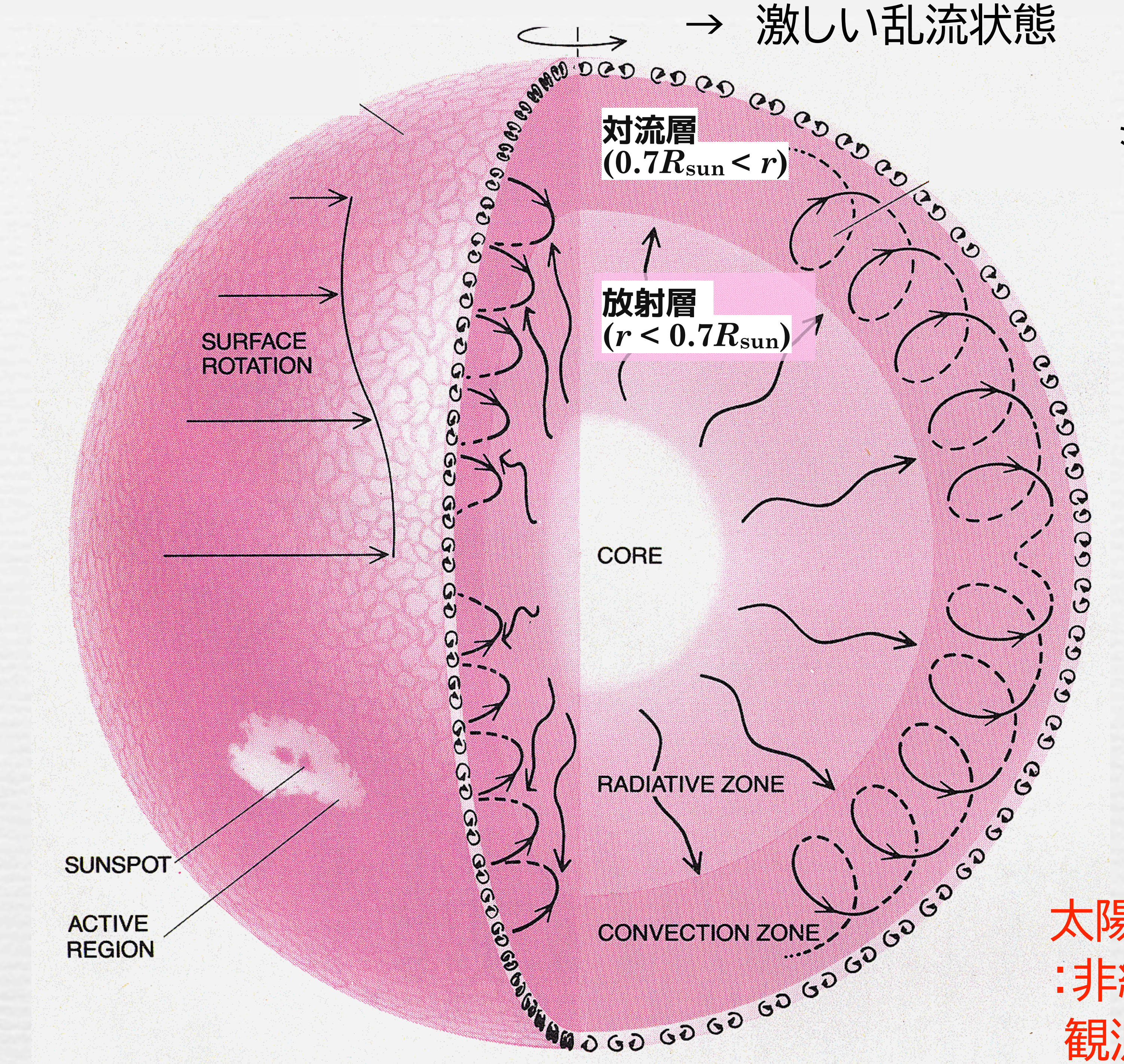

Hinode SOT(太陽表面の約1/100)

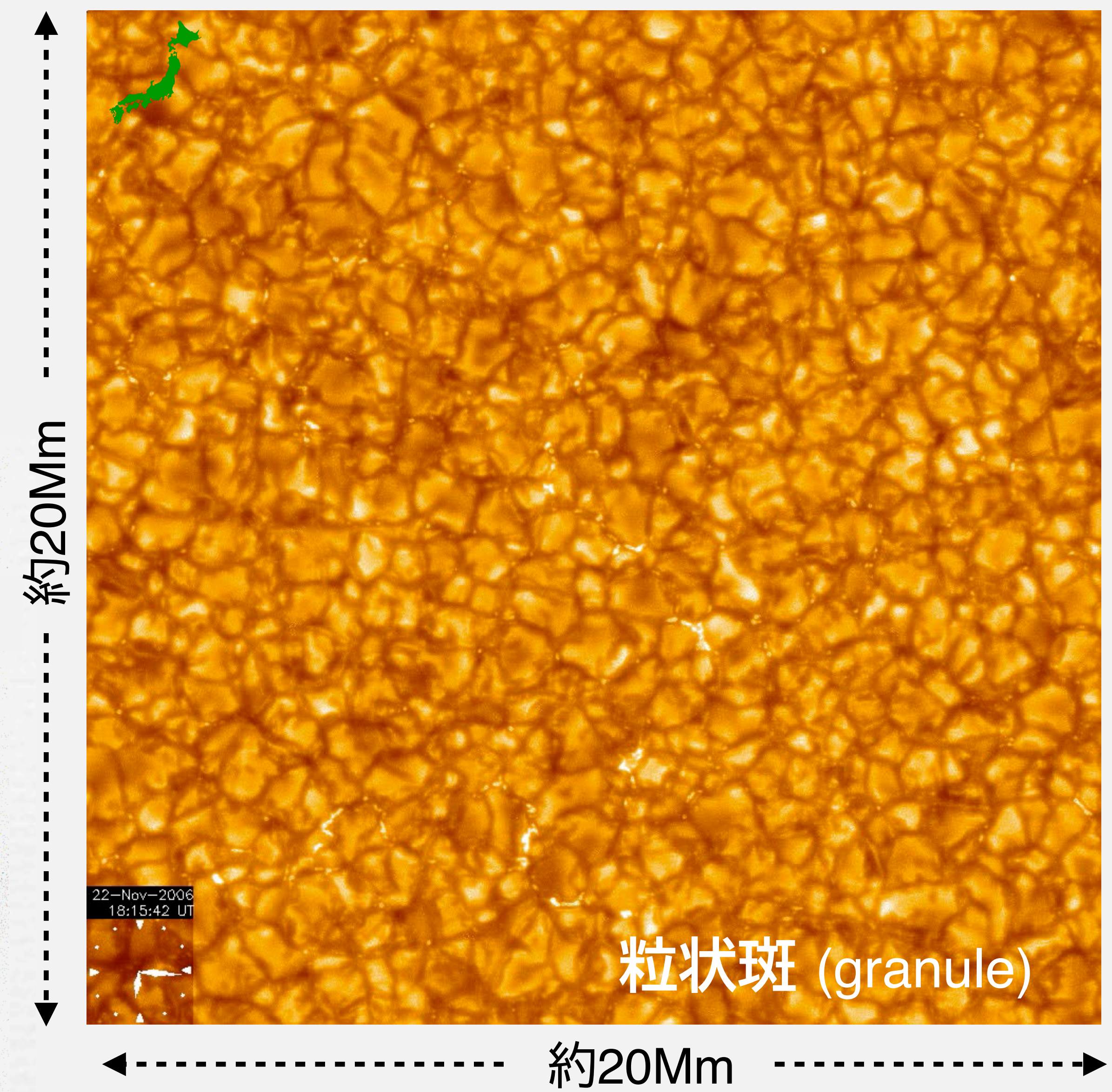

※特徴的な３つの対流構造

①粒状斑 (granule) ~ 1Mm

②超粒状斑 (super-granule) ~ 30Mm

③巨大胞 (giant cell) ~ 100Mm

（熱対流のマルチスケール性）

太陽のプラズマの流れ

：非線形性の強い宇宙流体現象を空間解像して観測・研究できる希少なケース

標準太陽モデル(SSM)

e.g., Christensen-Dalsgaard+ 96
Bahcall & Pinsonneault 95

星の進化計算 → 標準太陽モデル(Standard Solar Model):

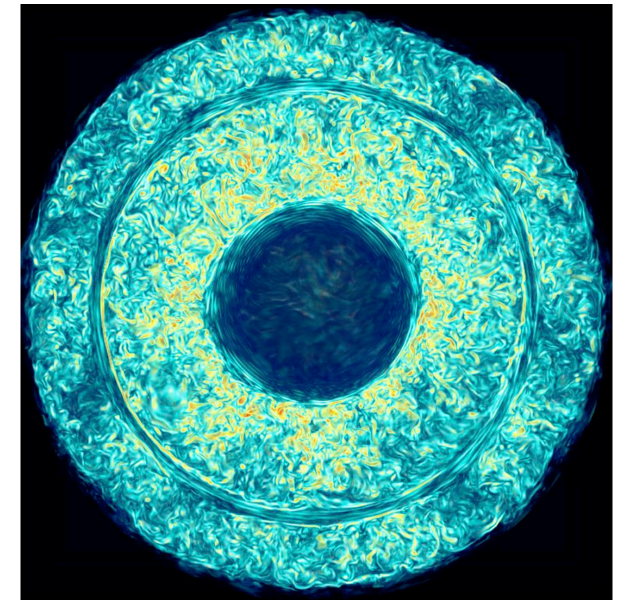

- 球対称一次元(太陽の質量は1Msunで不変)
- 準静的進化(静水圧平衡)
- 初期状態 (zero-age main-sequence : ZAMS):一様な化学組成
- 核融合反応を解いて, 化学組成の進化を追う

例) $4p \rightarrow {}^4He + 2e^+ + 2\nu_e + 26.73MeV$

- それにともなう熱的進化を追う(46億年) → 現在の太陽で期待される内部構造
(動径方向のエネルギー輸送を解く; 媒体:放射拡散 or 対流)

$$\frac{\partial r}{\partial m} = \frac{1}{4\pi r^2 \varrho},$$ mass continuity

$$\frac{\partial P}{\partial m} = -\frac{Gm}{4\pi r^4},$$ hydrostatic balance

$$\frac{\partial l}{\partial m} = \varepsilon_n - \varepsilon_\nu - c_P \frac{\partial T}{\partial t} + \frac{\delta}{\varrho}\frac{\partial P}{\partial t},$$ energy equation

$$\frac{\partial T}{\partial m} = -\frac{GmT}{4\pi r^4 P}\nabla,$$ heat transport

$$\frac{\partial X_i}{\partial t} = \frac{m_i}{\varrho}\left(\sum_j r_{ji} - \sum_k r_{ik}\right), \quad i = 1, \ldots, I.$$ composition changes

対流安定条件:
(Ledoux criterion)

$$\nabla_{\rm rad} < \nabla_{\rm ad} + [\phi/\delta]\nabla\mu,$$

満たされる場合 : $\nabla = \nabla_{\rm rad}$

満たされない場合 : $\nabla \rightarrow$ 対流による輸送フラックス

$$F_{\rm conv} = \rho c_P T \left(\frac{\ell_{\rm m}}{H_P}\right)^2 \sqrt{\tfrac{1}{2} g H_P}\,(\nabla - \nabla_{\rm ad})^{3/2}.$$

これに $F_{\rm conv} = L/4\pi r^2$ を代入して, ∇を決める(後で).

標準太陽モデル(SSM)

46億年後に太陽が現在の半径, 表面温度, 光度, 元素組成になるよう境界条件を課す.
(ヘリウム量と混合距離パラメータはフリーパラメータ)

- 恒星進化論 → HR図を定量的に説明

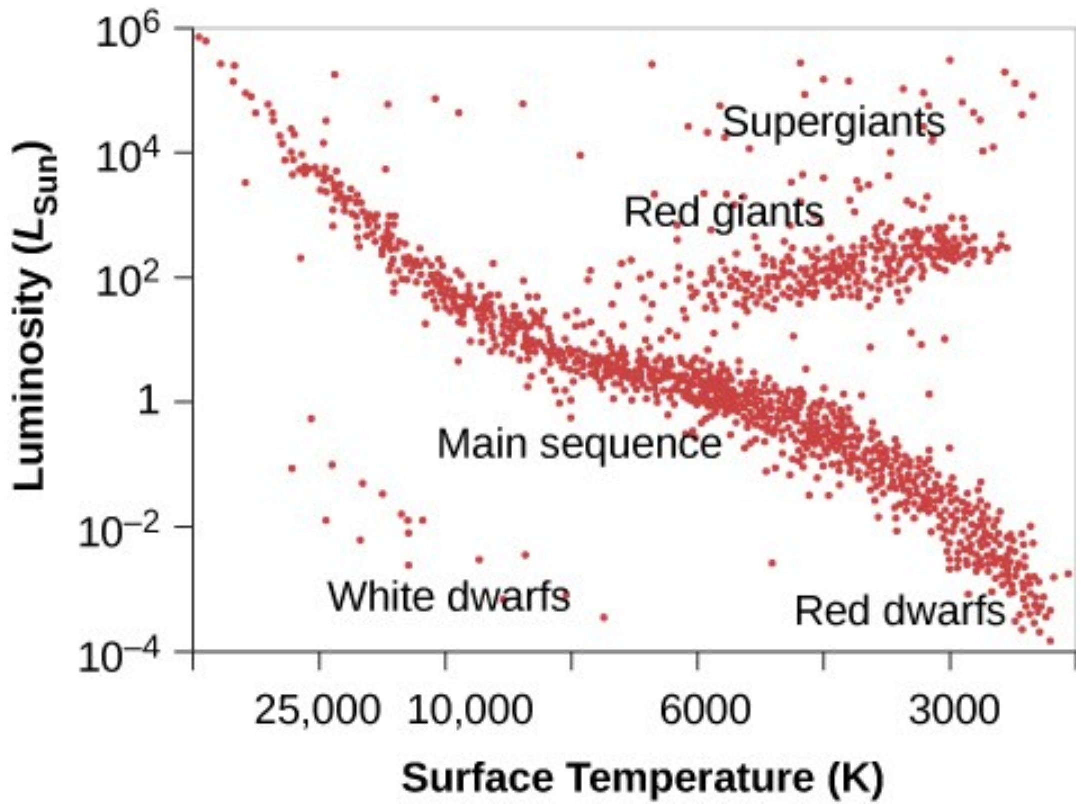

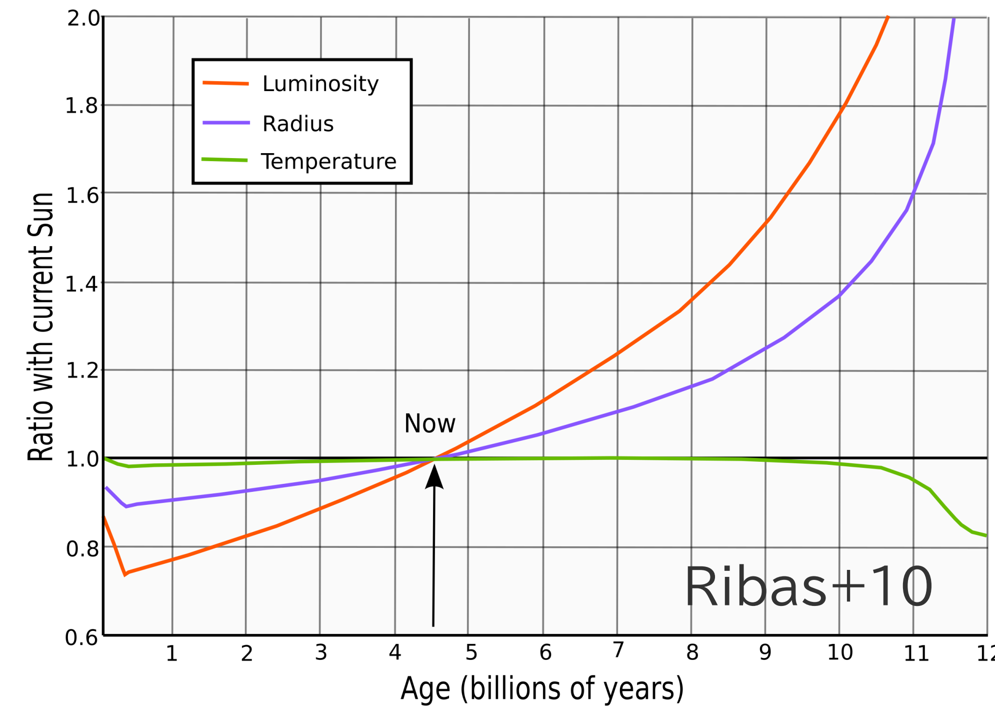

- 日震学観測とニュートリノ実験で検証
  - 太陽表面の固有振動の解析→内部構造を推定
  - 太陽由来のニュートリノの
    スーパーカミオカンデによる観測実験
    (ニュートリノ振動まで考慮に入れるとSSMと整合的)

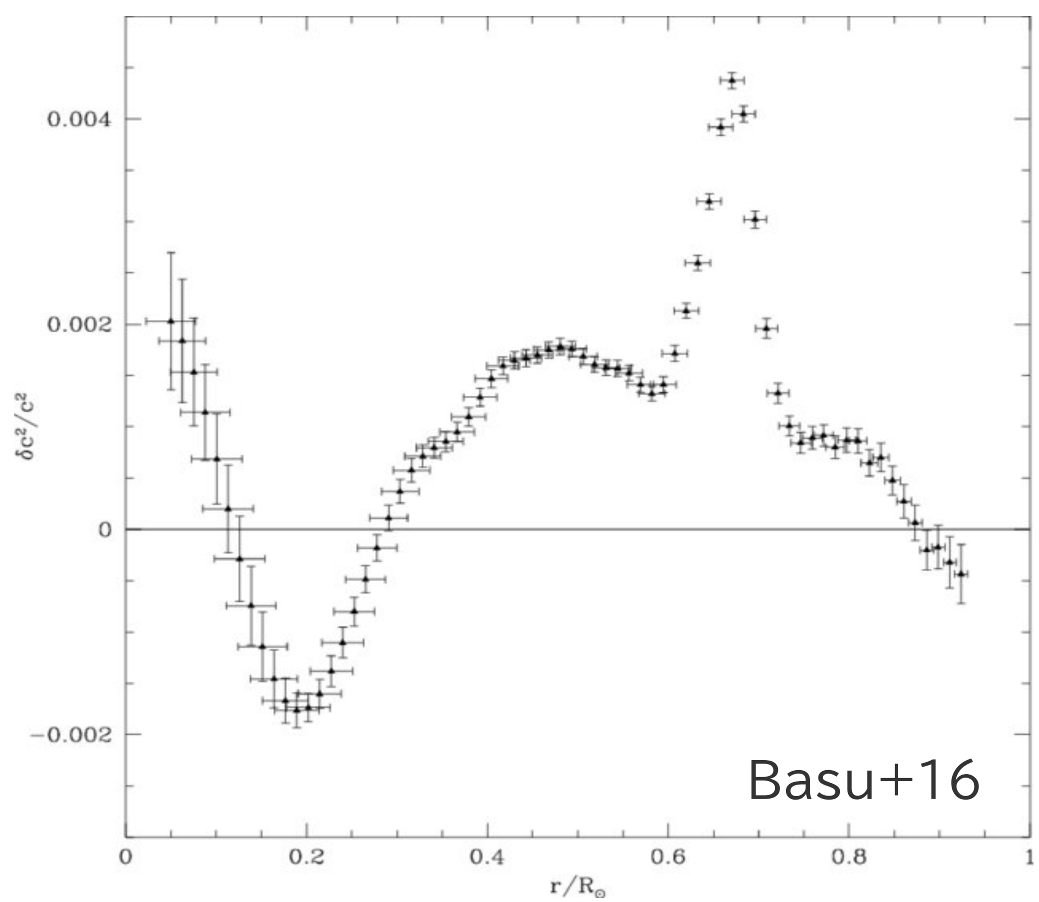

太陽の内部構造②内部回転分布（平均流）

日震学診断 → 太陽内部回転則の推定

①対流層 ($0.71R_{sun} < r < 1.0R_{sun}$ ：対流不安定)

：差動回転 ($\partial\Omega/\partial\theta \neq 0$ or $\partial\Omega/\partial r \neq 0$)

- 赤道加速
- 大部分はconicalな等角速度線
  ($\partial\Omega/\partial r \sim 0$ and $\partial\Omega/\partial\theta \neq 0$)
- Near-surface shear layer (NSSL)

②Tachocline（タコクライン）

($0.68R_{sun} < r < 0.71R_{sun}$ ：対流安定)

：差動回転 ($\partial\Omega/\partial\theta \neq 0$ or $\partial\Omega/\partial r \neq 0$)

- 強い動径シア ($\partial\Omega/\partial r \neq 0$)

③放射層

($r < 0.68R_{sun}$ ：対流安定)

：剛体回転

($\partial\Omega/\partial\theta \sim 0$ or $\partial\Omega/\partial r \sim 0$)

> **※太陽の自転周期：**
> 24 days @E.P.
> 〜 38 days @pole
> (平均：27日)

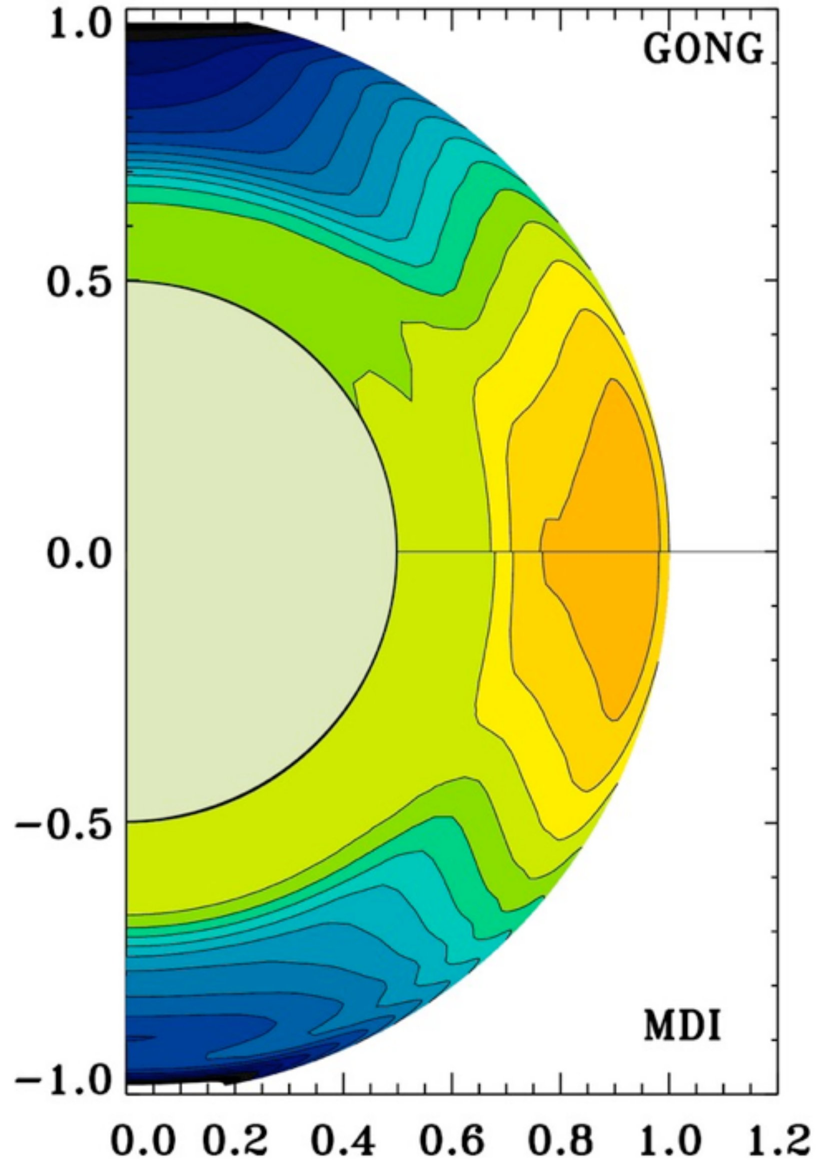

Howe+ 2003

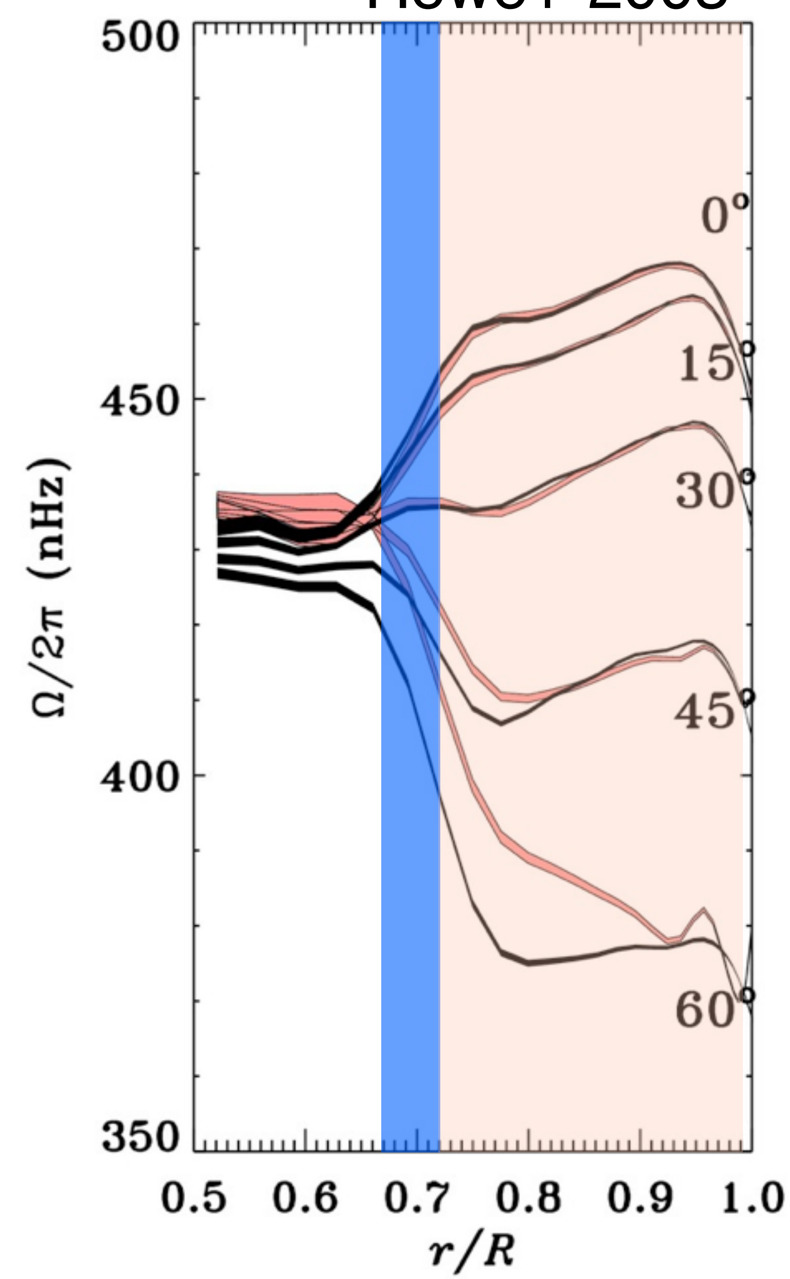

太陽の内部構造③子午面循環流（平均流）

Hanasoge 22

日震学診断 → 太陽内部子午面流の推定

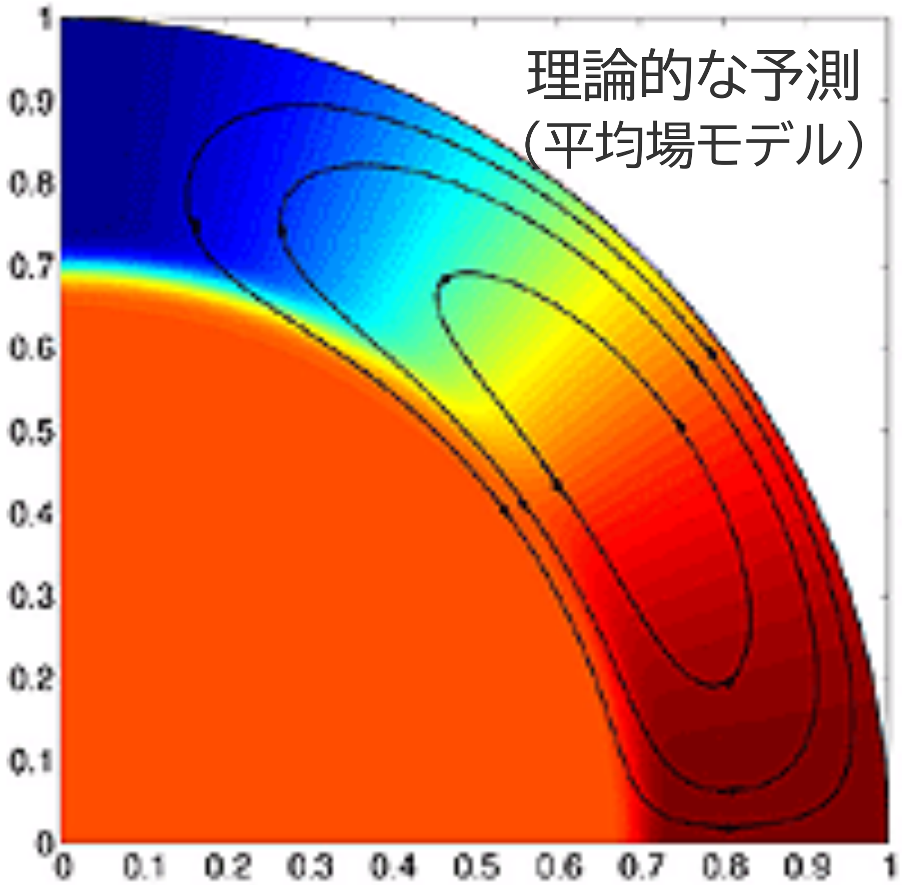

Fig. 15 Comparison between inversions of MC profiles obtained by Chen and Zhao (2017); Rajaguru and Antia (2015); Gizon et al. (2020) and Jackiewicz et al. (2015); positive velocities indicate northward flow and vice versa. The choice

・観測的には2つの可能性：

- single cell
- double cell (multi-cell)

未決着

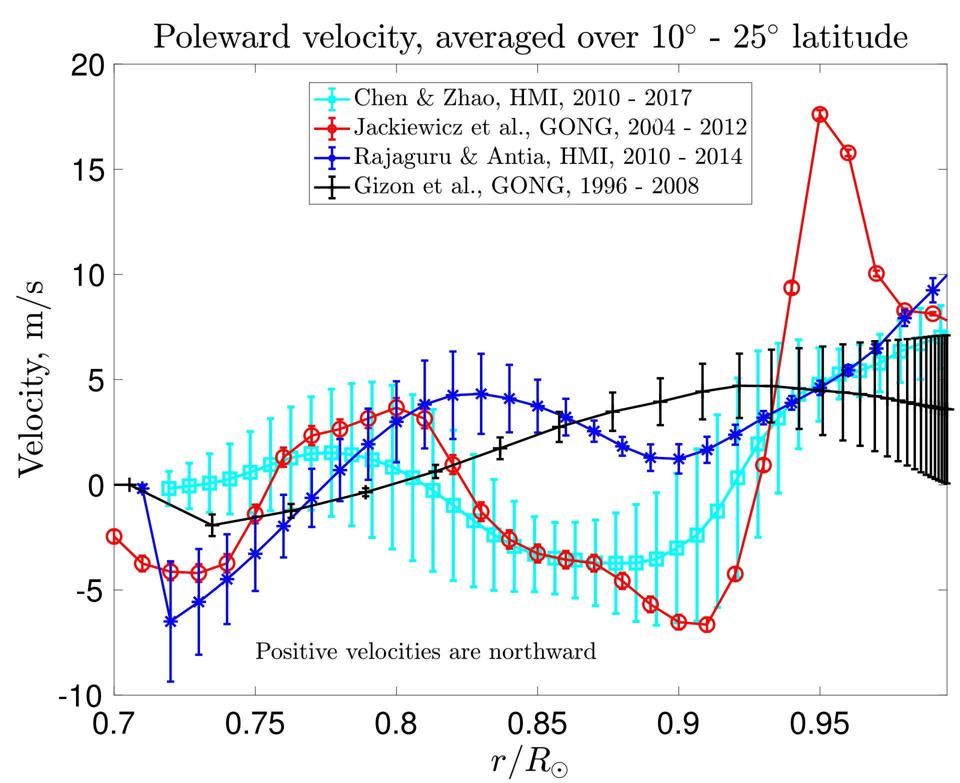

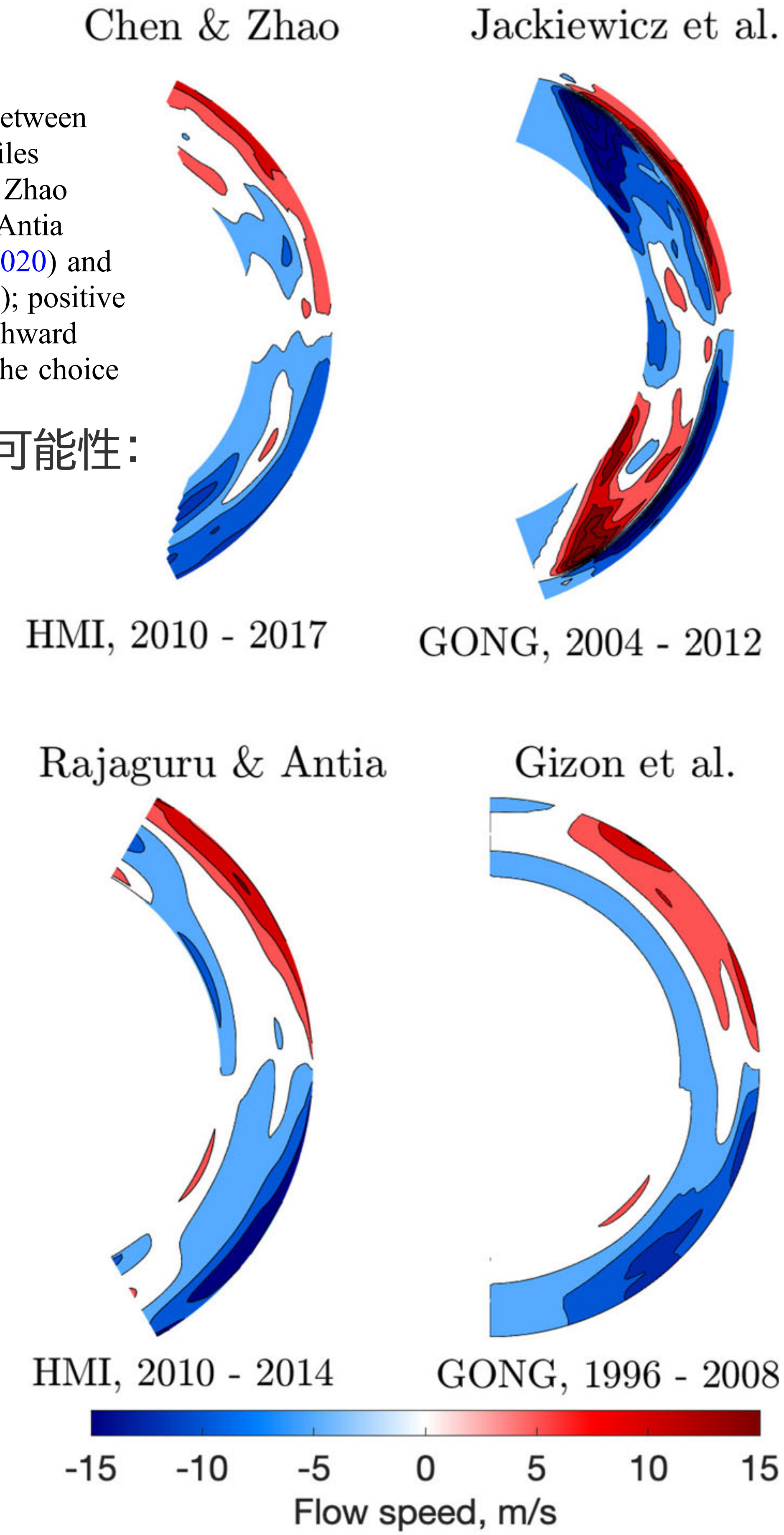

日震学と太陽内部の温度・密度分布

日震学（Helioseismology）診断

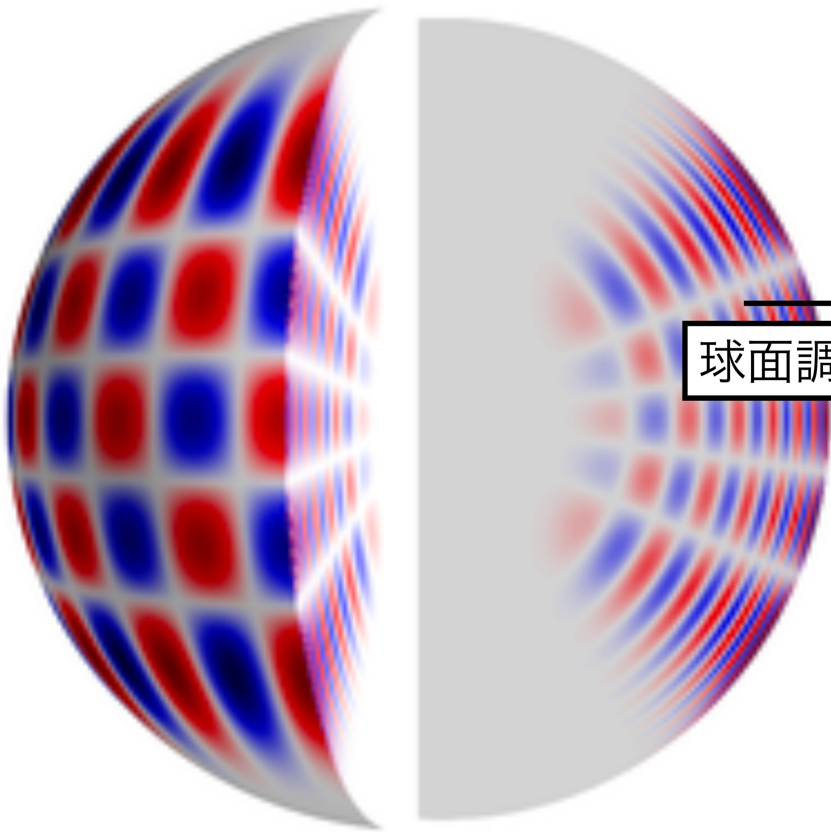

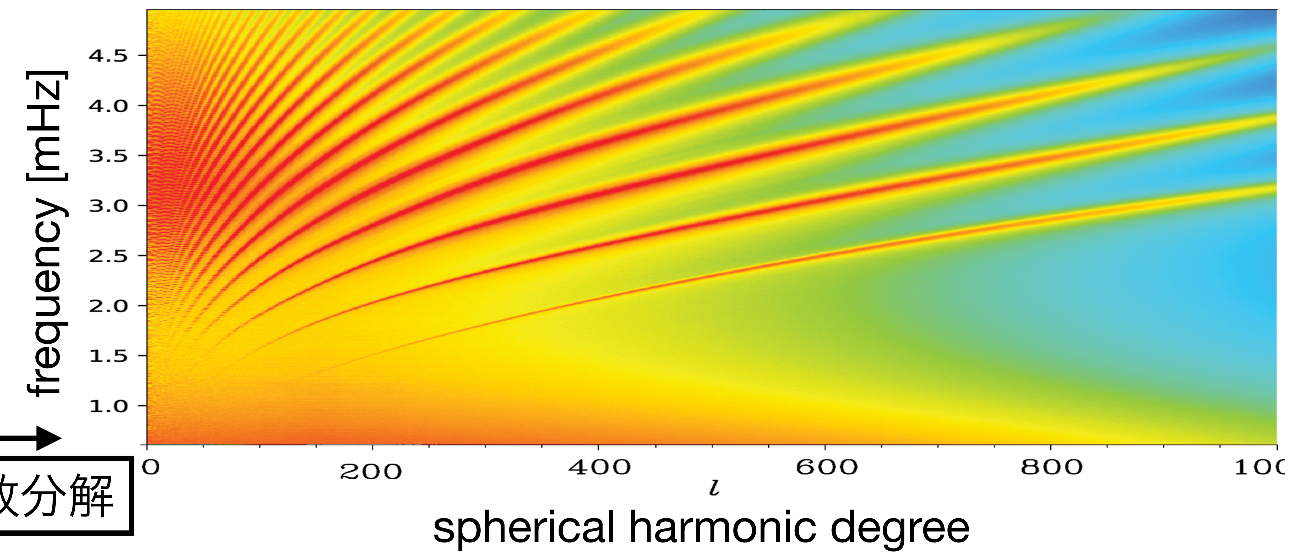

n=2
n=1
n=0
動径方向の
モードの違い

●太陽面速度場から内部を推定

固有振動数 → 太陽内部構造
（inversion）↓

標準太陽モデル（SSM）
(99.5%の精度)

得られる物理量：
- 内部の密度・温度分布
- 内部の回転分布・子午面流分布

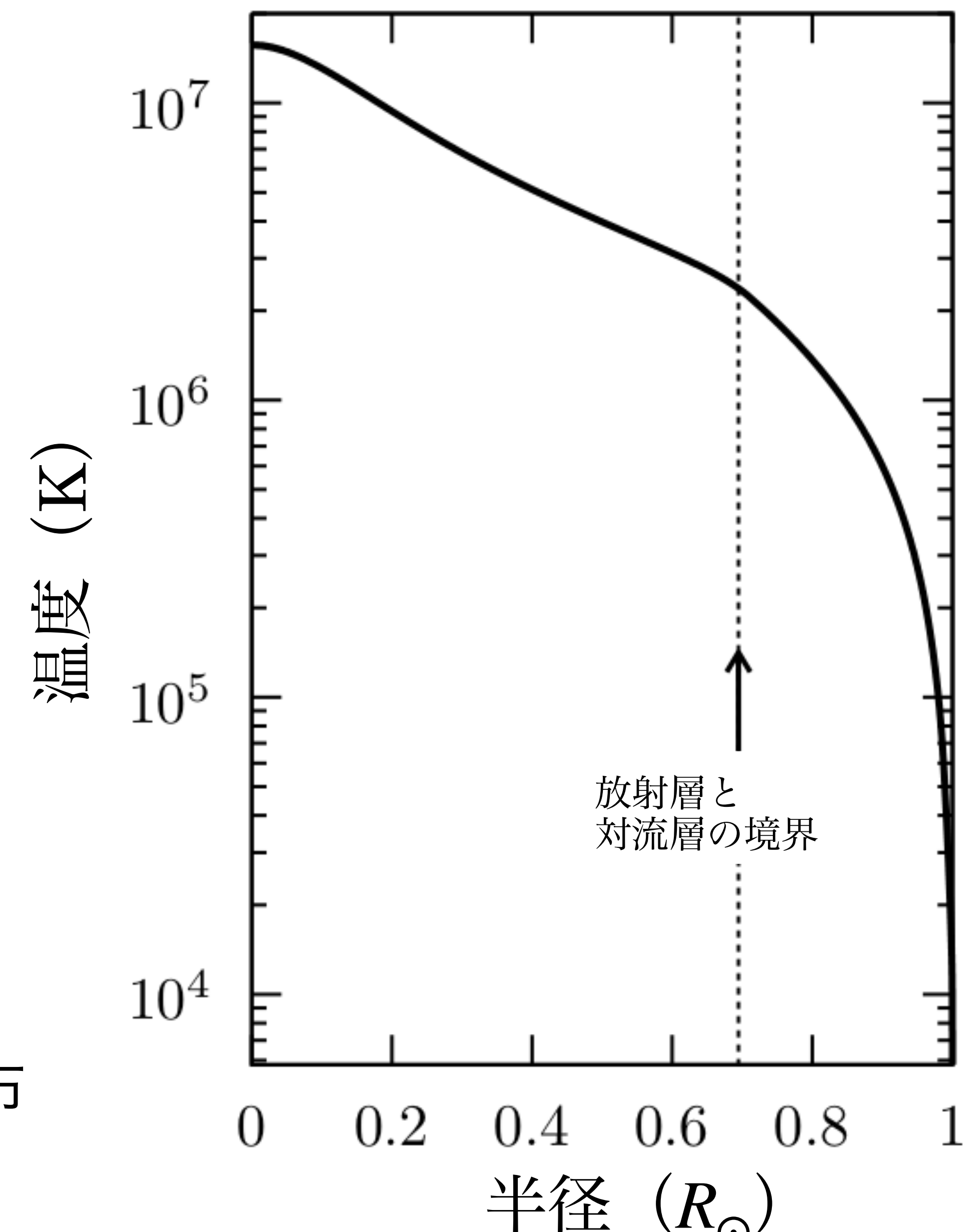

エネルギー流束：

$$F \propto \kappa \frac{\partial T}{\partial r}$$

・太陽では放射拡散係数κが外側に向かって減少
↓
・Fを一定に保つために大きな温度勾配が必要

温度勾配が急 ⇆ 対流

$r \lesssim 0.7R_\odot$ ：**放射層**
$0.7R_\odot \lesssim r$ ：**対流層**

補足資料

・超音波エコーによる測定

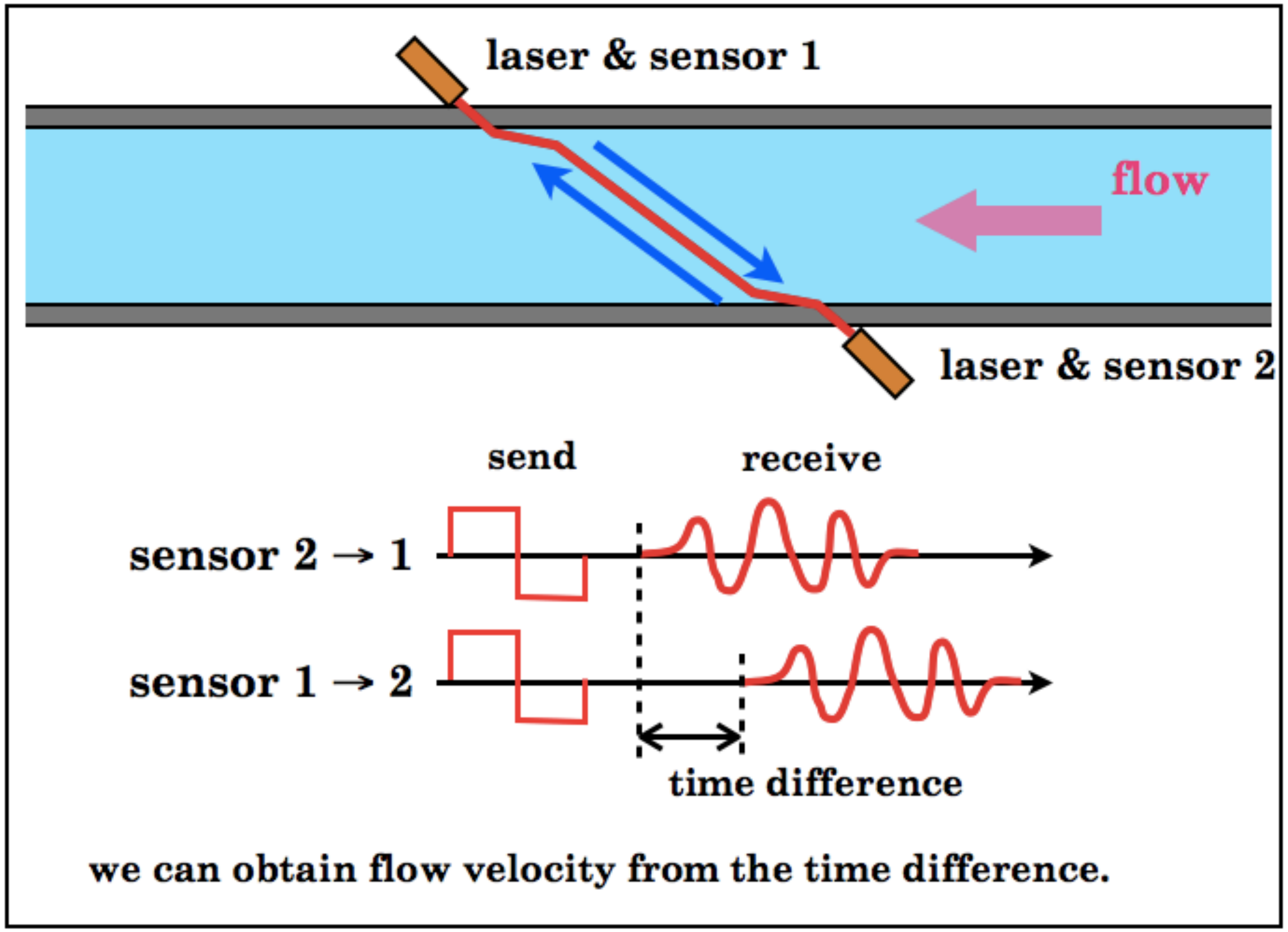

・日震学

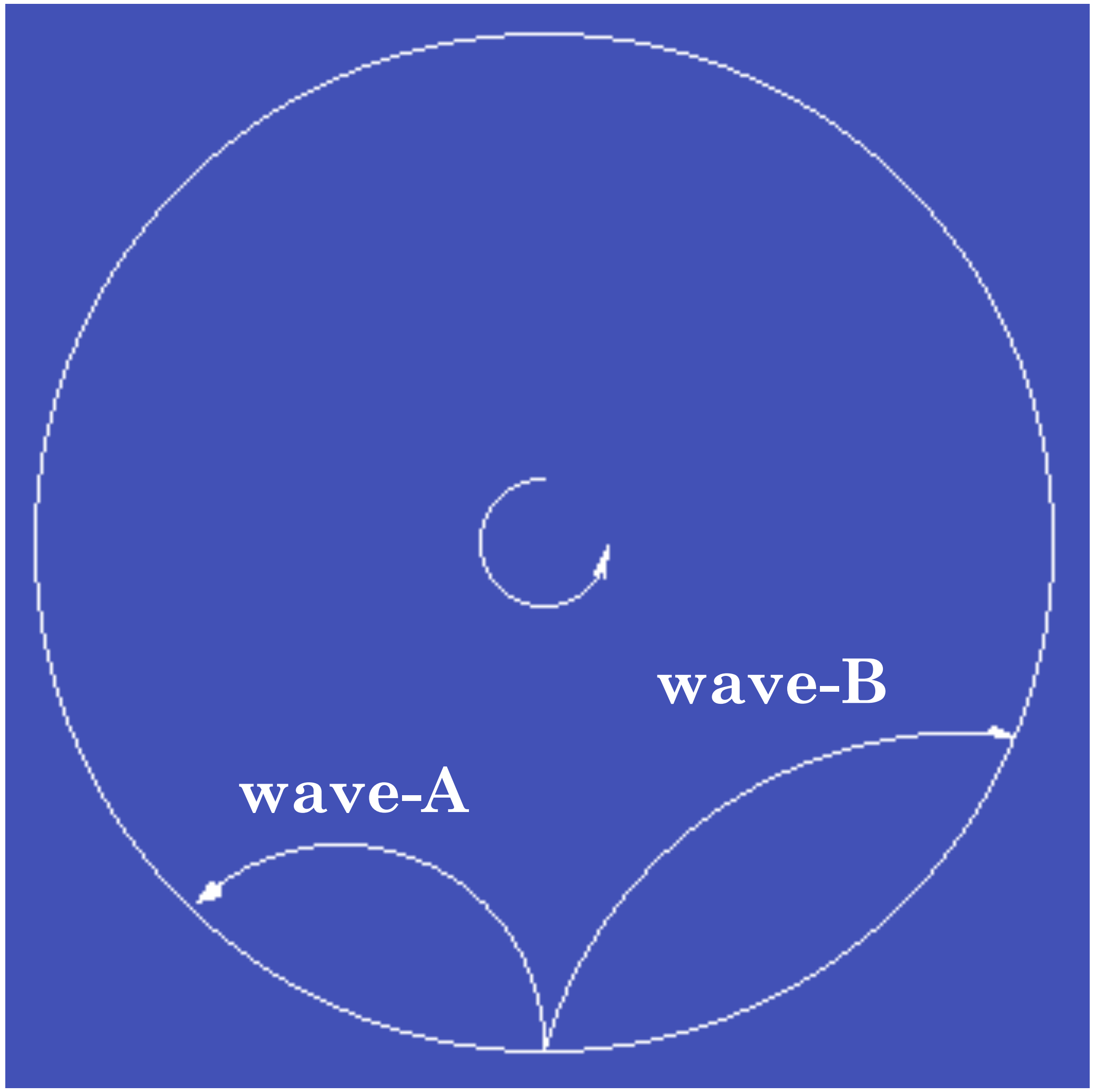

ドップラーシフト：流体運動に起因して音波のピッチ（音の周波数）が変化

■ 回転によって異なる経路を通る音波Aと音波Bの伝搬距離に違いが生じる
→ 振動周波数のスプリット → スプリットの幅から角速度の情報を抽出

対流理論・
太陽のマルチスケール熱対流描像

対流の線形理論

流体要素に変位Δrを加えた時, 周囲の媒質との密度差$\Delta\rho$は

$$\Delta\rho = [(\mathrm{d}\rho/\mathrm{d}r)_e - (\mathrm{d}\rho/\mathrm{d}r)_s]\Delta r$$

$\Delta\rho < 0$の時, $F_r = -g\Delta\rho > 0$となり浮力を得る. ここで,

$$\cdot\ (\mathrm{d}\rho/\mathrm{d}r)_e = \rho[(\mathrm{d}\ln P/\mathrm{d}r)_e - (\mathrm{d}\ln T/\mathrm{d}r)_e]$$

$$\cdot\ (\mathrm{d}\rho/\mathrm{d}r)_s = \rho[(\mathrm{d}\ln P/\mathrm{d}r)_s - (\mathrm{d}\ln T/\mathrm{d}r)_s]$$

と書ける. さらに, $\Delta P = 0$（圧力平衡）を仮定すると

$$\Delta\rho = [-\rho(\mathrm{d}\ln T/\mathrm{d}r)_e + \rho(\mathrm{d}\ln T/\mathrm{d}r)_s]\Delta r$$

圧力スケールハイト$H_P = -\mathrm{d}r/\mathrm{d}\ln P$を使って書き換えると

$$\Delta\rho = \rho[(\mathrm{d}\ln T/\mathrm{d}\ln P)_e - (\mathrm{d}\ln T/\mathrm{d}\ln P)_s]\Delta r/H_P$$
$$= \rho[\nabla_e - \nabla_s]\Delta r/H_P$$

流体要素と媒質の間で熱交換が無いことを仮定すると
（*i.e.*, 断熱膨張）, $\nabla_e = \nabla_{\mathrm{ad}}$と書ける. この時, 不安定条件は,

$$\delta \equiv \nabla_s - \nabla_{\mathrm{ad}} > 0 \quad \text{(Schwarzschild criterion)}$$

(adiabaticity)

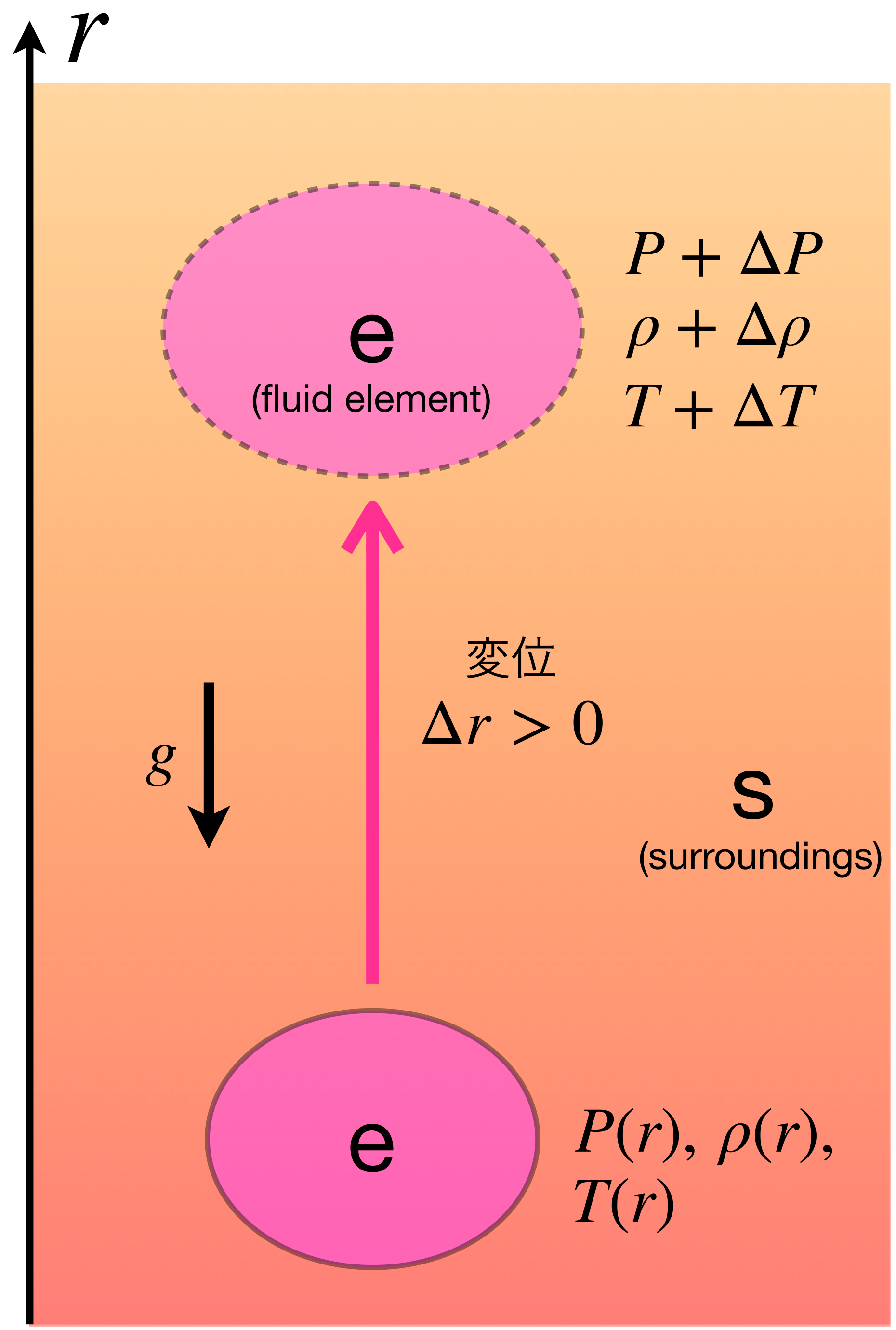

(Bohm-Vitense 1958, Gough 1977, Canuto & Mazzitelli 1992)

$F_r = -g\Delta\rho$より, 流体要素の運動方程式（働く力は浮力）, 及び帰結としての線形成長率は

$$\partial_t^2\Delta r = -(g/H_P)[\nabla_{\mathrm{ad}} - \nabla_s]\Delta r \quad \leftrightarrows \quad \sigma = \sqrt{(g/H_P)\delta} \quad \text{（線形成長率）}$$

（局所線形化 $\Delta \propto \exp(\sigma t)$）

乱流エネルギー輸送と混合距離理論

- 対流が運ぶ乱流エネルギーフラックス(TEF)：$F_{\rm cv} \propto \rho \langle \Delta v \Delta T \rangle$　　ただし, ⟨・⟩はアンサンブル平均
- 前述の線形理論に基づきTEFを記述する枠組み：混合距離理論 (Mixing-length theory: MLT)

$$\Delta v \approx \sigma \times l_m, \quad \Delta T/T \approx \Delta\rho/\rho = \delta l_m/H_P$$ （δ：adiabaticity)

l_m は任意のパラメータで混合距離と呼ばれる (ここで行っているのは$\Delta r \rightarrow l_m$の置き換え).
混合距離（〜エネルギーの典型的な輸送距離）として, $l_m \sim H_P$ を選ぶと, TEFは,

$$\boxed{F_{\rm cv} \propto \rho\,(\sigma H_P \delta) T \quad \text{where} \quad \sigma = \sqrt{(g/H_P)\delta},\ \ \delta = \nabla_s - \nabla_{\rm ad}}$$

と書き換えられる.

- ある半径における密度と圧力：$\rho(r), T(r)$
- ある半径でのadiabaticity：δ
- ある半径でのスケールハイト：$H_P(r)$

(全て局所的に与えられる量)

浮力が生じる典型的なスケールがH_P:

$$\Delta\rho = \rho[\nabla_e - \nabla_s] l_m/H_P$$

→ H_P のサイズの渦による輸送描像.

スケールハイトは

$$H_P \equiv C_s^2/g \propto T(r)$$

外向きに温度や密度が減少するような分布の場合, 対流層の底部ほど大きく, 対流層の上部ほど小さい

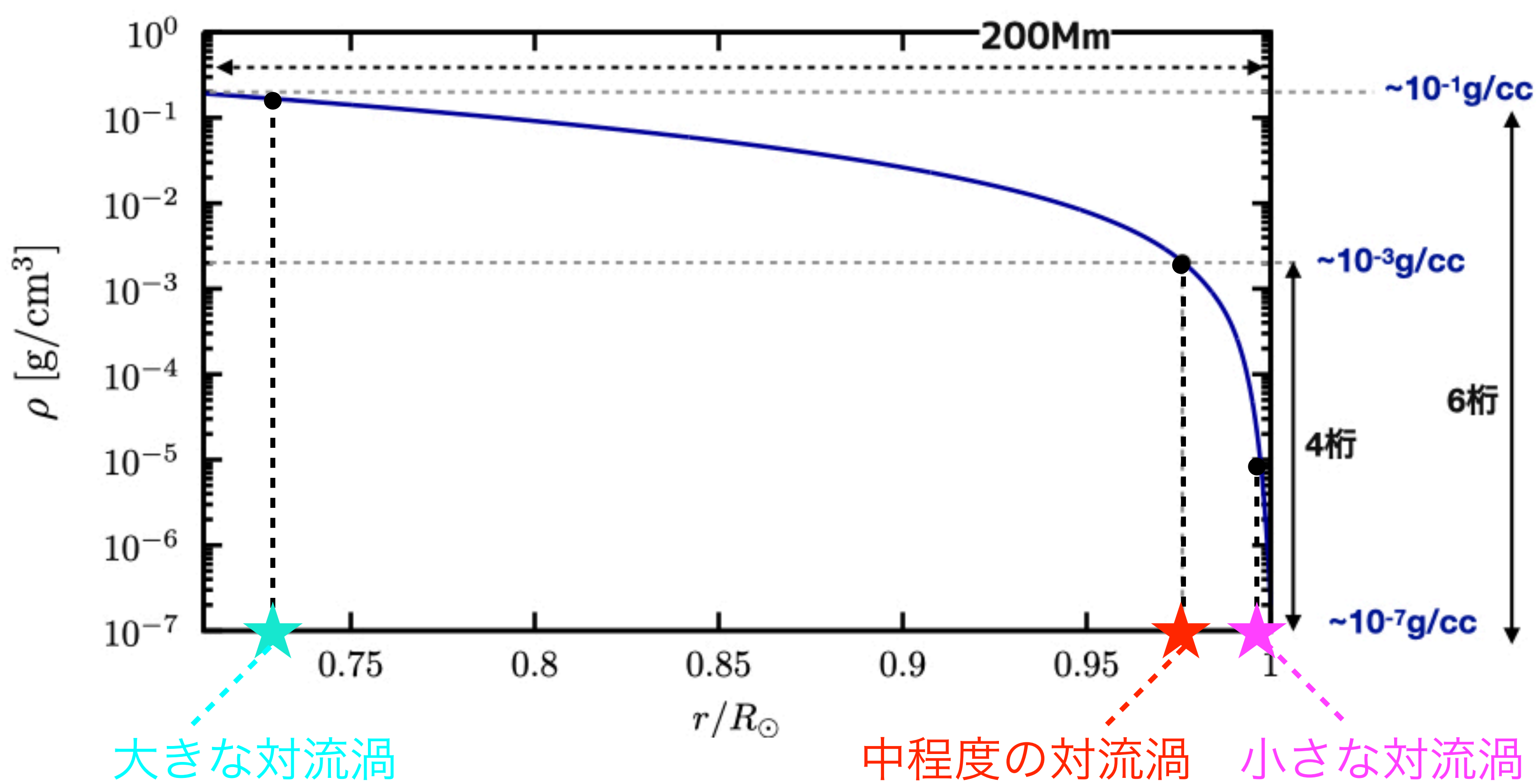

太陽のマルチスケール熱対流描像

太陽のマルチスケール熱対流描像

The Swedish 1-meter Solar Telescope / Institute for Solar Physics, Observer & Data reduction:
Luc Rouppe van der Voort, Oslo 18 Jun 2006 (Wavelength: 656.3nm H-Alpha)

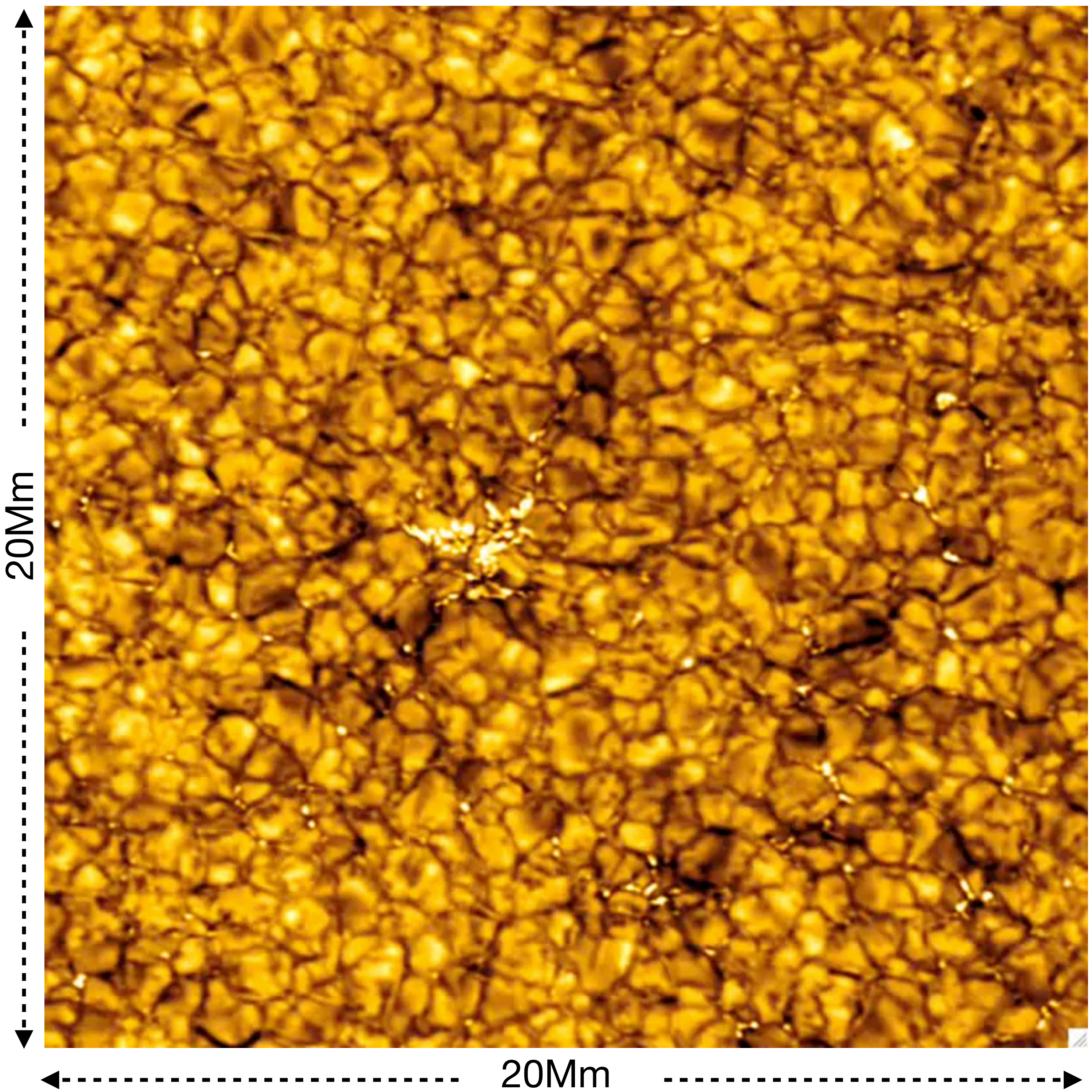

- **Conventional view on Sun's CZ (cartoon)**

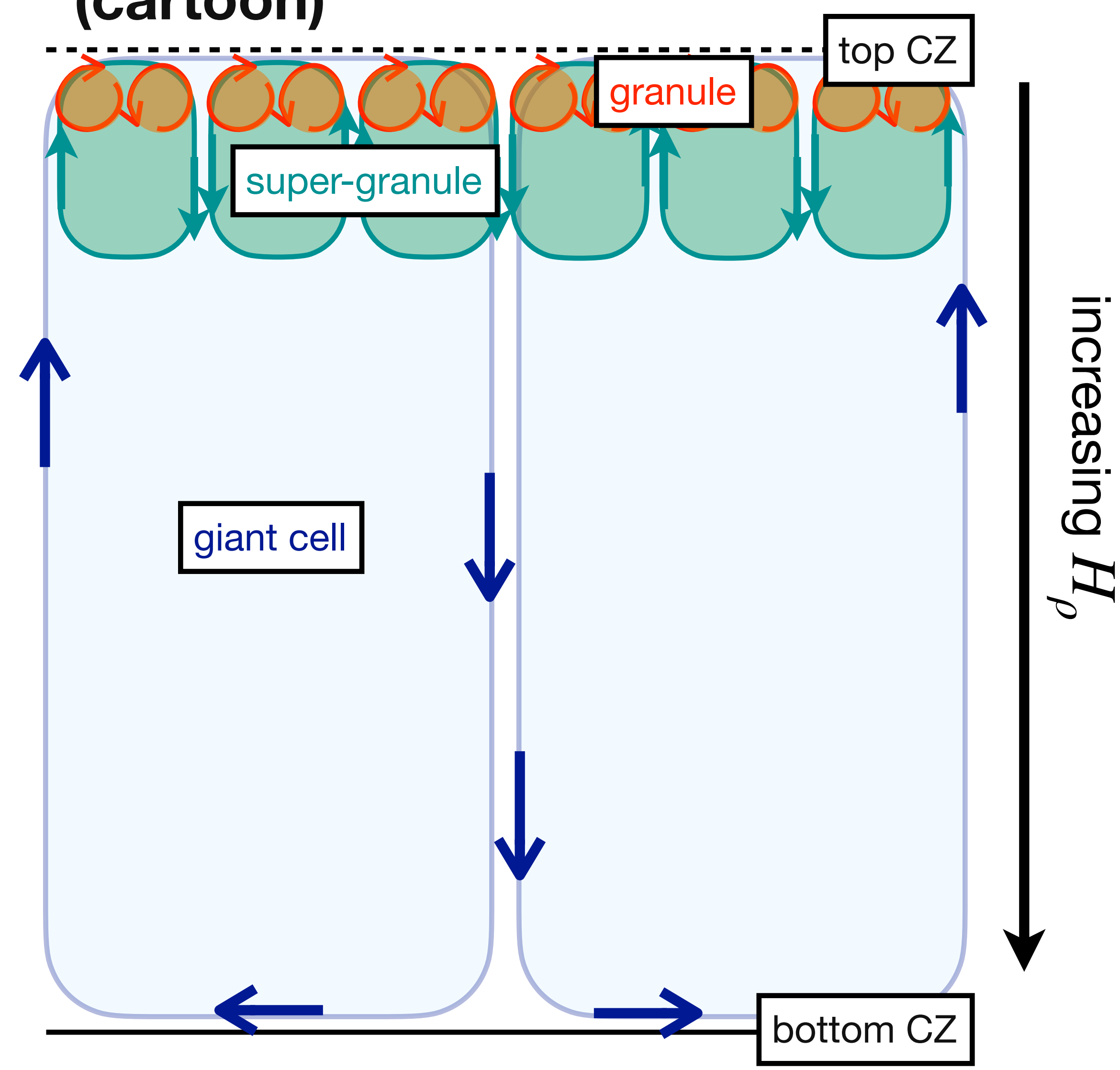

スケールハイトが大きく変化する
ので様々な駆動スケールの渦が混在
（対流層上部ほどスケールハイトが
小さくなり対流渦が小さくなる）

- 粒状斑　: typical size ≈ 1000km,　typical lifetime ≈ 10 min.
- 超粒状斑　: typical size ≈ 30Mm,　typical lifetime ≈ 20 hours
- 巨大胞　: typical size ≈ 200Mm,　typical lifetime ≈ 1 month

太陽磁場の観測

太陽磁場の時空間進化

- **準周期的な時空間進化：**
  - 11年の磁気活動周期（22年の極性周期）
  - 蝶形パターンのマイグレーション
    (アクティビティベルト < ±30°)
  - 黒点はO(1) kG
    大局的磁場はO(10) G (双極 時々 四重極)
- **蝶形図（バタフライダイアグラム）**
  （太陽表面磁場の時間-緯度分布）
  - 高い時空間コヒーレンス

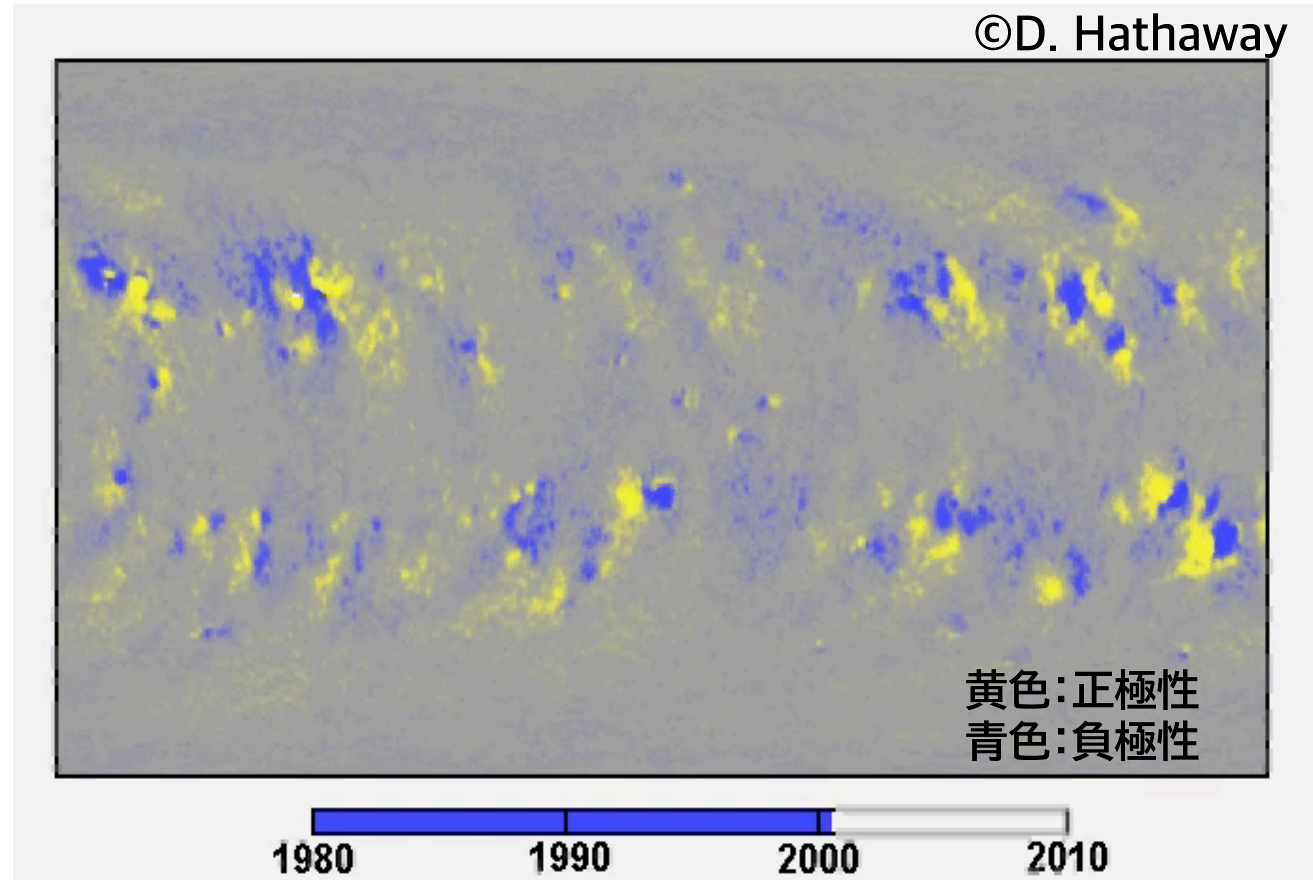

方位角平均

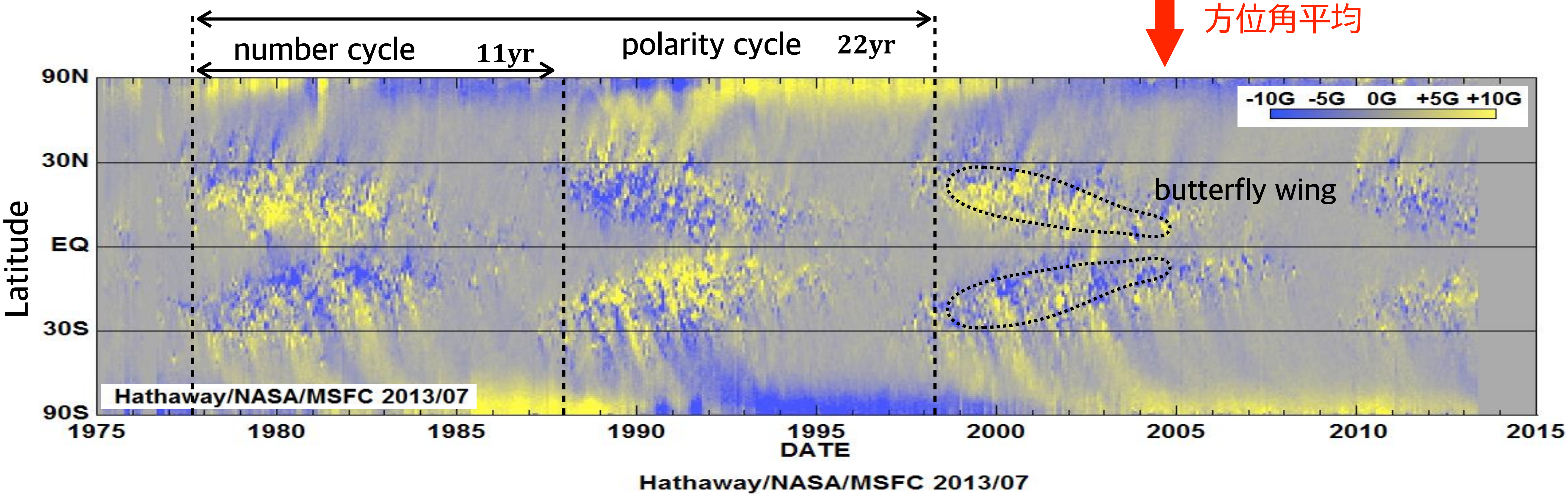

太陽黒点の特徴：大局性・収束性・周期性

©J. Okamoto

太陽磁場（黒点）の3つの特徴

① 大局性：黒点 ≫ 対流セル（粒状斑）

② 収束性（集中性）：局在化
（× diffuse structure）

③ 周期性：
- 11年周期（22年周期）：5つの経験則（次ページ）
（× ランダムな磁場）

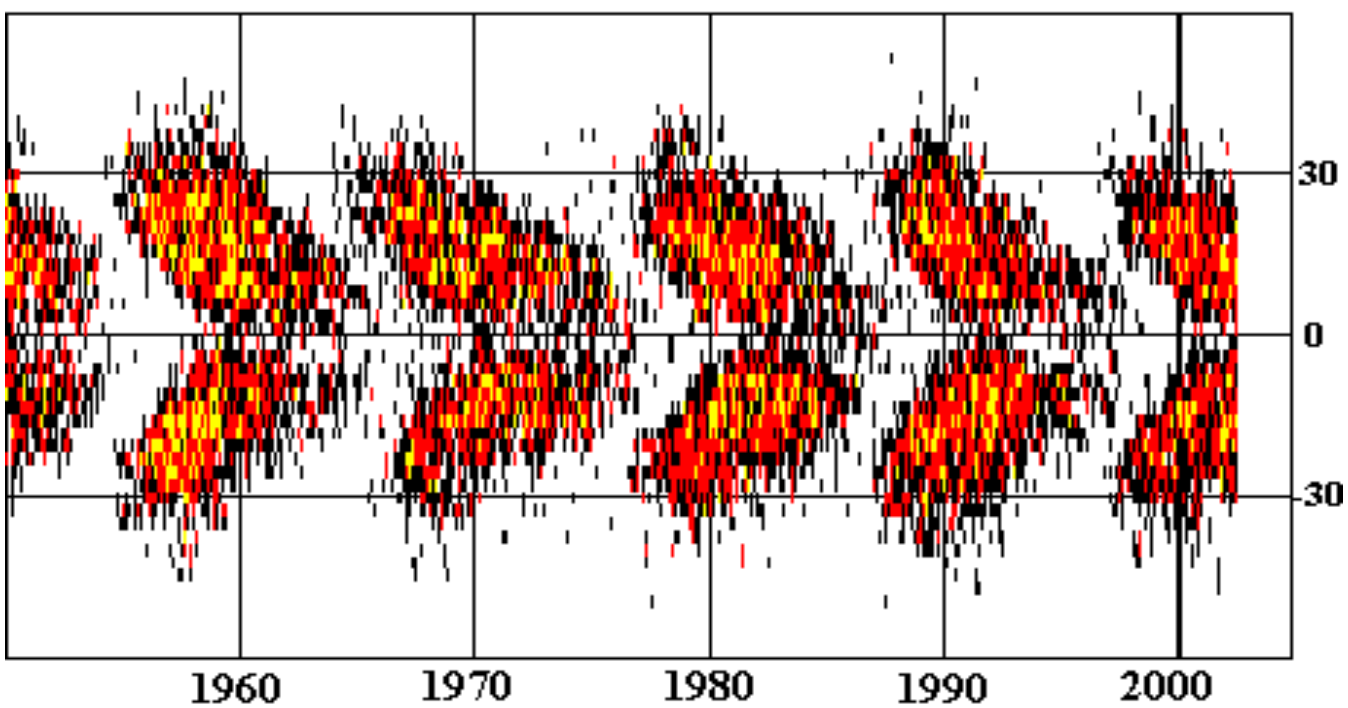

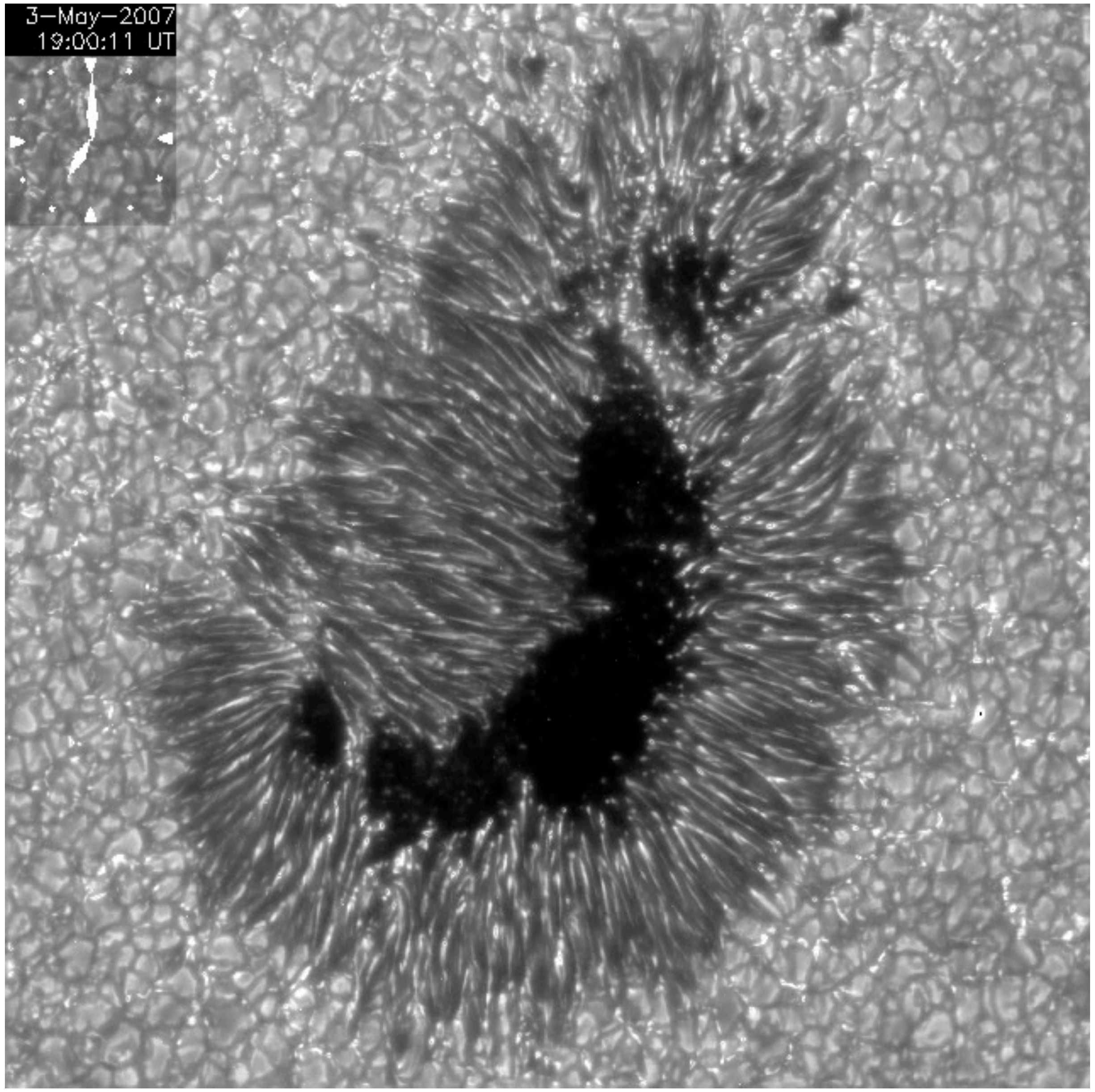

黒点：暗部 + 半暗部

プラズマ物理（MHD）のフレームワークで
これらの「内部流れ場」および「磁場」の観測結果を説明しなければならない.

太陽磁場の5つの経験則と例外(マウンダー極小期)

(a) Hale-Nicolson's law & Joy's law [経験則(1)と(2)]

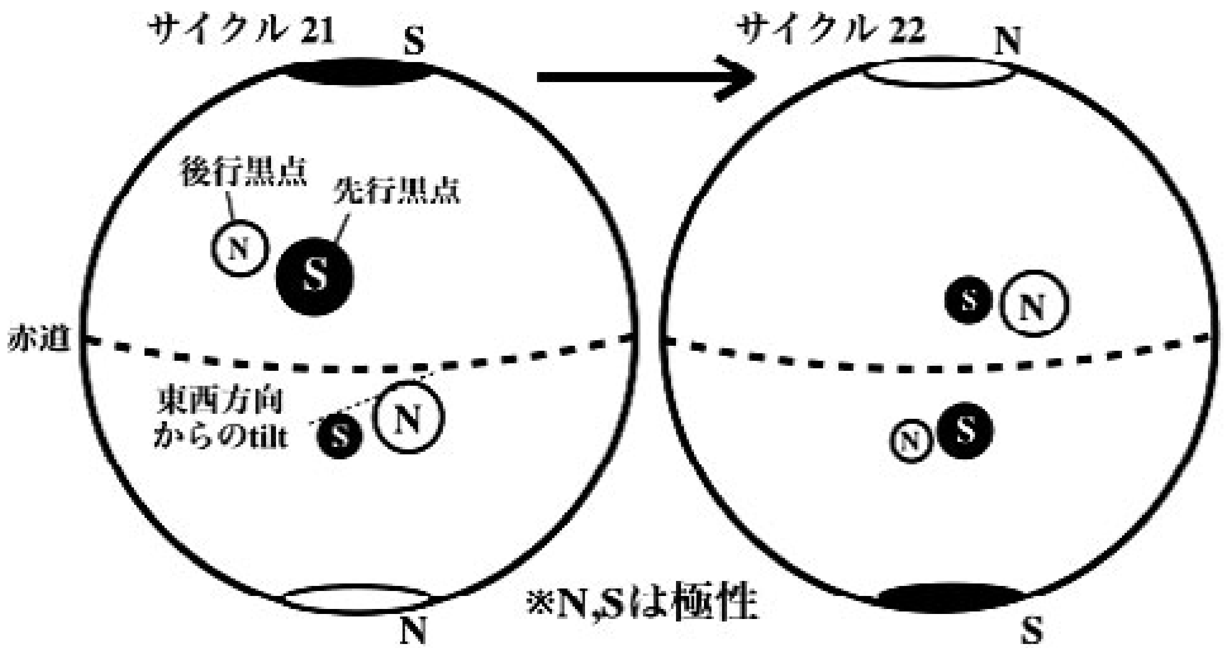

（1）黒点は正極と負極の双極（対）構造で出現する.

（2）黒点対を結ぶ軸は東西方向から約５度傾いている.

（3）黒点数は約11年周期で増減を繰り返す.

(b) Schwabe's law [経験則(3)]

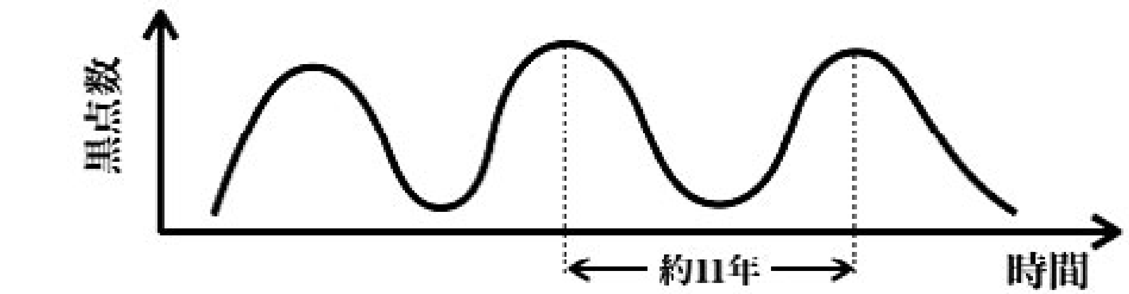

(c) Carrington-Spörer's law [経験則(4)と(5)]

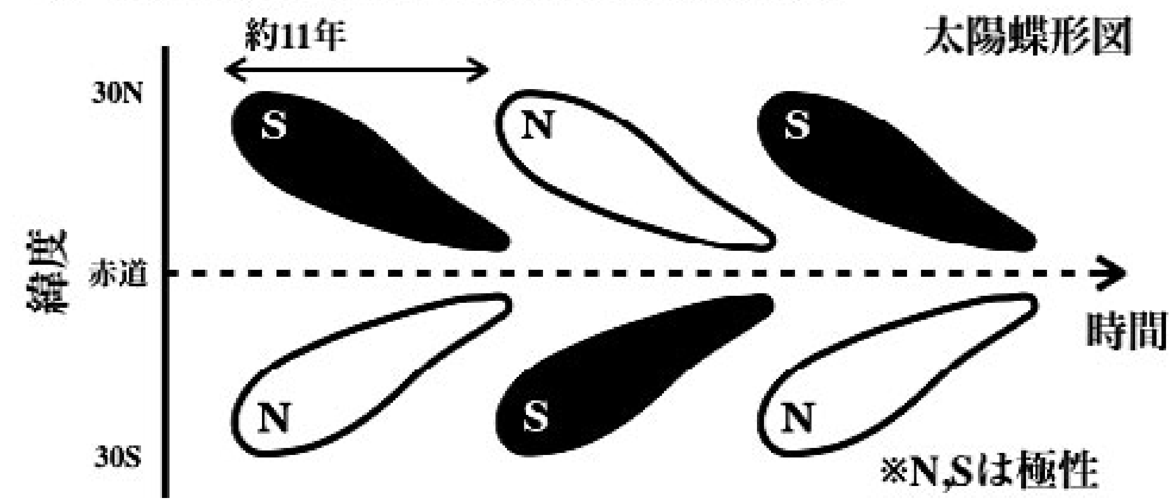

（4）黒点対の極性は南北反対称で周期ごとに反転する（極性反転を考慮すると太陽サイクルは約22年）.

（5）黒点の出現緯度は時間とともに中緯度から赤道へ向かってドリフトする.

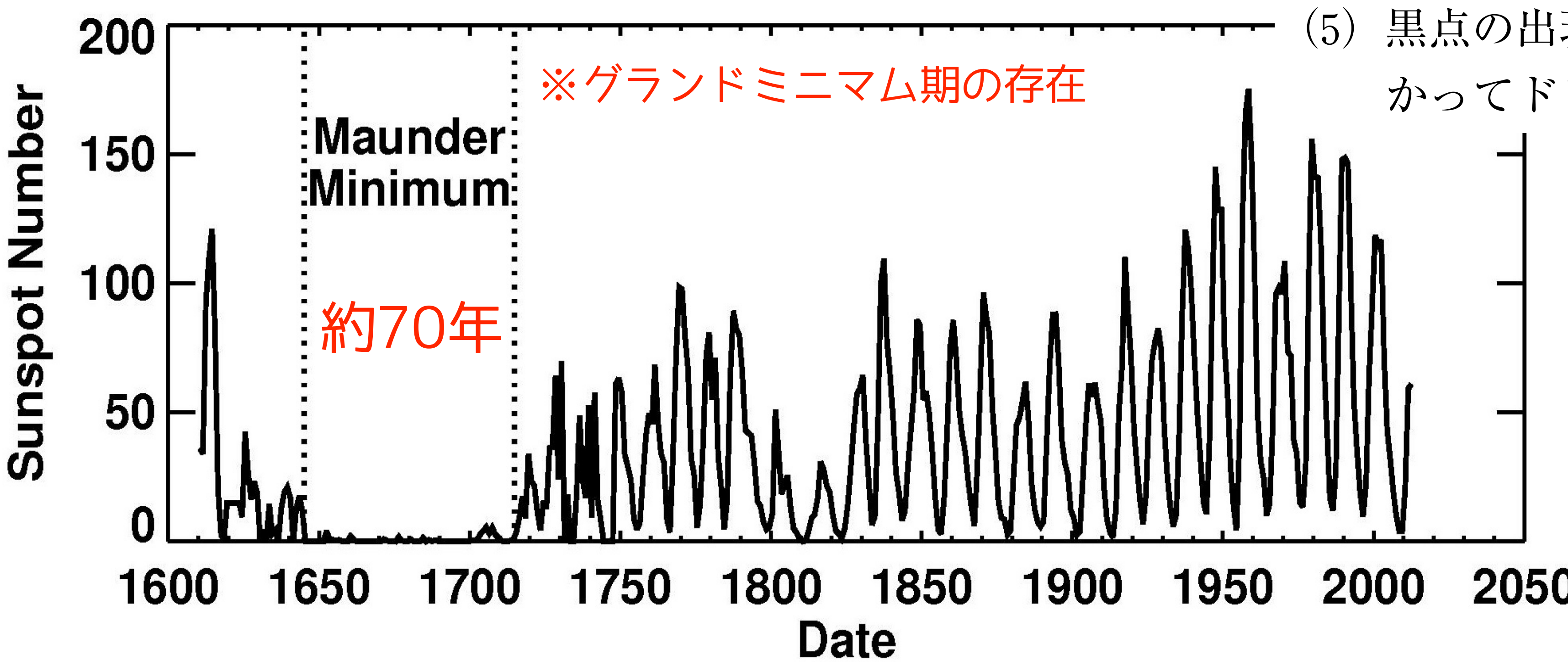

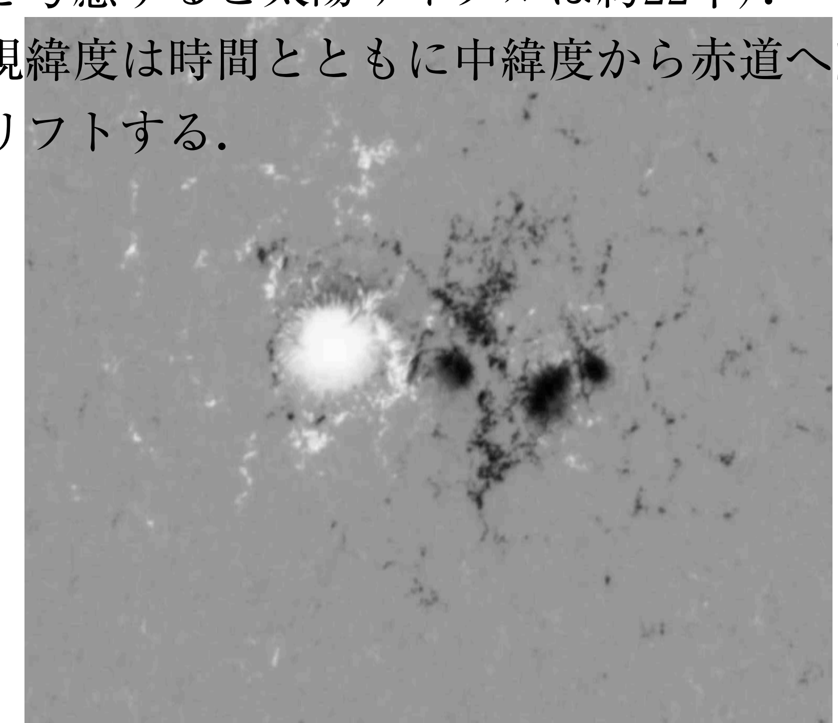

極域磁場 Polar field reversal as observed with Hinode

Ito & Tsuneta 10

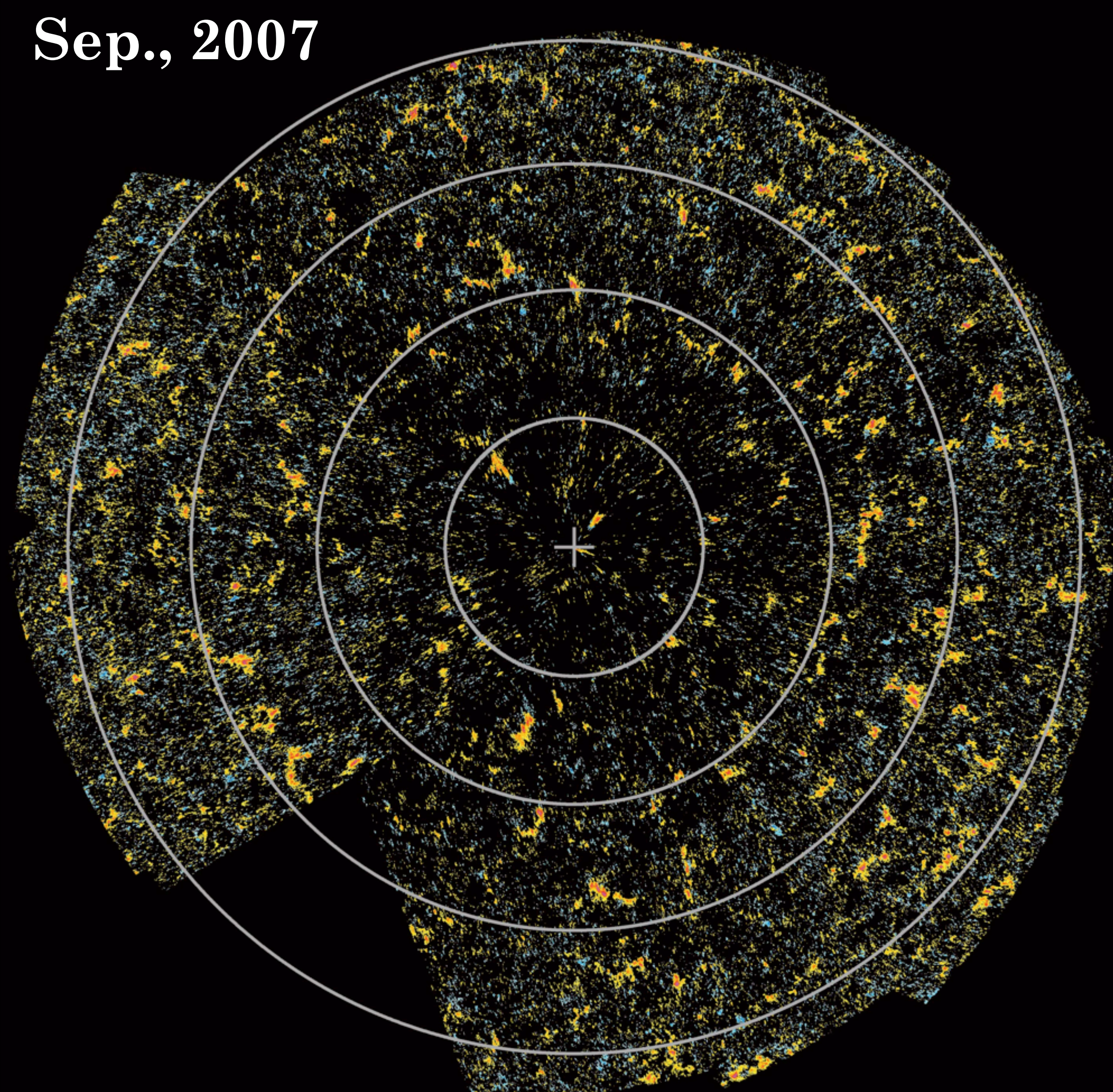

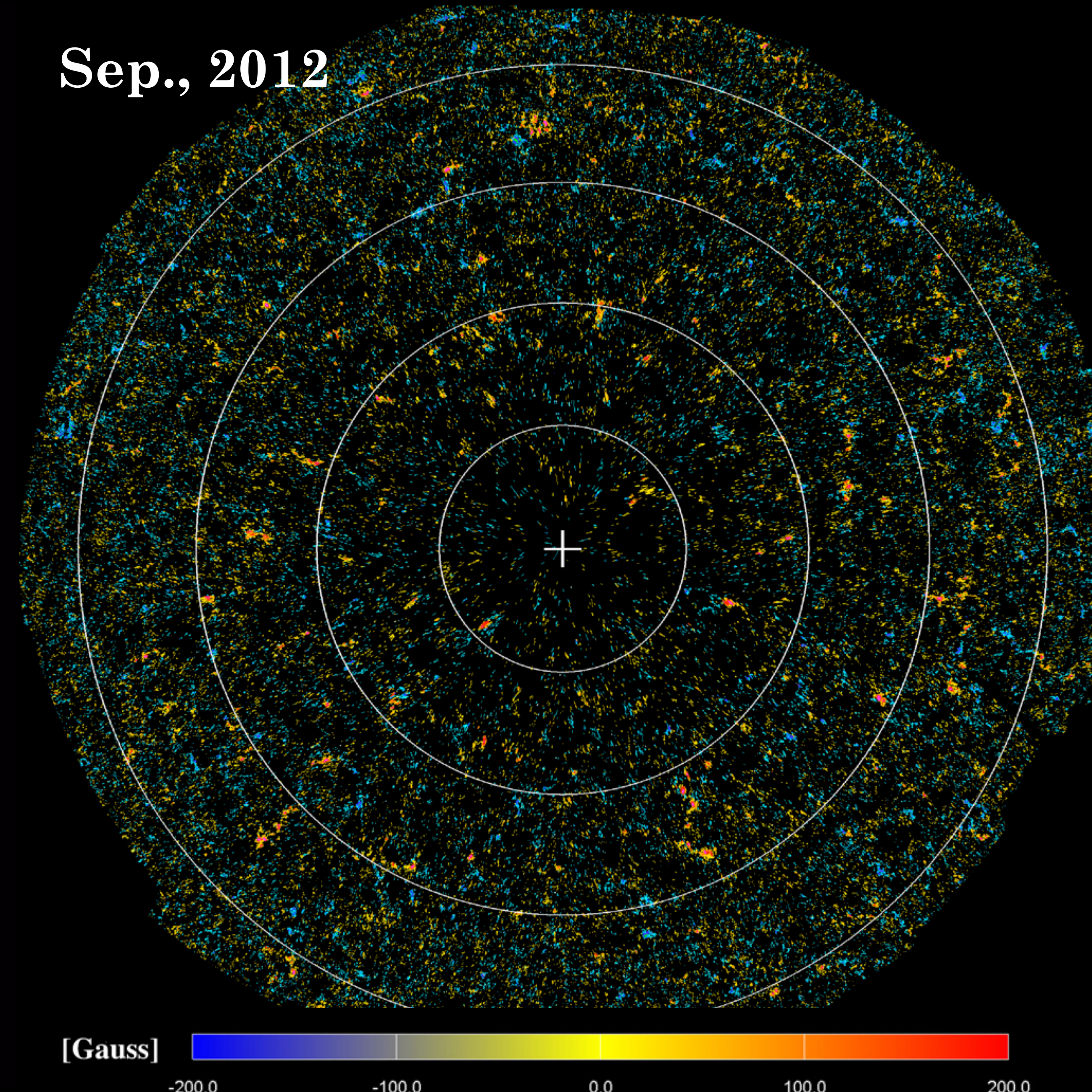

極域磁場の構造:

× 一様な磁場 → 双極磁場

○ kGパッチ → 双極磁場

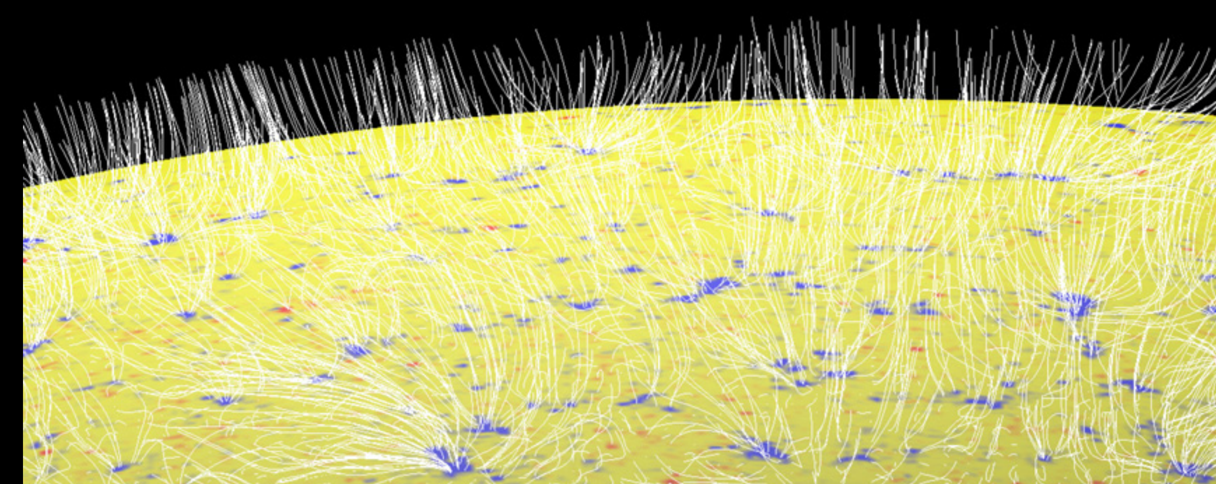

太陽MHDを考える上で
頭に入れておくべき基礎知識

太陽プラズマを考える上で必要な補足情報①

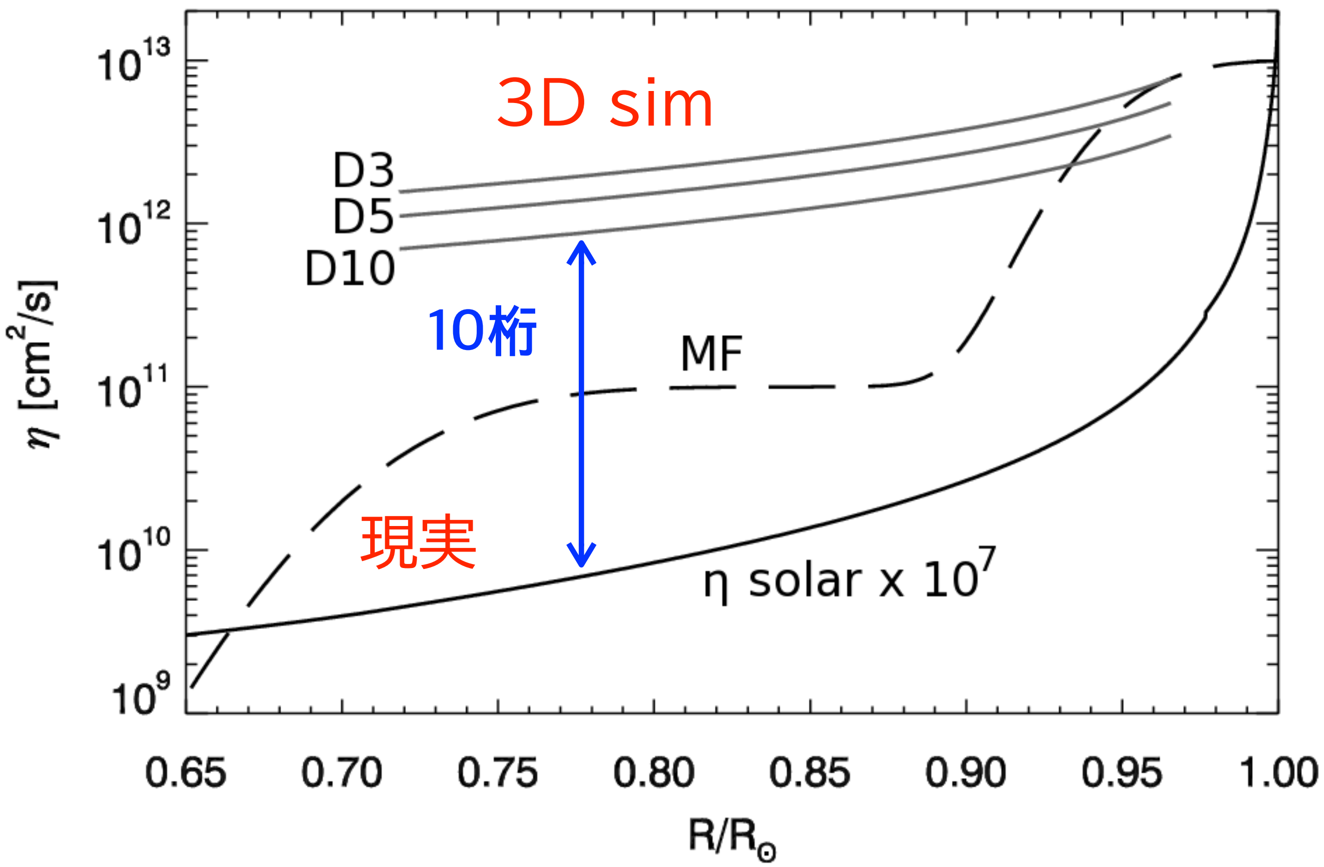

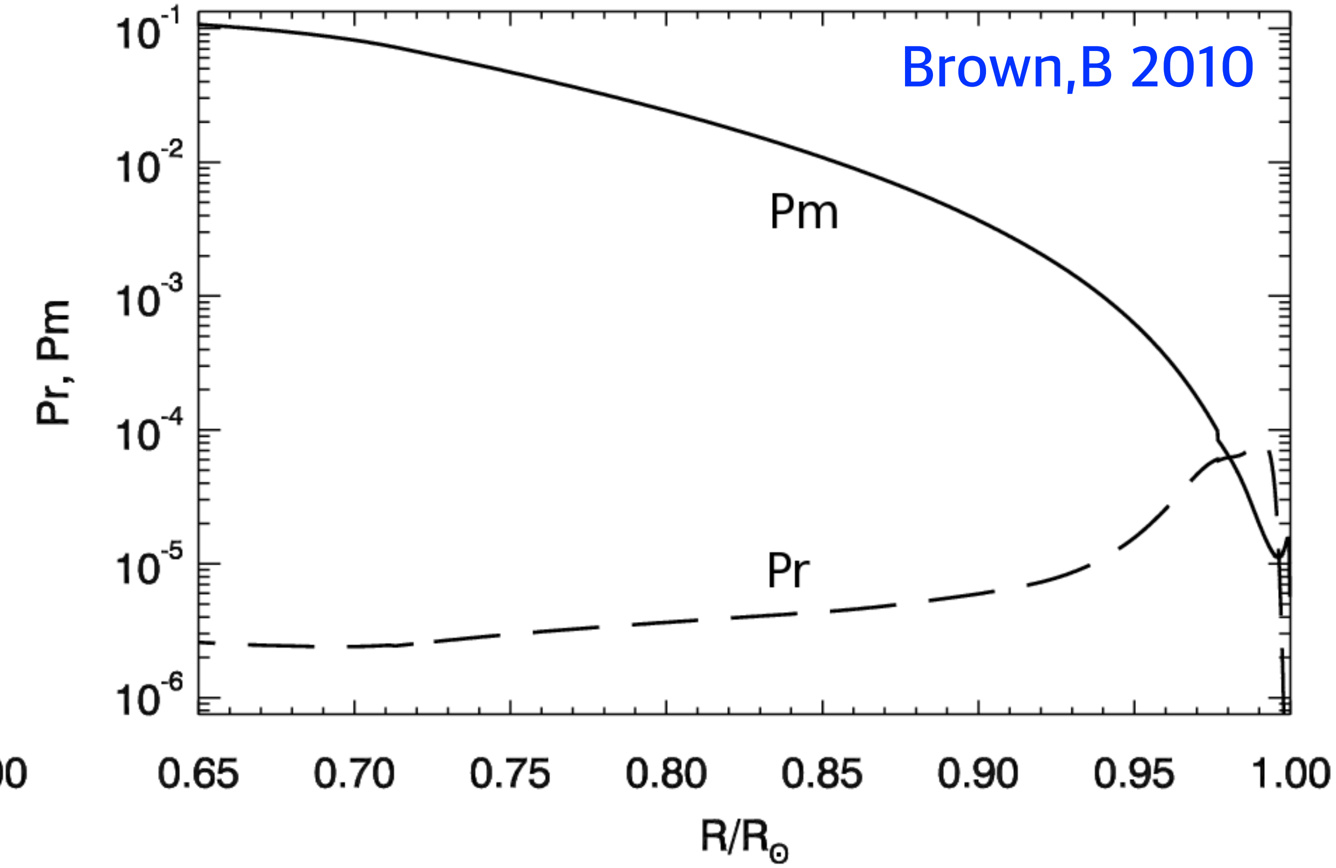

太陽プラズマ(対流層)を
特徴づける無次元パラメータ:

$Re = 10^{12} - 10^{14}$
$Re_M = 10^{8} - 10^{10}$
$Ra = 10^{22} - 10^{24}$
$Pr = 10^{-6} - 10^{-5}$
$Pr_m = 10^{-5} - 10^{-2}$
$Ek = 10^{-15}$ (=Ro/Re)

対流層の密度コントラスト:7桁
0.2g/cm³ @底, 2×10⁻⁶ g/cm³@光球

中心からの距離	圧力	温度	密度	内部の質量	輻射量	水素含有量
(太陽半径=1.0)	(10^{15} dyn/cm^2)	(10^6K)	(g/cm^3)	(太陽の質量=1.0)	(表面総輻射量=1.0)	(質量比)
0.0	240	15.8	156	0.0	0.0	0.333
0.1	137	13.2	88	0.08	0.46	0.537
0.2	43	9.4	35	0.35	0.94	0.678
0.3	10.9	6.8	12.0	0.61	1.0	0.702
0.4	2.7	5.1	3.9	0.79	1.0	0.707
0.6	0.21	3.1	0.50	0.94	1.0	0.712
0.8	0.017	1.37	0.09	0.99	1.0	0.735
1.0	1.3×10^{-10}	0.0064	2.7×10^{-7}	1.00	1.0	0.735

(Bahcall and Pinsonneault: Rev. Mod. Phys., 67, 781, 1995)

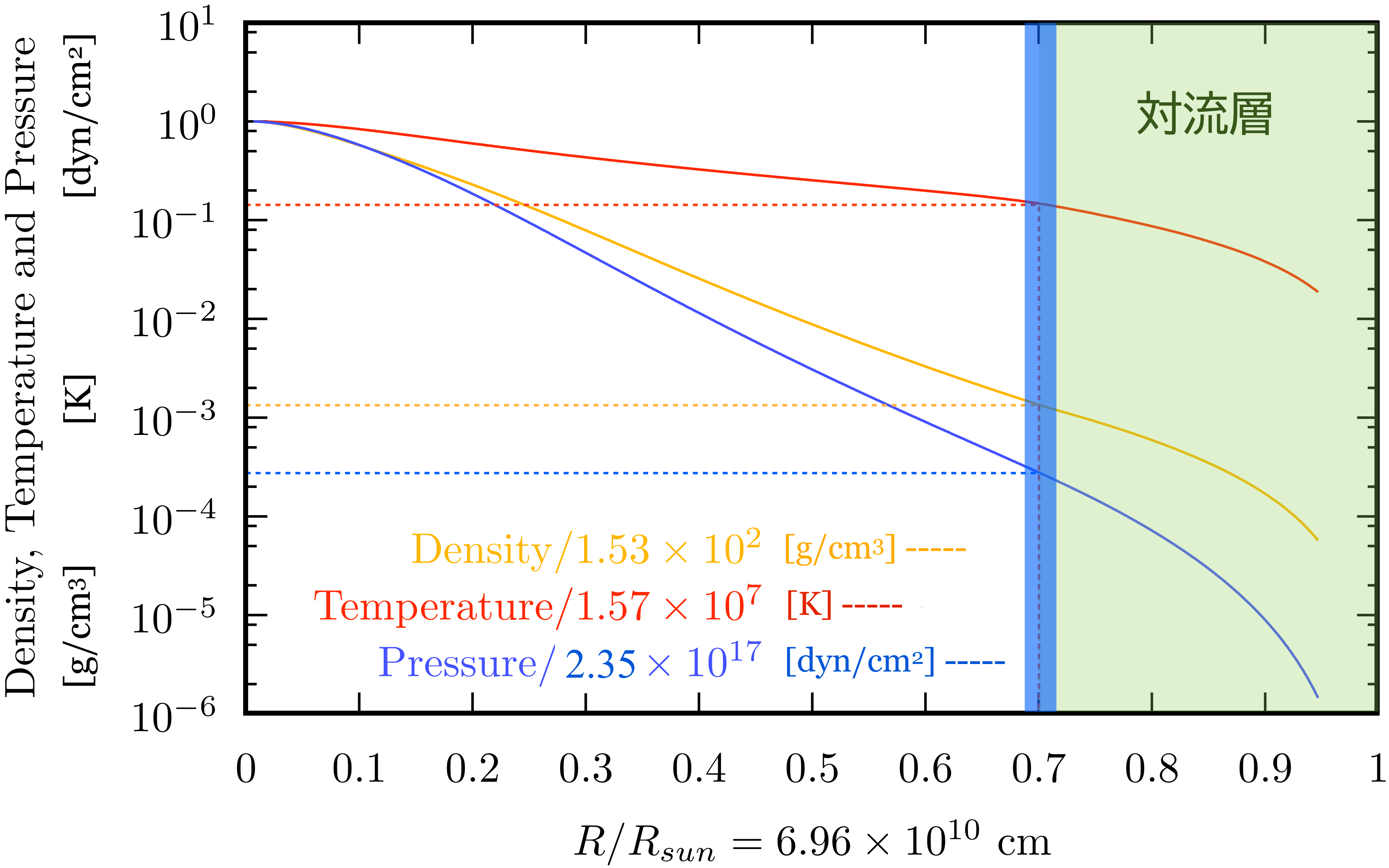

密度換算：1 [g/cm^3] = 10^3 [kg/m^3] 〜10^{30} [m^{-3}]

温度換算：1 [K] ~ 10^{-4} [eV]

圧力換算：1 [dyn/cm^2] ~ 0.1 [N/m^2]

太陽プラズマを考える上で必要な補足情報②

Ro-Re相図：太陽系天体（太陽・惑星）および宇宙物理的天体（恒星・降着円盤）の位置関係

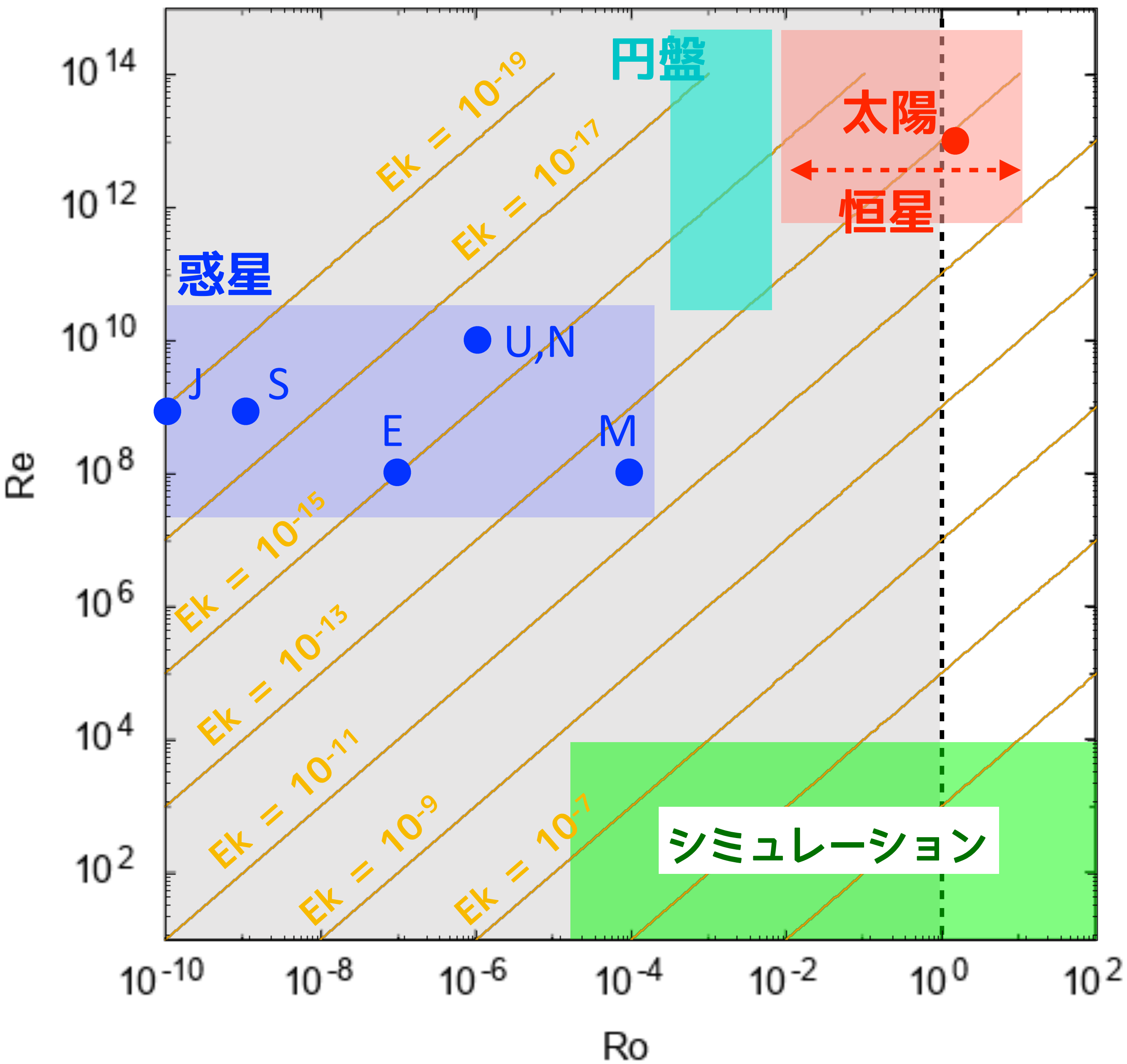

Dynamo	E	Pr	Pm	Rm	Ro	Re
Mercury	10^{-12}	0.1	10^{-6}	10^2	10^{-4}	10^8
Earth	10^{-15}	0.1	10^{-6}	10^2	10^{-7}	10^8
Jupiter	10^{-19}	0.1	10^{-7}	10^2	10^{-10}	10^9
Ganymede	10^{-13}	0.1	10^{-6}	10^2	10^{-5}	10^8
Saturn	10^{-18}	0.1	10^{-7}	10^2	10^{-9}	10^9
Uranus	10^{-16}	10	10^{-8}	10^2	10^{-6}	10^{10}
Neptune	10^{-16}	10	10^{-8}	10^2	10^{-6}	10^{10}
(ref. Schubert & Soderlund 2011)						
Sun (ref. Kapyla 2011)	**10^{-13}**	**10^{-7}**	**10^{-5}**	**10^9**	**10^{-1}**	**10^{13}**

※Ek ～ Ro/Re（図中の黄色点線はEk一定の線）

$$\mathrm{Ro} \equiv \frac{V}{2\Omega L} = \frac{\text{慣性力}\ (V^2/l)}{\text{コリオリ力}\ (2\Omega V)}$$

- 恒星や太陽のプラズマの流れは，惑星内部の流れに比べて比較的小さなRo
  → 太陽はslow rotator ↔ 慣性力のダイナミクスへの影響が大きい
- 恒星や太陽のプラズマの流れは，惑星内部の流れに比べて比較的大きなRe
  → 激しい乱流状態

天体プラズマの特徴と磁場の普遍性

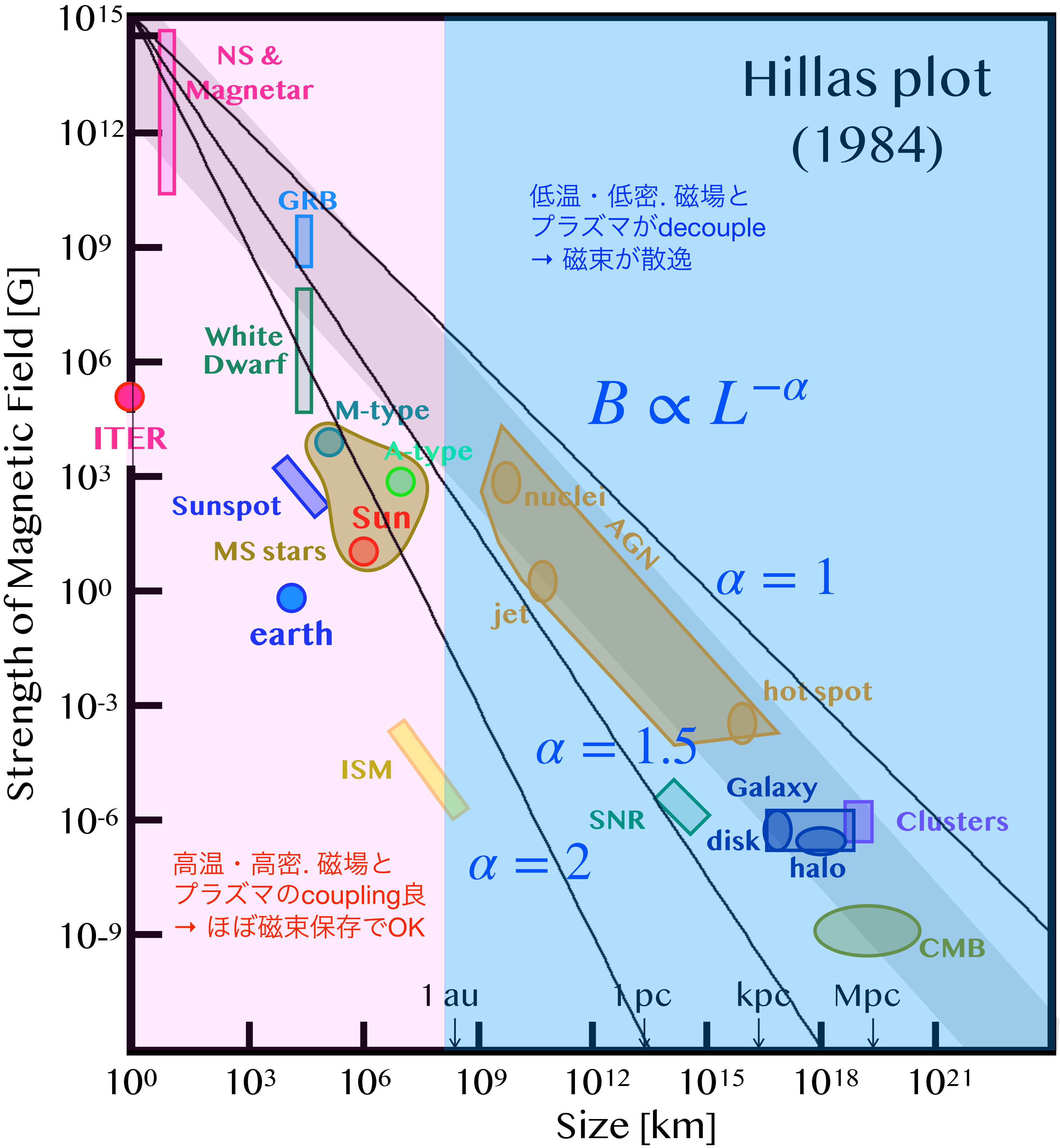

Hillas plot (1984)：

- あらゆるスケールの
  天体プラズマに磁場が存在
- 規則性： サイズ↓磁場↑
- 天体の進化 ⇆ 重力収縮

> 銀河（星間ガス）
> 重力収縮 → 恒星
> 重力収縮 → コンパクト天体

- 磁束保存則（理想MHD）：

$$\frac{d\Phi}{dt} = \frac{d}{dt}\int \boldsymbol{B}\cdot d\boldsymbol{S} = 0$$

$$\therefore B \propto S^{-1} \propto L^{-2} \text{(理論予測)}$$

$$\leftrightarrow B \propto L^{-\alpha} \text{(for fitting)}$$

- 全体的に見れば観測は $\alpha \approx 1$ を示唆
- 天体が密度の高い状態に進化する
  につれて, 磁場が散逸していく描像
- 一方, 星→コンパクト天体のレジーム
  では $\alpha \approx 2$. 第0近似では磁束保存でOK.

サポートスライド

Unsolved Issue ① Origin of Conical Profile

- Before helioseismology,
  - cylindrical profile is expected.
  - i.e., Taylor-Proudmann state.
  - Why conical in the actual Sun ?

Discuss later in more detail.

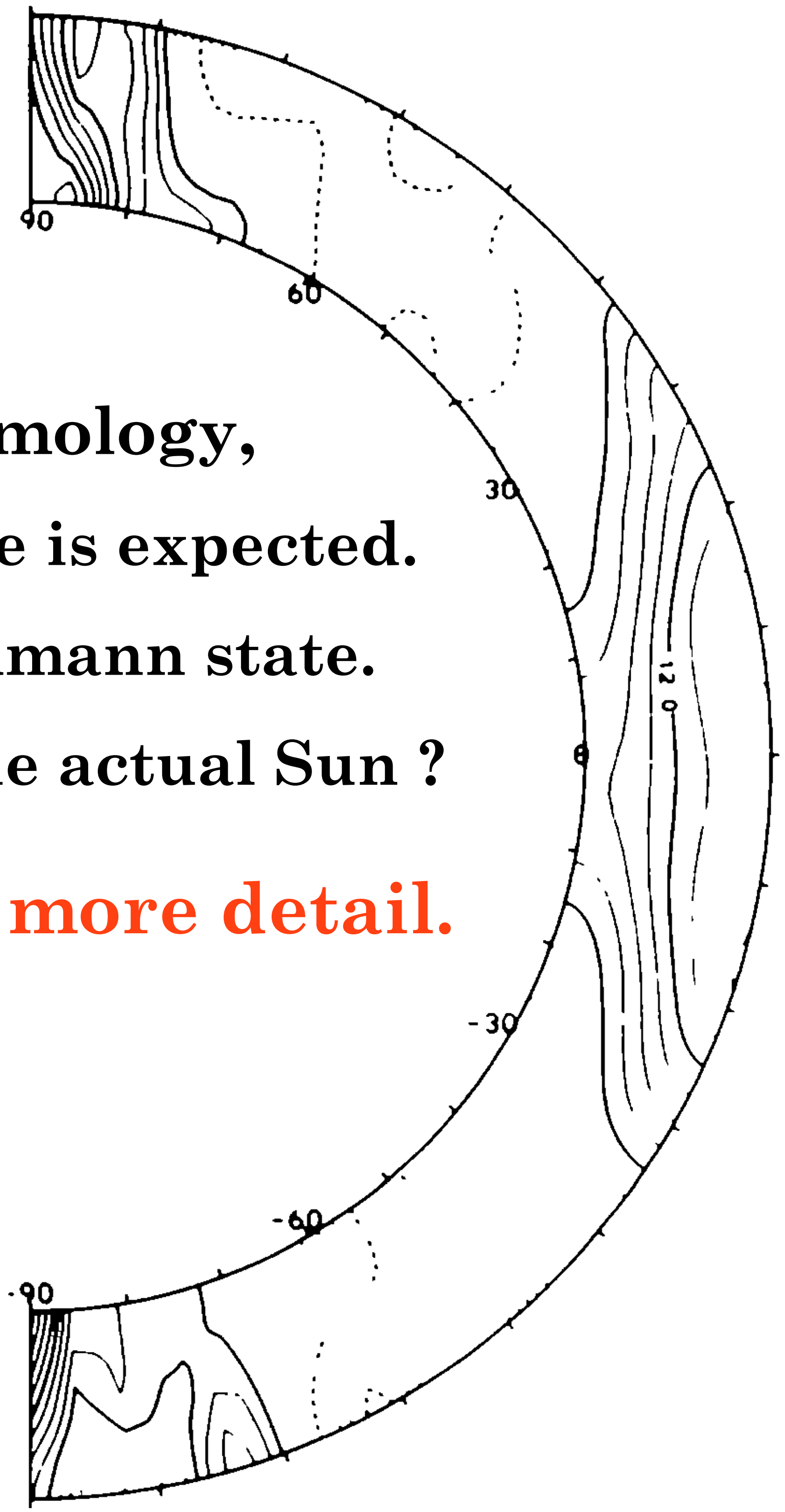

Gilman & Miller 1986

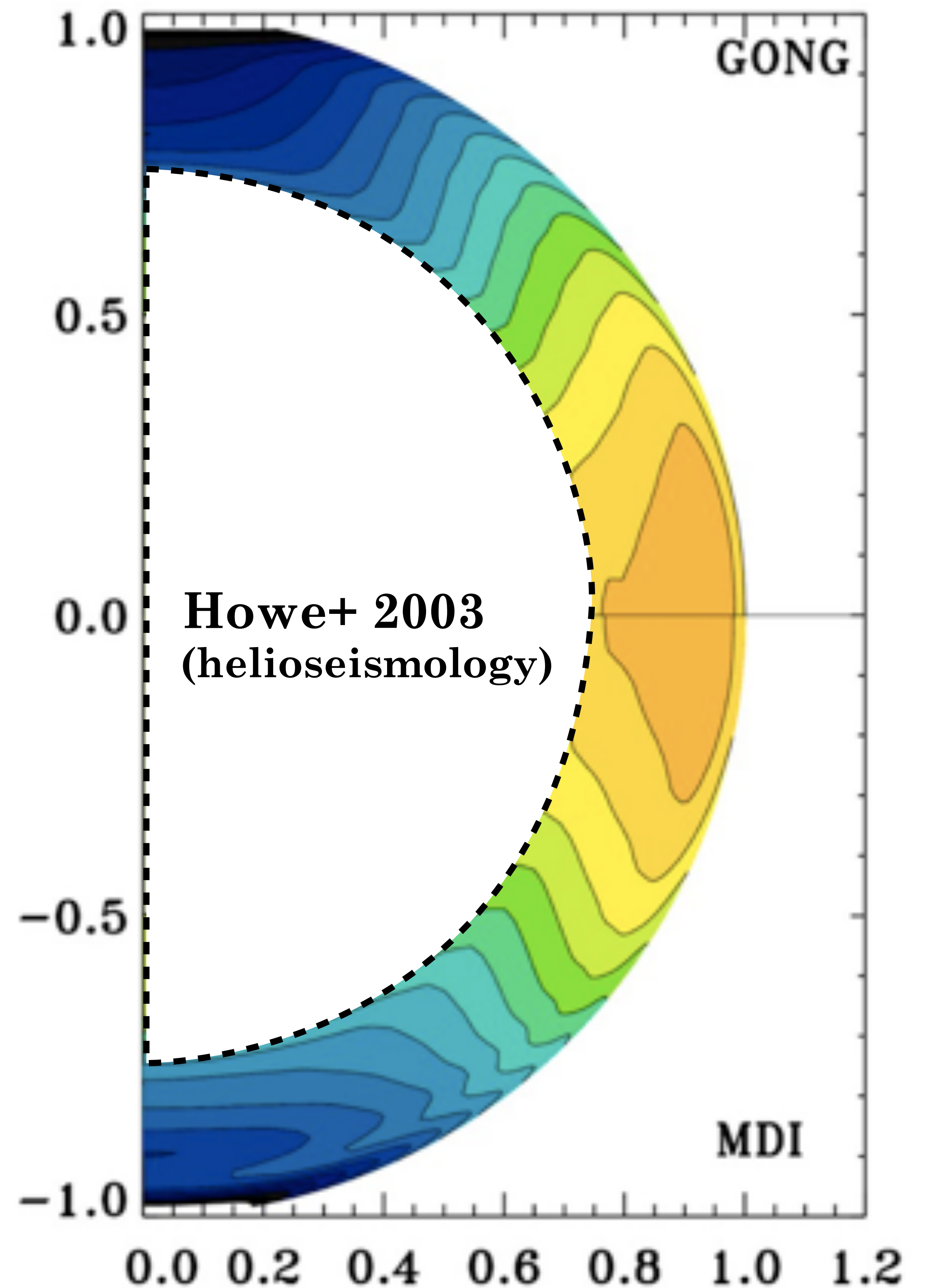

Unsolved Issue ② Origin of Thin Tachocline

“ Tachocline ” **(Spiegel & Zahn 1992)**

: ***A transition layer from the differentially rotating convectively unstable envelope to the rigidly rotating, convectively stable region.***

Q: ***Why does the tachocline becomes a issue ?***

A: ***Because it is too thin, physically.***

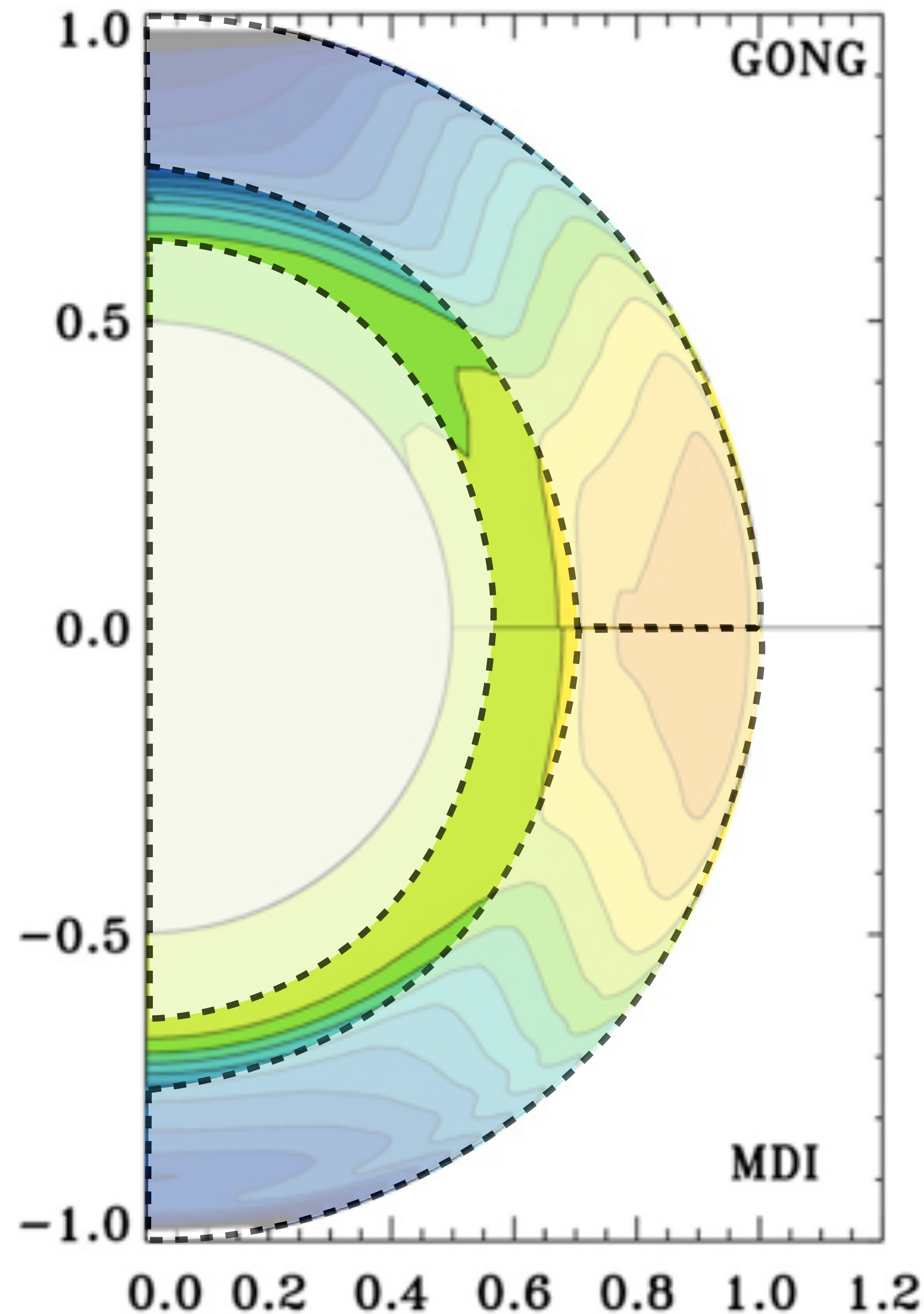

Unsolved Issue ② Origin of Thin Tachocline

Suppose the situation with a moving fluid layer overlying the stationary fluid layer

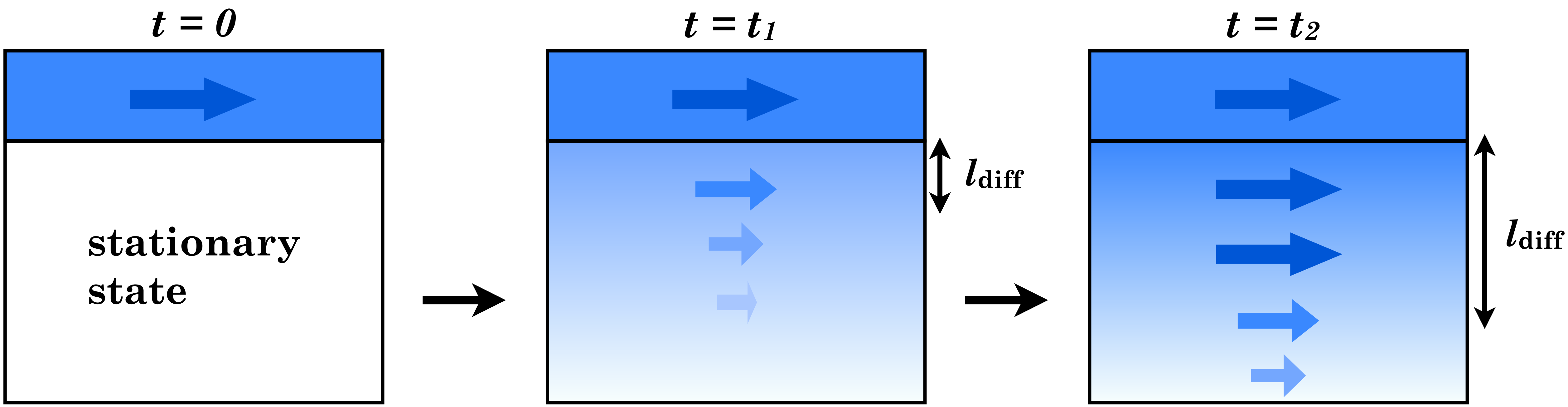

1. Because of the diffusivities (such as viscosity and conductivity), the initially stationery fluid is dragged by the overlying moving fluid.
2. The region with moving fluid gradually spread with a diffusion time if the velocity of the overlying moving fluid is maintained.

diffusion length: $l_{\mathrm{diff}} \sim (\nu t)^{1/2}$ [ν: diffusivity, t: time]

In the case of the Sun with the age $t \sim 4.5$ G years,

$l_{\mathrm{diff}} \sim 0.3 R_{\mathrm{sun}} \gg$ tachocline thickness with $O(10^{-2})\ R_{\mathrm{sun}}$

→ **Tachocline confinement problem** (Spiegel & Zahn 1992; Gough & McIntyre 1998, Hughes et al. 2007 ....etc....)

Brief Summary 1 - Solar Internal Rotation -

※ There are three characteristic layers:

① **Convection envelope**
: Differential Rotation
- Equatorial acceleration
- Conical iso-rotation profile

② **Tachocline** (※ convectively stable)
: Differential Rotation

③ **Radiative Zone**
: Rigid Rotation

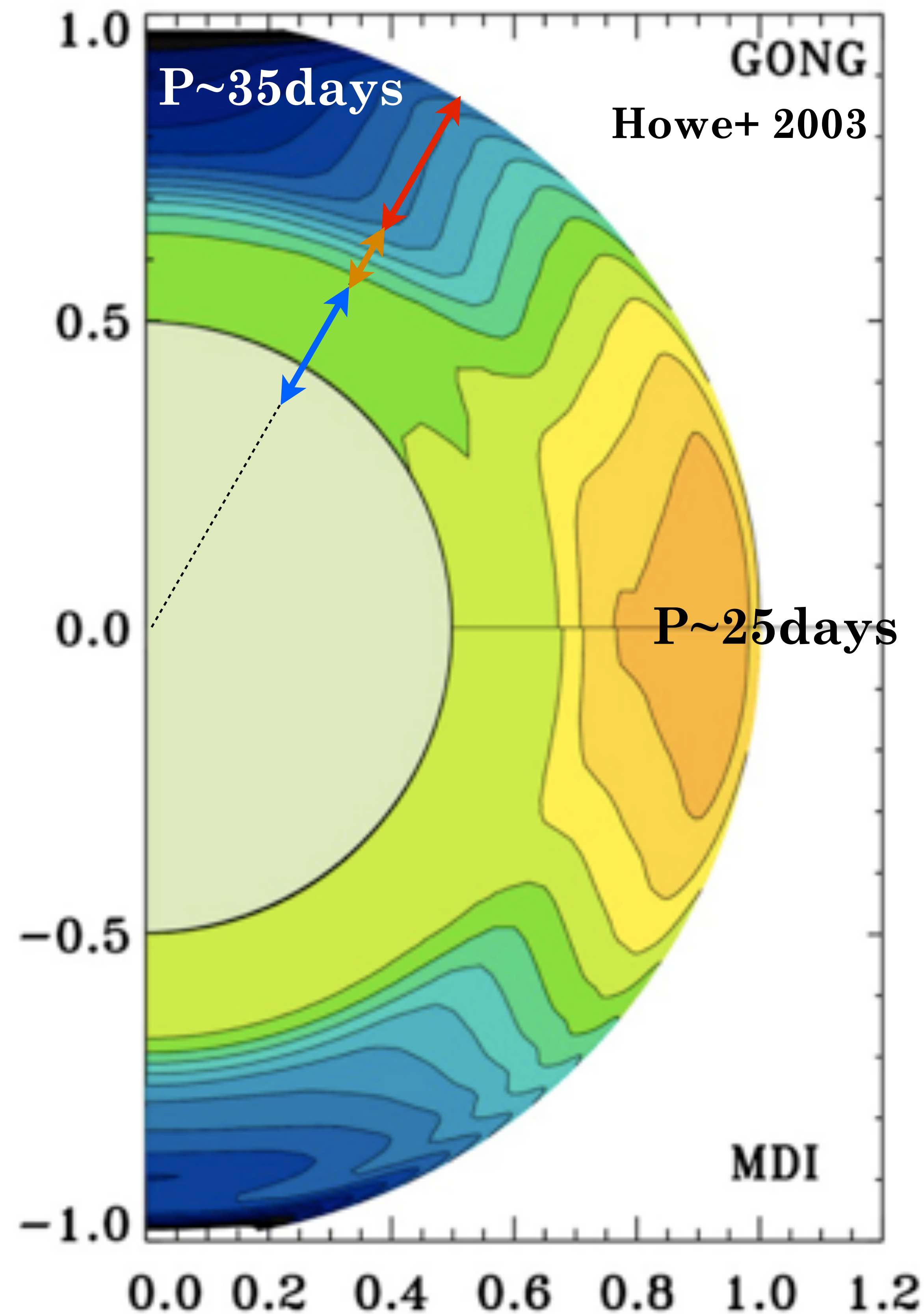

※ There are two important unsolved issues:

(1) Origin of conical profile

(2) Origin of thin tachocline

Contents

1. Solar Rotation Profile, and Unsolved Issues

2. Basic Hydrodynamics in the Solar Interior

   2-1. Properties of the Solar Convection

   2-2. Angular Momentum Transport in the Sun

   ~ MHD effects are ignored here ~

   ~ Differential rotation in the CZ is highlighted here ~

3. Recent Progress and Future Prospects

The rotating stratified convection transports angular momentum in the Sun

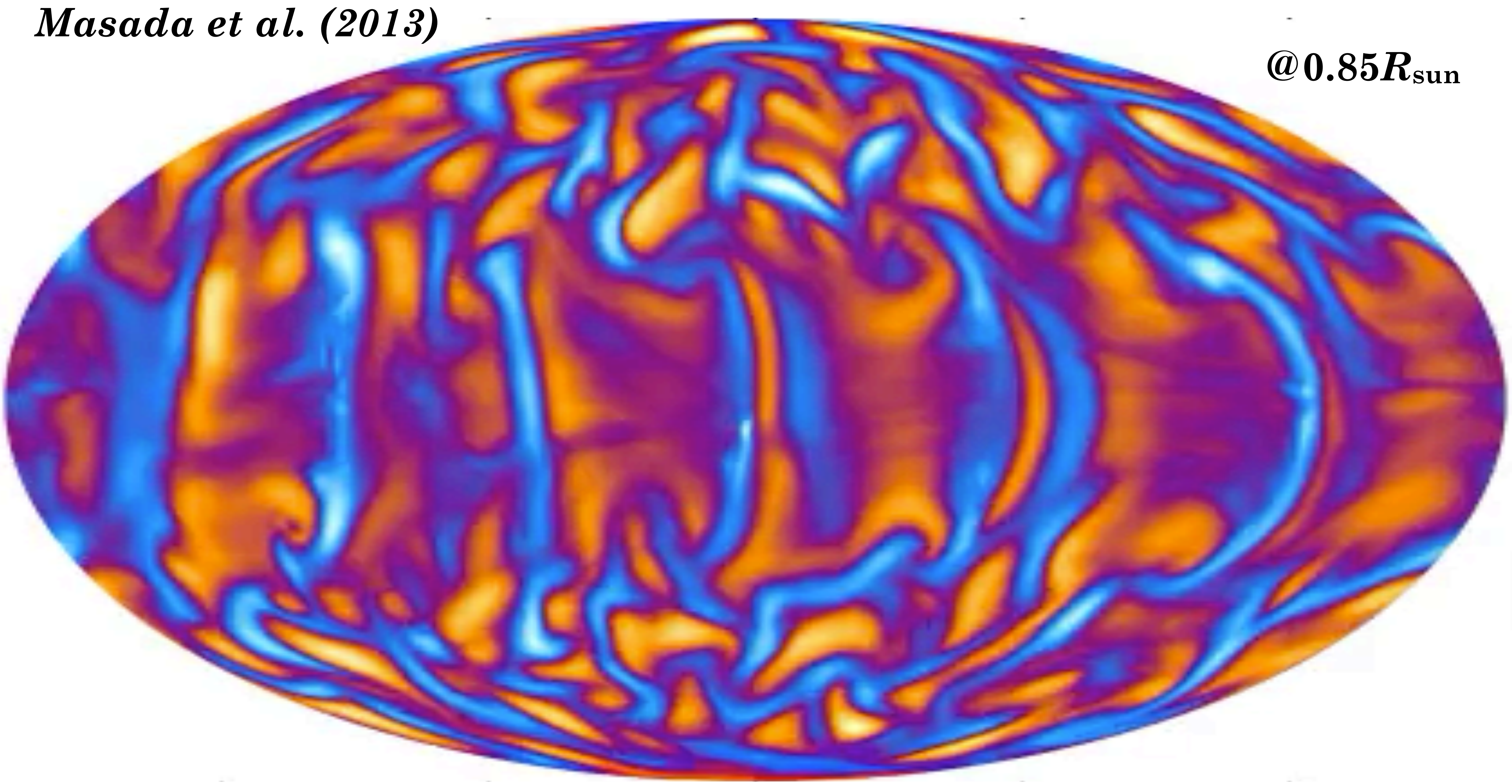

A similar convective motion (@mid-CZ) is commonly observed in the simulation of the other groups.

To deepen the understanding of the rotation profile, we should begin with the physical properties of the convection in the Sun.

Properties of the Solar Convection

The rotating stratified convection transports A.M.

To deepen the understanding of the rotation profile, we should begin with the physical properties of the convection in the Sun.

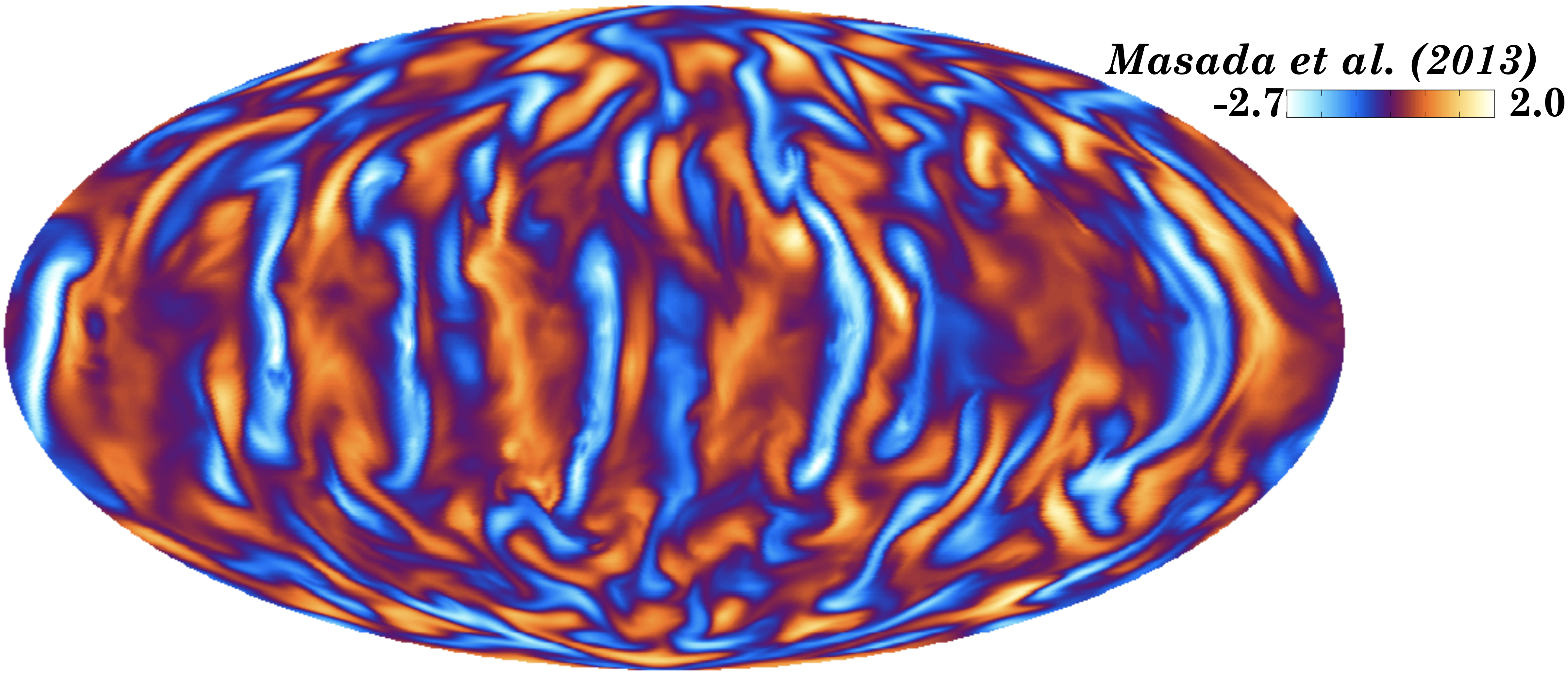

The solar convective motion is characterized by

(1) Narrower & faster downflow + broader & slower upflow

(2) Elongated convective cells aligned with the rotation axis

: solar convection profile has asymmetric features.

Effects of the Stratification - up-down asymmetry -

▪ Effects of the stratification on the convection (Spruit et al. 1990 for review)

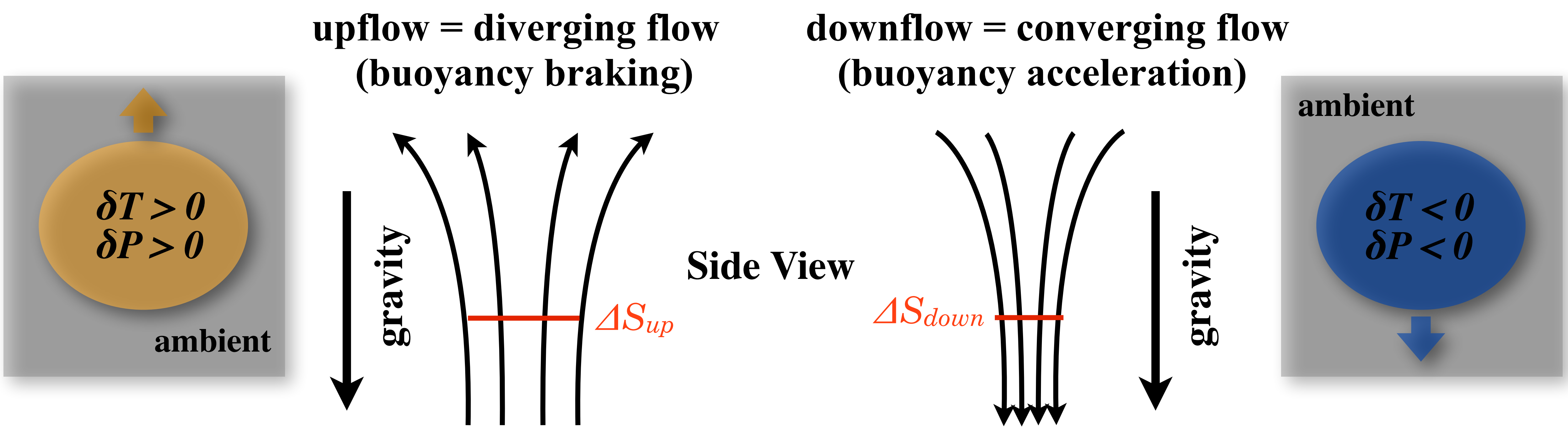

The downflow region is thus narrower than the upflow region.

※ The conservation of the mass flux:

$$\int \nabla \cdot (\rho \boldsymbol{u}) \, \mathrm{d}V = \sum \rho u_r \Delta S = 0$$

$$\therefore \; u_{\mathrm{down}}/u_{up} \sim -S_{up}/S_{down} > 1 \quad (S_{up} = \Sigma \Delta S_{up},\ S_{down} = \Sigma \Delta S_{down})$$

The faster downflow is a natural outcome of the stratified convection.

These are the reason why the up-down asymmetry arises in the solar convection (→ Narrower & Faster downflow + Broader & Slower Upflow).

Effects of the Rotation ① Helical motion

- **Effects of the rotation on the convection ①** (Spruit et al. 1990 for review)

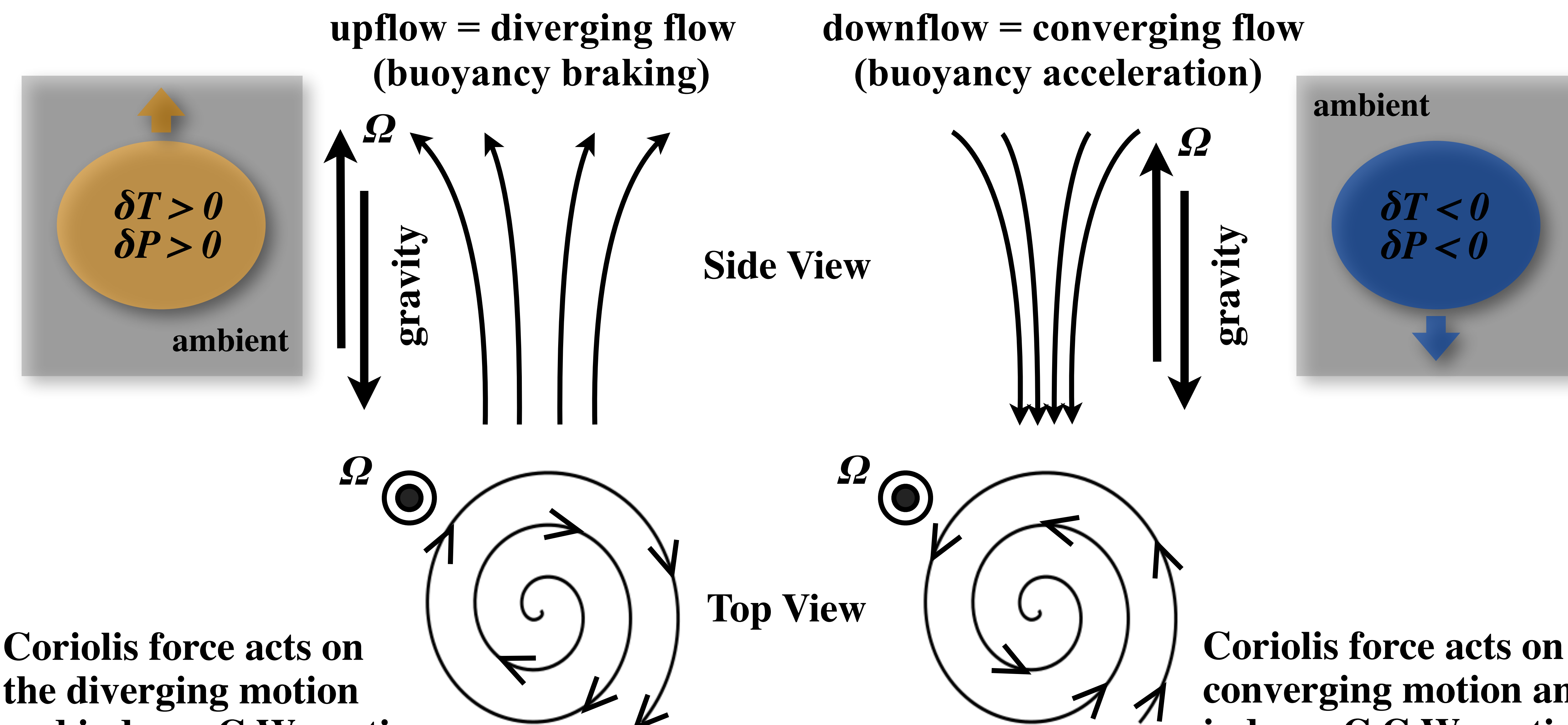

Coriolis force acts on the diverging motion and induces C.W. motion.

Coriolis force acts on converging motion and induces C.C.W. motion

- Coriolis force → helical convective motion.
- CCW motion of the downflow >> CW motion of the upflow (because of the up-down asymmetry).

Effects of the Rotation ② Alignment

- **Effects of the rotation on the convection ②**

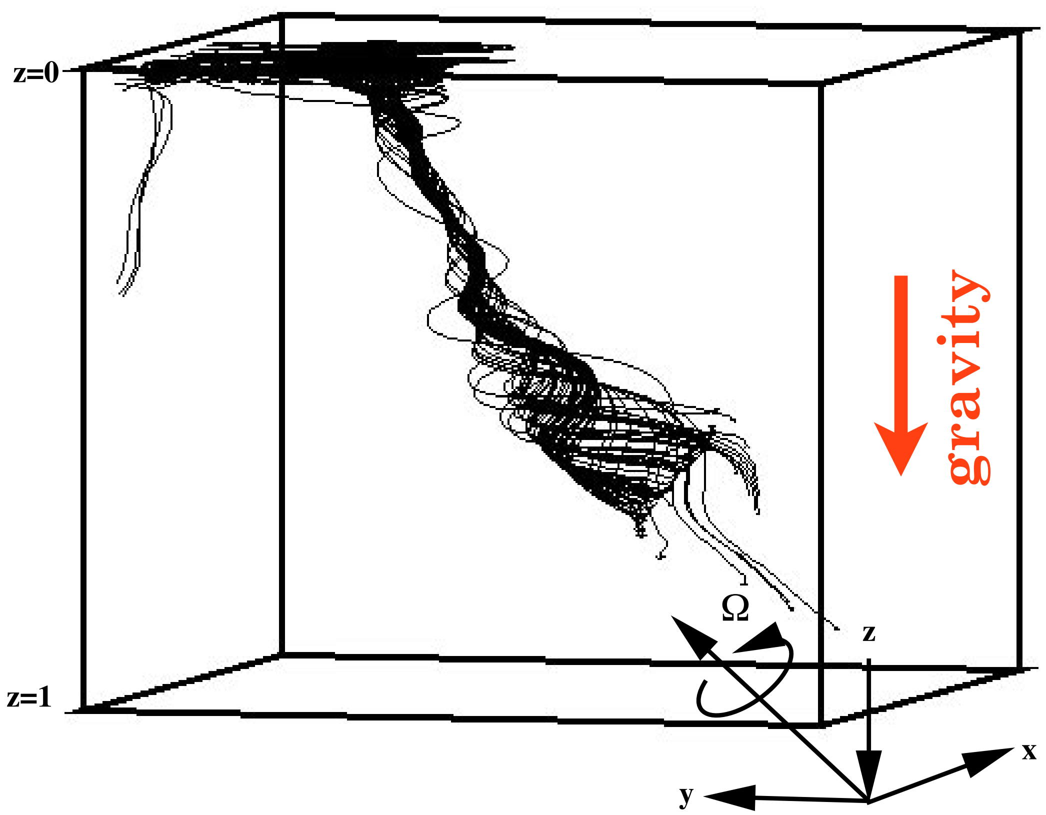

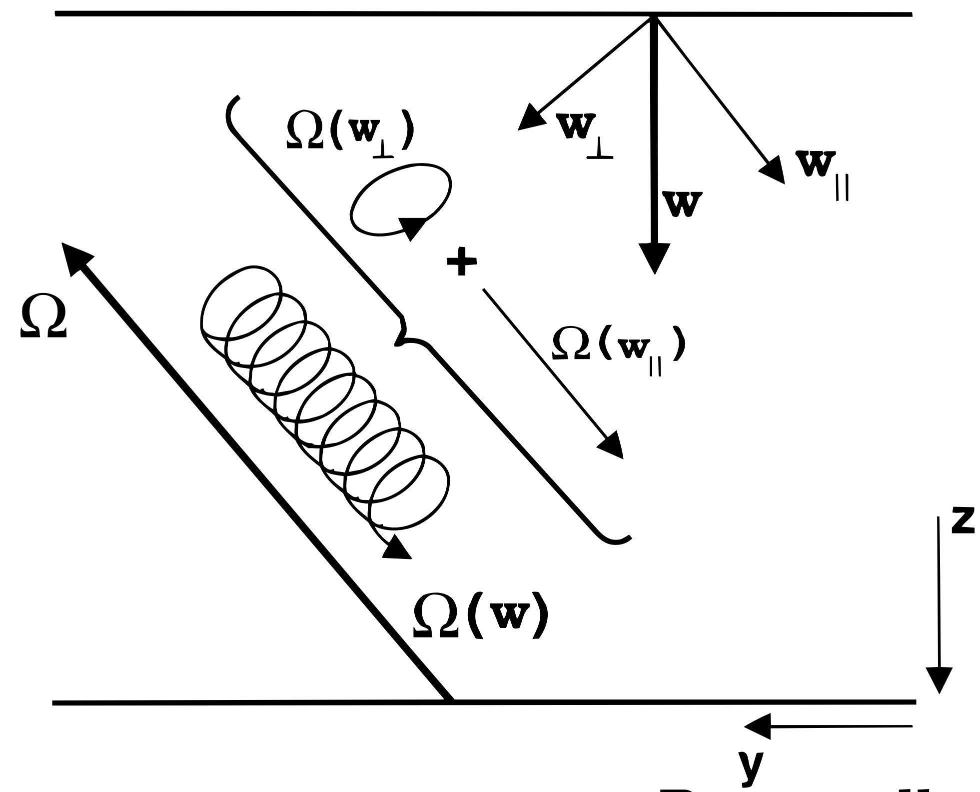

Brummell et al. 1996

※The convective motion is aligned with the rotation axis due to the Coriolis force ($\propto \boldsymbol{u} \times \boldsymbol{\Omega}$) when $\boldsymbol{\Omega}$ is not parallel to $\boldsymbol{g}$.

The motion parallel to Ω experiences no Coriolis acceleration, whereas that perpendicular to Ω feels a force which will tend to move a fluid parcel in an inertial circle in the plane perpendicular to the rotation vector.

- **Analogy with the cyclotron motion of charged particles moving in the magnetic field due to the Lorentz force $\propto v \times B$**

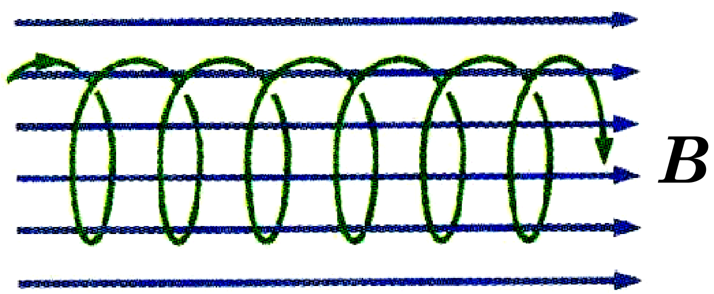

Effects of the Rotation ③ Elongation

- **The size of convective cell is determined by both the scale-height and the Coriolis force** (see Cowling 1951):
- **Simple version of dispersion relation for the convection** (c.f., Hathaway 1984)

$$\sigma^2 = \frac{g}{T_0}\nabla\Delta T\left[\frac{k_\theta{}^2 + k_\phi{}^2}{k_\theta{}^2 + k_\phi{}^2 + k_r{}^2} - F^2\,\frac{(k_\theta \sin\theta - k_r\cos\theta)^2}{k_\theta{}^2 + k_\phi{}^2 + k_r{}^2}\right],$$

(no diffusivities)

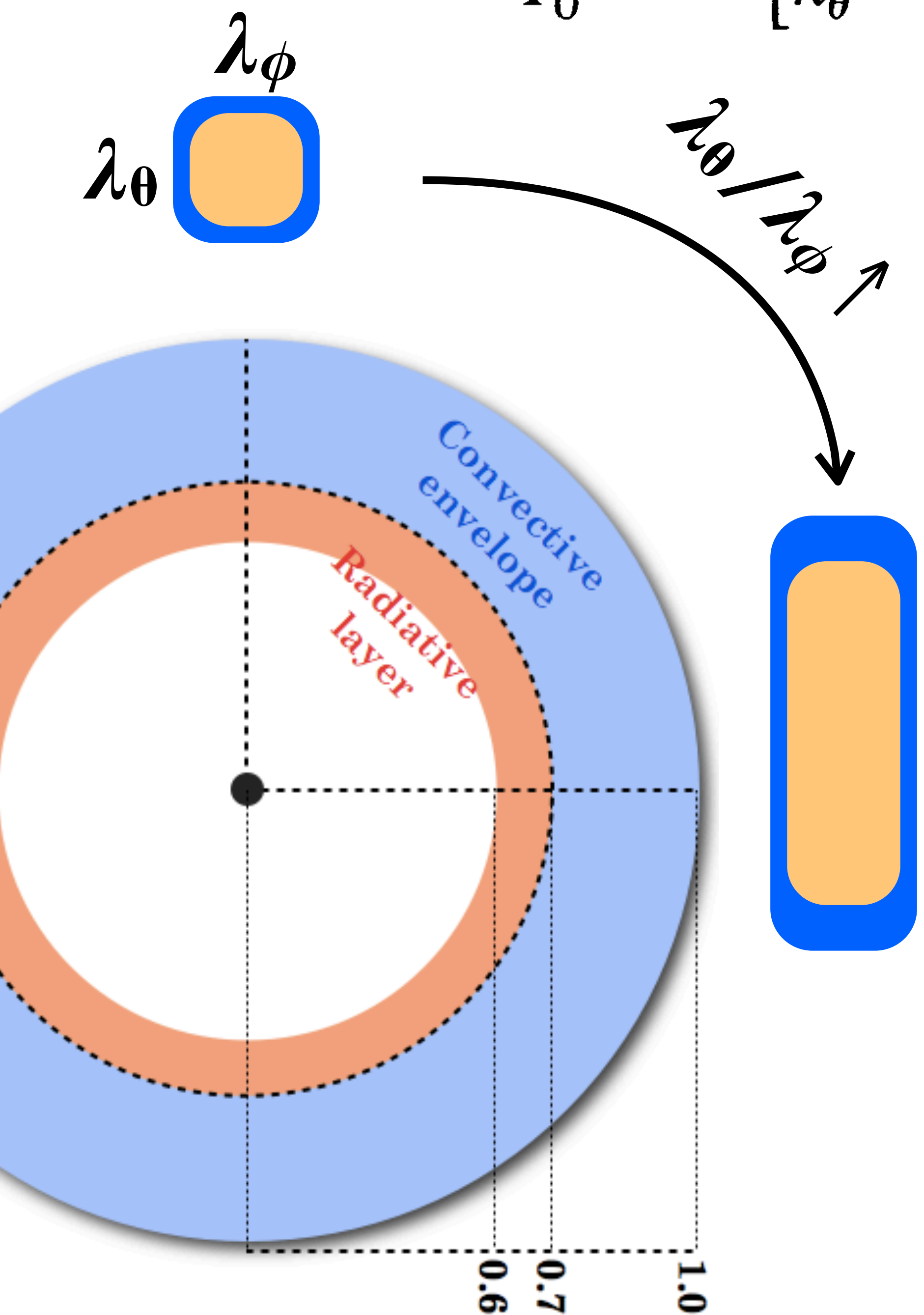

- **When we neglect Ω_r, this can be reduced to**

$$\lambda_\theta / \lambda_\varphi \propto [1 - (\Omega_\theta / N)^2 \sin^2\theta]^{-1/2}$$

λ_θ : latitudinal wavelength of convective instability.
λ_ϕ : longitudinal wavelength of convective instability.
θ : colatitude
N : Brunt-Vaisala frequency
Ω_θ : Latitudinal component of rotational frequency

- The ratio of λ_θ and λ_ϕ increases with θ

(this is the reason why the convective cell is elongated in the latitudinal direction)

→ The elongation of the cell is controlled by Ω_θ

Brief Summary 2-1 - Anisotropy in the Solar Convection -

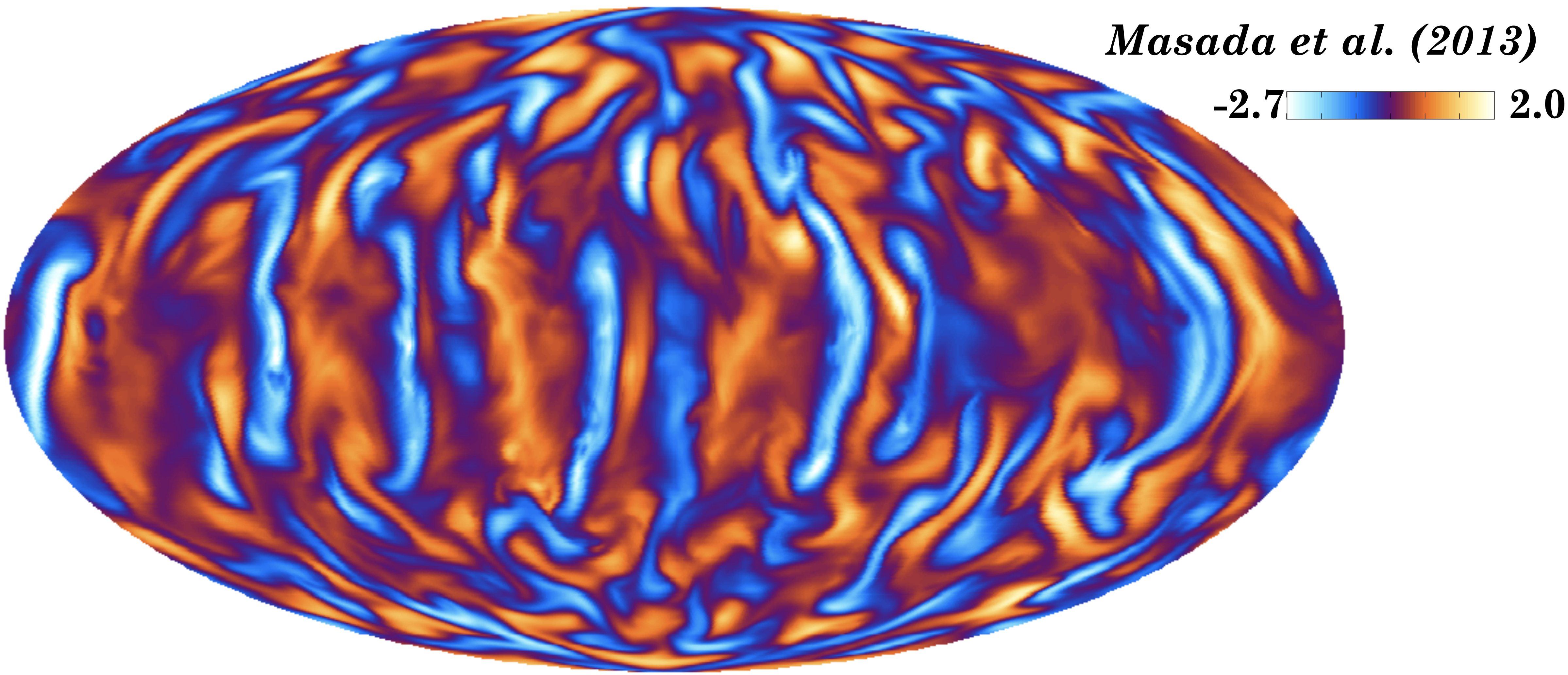

There are two sources of anisotropy in the solar convection:

(a) Density Stratification → **Up-down asymmetry in the convection.**

(b) Rotation (Coriolis force):

- **helical convective motion (CCW downflow >> CW upflow).**
- **convective motion is aligned with the rotation axis.**
- **convection cell is elongated in the direction of the rotation axis.**

Contents

Angular Momentum Transport in the Sun

Q: ***Why does the equator rotate faster than the pole ?***

To answer this question, we should understand the "angular momentum transport process" in the Sun.

solar interior

$L = \rho\lambda^2\Omega$

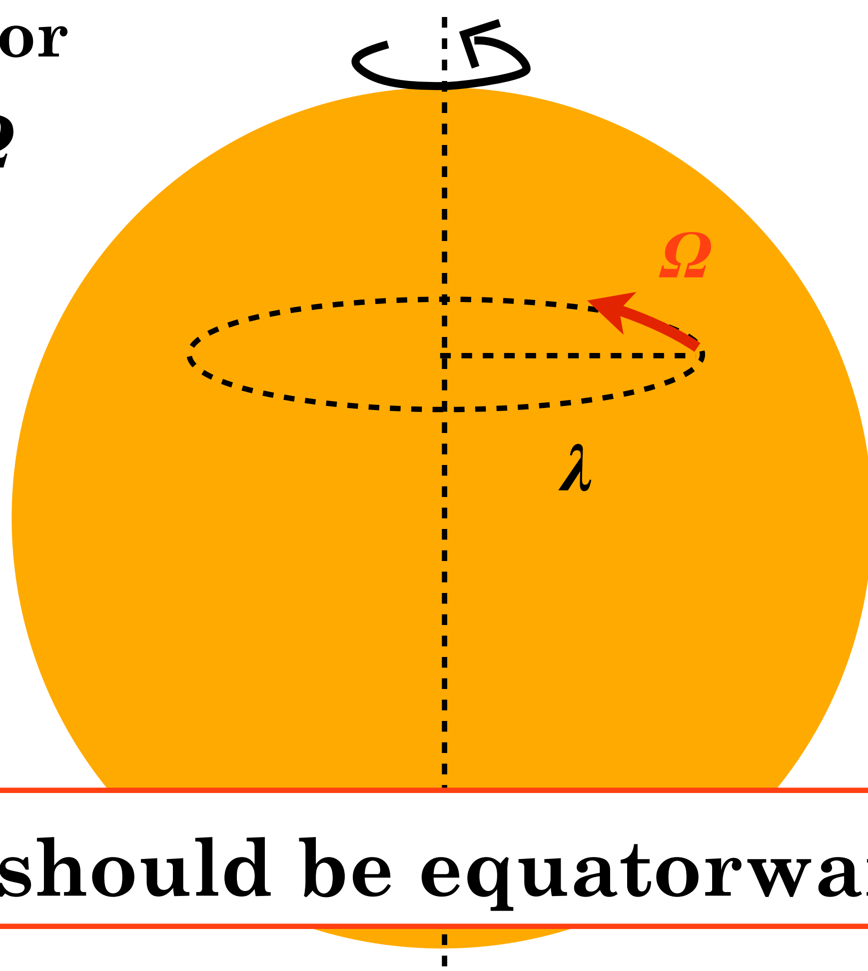

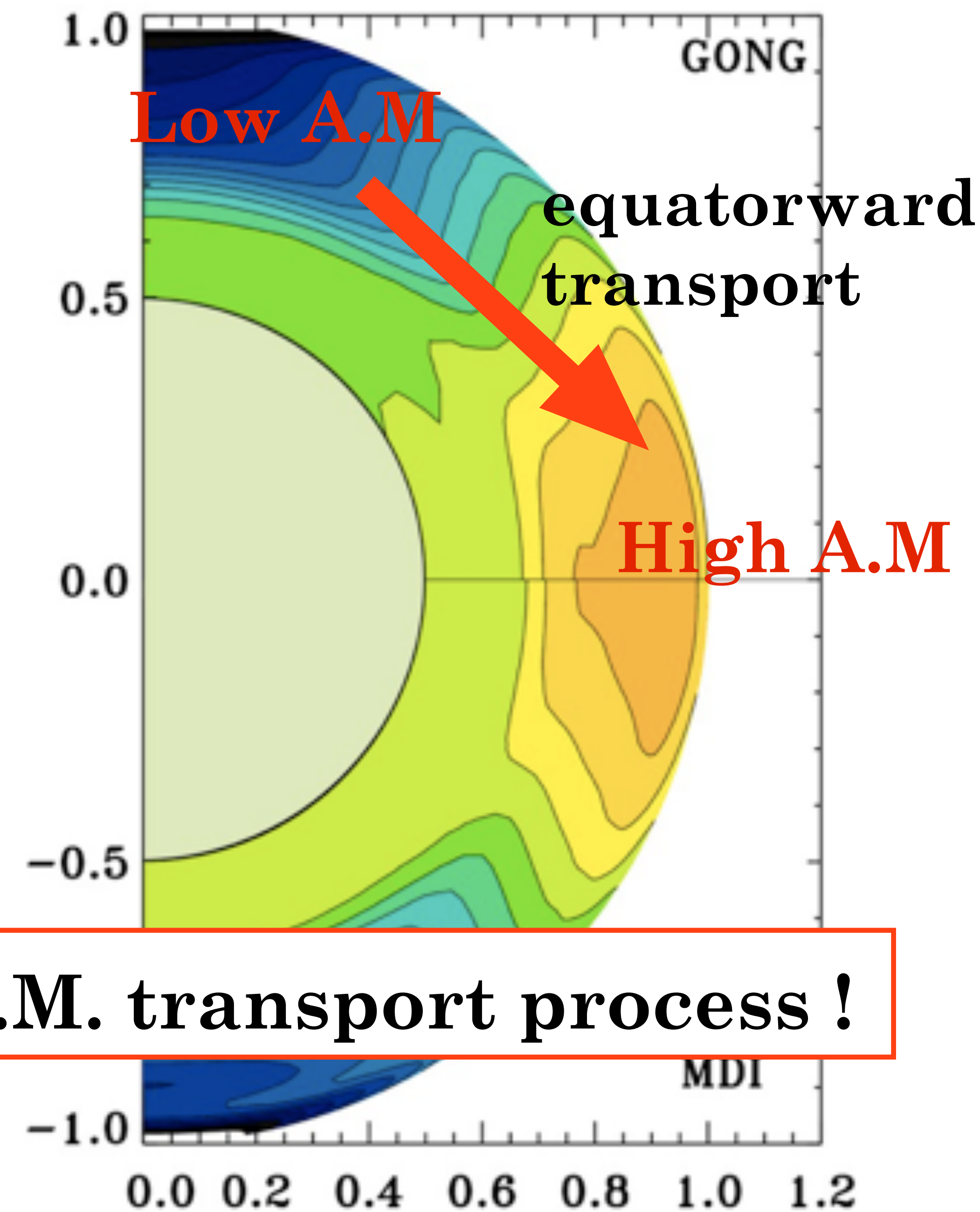

There should be equatorward A.M. transport process !

Turbulent Transport by Reynolds Stress

Transporter = turbulent Reynolds stress:

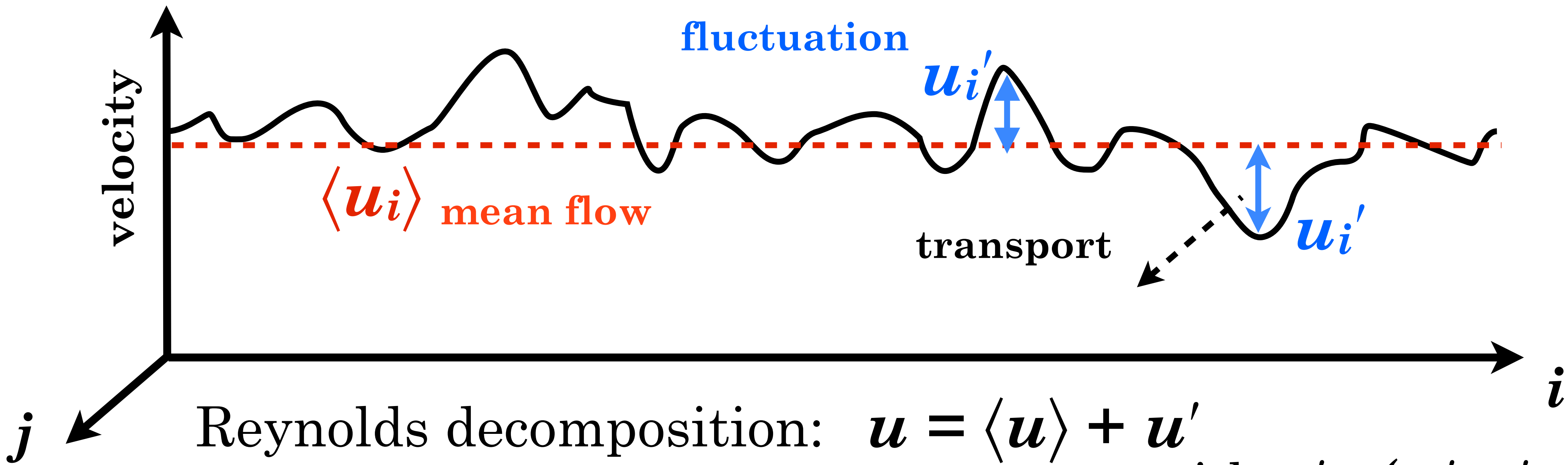

Reynolds decomposition: $\boldsymbol{u} = \langle \boldsymbol{u} \rangle + \boldsymbol{u}'$

with $\boldsymbol{u}' = (u_\mathrm{i}', u_\mathrm{j}', u_\mathrm{k}')$

Reynolds stress:

the stress that arises when the fluctuated momentum ($\rho u_i'$) is transported by fluctuation velocities u_j'or u_k' . The momentum flux is then ($\rho u_i' u_j'$) or ($\rho u_i' u_k'$). The mean flow is changed by these fluctuated momentum being transported.

In the case of the Sun,

$$\boldsymbol{F}_{\mathrm{RS}} \propto \underline{\rho u_r' u_\phi'},\ \underline{\rho u_\theta' u_\phi'},\ \rho u_r' u_\theta'$$

The first and second components are related to the differential rotation in the Sun because these describe the transport of the zonal momentum ($\rho u_\phi'$).

An Origin of Velocity Correlation = Coriolis force

※Coriolis force yields a correlation in two velocity components

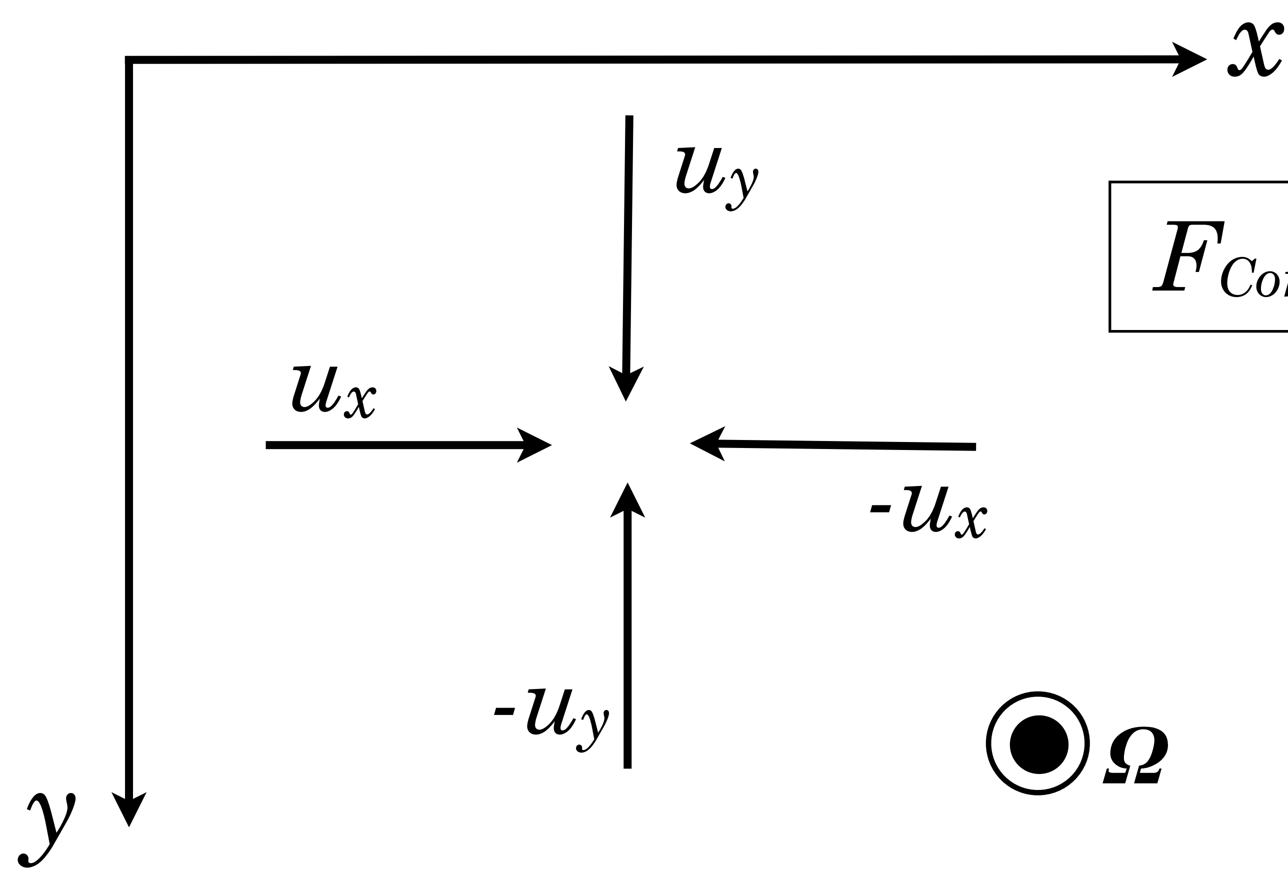

$$F_{Coriolis} \propto \boldsymbol{u} \times \boldsymbol{\Omega}$$

- Assume four fluctuated velocity components $\pm u_x$ and $\pm u_y$.
- The rotation axis is perpendicular to this slide in the rotating frame.
- Then how does the Coriolis force act on these velocity components ?

An Origin of Velocity Correlation = Coriolis force

※Coriolis force yields a correlation in two velocity components

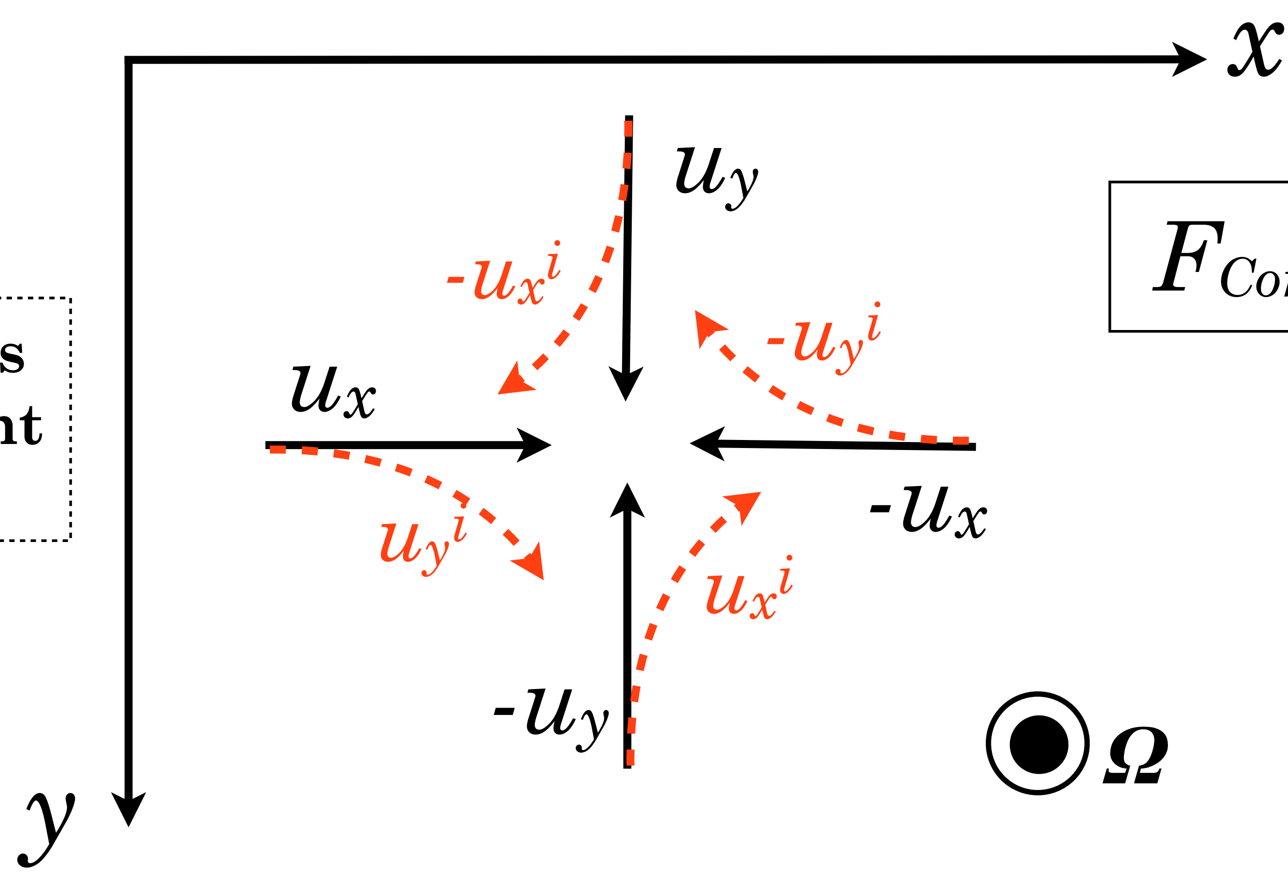

$F_{Coriolis} \propto \boldsymbol{u} \times \boldsymbol{\Omega}$

superscript "*i*" denotes the induced component by the Coriolis force.

$$u_x \rightarrow \ u_x u_y{}^i > 0,\ -u_x \rightarrow u_x u_y{}^i > 0$$

$$u_y \rightarrow \ u_x{}^i u_y < 0,\ -u_y \rightarrow u_x{}^i u_y < 0$$

if the amplitudes of $|u_x|$ and $|u_y|$ *are comparable*, the spatial average of the velocity correlation $\langle u_x u_y \rangle$ becomes zero.

※There should be anisotropy in the fluid motion for generating the mean momentum flux.

Radial Transport of Zonal Angular Momentum

Q: ***Is the fluctuated zonal momentum $\rho u_\phi'$ transported radially inward or outward ?***

※Coriolis force introduces the correlation between u_r' and u_ϕ'.

$$\boxed{F_{Coriolis} \propto \boldsymbol{u} \times \boldsymbol{\Omega}}$$

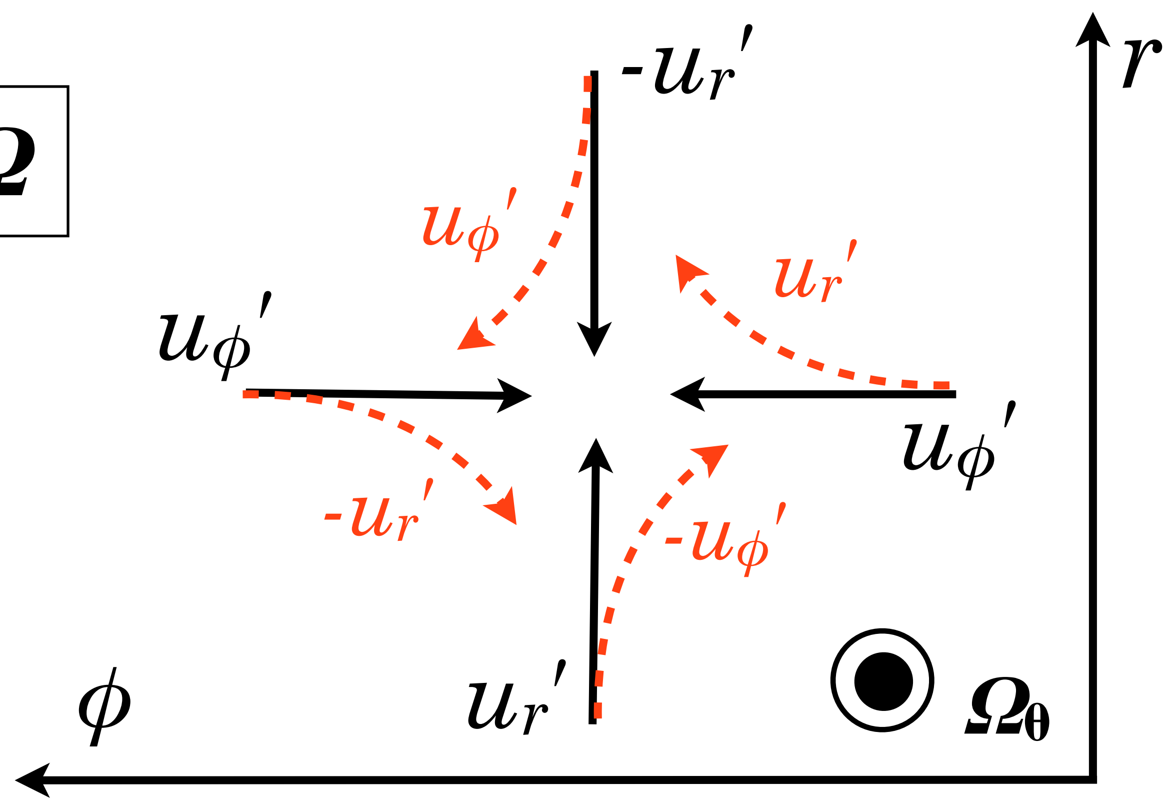

$u_r' \rightarrow u_r'u_\phi' < 0$

$-u_r' \rightarrow u_r'u_\phi' < 0$

$u_\phi' \rightarrow u_r'u_\phi' > 0$

$-u_\phi' \rightarrow u_r'u_\phi' > 0$

In the solar convection, the radial convective velocity is much larger than the azimuthal convective velocity, that is $\boldsymbol{u_r' > u_\phi'}$. The mean correlation $\langle \boldsymbol{u_r' u_\phi'} \rangle$ thus becomes negative, that is $\langle \boldsymbol{u_r' u_\phi'} \rangle \boldsymbol{< 0}$.

A: ***the angular momentum ($\propto \rho u_\phi'$) is transported to radially inward direction.***

Latitudinal Transport of Zonal Angular Momentum

Q: ***Is the fluctuated zonal momentum $\rho u_\phi'$ transported poleward or equatorward ?***

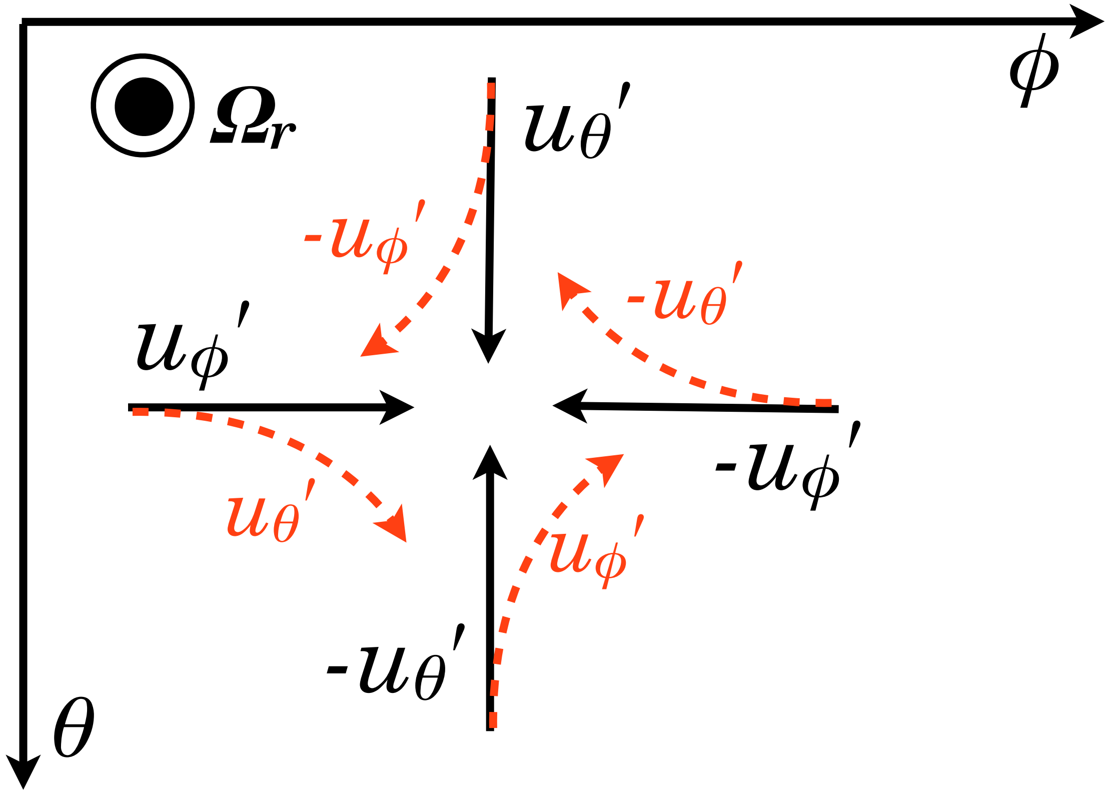

$u_\phi' \rightarrow u_\phi' u_\theta' > 0 \quad u_\theta' \rightarrow u_\phi' u_\theta' < 0$

$-u_\phi' \rightarrow u_\phi' u_\theta' > 0 \quad -u_\theta' \rightarrow u_\phi' u_\theta' < 0$

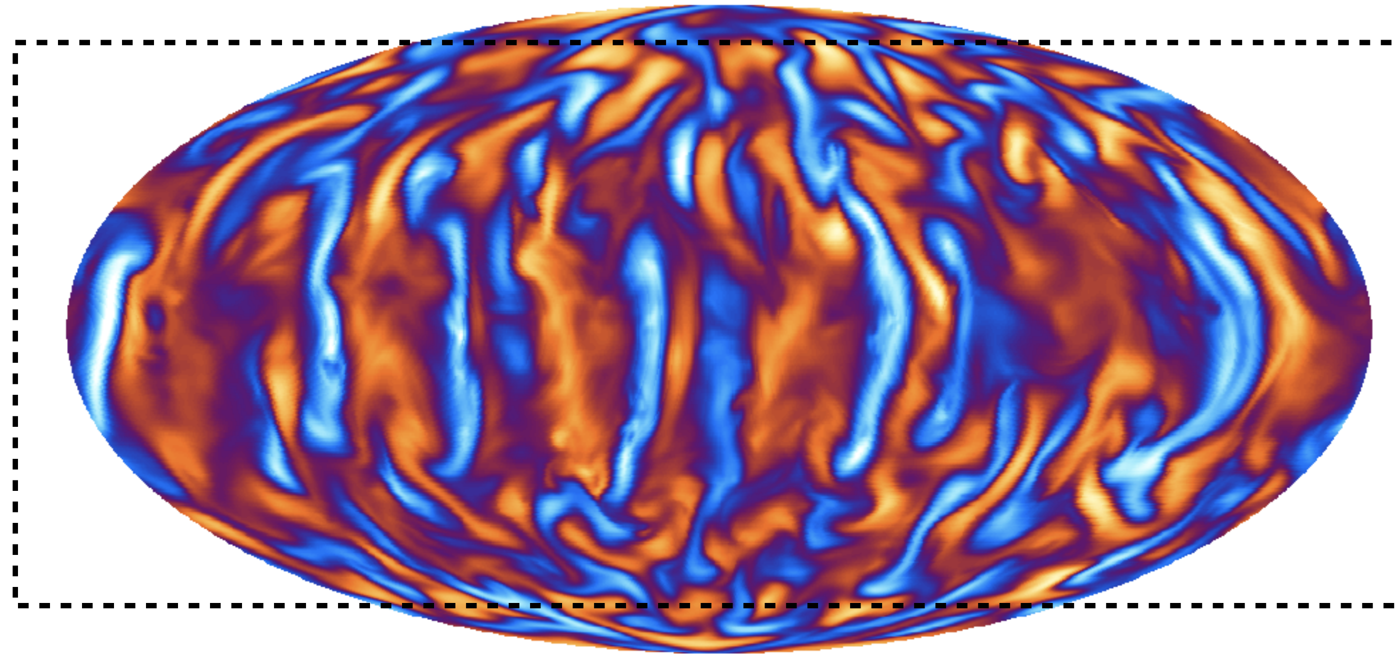

The convective cells are elongated in the $\boldsymbol{\theta}$-direction and aligned with the rotation axis.

➡ $\boldsymbol{u_\phi' > u_\theta'}$

(The asymmetry is induced by the rotation)

The mean correlation $\langle u_\theta' u_\phi' \rangle$ thus becomes positive ($\langle u_\theta' u_\phi' \rangle > 0$).

A: ***the angular momentum ($\propto \rho u_\phi'$) is transported to the equatorial direction.***

Turbulent Angular Momentum Transport in the Sun

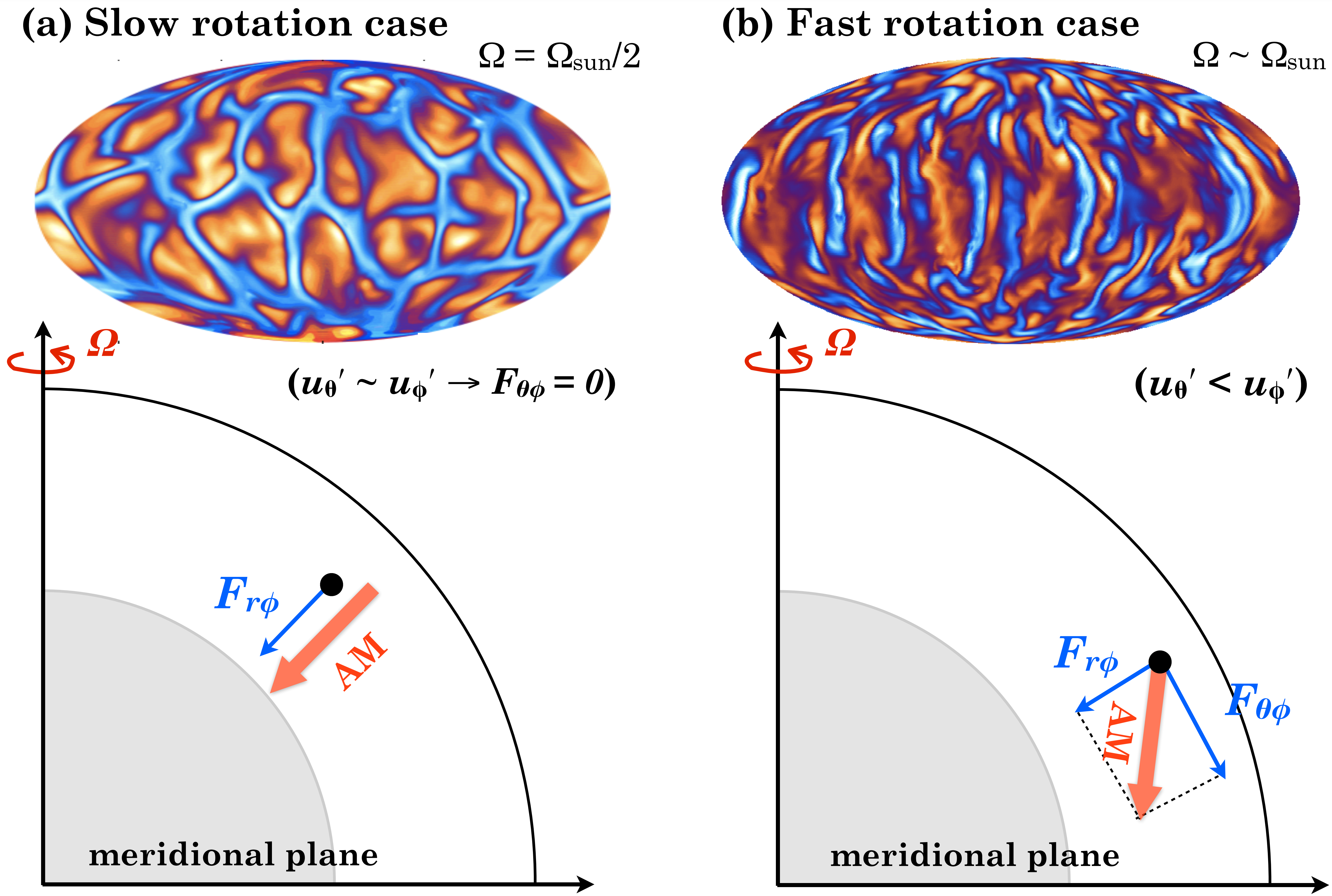

Mean Field Transport of Angular Momentum

The mean-field EOM in a rotating frame with $\boldsymbol{\Omega}_0$: (※$\boldsymbol{\Omega}_0 = \Omega_0\, \boldsymbol{e}_z$)

$$\boxed{\frac{\partial \boldsymbol{u}}{\partial t} + (\boldsymbol{u}\cdot\nabla)\boldsymbol{u} = -\frac{1}{\rho}\nabla P - 2\boldsymbol{\Omega}_0 \times \boldsymbol{u} + \boldsymbol{g} + \frac{1}{\rho}\nabla\cdot(\boldsymbol{F}_{\mathrm{RS}})}$$

※ $\boldsymbol{F}_{\mathrm{RS}} \propto$ Reynolds stress

when considering a steady sate with $\partial \boldsymbol{u}/\partial t = 0$

Meridional component **($\boldsymbol{r},\boldsymbol{\theta}$)**

curl

$$r\sin\theta\frac{\partial\Omega^2}{\partial z} = \frac{g}{\gamma C_v}\frac{1}{r}\frac{\partial S}{\partial\theta}$$

$$\frac{\partial S}{\partial\theta} \propto \nabla P \times \nabla\rho$$

(Thermal Wind Balance eq.)

Zonal component **($\boldsymbol{\phi}$)**

$$\mathcal{L} = \lambda^2\Omega \equiv \lambda(\lambda\Omega_0 + u_\phi)$$

$$\boxed{\rho\boldsymbol{u}_m\cdot\nabla_m\mathcal{L} = -\nabla\cdot(\boldsymbol{F}_{\mathrm{RS}})}$$

Anelastic approximation
$\rightleftarrows \nabla\cdot(\rho\boldsymbol{u}_{\mathrm{m}})$

$$\boldsymbol{u}_m \equiv u_r\boldsymbol{e}_r + u_\theta\boldsymbol{e}_\theta$$

$$\nabla\cdot(\boldsymbol{F}_{\mathrm{MC}} + \boldsymbol{F}_{\mathrm{RS}}) = 0$$

where

$$\boldsymbol{F}_{\mathrm{MC}} \equiv \rho(r\sin\theta)^2\Omega\boldsymbol{u}_m = \rho\mathcal{L}\boldsymbol{u}_m$$

$$\boldsymbol{F}_{\mathrm{RS}} \equiv \rho(r\sin\theta)(\langle u_r' u_\phi'\rangle\boldsymbol{e}_r + \langle u_\theta' u_\phi'\rangle\boldsymbol{e}_\theta)$$

Gyroscopic Pumping (Zonal Balance eq.)

gyroscopic pumping after McIntyre 1998

The mean flow profile is determined to satisfy these two equations.

Angular Momentum of Rotating Star

回転星の角運動量分布（≠角速度分布）：円柱状

理由：角運動量（$L \propto \lambda^2\Omega$）の視点で見れば恒星内部の回転則はほぼ剛体回転

(太陽の極-赤道の角速度差は高々20%)

$$\boxed{\therefore\ \partial L/\partial z \sim 0,\ \partial L/\partial \theta > 0}$$

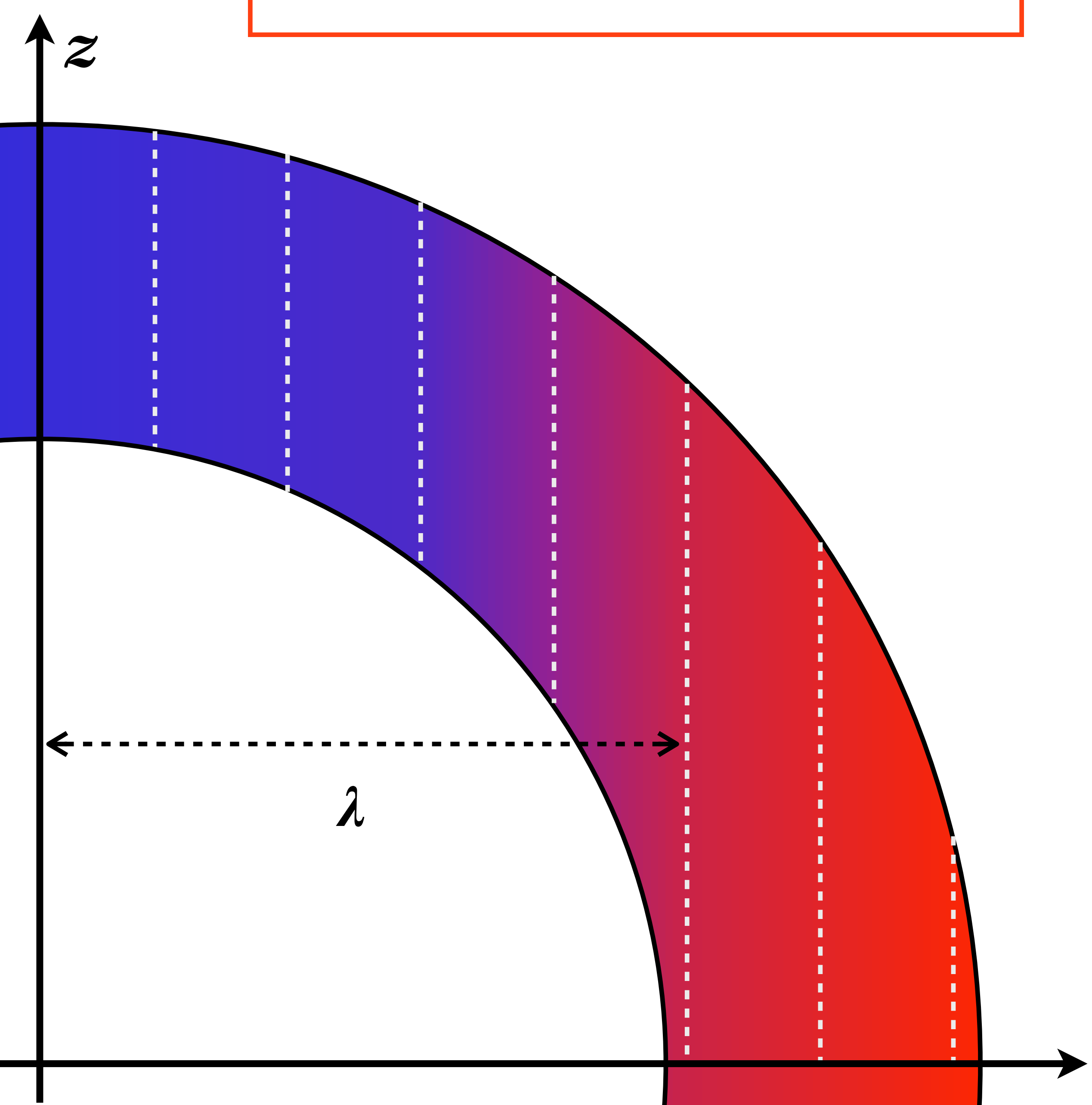

$$\boxed{\rho \boldsymbol{u}_m \cdot \nabla_m \mathcal{L} = -\nabla \cdot (\boldsymbol{F}_{\mathbf{RS}})}$$

Anelastic approximation $\rightleftarrows \nabla \cdot (\rho \boldsymbol{u}_{\mathrm{m}})$ $\updownarrow$ $\boldsymbol{u}_m \equiv u_r \boldsymbol{e}_r + u_\theta \boldsymbol{e}_\theta$

$$\nabla \cdot (\boldsymbol{F}_{\mathbf{MC}} + \boldsymbol{F}_{\mathbf{RS}}) = 0$$

where

$$\boldsymbol{F}_{\mathbf{MC}} \equiv \rho (r \sin\theta)^2 \Omega \boldsymbol{u}_m = \rho \mathcal{L} \boldsymbol{u}_m$$

$$\boldsymbol{F}_{\mathbf{RS}} \equiv \rho (r \sin\theta)(\langle u_r' u_\phi' \rangle \boldsymbol{e}_r + \langle u_\theta' u_\phi' \rangle \boldsymbol{e}_\theta)$$

- $\boldsymbol{F}_{\mathrm{RS}}$の向きがわかれば、循環流の向きがわかる.

Mean Field Transport of Angular Momentum (1)

回転星の角運動量分布（≠角速度分布）：円柱状

理由：角運動量（$L \propto \lambda^2\Omega$）の視点で見れば恒星内部の回転則はほぼ剛体回転

(太陽の極-赤道の角速度差は高々20%)

$$\boxed{\therefore\ \partial L/\partial z \sim 0,\ \partial L/\partial \theta > 0}$$

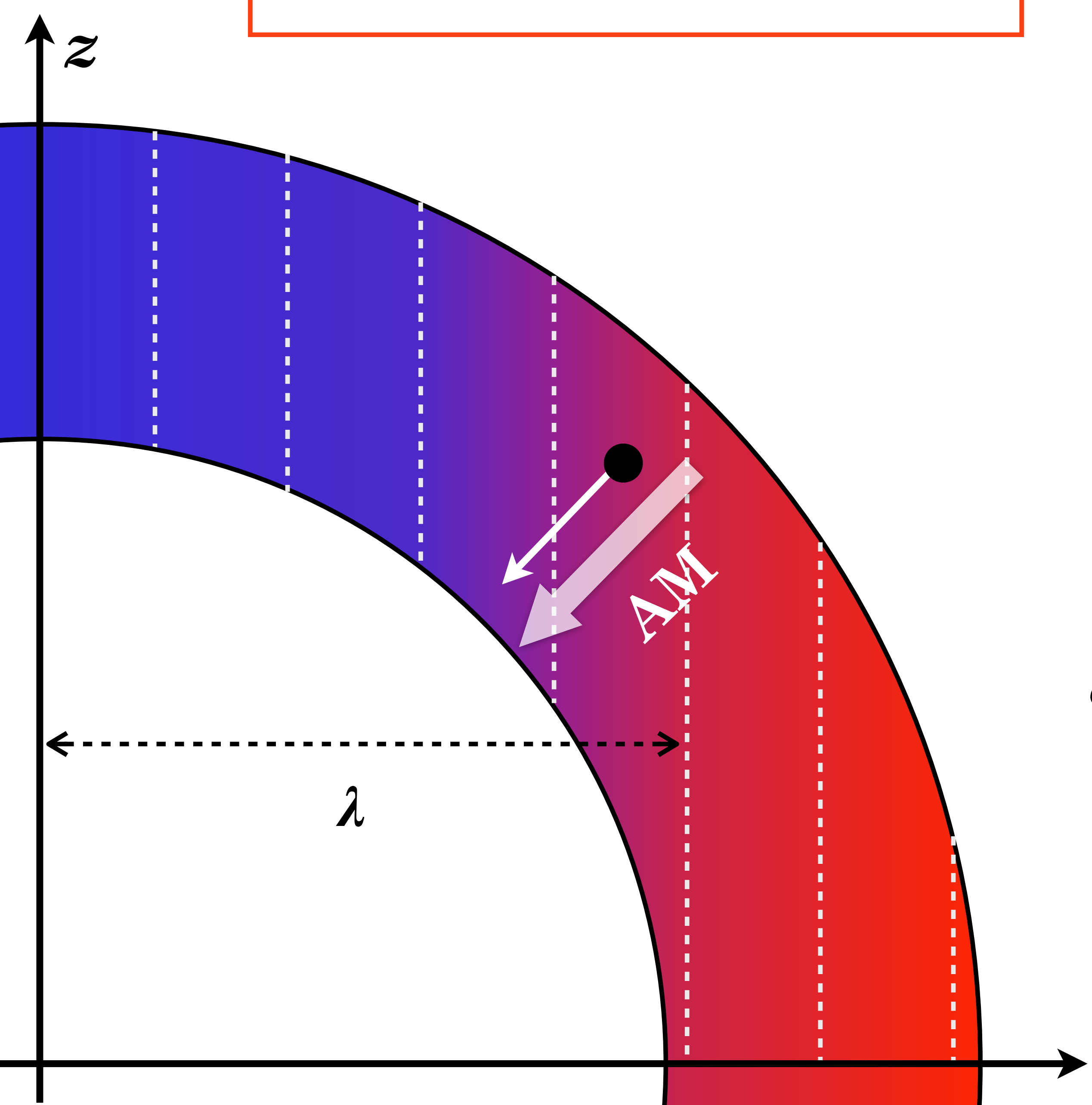

$$\boxed{\rho \boldsymbol{u}_m \cdot \nabla_m \mathcal{L} = -\nabla \cdot (\boldsymbol{F}_{\mathrm{RS}})}$$

Anelastic approximation
$\rightleftarrows \nabla \cdot (\rho \boldsymbol{u}_{\mathrm{m}})$

$\boldsymbol{u}_m \equiv u_r \boldsymbol{e}_r + u_\theta \boldsymbol{e}_\theta$

$$\nabla \cdot (\boldsymbol{F}_{\mathrm{MC}} + \boldsymbol{F}_{\mathrm{RS}}) = 0$$

where

$$\boldsymbol{F}_{\mathrm{MC}} \equiv \rho (r \sin\theta)^2 \Omega \boldsymbol{u}_m = \rho \mathcal{L} \boldsymbol{u}_m$$

$$\boldsymbol{F}_{\mathrm{RS}} \equiv \rho (r \sin\theta)(\langle u_r' u_\phi' \rangle \boldsymbol{e}_r + \langle u_\theta' u_\phi' \rangle \boldsymbol{e}_\theta)$$

- **回転が遅い場合：**

- F_{RS}が動径方向負の向き = F_{RS}は負の値

$\partial F_{\mathrm{RS}}/\partial r > 0$ @upper, $\partial F_{\mathrm{RS}}/\partial r < 0$ @bottom

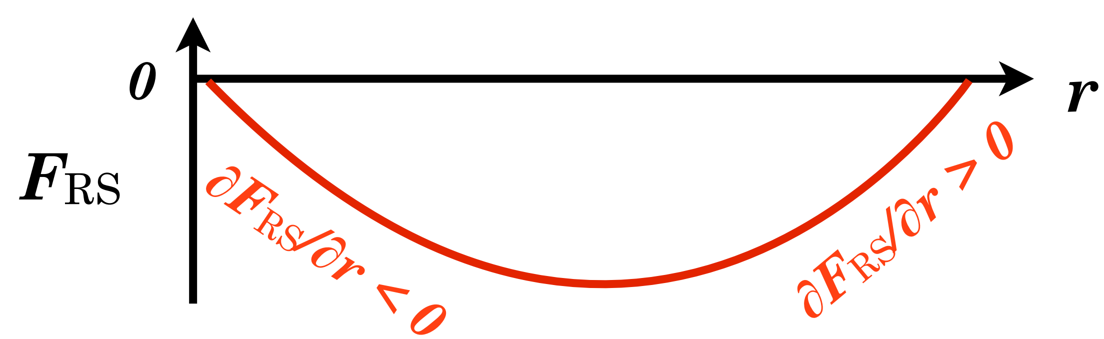

Mean Field Transport of Angular Momentum (2)

回転星の角運動量分布（≠角速度分布）：円柱状

理由：角運動量（$L \propto \lambda^2 \Omega$）の視点で見れば恒星内部の回転則はほぼ剛体回転

(太陽の極-赤道の角速度差は高々20%)

$$\boxed{\therefore\ \partial L/\partial z \sim 0,\ \partial L/\partial \theta > 0}$$

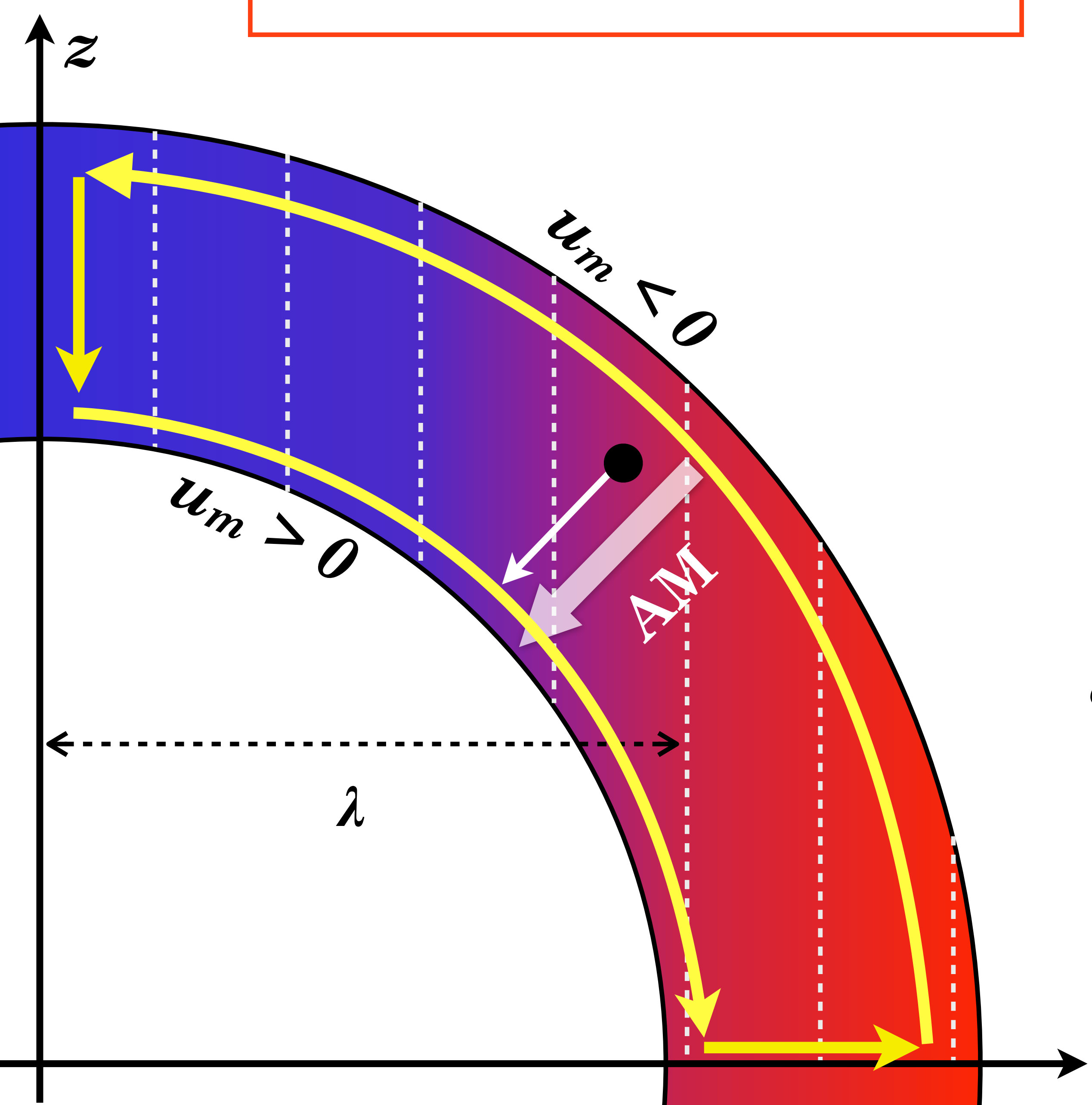

$$\boxed{\rho \boldsymbol{u}_m \cdot \nabla_m \mathcal{L} = -\nabla \cdot (\boldsymbol{F}_{\mathbf{RS}})}$$

Anelastic approximation $\rightleftarrows \nabla \cdot (\rho \boldsymbol{u}_m)$ $\qquad \boldsymbol{u}_m \equiv u_r \boldsymbol{e}_r + u_\theta \boldsymbol{e}_\theta$

$$\nabla \cdot (\boldsymbol{F}_{\mathbf{MC}} + \boldsymbol{F}_{\mathbf{RS}}) = 0$$

where

$$\boldsymbol{F}_{\mathbf{MC}} \equiv \rho (r \sin\theta)^2 \Omega \boldsymbol{u}_m = \rho \mathcal{L} \boldsymbol{u}_m$$

$$\boldsymbol{F}_{\mathbf{RS}} \equiv \rho (r \sin\theta)(\langle u'_r u'_\phi \rangle \boldsymbol{e}_r + \langle u'_\theta u'_\phi \rangle \boldsymbol{e}_\theta)$$

- **回転が遅い場合：**

- F_{RS}が動径方向負の向き = F_{RS}は負の値

$\partial F_{RS}/\partial r > 0$ @upper, $\partial F_{RS}/\partial r < 0$ @bottom

$u_m < 0$ @upper

$u_m > 0$ @bottom

（上昇・下降流は質量流速の保存）

Mean Field Transport of Angular Momentum (3)

回転星の角運動量分布（≠角速度分布）：円柱状

理由：角運動量（$L \propto \lambda^2\Omega$）の視点で見れば恒星内部の回転則はほぼ剛体回転

(太陽の極-赤道の角速度差は高々20%)

$\therefore\ \partial L/\partial z \sim 0,\ \partial L/\partial\theta > 0$

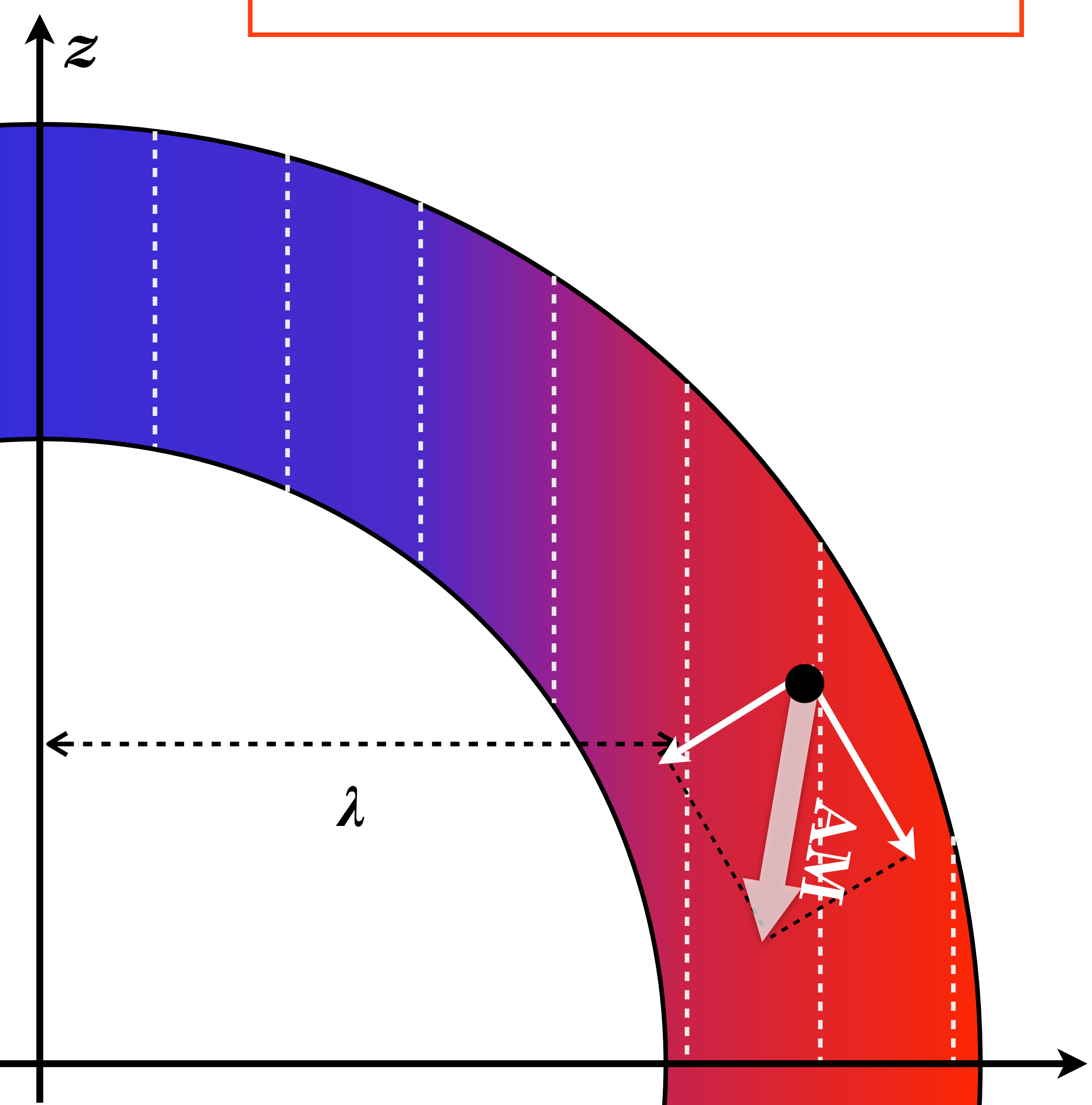

$$\boxed{\rho \boldsymbol{u}_m \cdot \nabla_m \mathcal{L} = -\nabla \cdot (\boldsymbol{F}_{\mathbf{RS}})}$$

Anelastic approximation $\rightleftarrows \nabla \cdot (\rho \boldsymbol{u}_\mathrm{m})$ $\quad \boldsymbol{u}_m \equiv u_r \boldsymbol{e}_r + u_\theta \boldsymbol{e}_\theta$

$$\nabla \cdot (\boldsymbol{F}_{\mathbf{MC}} + \boldsymbol{F}_{\mathbf{RS}}) = 0$$

where

$$\boldsymbol{F}_{\mathbf{MC}} \equiv \rho (r\sin\theta)^2 \Omega \boldsymbol{u}_m = \rho \mathcal{L} \boldsymbol{u}_m$$

$$\boldsymbol{F}_{\mathbf{RS}} \equiv \rho (r\sin\theta)(\langle u_r' u_\phi' \rangle \boldsymbol{e}_r + \langle u_\theta' u_\phi' \rangle \boldsymbol{e}_\theta)$$

- **回転が速い場合：**

- F_RSがz方向負の向き = F_RSは負の値

$\partial F_\mathrm{RS}/\partial\theta < 0$ @high-z, $\partial F_\mathrm{RS}/\partial z > 0$ @low-z

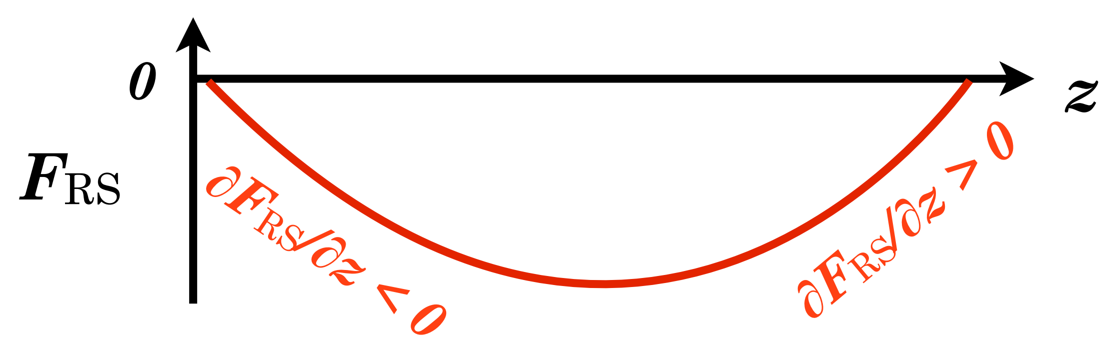

Mean Field Transport of Angular Momentum (3)

回転星の角運動量分布（≠角速度分布）：円柱状

理由：角運動量（$L \propto \lambda^2\Omega$）の視点で見れば恒星内部の回転則はほぼ剛体回転

(太陽の極-赤道の角速度差は高々20%)

$$\boxed{\therefore\ \partial L/\partial z \sim 0,\ \partial L/\partial \theta > 0}$$

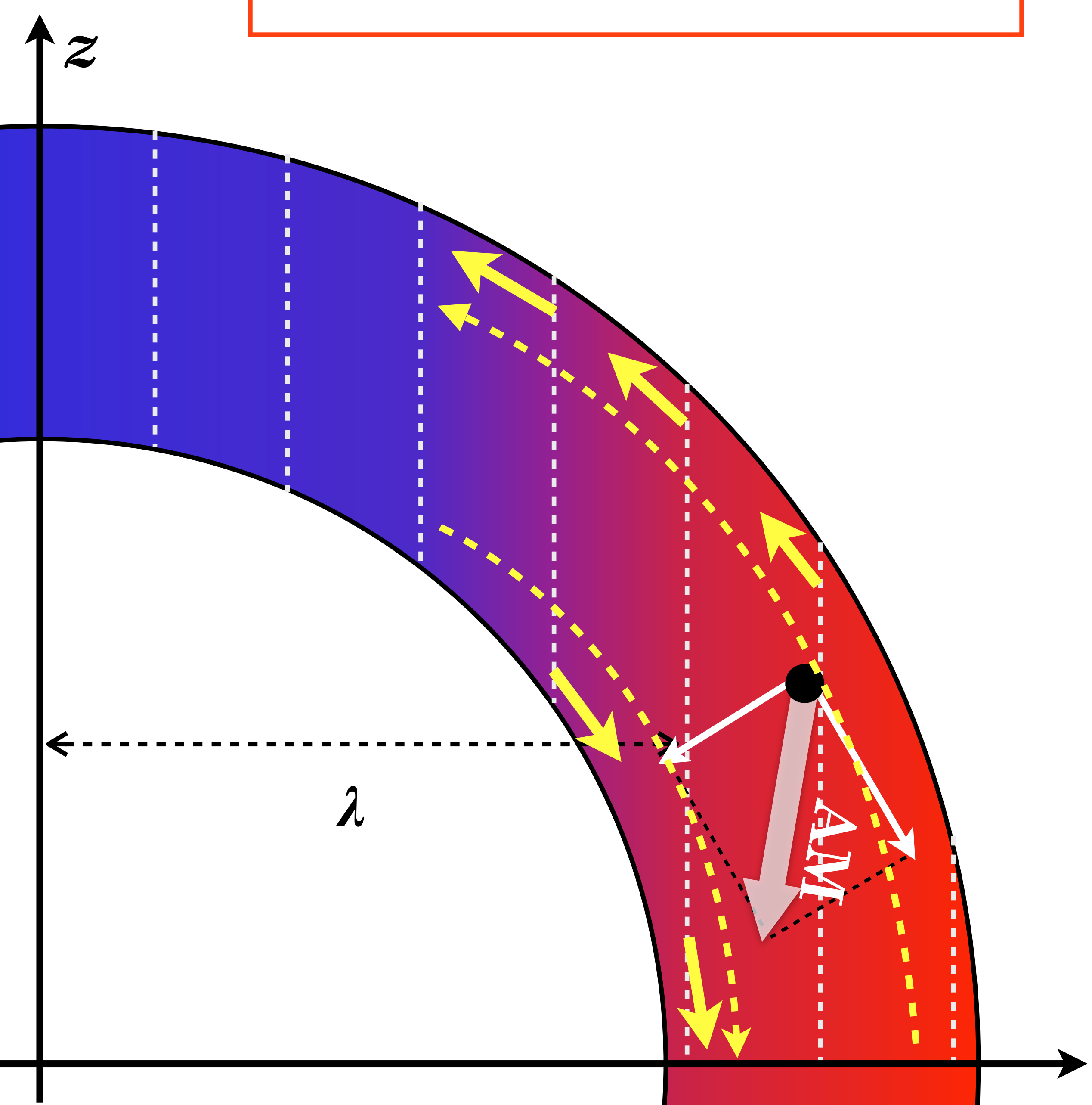

$$\boxed{\rho \boldsymbol{u}_m \cdot \nabla_m \mathcal{L} = -\nabla \cdot (\boldsymbol{F}_{\mathrm{RS}})}$$

Anelastic approximation $\rightleftarrows \nabla \cdot (\rho \boldsymbol{u}_\mathrm{m})$

$\boldsymbol{u}_m \equiv u_r \boldsymbol{e}_r + u_\theta \boldsymbol{e}_\theta$

$$\nabla \cdot (\boldsymbol{F}_{\mathrm{MC}} + \boldsymbol{F}_{\mathrm{RS}}) = 0$$

where

$$\boldsymbol{F}_{\mathrm{MC}} \equiv \rho (r \sin\theta)^2 \Omega \boldsymbol{u}_m = \rho \mathcal{L} \boldsymbol{u}_m$$

$$\boldsymbol{F}_{\mathrm{RS}} \equiv \rho (r \sin\theta)(\langle u'_r u'_\phi \rangle \boldsymbol{e}_r + \langle u'_\theta u'_\phi \rangle \boldsymbol{e}_\theta)$$

- **回転が速い場合：**

- F_{RS}がz方向負の向き = F_{RS}は負の値

$\partial F_{\mathrm{RS}}/\partial\theta < 0$ @high-z, $\partial F_{\mathrm{RS}}/\partial z > 0$ @low-z

$u_m < 0$ @high-z

$u_m > 0$ @low-z

Mean Field Transport of Angular Momentum (4)

※重要なこと：Gyroscopic Pumpingが回転分布を決めているわけではない

→ **ある回転分布における角運動量輸送のバランスを記述している**

(a) 回転が遅い場合

– 子午面流は角運動量を極向きに輸送

– レイノルズ応力は角運動量を動径方向内向きに輸送

→ この二つの輸送プロセスの帰結としてある回転分布が決まる.

(b) 回転が速い場合

– 子午面流は角運動量を極向きに輸送

– レイノルズ応力は角運動量を赤道向きに輸送

→ この二つの輸送プロセスの帰結としてある回転分布が決まる.

Demonstration with Simulation Models

(a) Slow rotation case **(b) Fast rotation case**

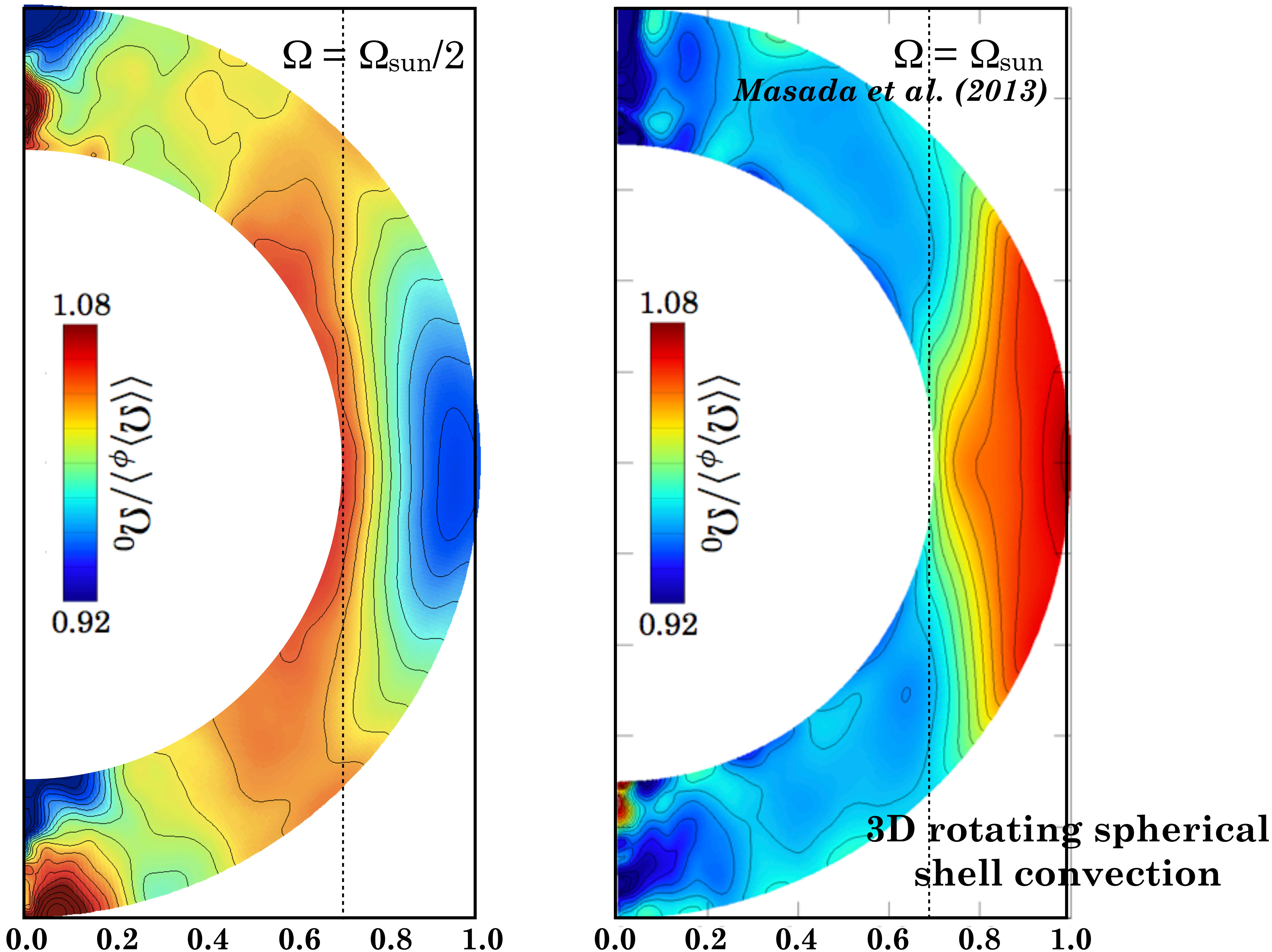

GFDセミナー@休暇村支笏湖
（R7. 3/15-16）

太陽内部のプラズマの流れ：診断・モデル化・推定

政田洋平（福岡大学）

共同研究者
横井喜充（東大生産研），滝脇知也（NAOJ），原田了（茨城高専），
仲田資季（駒澤大学），本武陽一（一橋大学），佐野孝好（大阪大学）

太陽内部のプラズマの流れ:
診断・モデル化・推定

①診断 : 太陽内部のプラズマの流れの観測

- 太陽の内部構造モデルと日震学
- 標準太陽モデルと熱対流の物理
- 太陽磁場の観測と太陽MHDを考える上で知っておくべきこと

②モデル化 : 太陽内部MHDモデリング

- 太陽ダイナモモデル(ダイナモの基礎・標準シナリオ)
- グローバルモデルと過去20年の研究の進展
- セミグローバルモデルとダイナモのロスビー数依存性

③推定 : 太陽熱対流の難問:計算・データサイエンス手法を使った対流駆動機構の検討と推定

- Convection conundrum と 非局所駆動型熱対流
- Topological Data Analysis (TDA)の基礎
- 太陽熱対流のトポロジカルな特徴(モデル vs. 観測)

Convection conundrum
（解決困難な熱対流の難問）

太陽のマルチスケール熱対流描像(パラダイム)

The Swedish 1-meter Solar Telescope / Institute for Solar Physics, Observer & Data reduction:
Luc Rouppe van der Voort, Oslo 18 Jun 2006 (Wavelength: 656.3nm H-Alpha)

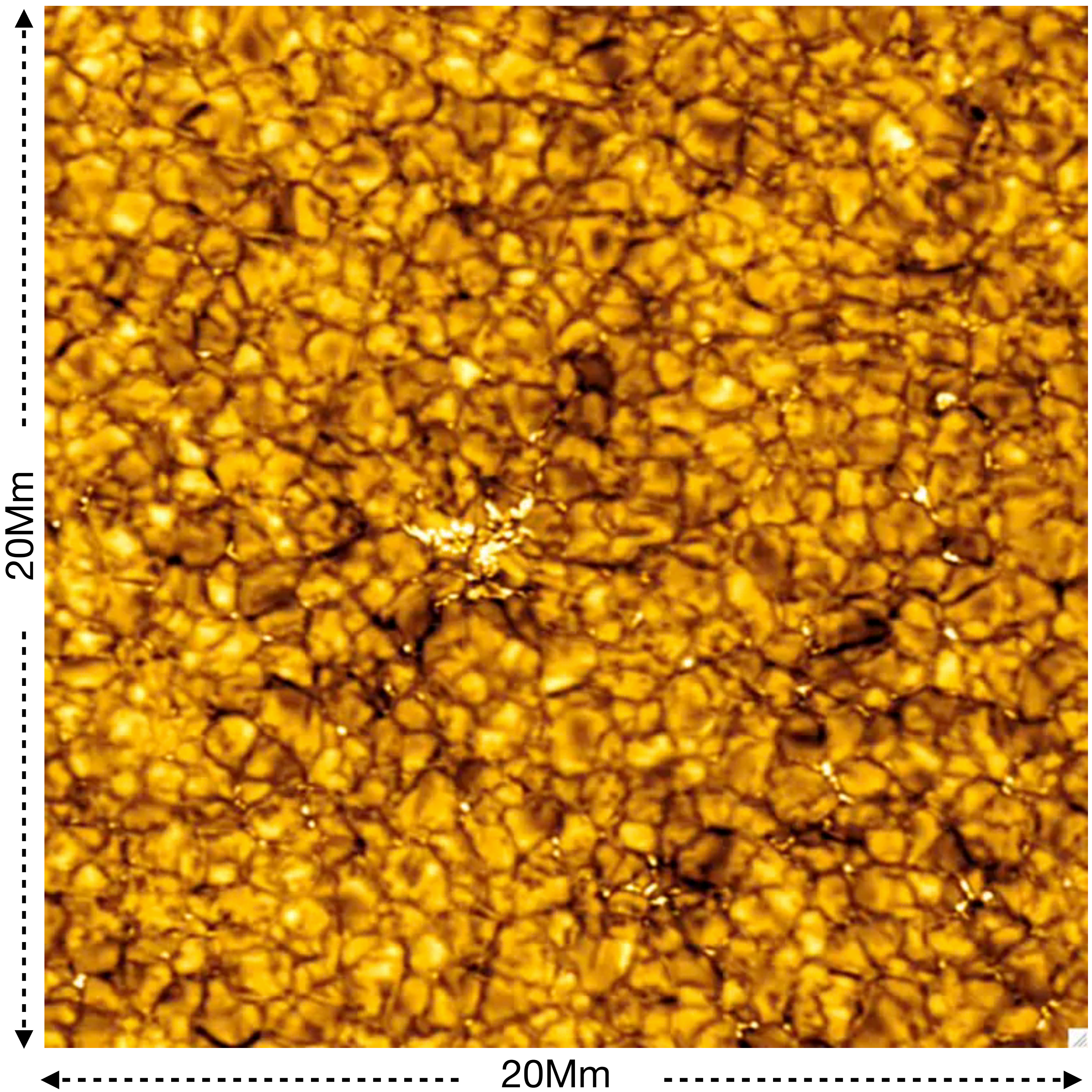

● 太陽対流層の(伝統的な)描像

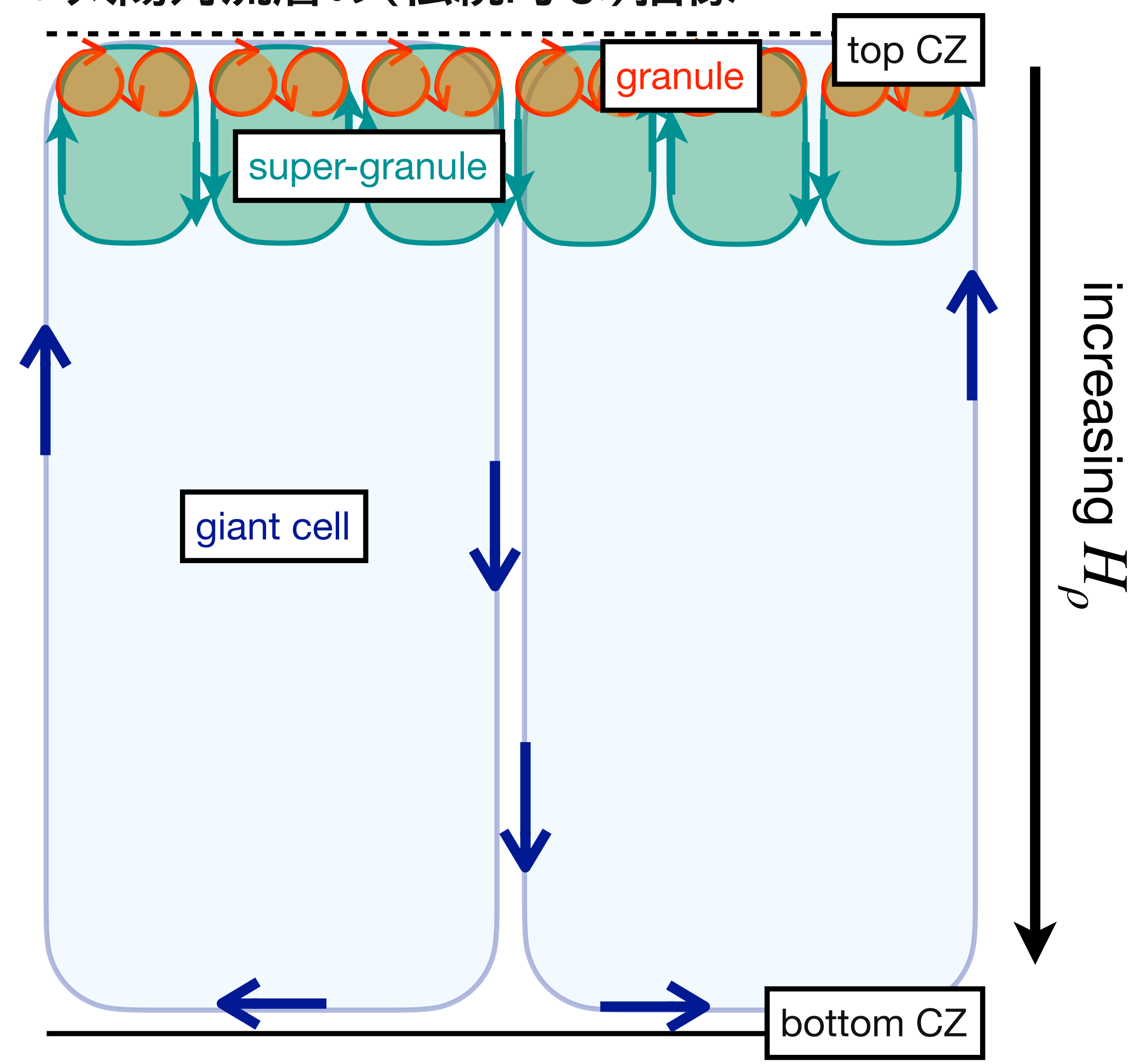

● 太陽対流層の対流渦は階層構造を持つ:
- 対流の駆動スケール ∝ 圧力スケール長(H_P)
- 太陽対流層の圧力変化は4桁 → H_Pも4桁変化
  (背景にあるのは混合距離理論と勾配拡散近似)

近年, このパラダイムに疑問符が

- 粒状斑 : typical size ≈ 1Mm, typical lifetime ≈ 10 min.
- 超粒状斑 : typical size ≈ 30Mm, typical lifetime ≈ 20 hours
- 巨大胞 : typical size ≈ 200Mm, typical lifetime ≈ 1 month

太陽熱対流の難問：巨大胞はどこへ行った！？

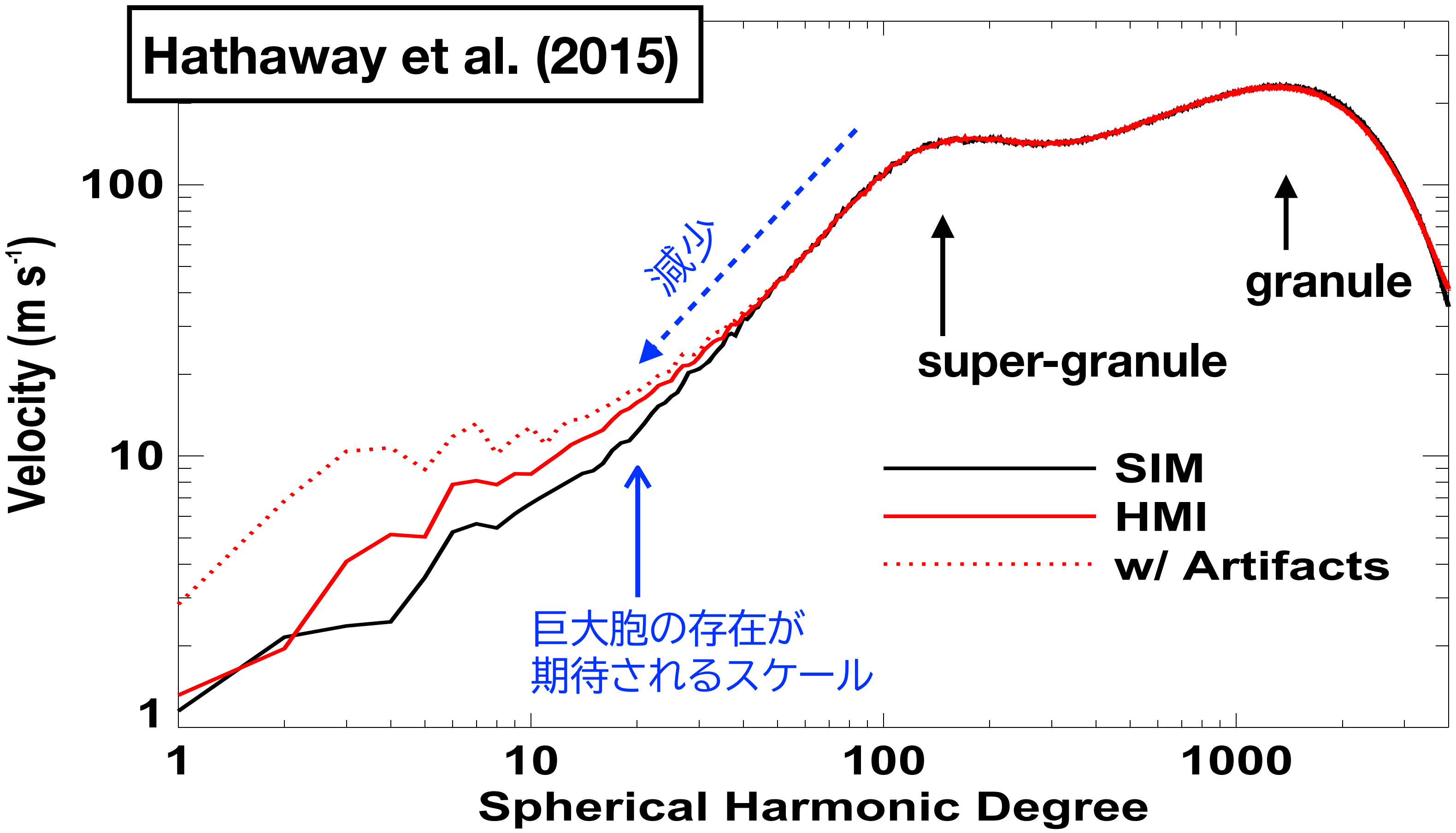

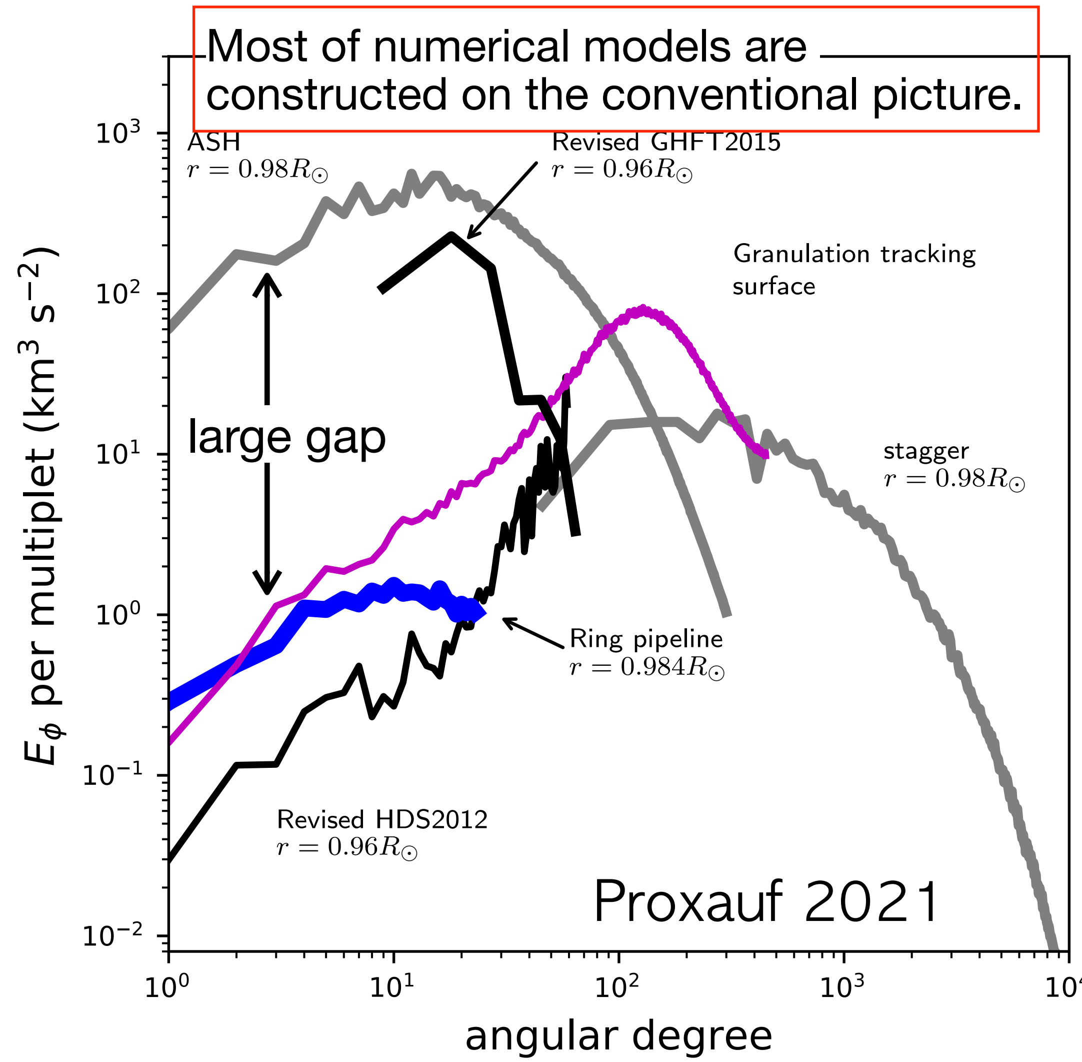

- **Hathaway et al. (2015):**
  太陽対流層表面（光球面）での対流速度スペクトル：
  → 長時間積分しても期待されるスケールに巨大胞の存在が確認できない
- **Hanasoge et al. (2012): see also e.g., Greer+15; Proxauf 21:**
  日震学診断による対流速度スペクトル（表面直下）（※理論予測 ↔ 混合距離理論に基づく輸送）
  → 低波数レジームの対流速度の観測値が理論予測より2桁以上小さい
  - 巨大胞が存在しない → 対流層の内側から輸送されてくる熱エネルギーが不足するはず
  - 観測的には表面に輸送されている熱エネルギーに不足は無い（太陽光度）

・どうやってエネルギーは運ばれているのか？ Convection Conundrum
・近年の太陽MHDモデルは現実の太陽とは全く異なる対流の中でダイナモを解いている？？

対流層の計算モデルを構築する際, どうしているか？

太陽の内部構造モデル･･･ポリトロープ大気： $P = \rho^{1+1/m}$

$$\nabla s = 1/(m+1), \qquad \nabla_{ad} = 1 - 1/\gamma$$

$\nabla_{ad} - \nabla_s < 0$ (Schwarzschild criterion for unstable)

γ = 5/3を仮定すると, m < 3/2が不安定条件. m = 1.49 (YM&Sano16)とか適当に値を与えて
浮力駆動の対流を対流層で起こす → 浮力駆動のMLT描像に近い対流が発達

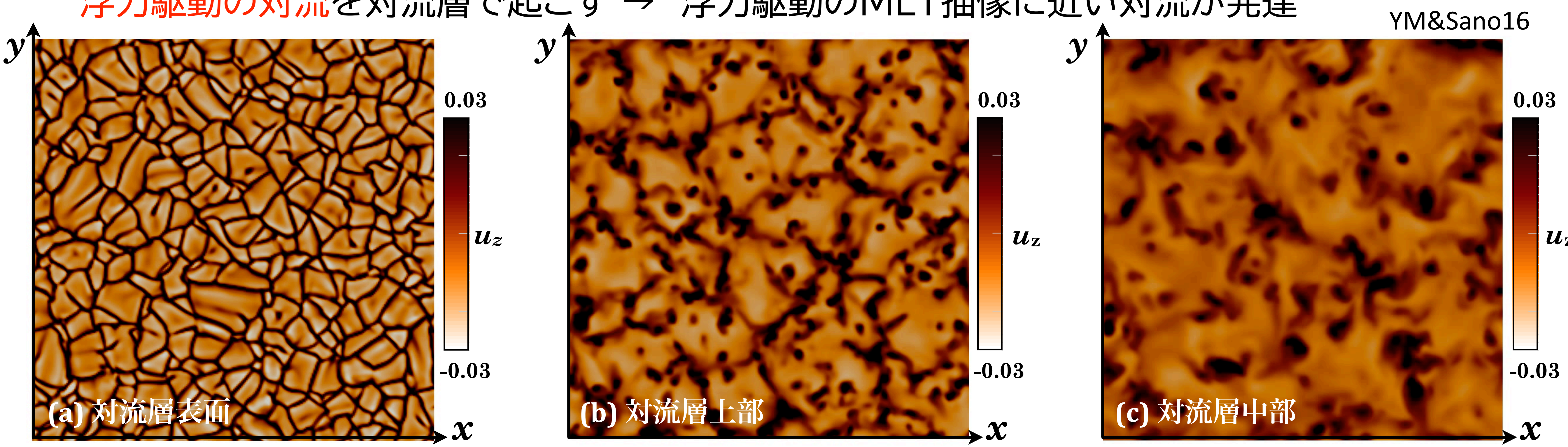

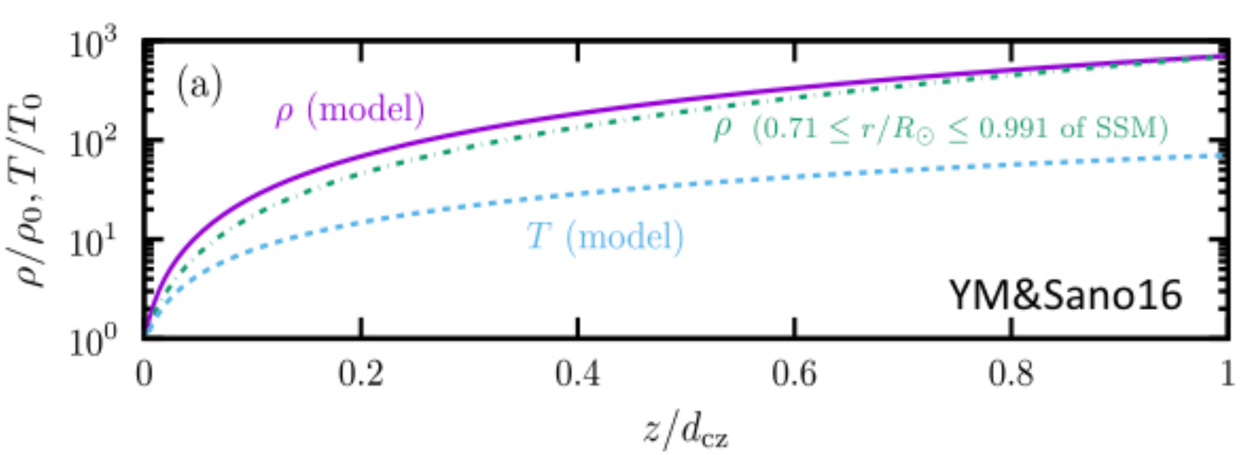

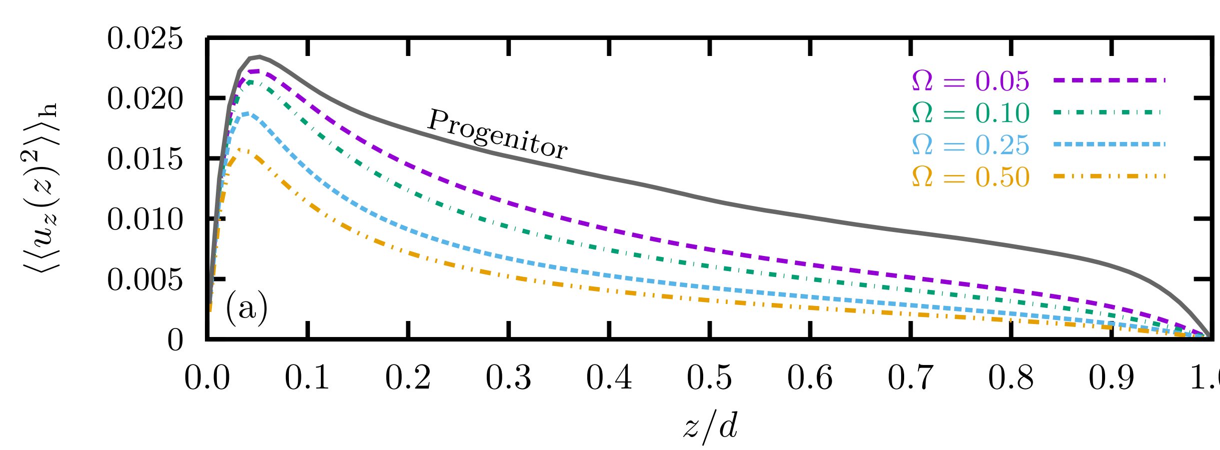

対流層の底ほどHpは大きいので, 速度は小さく, 空間スケールの大きな対流セル.
これは対流を局所プロセスとして取り扱っている(与えている)帰結.

Are we headed in the right direction?

How to resolve the convection conundrum ? several possible solutions are proposed:

① rotationally-constrained convection (e.g., Featherstone and Hindman 2016; Vasil et al. 2021)

② mostly adiabatic CZ (e.g., Spruit 1997; Rast 1998; Brandenburg 2016; Cossette & Rast 2017)

③ large effective Prandtl number (e.g. O'Mara et al. 2016; Bekki et al. 2017; Karak et al. 2018)

④ higher resolution + SSD (e.g., Hotta & Kusano 21)

■ conventional view : multi-scale convection

$\delta = \nabla_s - \nabla_{ad} > 0$ (for whole the CZ)

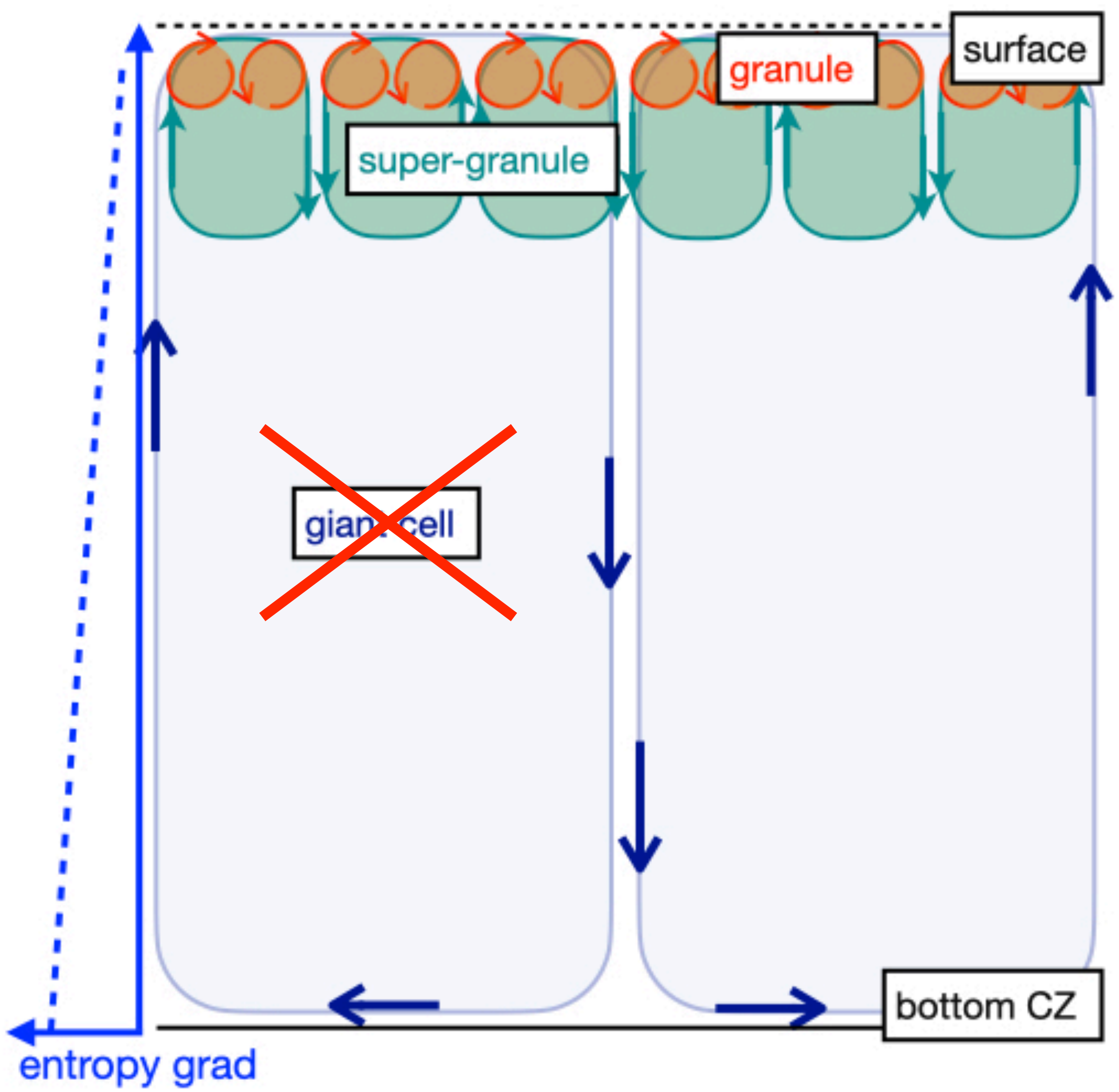

Because of the high density contrast in the solar CZ (6 orders of magnitude difference in the density over whole CZ), the scale height varies largely there. So, we believe that the size of the convective eddies should vary largely in the solar CZ.

Brief review of mixing-length concept:

- How is the energy transported inside the sun ?
  - two transporters:

$$\underbrace{F_r}_{\text{radiative diffusion}} + \underbrace{F_e}_{\text{convection}} = \frac{L_\odot}{4\pi r^2}$$

with $F_e \propto \rho \boxed{\langle \delta u_r \delta e_i \rangle}$: enthalpy flux

(energy transported by the convection)

- The turbulent energy flux is naively modeled by :

$$\delta u_r \delta e_i \sim \kappa_E \frac{\partial e_i}{\partial r}, \quad \text{where} \quad \kappa_E = \sqrt{\langle \delta u_r^2 \rangle}\ l$$

: turbulent transport coef.

$\boxed{\text{gradient diffusion model}}$ (GD model)

(l: mixing length ~ size of the convective eddies)

With choosing the scale-height H_ρ as the mixing-length l, the amplitude of the turbulent transport coef. κ_E is determined.

- The natural depiction derived from the GD model is the multi-scale convection in the sun.
- CC suggests that the absence of the giant cell which should be the main energy transporter.

Is there an alternative to giant cells ?

solar CZ is an open system
(energy loss from the photosphere)

one pos

(The driv

Simple

(YM in pr

- polytr
  - densi
  - 2D hy
- \+ Gaus
  - FWH
  - mini

ABSTRACT. Progress in the theory of stellar convection over the past decade is reviewed. The similarities and differences between convection in stellar envelopes and laboratory convection at high Rayleigh numbers are discussed. Direct numerical simulation of the solar surface layers, with no other input than atomic physics, the equations of hydrodynamics and radiative transfer is now capable of reproducing the observed heat flux, convection velocities, granulation patterns and line profiles with remarkably accuracy. These results show that convection in stellar envelopes is an essentially non-local process, being driven by cooling at the surface. This differs distinctly from the traditional view of stellar convection in terms of local concepts such as cascades of eddies in a mean superadiabatic gradient. The consequences this has for our physical picture of processes in the convective envelope are illustrated with the problems of sunspot heat flux blocking, the eruption of magnetic flux from the base of the convection zone, and the Lithium depletion problem.

stellar convection should be driven by cooling at the surface !

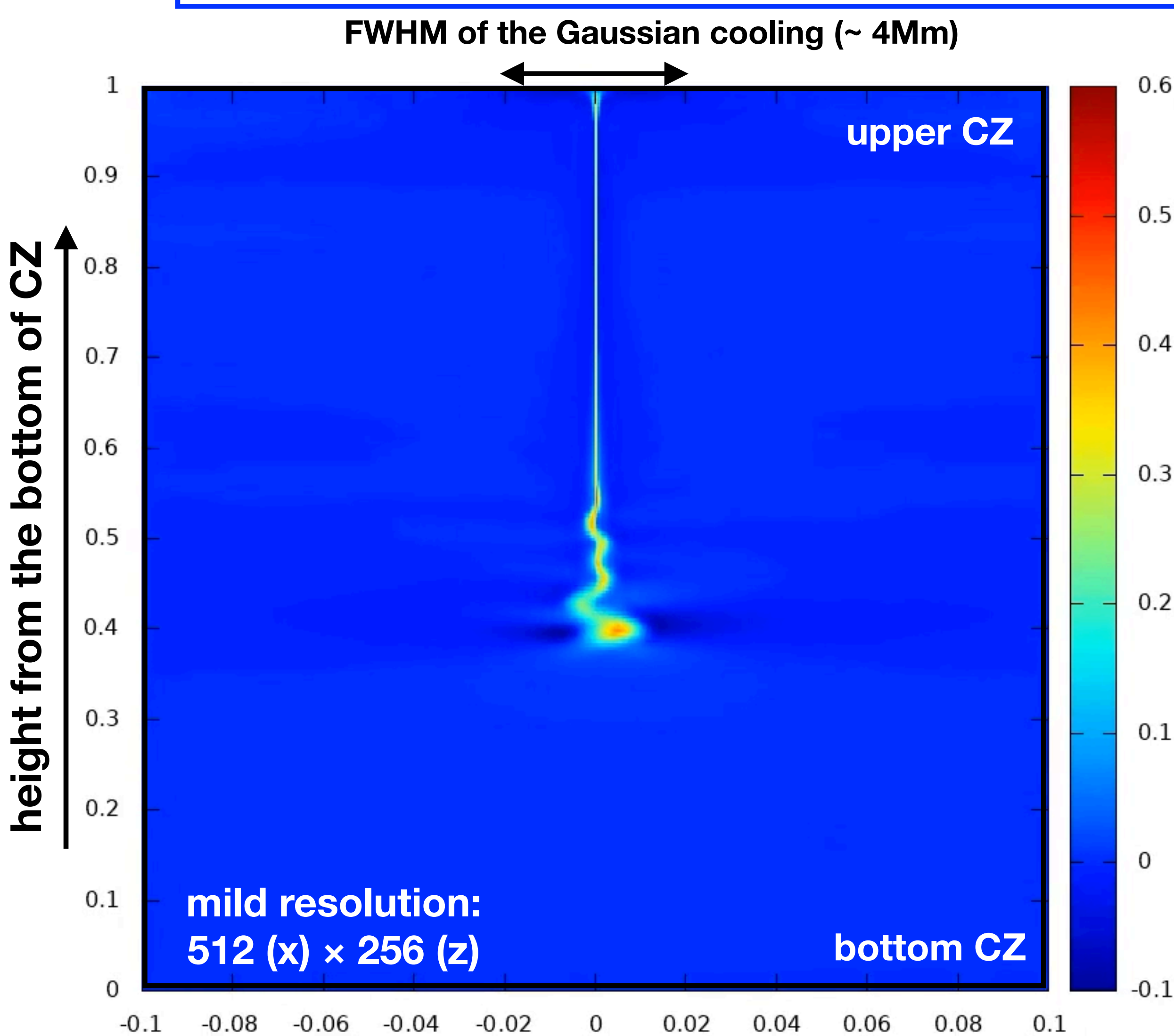

This alternative model has been proposed theoretically already in late 90's, but has not been studied carefully until recently.

CONVECTION IN STELLAR ENVELOPES: A CHANGING PARADIGM

H.C. SPRUIT
Max Planck Institute

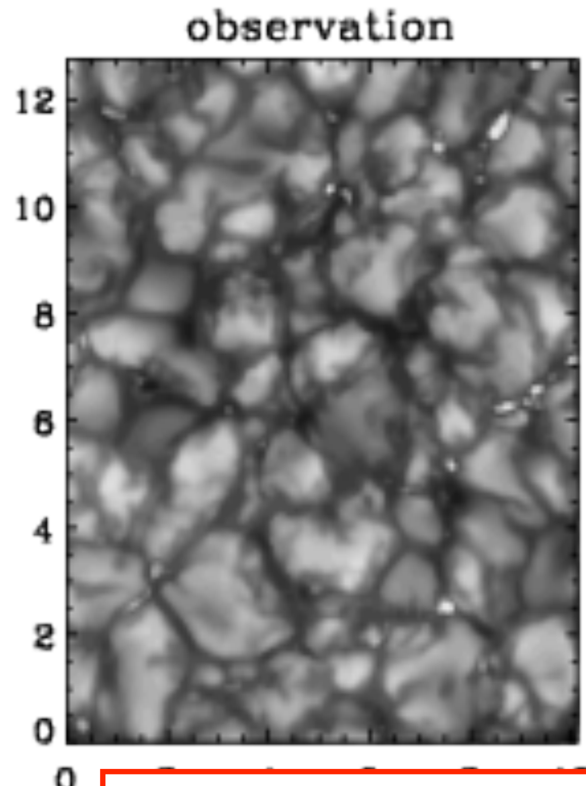

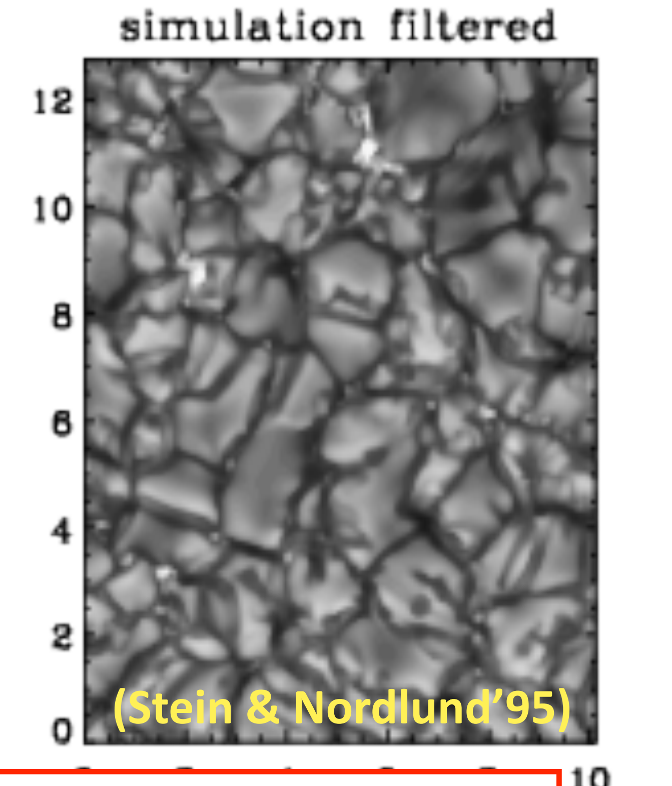

Quantitative agreement between surface convection simulations with radiation and observational results.

Possible Two Convection Models :

(a) Cooling-driven model: super-adiabatic surface due to the radiative cooling **(c.f., Spruit 1997)**

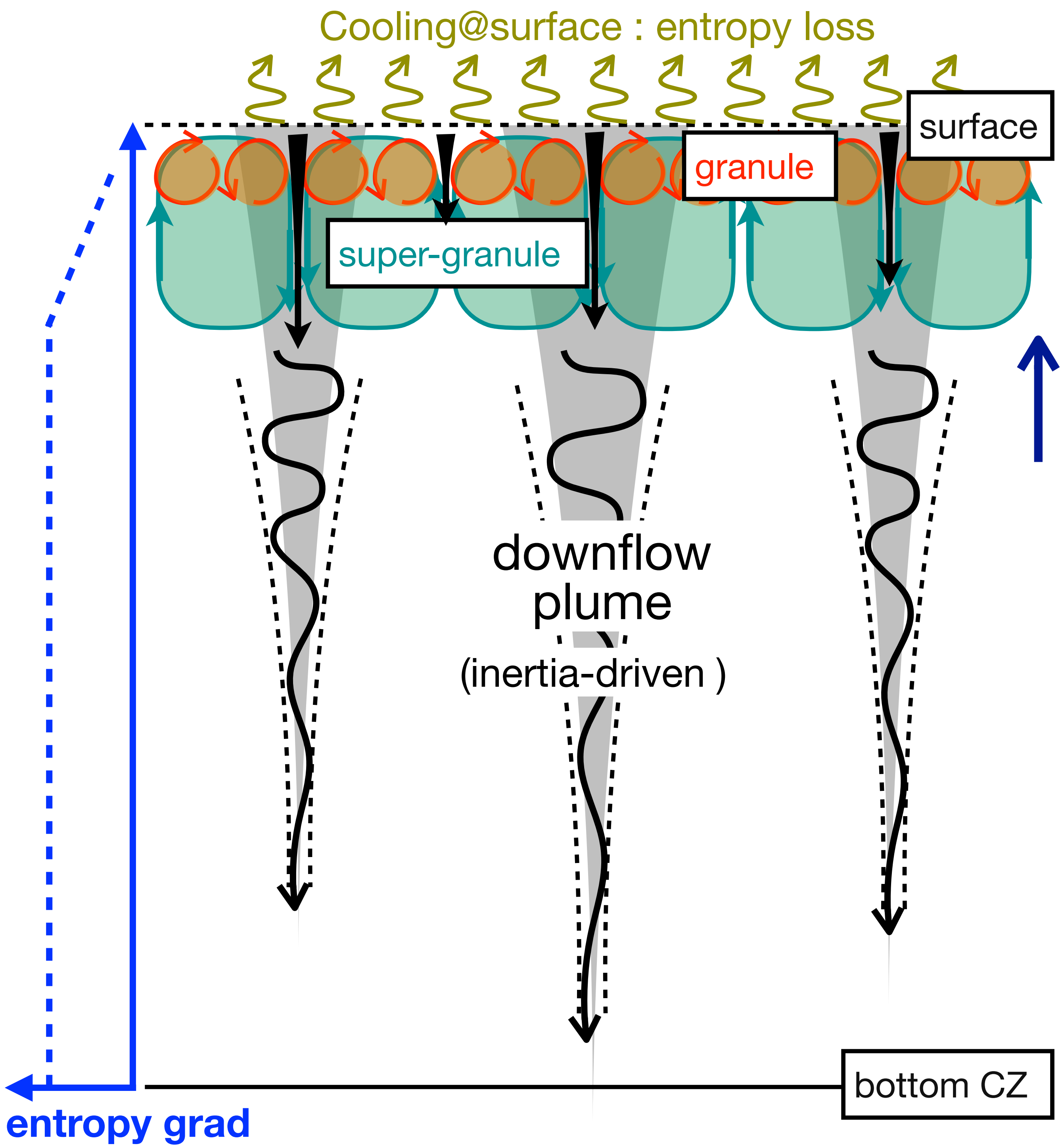

・radiative cooling makes the surface super-adiabatic :

→ interface btw super-adiabatic and adiabatic layers determines the largest size of the convective cell

(b) S-grad-driven model: super-adiabatic entropy gradient over the whole CZ

$$\delta = \nabla_s - \nabla_{ad} > 0 \quad \text{(for whole the CZ)}$$

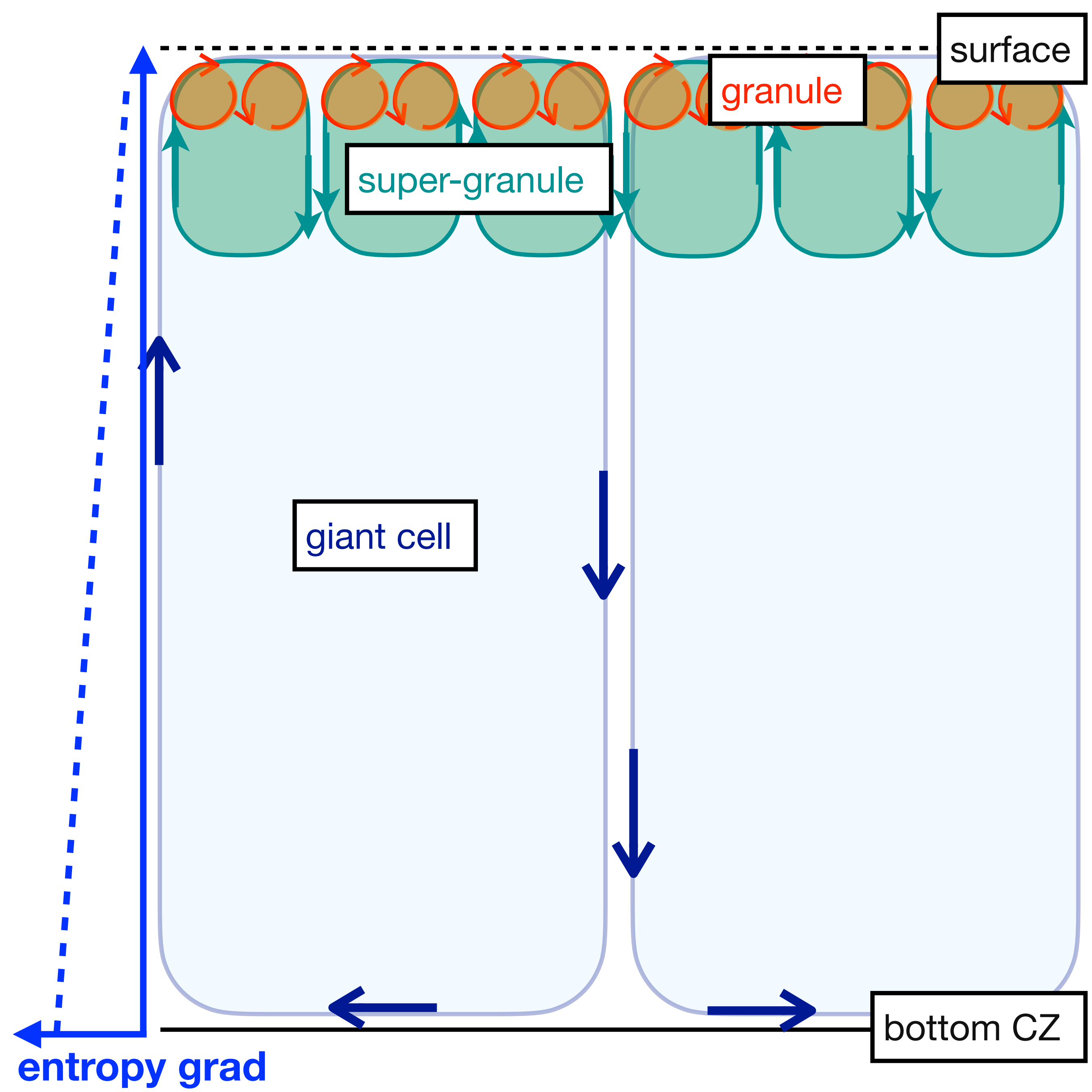

・In this model, the size of the convective eddies determined by the local scale-height.

→ broad spectrum from granule to giant cell

How does the convection model impact on the turbulent transport properties ?

表面での急激な冷却が担う太陽熱対流

(実験結果)

- 高レイリー数熱対流：buoyant fluidのthread (糸) or 細いplumeが熱を輸送
- $F_{conv} = \rho v C_p DT$, $v < 0$かつ$DT < 0$の時も, $F_{conv} > 0$ (外向きに熱エネルギーを輸送)
- 強密度成層 → 対流層底部 (ρ_b) と表面 (ρ_t) の密度比が10^6.
  → 底部からの上昇流が運ぶDTは, 表面からの下降流が運ぶDTの10^5 ~10^6分の1に過ぎない.
- 表面で急激に冷却された重いプルームが下降することで熱を輸送

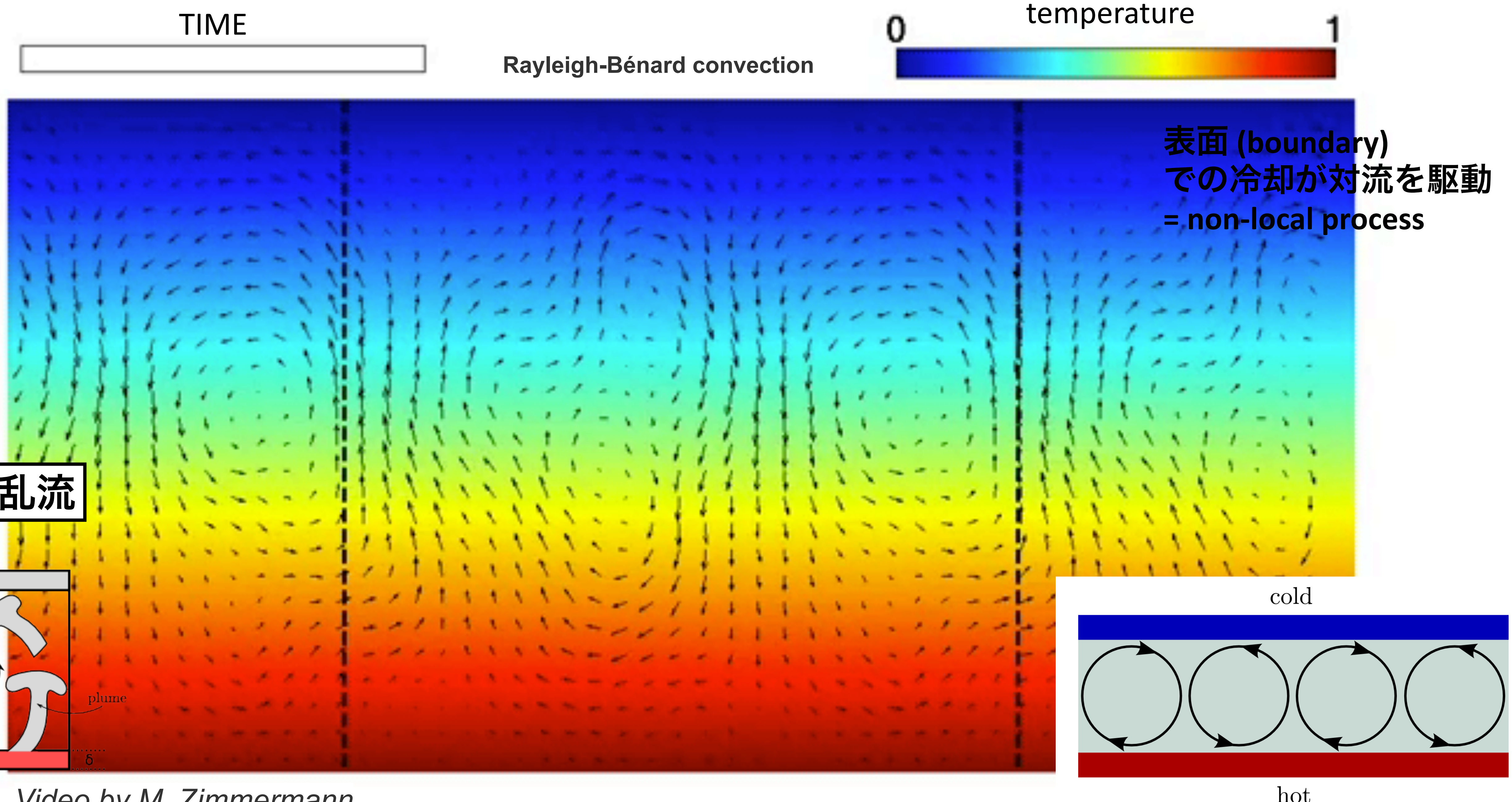

Video by M. Zimmermann

検証：熱対流モデルの違いが熱輸送に及ぼす影響

How different they are in the transport properties ?

Yokoi, YM+23, YM+25 (simulation similar to Cossette & Rast 2016)

- Basic eqs : compressible HD eqs [Cartesian box]
- polytropic atmosphere [CZ only] with an index m

  (aspect ratio : $L_x/L_z = L_y/L_z = 4$, no rotation)
- two-types of convection models are simulated :

  ① cooling-driven : m = 1.495 (upper 5%) + 1.5 (95%)

  ② S-grad-driven : m = 1.495 (whole CZ)

  (0.2% difference in the input energy between models)
- technical term : Newton cooling (only model ①)

$$\frac{\mathrm{D}\epsilon}{\mathrm{D}t} = -\frac{P}{\rho}\nabla\cdot v + \boxed{\frac{\epsilon - \epsilon_{\mathrm{ref}}}{\tau}}$$

This mimics the rad cooling and maintain super-adiabaticity in the upper CZ

- density contrast & resolution :

  $\rho_{\mathrm{bottom}}/\rho_{\mathrm{top}} = 300, \quad N_x \times N_y \times N_z = 512^2 \times 128$

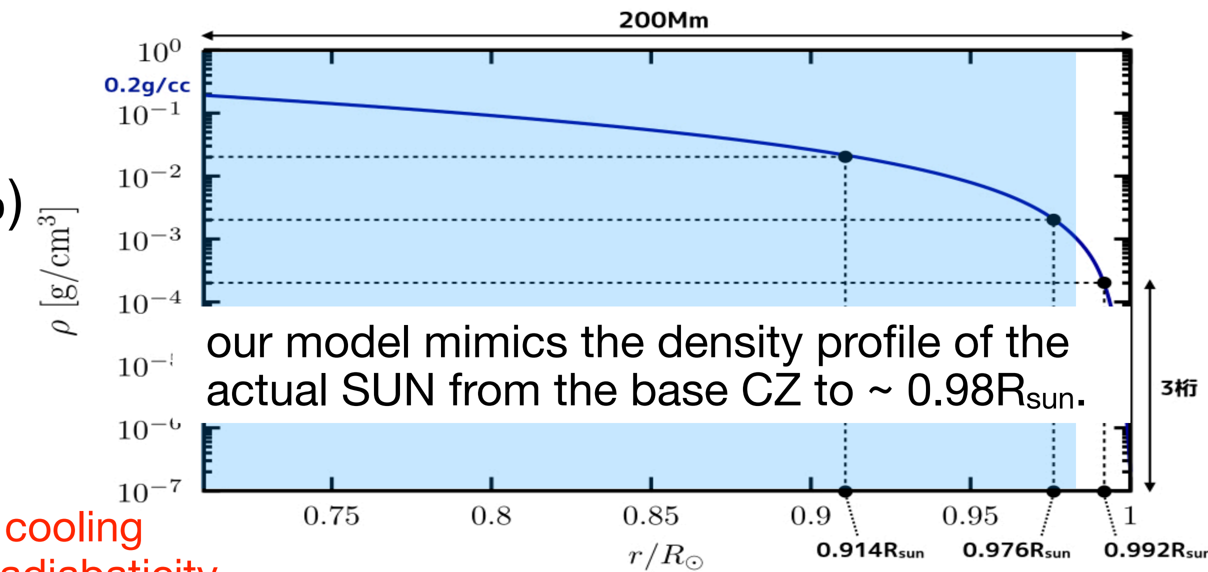

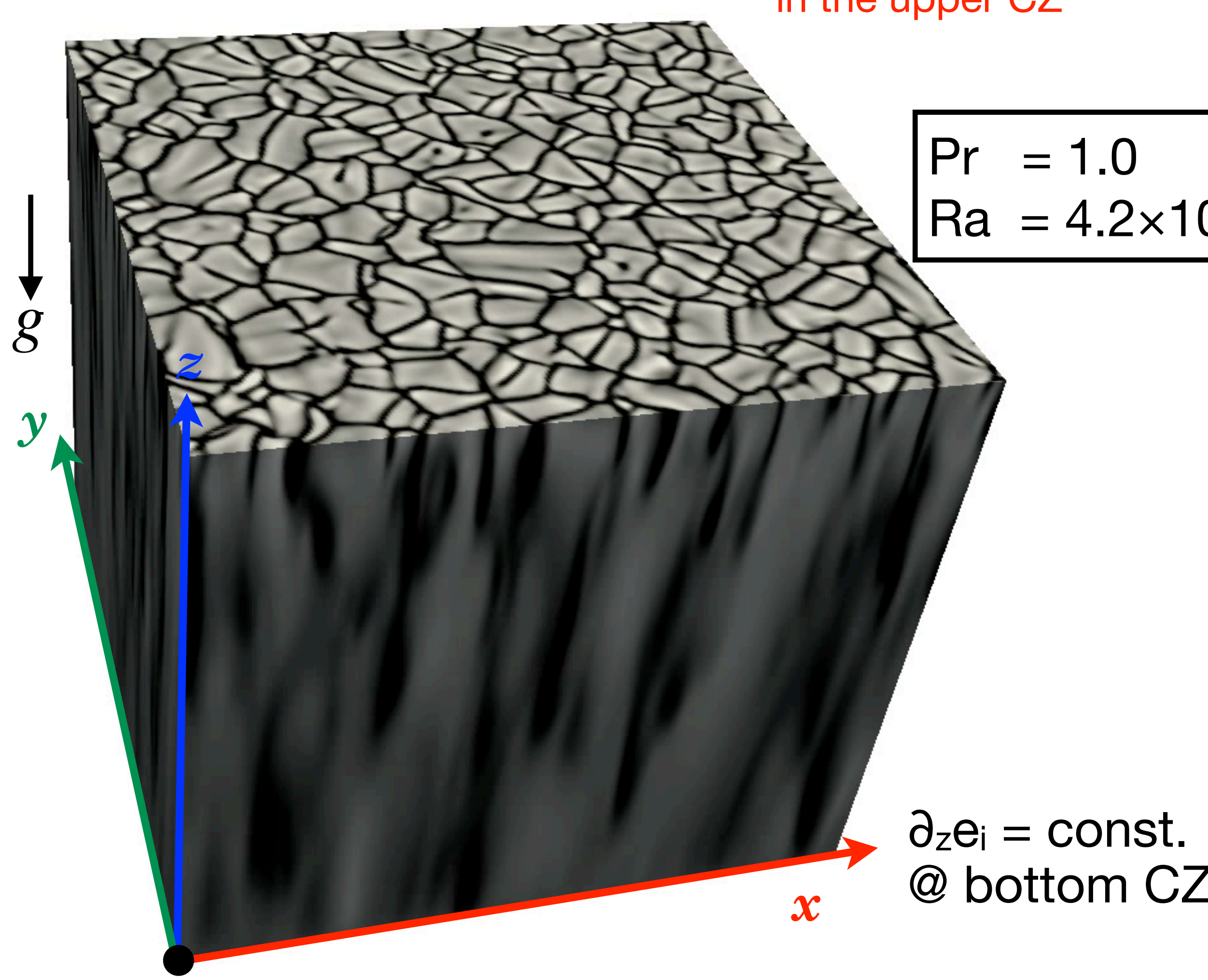

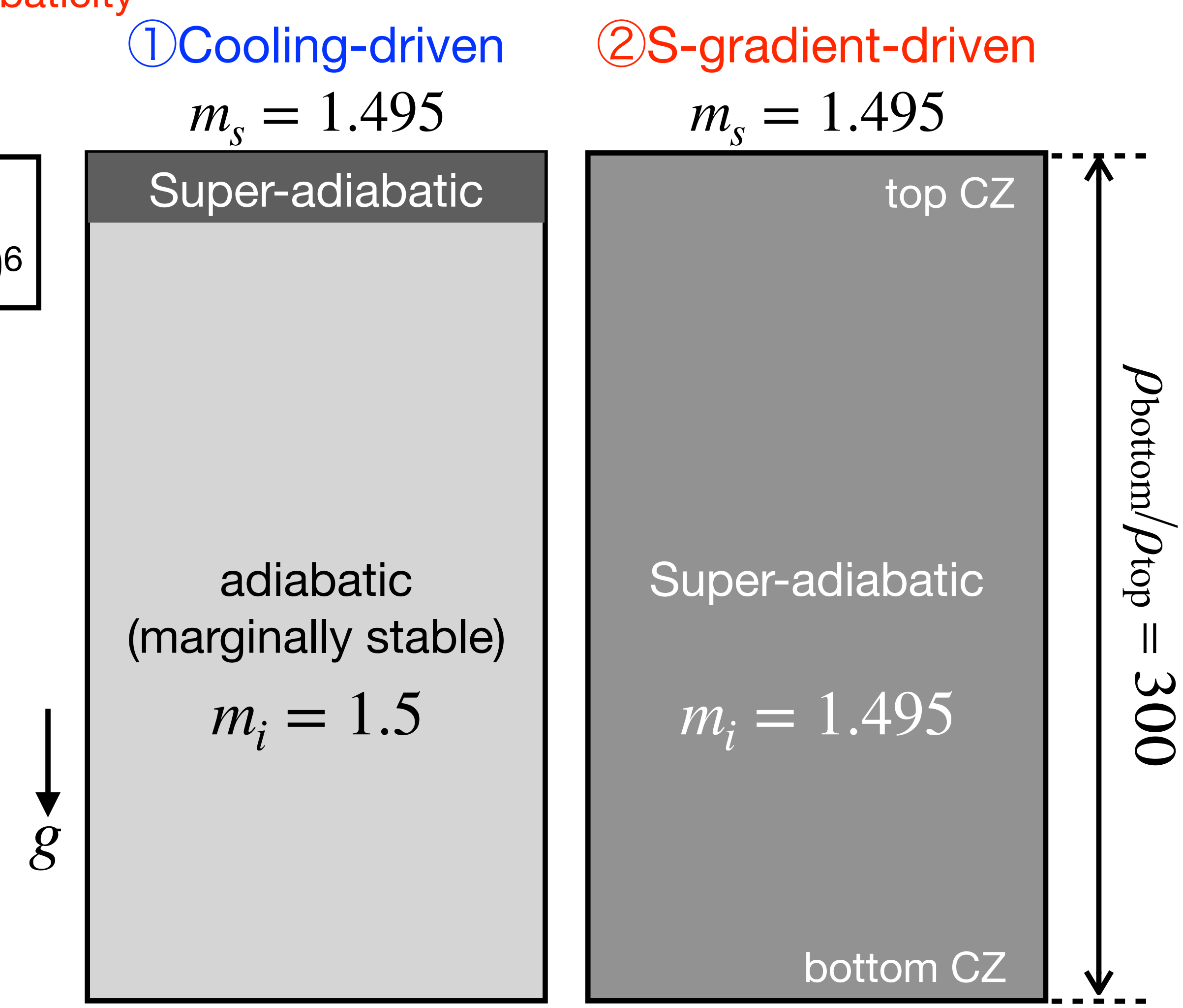

Convection Properties of Two models : Appearance

①Cooling-driven model (CD):

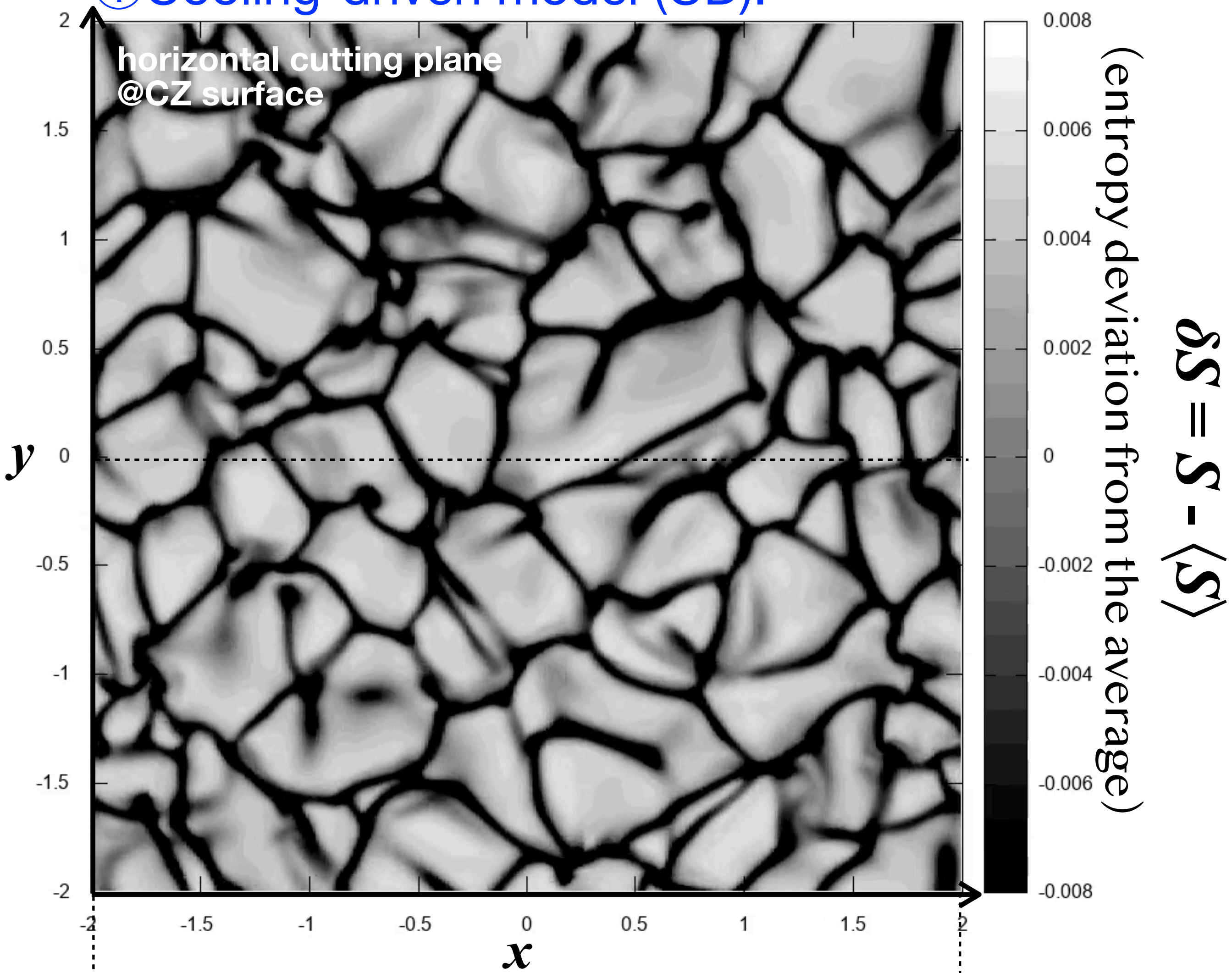

A lots of downflow plumes exist in the upper CZ

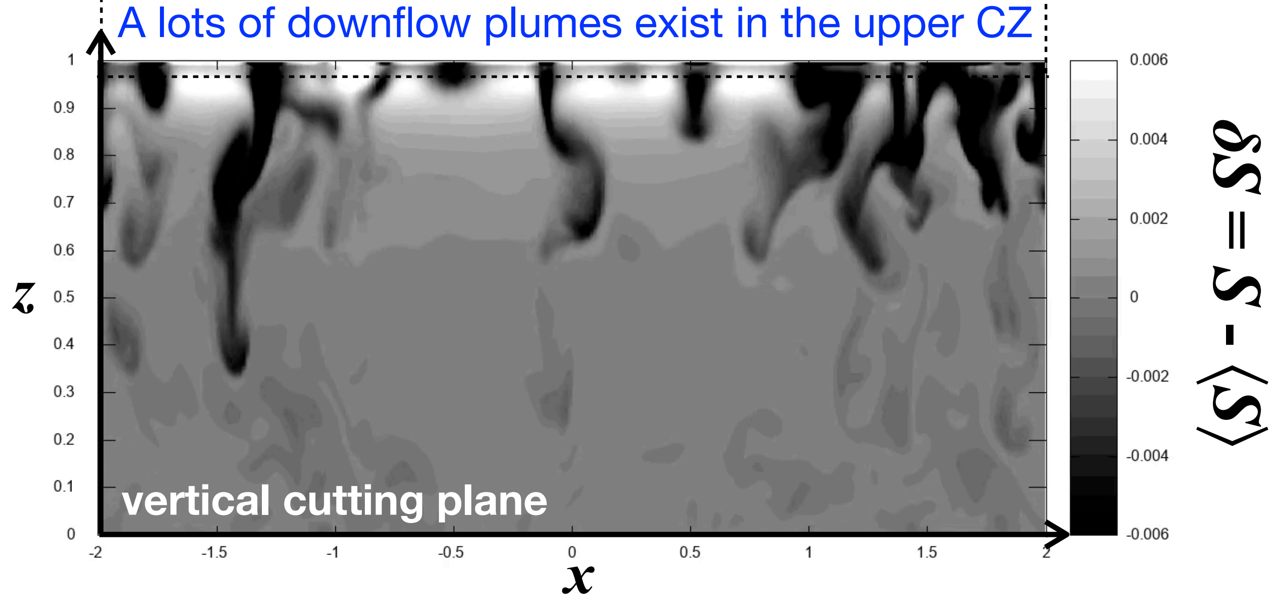

- Small convective cells prevail at the surface.
- A lot of downflow plumes appear in the upper CZ.

②S-grad-driven model (SD):

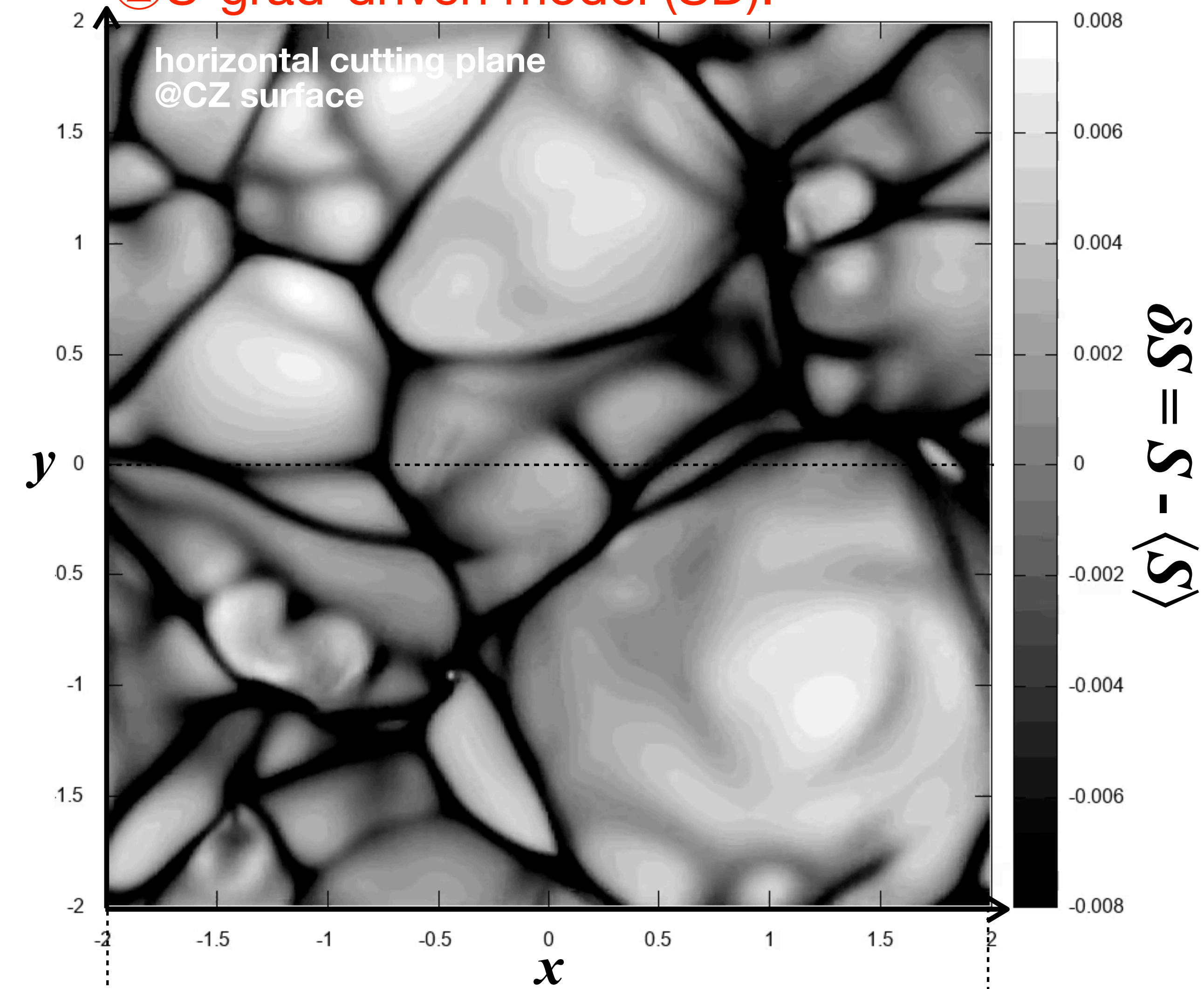

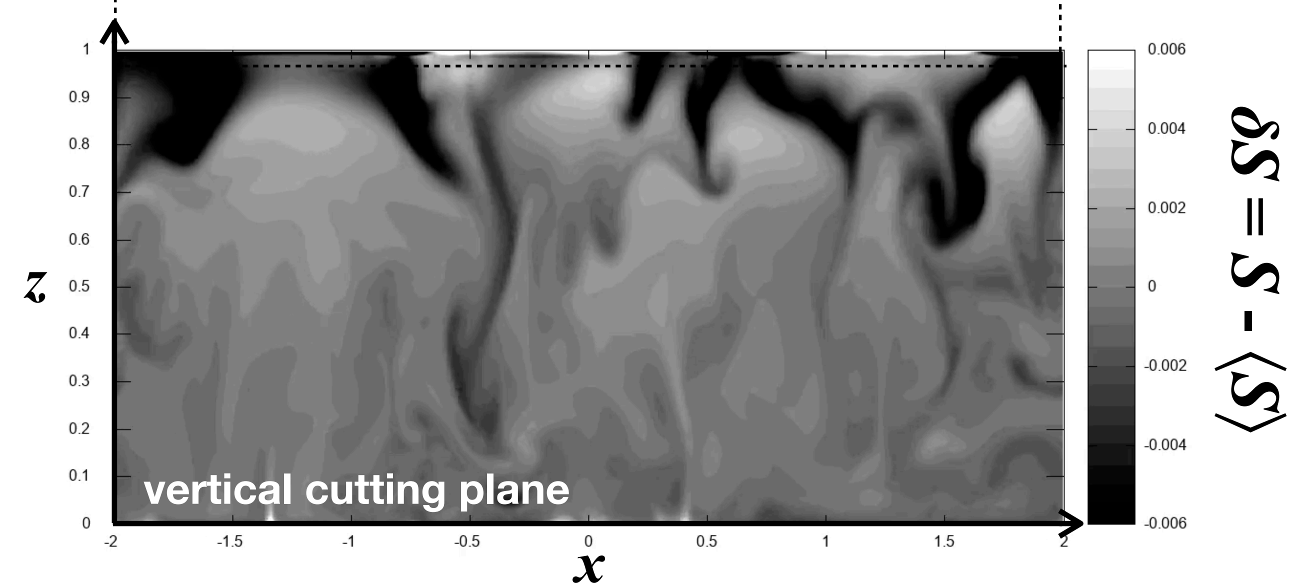

- Large convective cells are dominant at the surface.
- Large-scale flow motions across the entire domain.

Mean Convection Properties : Similarity and Difference

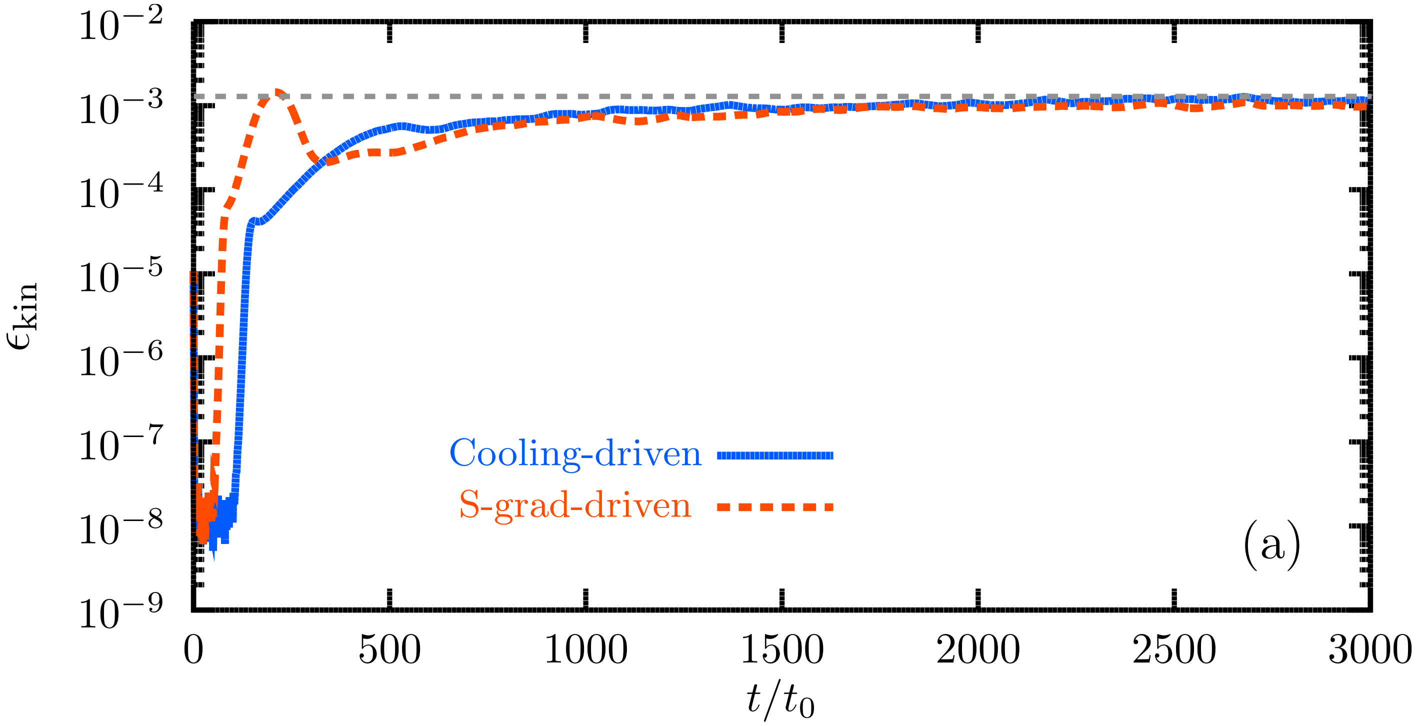

- Mean kinetic energies are almost same at saturated state between models.
- Kinetic energy spectra for v_z show a remarkable difference in the low k regime:
  - the convective energy is suppressed in low k in the cooling-driven model

  → **compatible with the NO giant cell obs.**

The cooling-driven model seems to be suitable for the solar convection. How do the other physical properties differ between the cooling-driven and S-grad-driven ?

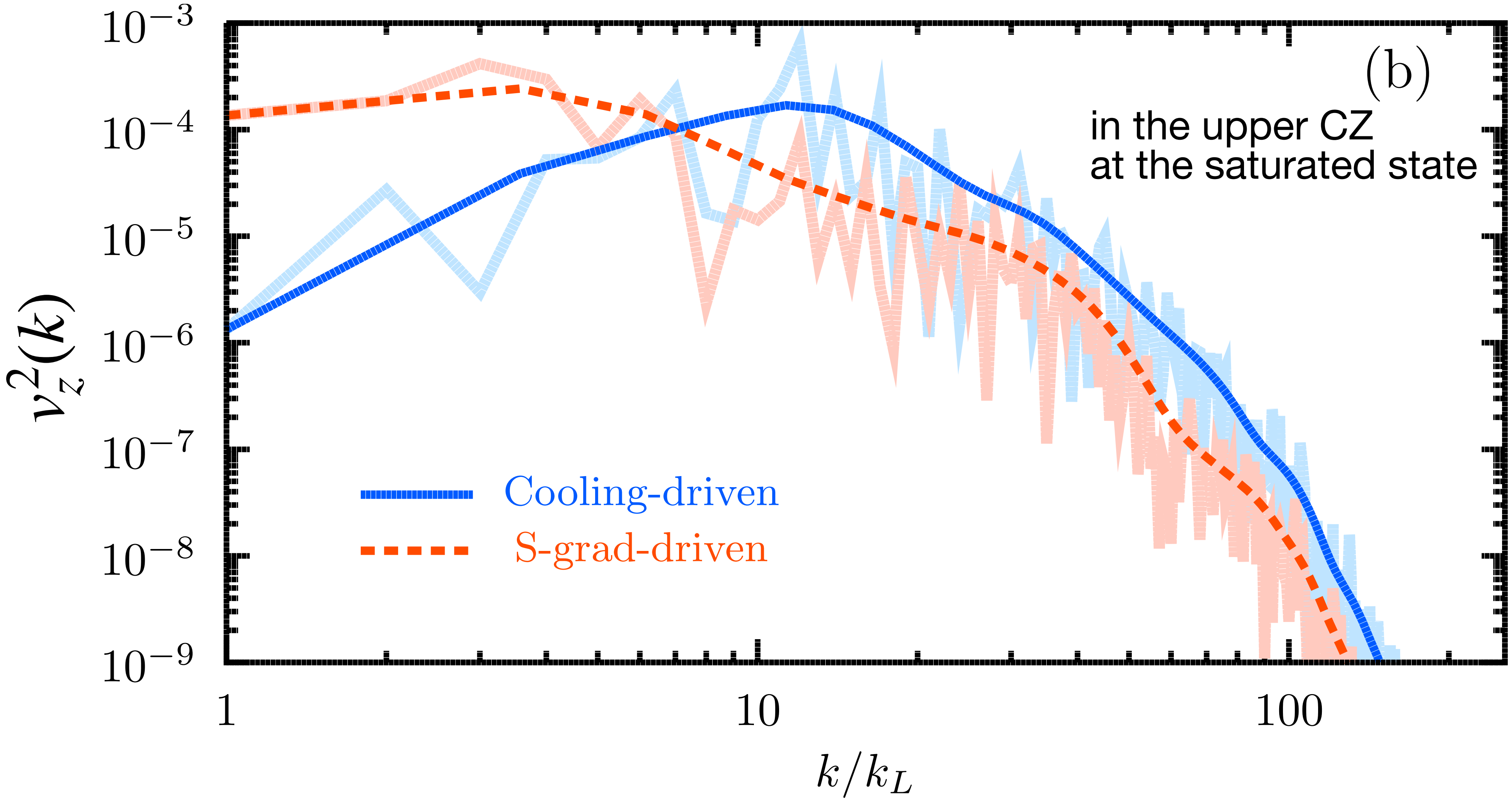

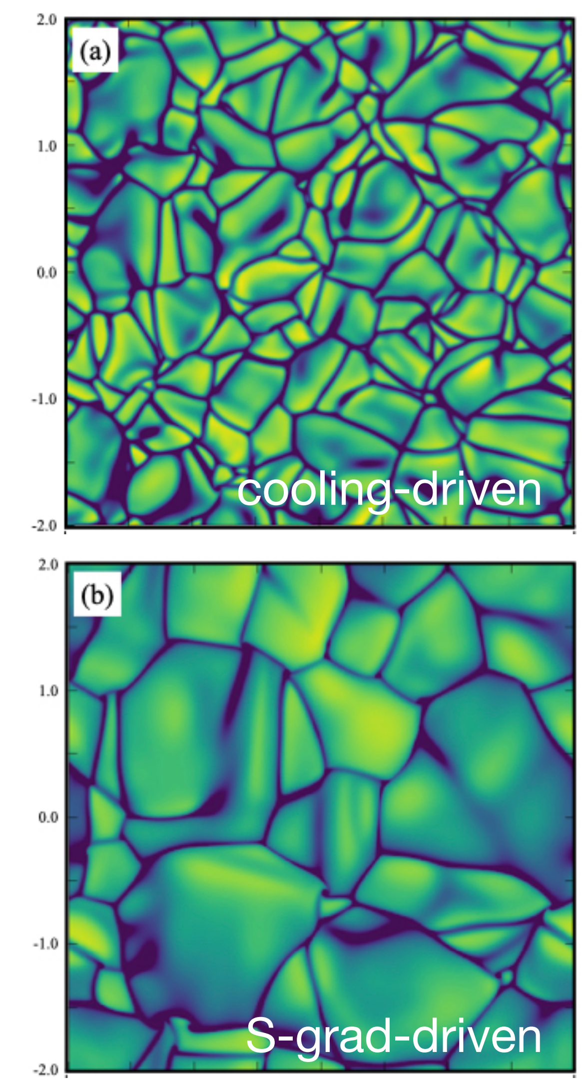

Statistical Properties of Convection : broad downflow wing

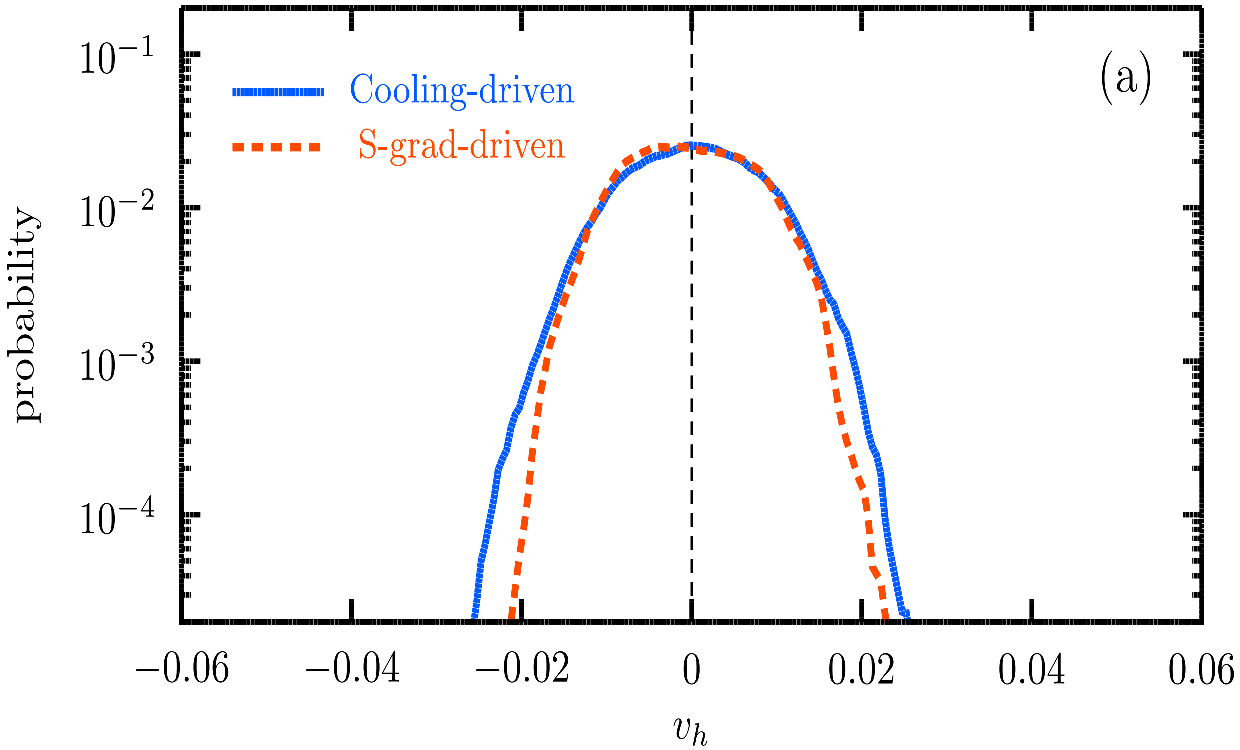

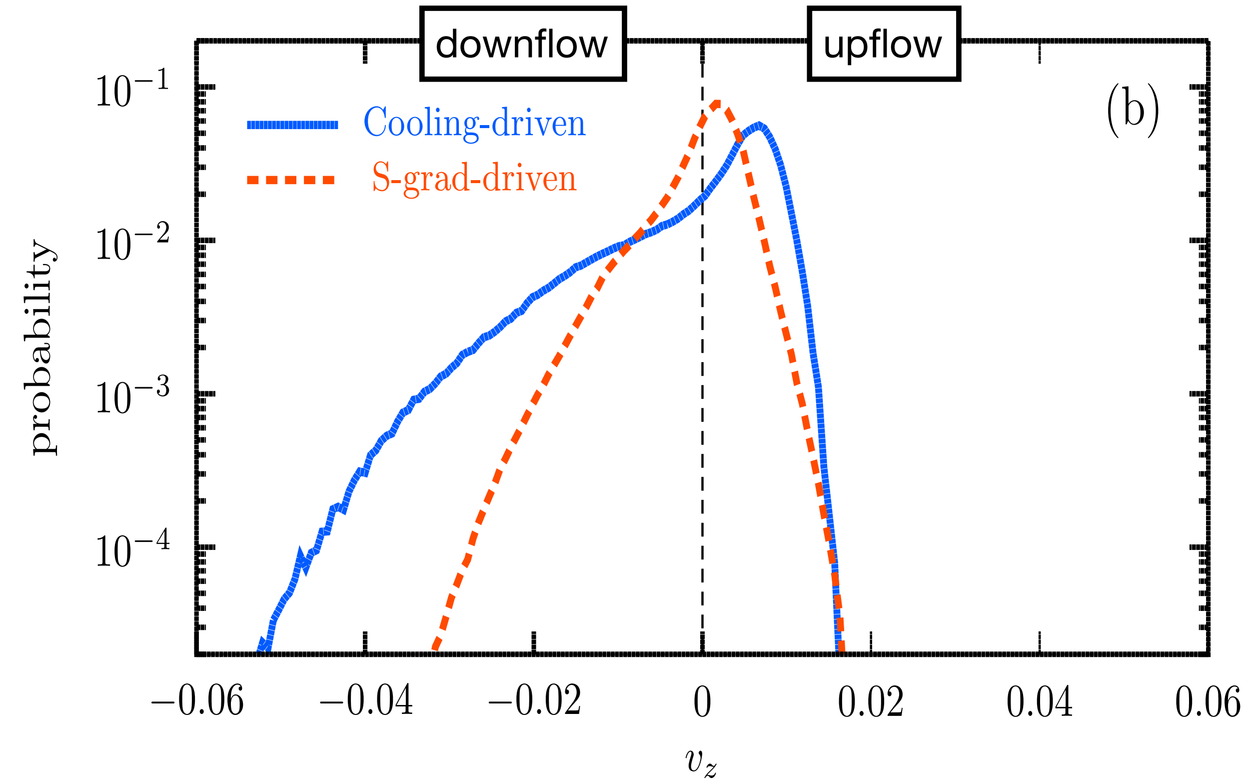

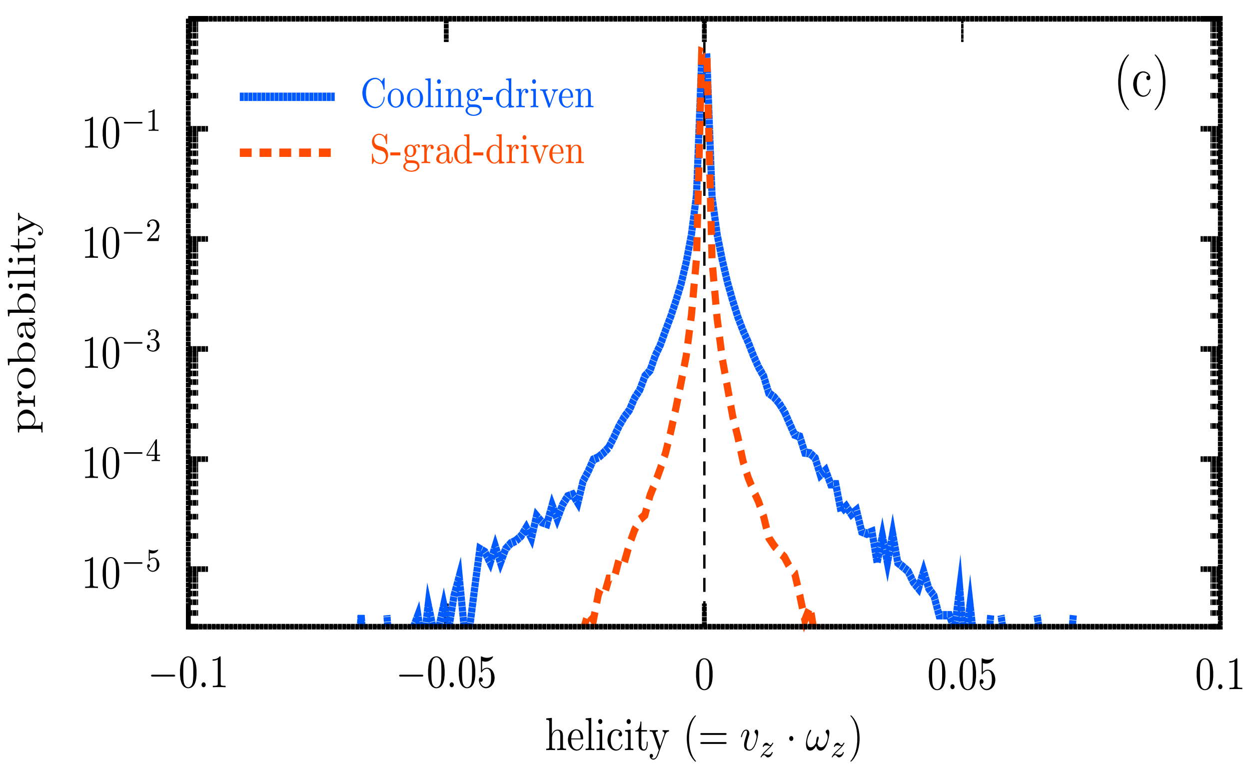

Regardless of the non-rotating model, kinetic helicity exists locally, while it becomes zero when taking sufficiently-long time average.

- Gaussian-like distribution of v_h for both models (a bit broader in the cooling-driven)
- Non-gaussian distribution of v_z for both models :
  - up-down asymmetry would be a natural outcome of compressible convection & mass flux conservation.
  - downflow has broader wing in the cooling-driven model than that in the S-gradient-driven model
  - → stochastic downflow (non-equilibrium process) plays an important role for the transport in the system
- Leptokurtic distribution of H for both models:
  - broader wing in the cooling-driven model

How should we treat such ``non-gaussian properties" of convection, that may be important in considering the transport in the stars.

Statistical Properties of Convection : probability density

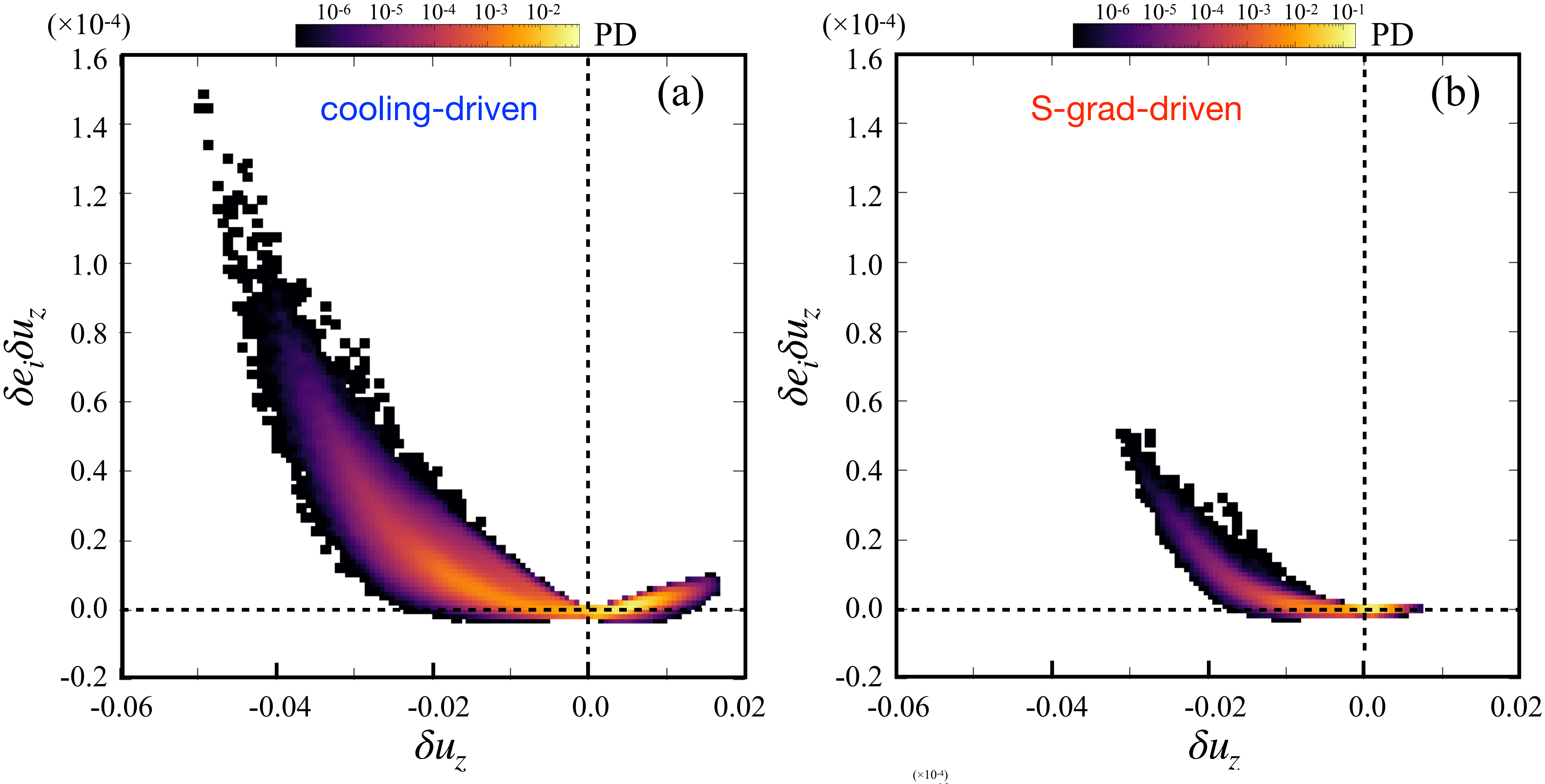

- Probability density is also different between models.
  - In the cooling-driven model, the faster downflow component transports more energy.
  - scaling law :

$$\delta u_z \delta e_i \propto |\delta u_z|^3$$

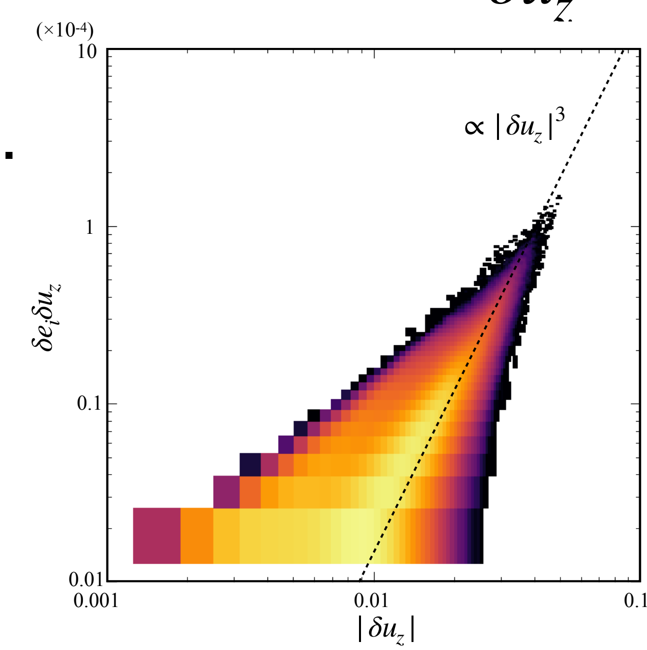

The impact of the convection mode on turbulent transport properties

Is there any difference in the turbulent energy flux $\langle \delta u_z \delta e_i \rangle$?

Yokoi, YM+23, YM+25

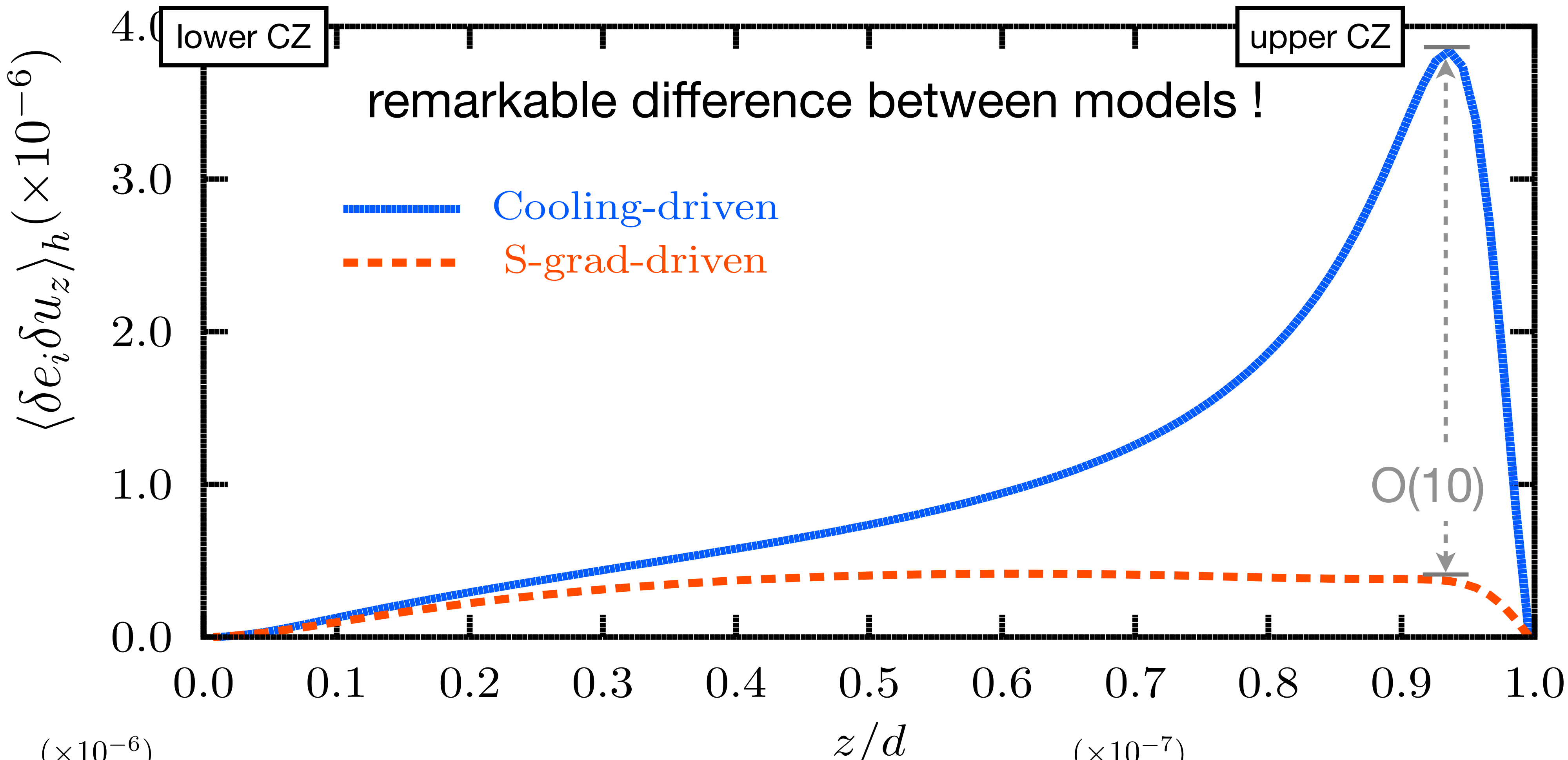

comparison with theoretical prediction

GD model :

$$\delta u_z \delta e_i \sim \kappa_{\mathrm{E}} \frac{\partial e_i}{\partial z},$$

where

$$\kappa_{\mathrm{E}} = \sqrt{\langle \delta u_z^2 \rangle}\ l$$

the box height L_z is chosen as the typical size of the eddies l.

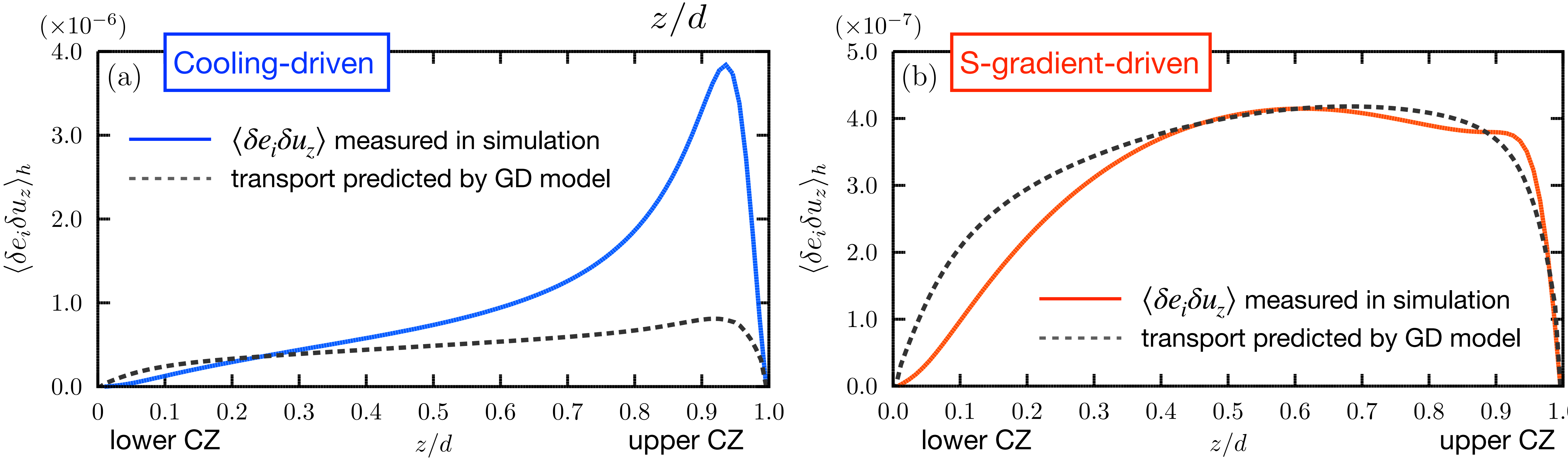

$\langle \delta u_z \delta e_i \rangle$ for the SD model is GD-type, but that for the CD model is far from the GD-type.

Averaging method to extract the non-equilibrium effect

Main difference btw cooling-driven and S-grad-driven models: stochastic downflow plume

(non-equilibrium process)

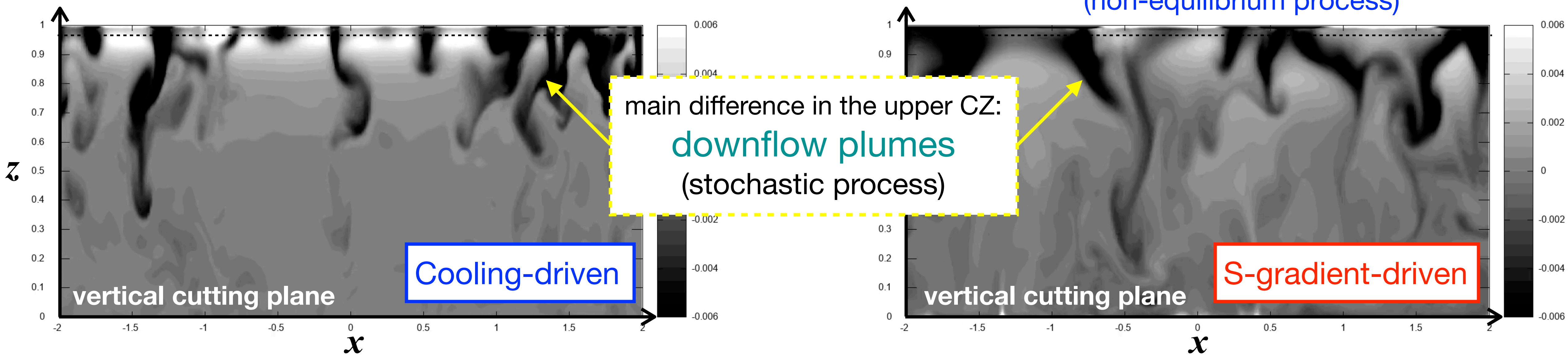

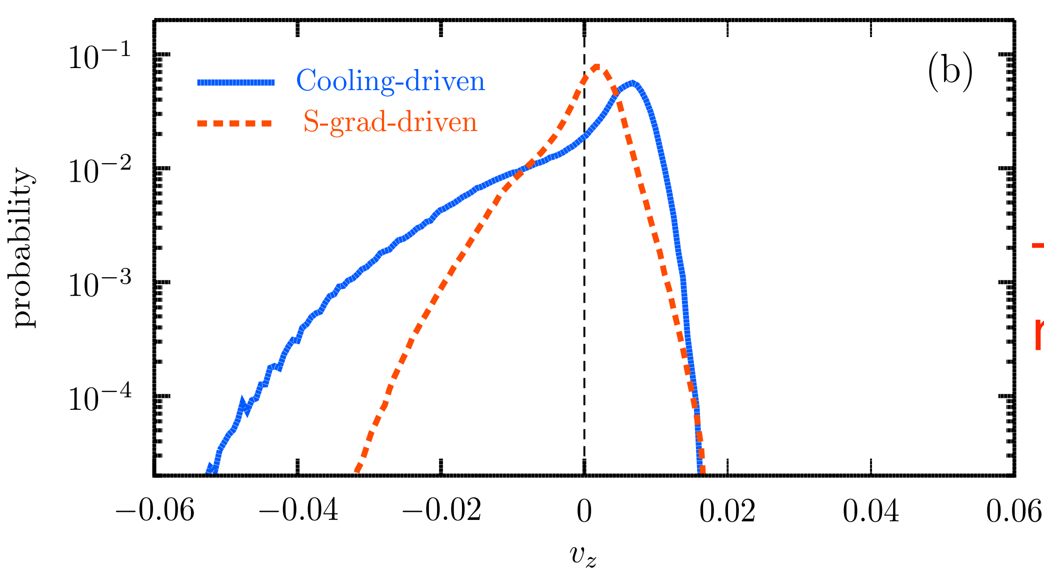

- Conventional GD model cannot adequately describe the non-equilibrium process in the cooling-driven convection.
- How can we implement it to the transport model ?

To gain insights to answer this question, we developed a new method for extracting the key non-equilibrium component.

Time-space double averaging (TSDA) method:

(see Yokoi, YM, Takiwaki 22, MNRAS for details)

A field quantity f is decomposed into three parts (overbar denotes time-average, $\langle \cdot \rangle$ denotes spatial average):

$$f = \langle \bar{f} \rangle + f' \qquad \text{(mean + fluctuation : usual decomposition)}$$

$$= \langle \bar{f} \rangle + \tilde{f} + f'' \qquad \text{(mean + spatially coherent fluctuation + incoherent (random) fluctuation)}$$

with $$\bar{f} = \langle \bar{f} \rangle + \tilde{f} \qquad \text{(time average = spatial average + deviation from the spatial average)}$$

By varying the time window applying for averaging the simulation data, we can extract the information of spatially coherent fluctuation like as downflow plumes.

Insights from the TSDA method

(= stochastic donwflow plume)

With TSDA, we can see the contribution of the coherent fluctuation to the time-average of u_z :

- Vertical profile of $\tilde{u}_z$ (RMS) as a coherent fluctuation of the vertical velocity for two models :

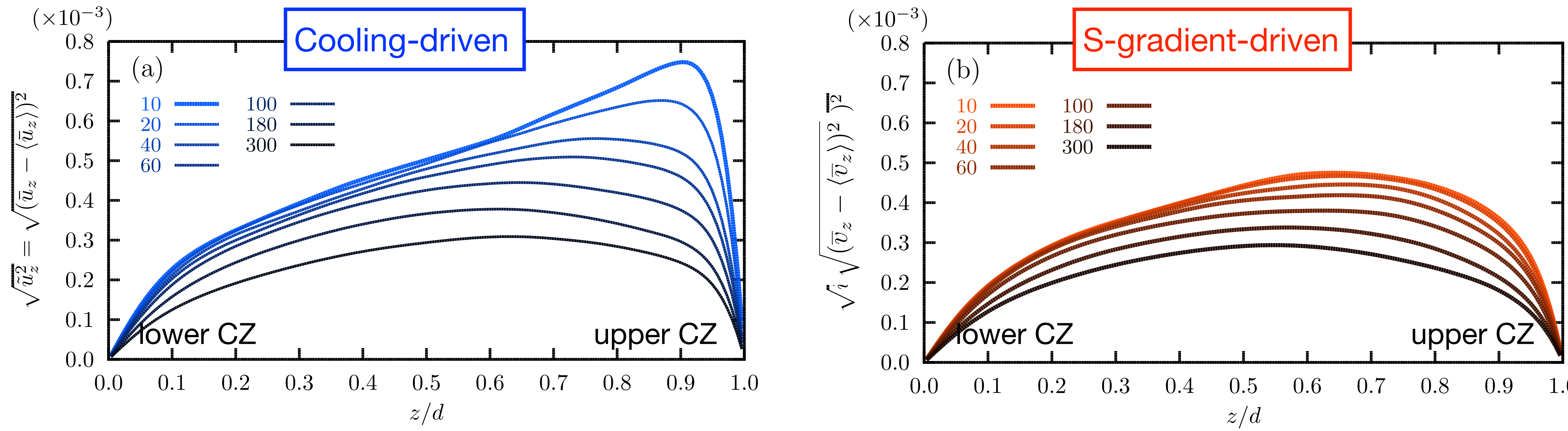

- RMS of $\tilde{u}_z$, i.e., $\sqrt{\tilde{u}_z^2} = \sqrt{(\bar{u}_z - \langle \bar{u}_z \rangle)^2}$ depends on the averaging time especially in the cooling-driven model:

  - The amplitude of the coherent fluctuation (i.e., plume motion) has an eminent peak near the CZ surface when taking short-time average.

    → The peak is at the same place as the strong peak of the turbulent energy flux, implying that the spatial distribution of it is determined by the coherent component of the fluctuation.

  - As the averaging time increases, the amplitude of $\tilde{u}_z$ becomes smaller especially in the upper CZ and finally the spatial profile becomes similar to the one in the S-gradient driven model.
    (when setting the averaging time sufficiently long (than the life time of the plume), they are smeared out)

    → This clearly shows that the characteristics of the cooling-driven convection related to plume motions can be described by the coherent component of the fluctuating motion.

$\boxed{\text{$\tilde{u}_z$ is the key for describing the contribution of the plume motion to the transport and the modification to the transport model.}}$

Modification to the Gradient Diffusion model

Yokoi, YM+23, YM+25

Enhancement of $\langle \delta u_z \delta e_i \rangle$ in the CD model can be well-explained by modified GD model with plume's contributions

$$\delta u_z \delta e_i \sim \kappa_\mathrm{E} \frac{\partial e_i}{\partial z},$$

with $\kappa_\mathrm{E} = \sqrt{\langle \delta u_z^2 \rangle}\ l$

conventional eddy diffusivity

(conventional GD model)

$$\delta u_z \delta e_i \sim \kappa_\mathrm{NE} \frac{\partial e_i}{\partial z},$$

with $\kappa_\mathrm{NE} = \kappa_\mathrm{E} \left[1 - C \langle \rho \rangle^{-1/3} \left\langle (\tilde{\boldsymbol{u}} \cdot \nabla) \overline{\boldsymbol{u}'^2} \right\rangle \right]$

correction due to the non-equilibrium process

(C : arbitrary parameter)

(modified GD model with non-equilibrium plume effect)

$\langle \delta u_z \delta e_i \rangle$

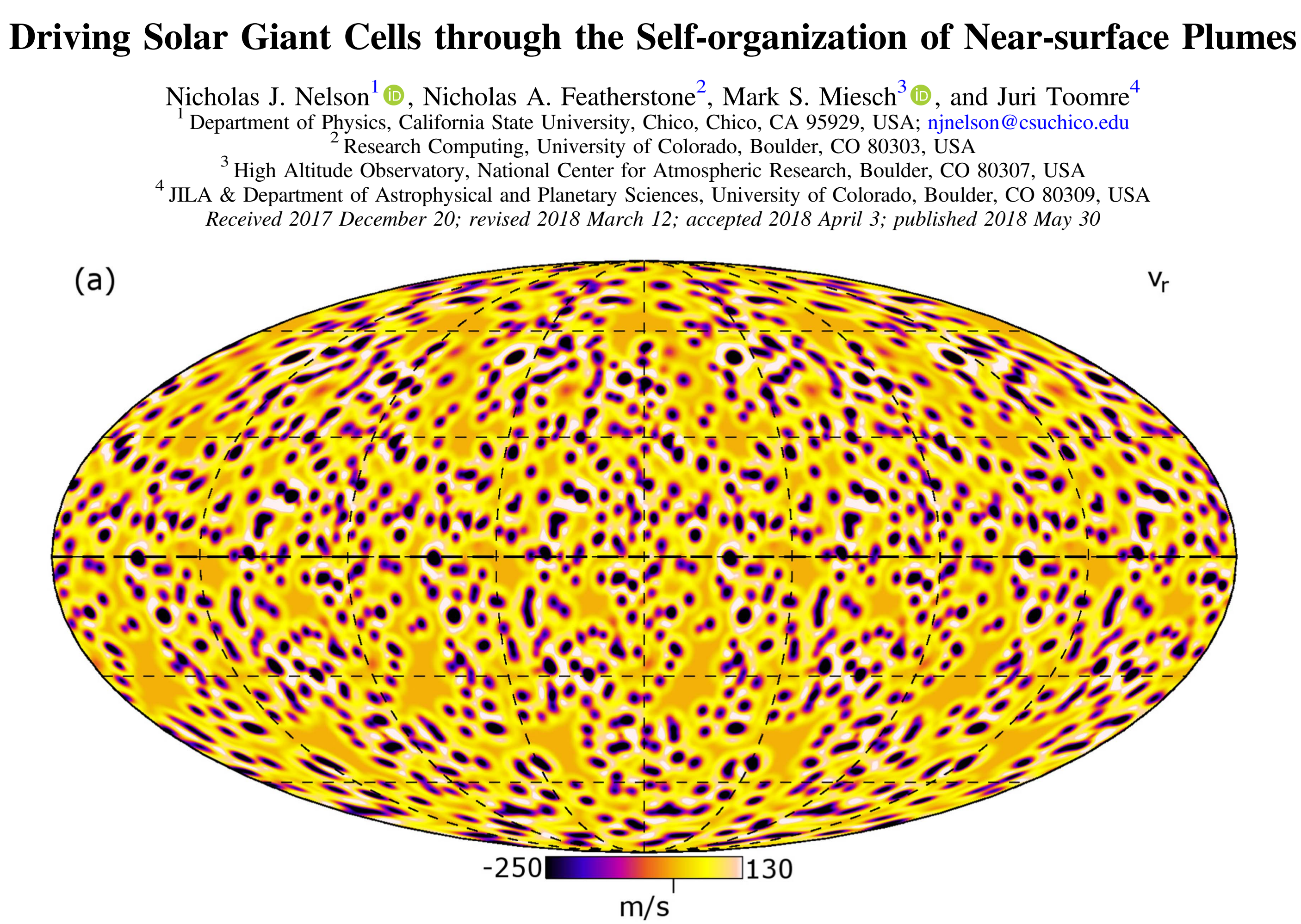

influence of the plume is studied in the HD simulation, but not MHD

oach can no longer be applied.
ocesses.

Then, what will happen to

α (and other dynamo coeff.)

in such a CD situation ????

How does the MHD dynamo change its properties under the CD convection ?

Global MHD dynamo under the cooling-driven convection should be studied to bridge the gap between models and obs.

Discussion ① penetration depth of downflow plume

Experiment : penetration depth of the plume seems to depend on Pr : (YM in prep.)

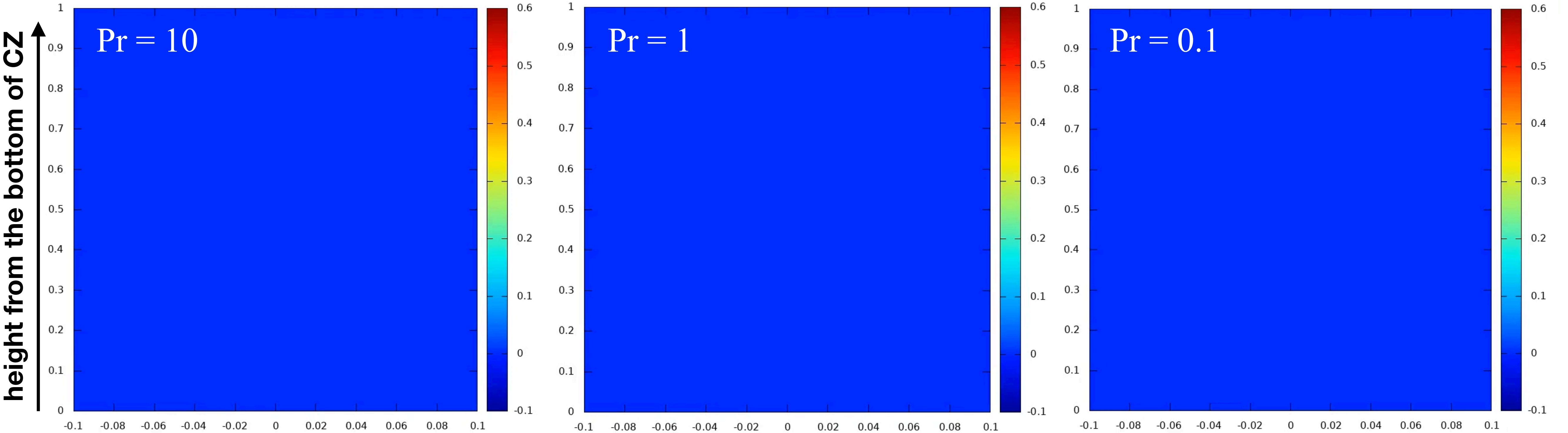

In the Sun and stars with Pr ≪ 1, a lot of plume may penetrate the entire CZ (like Spruit's concept)

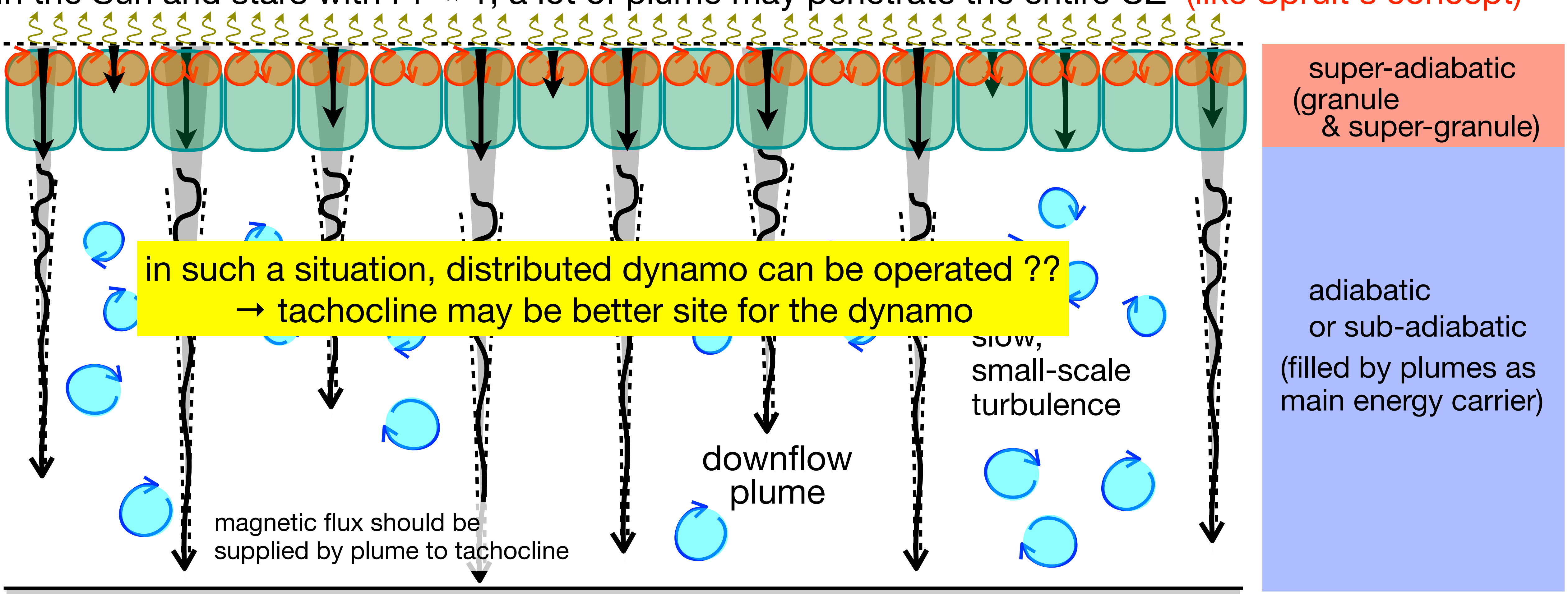

See, Bekki-san's talk in this session about the adiabaticity of the CZ deduced from the analysis of inertial modes.

Discussion ② impact of plume on the dynamo in M-dwarfs

Lx-Ro relationship (Wright & Drake 2016, see Wright+11)

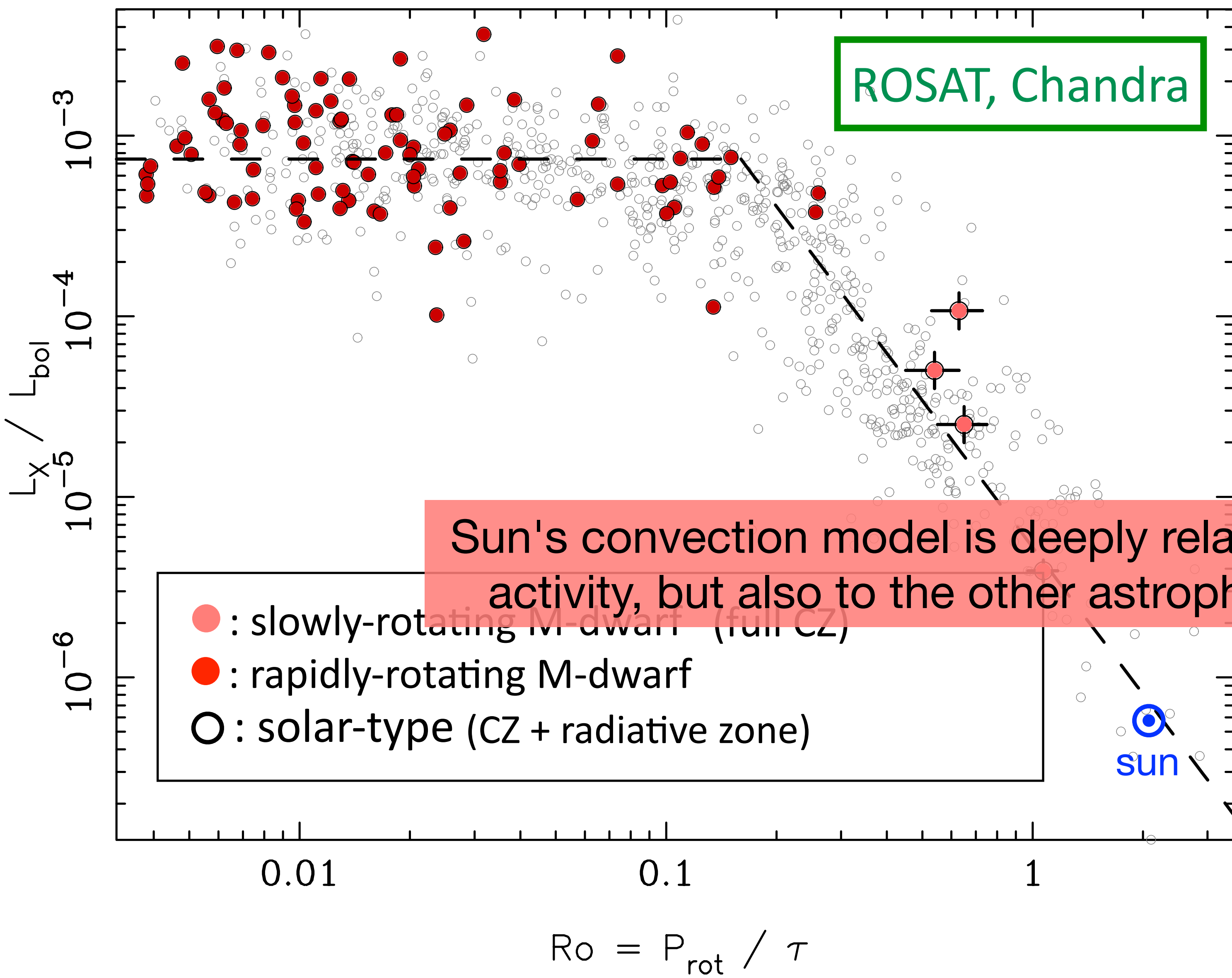

Sun's convection model is deeply related not only to solar/stellar activity, but also to the other astrophysical plasma dynamics.

- Lx : the indicator of the magnetic activity
- Regardless the internal structure, the Lx-Ro relationship is similar.

→ similar dynamo mechanism works in F,G,K and M

→ distributed dynamo should be that !
(because there should not be tachocline in M-dwarfs)

But, if the convection is cooling-driven,

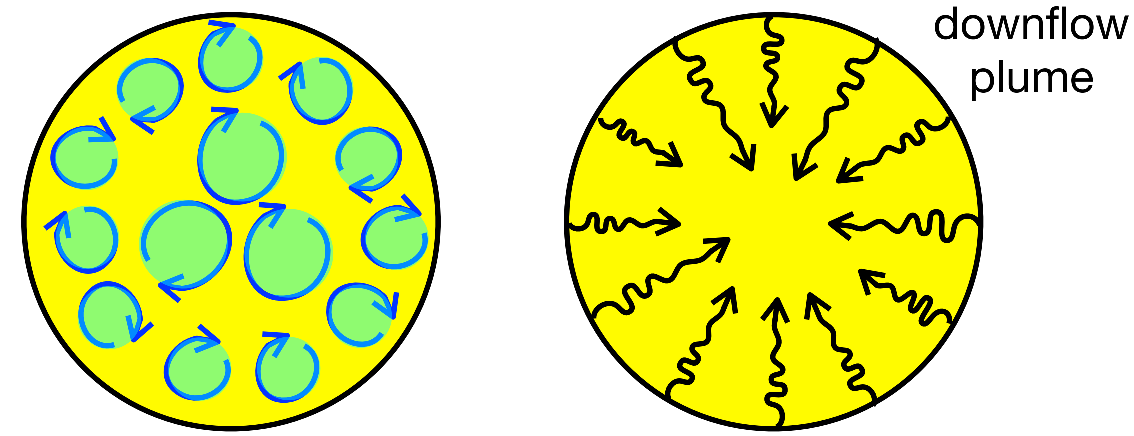

No tachocline

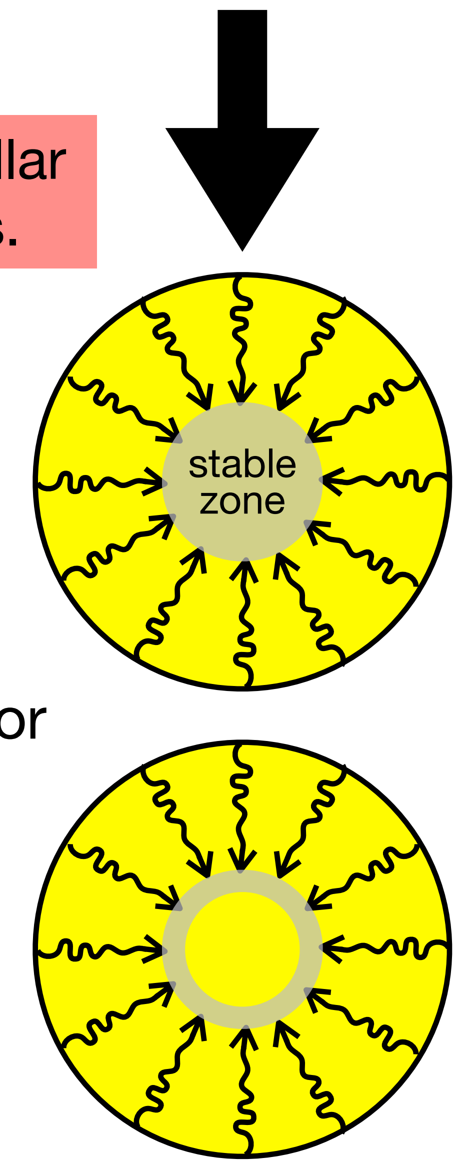

weekly
sub-adiabatic core

or

weekly
sub-adiabatic shell

just a speculation

tachocline-like
layer may exist ??

2種類の熱対流モデルを観測的に区別する方法はあるか？:トポロジカルデータ解析による推定

観測データから太陽熱対流の特徴量を抽出する

(エントロピー勾配駆動型と冷却駆動型、太陽の熱対流モデルとしてどちらが相応しいか)

Method : トポロジカルデータ解析（Topological Data Analysis：TDA）

- データセット: (1) S-grad-driven (SD), (2)Cooling-driven (CD), (3) Obs. (DKIST & Hinode/SOT)

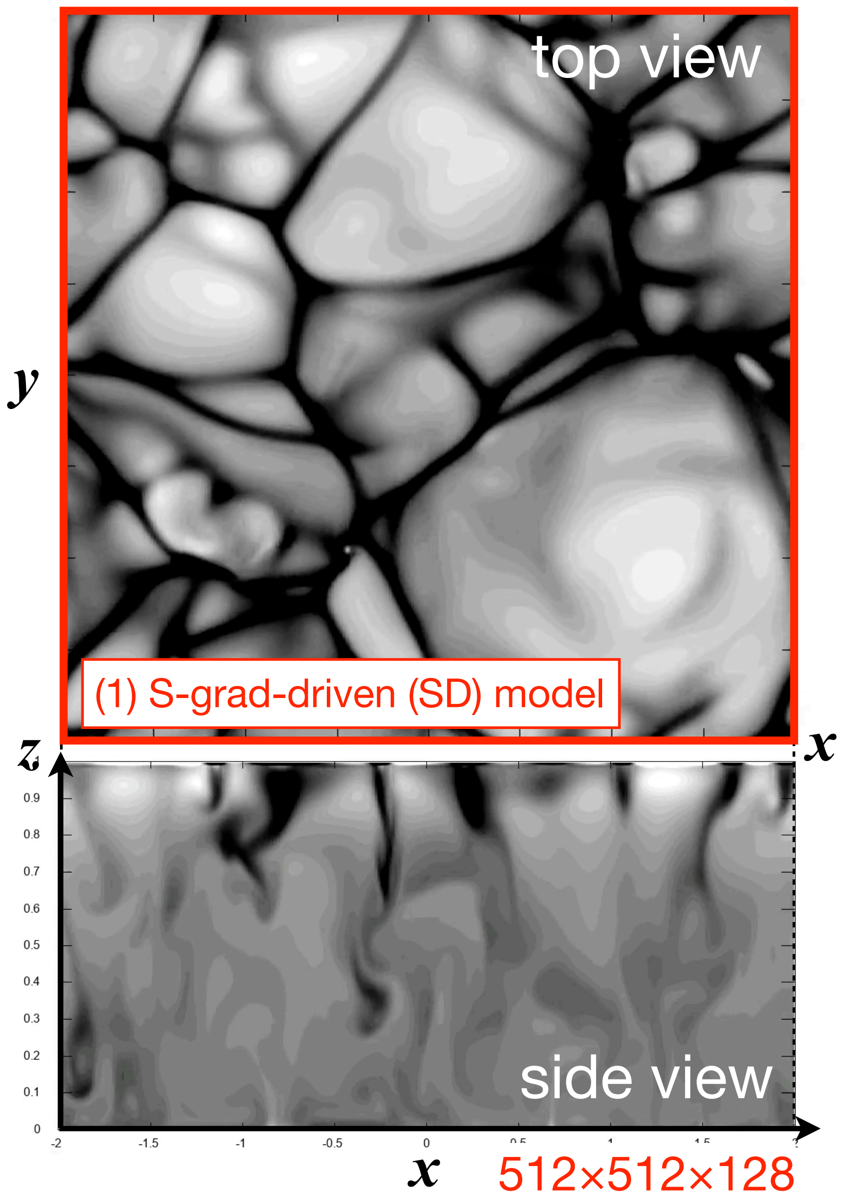

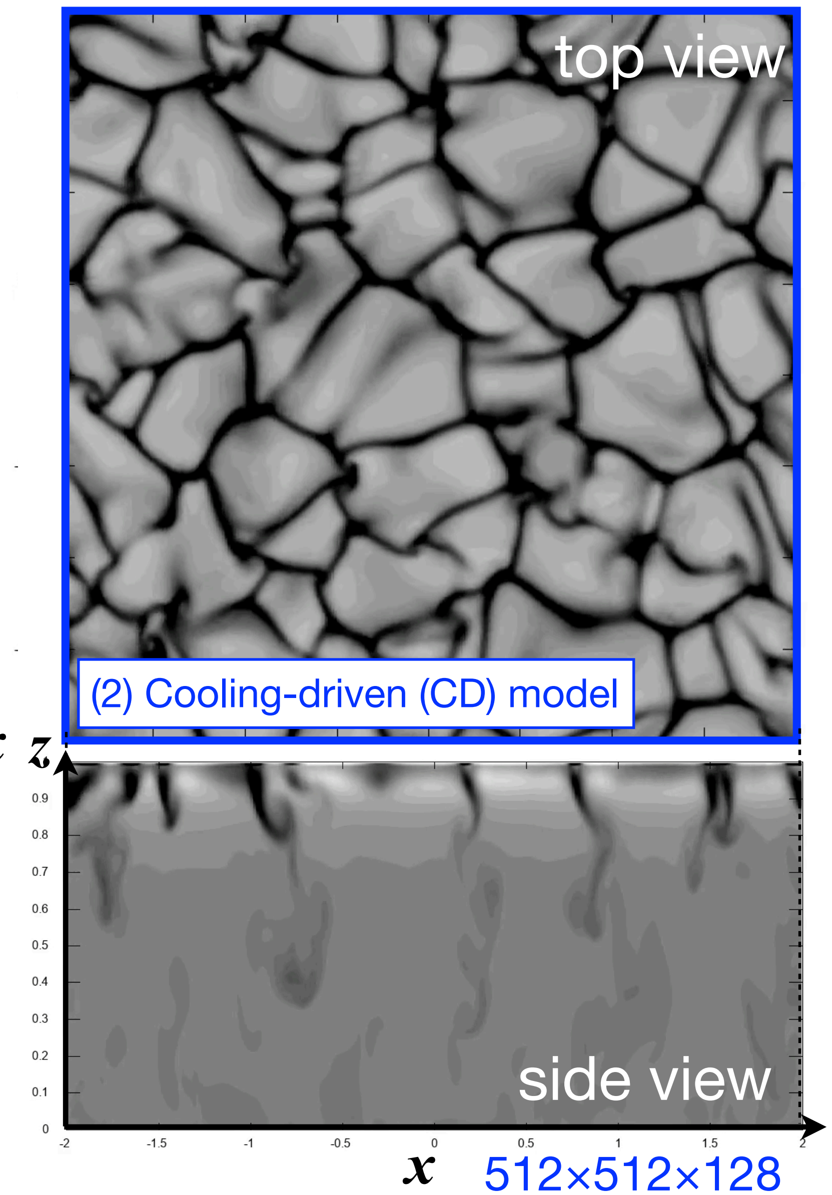

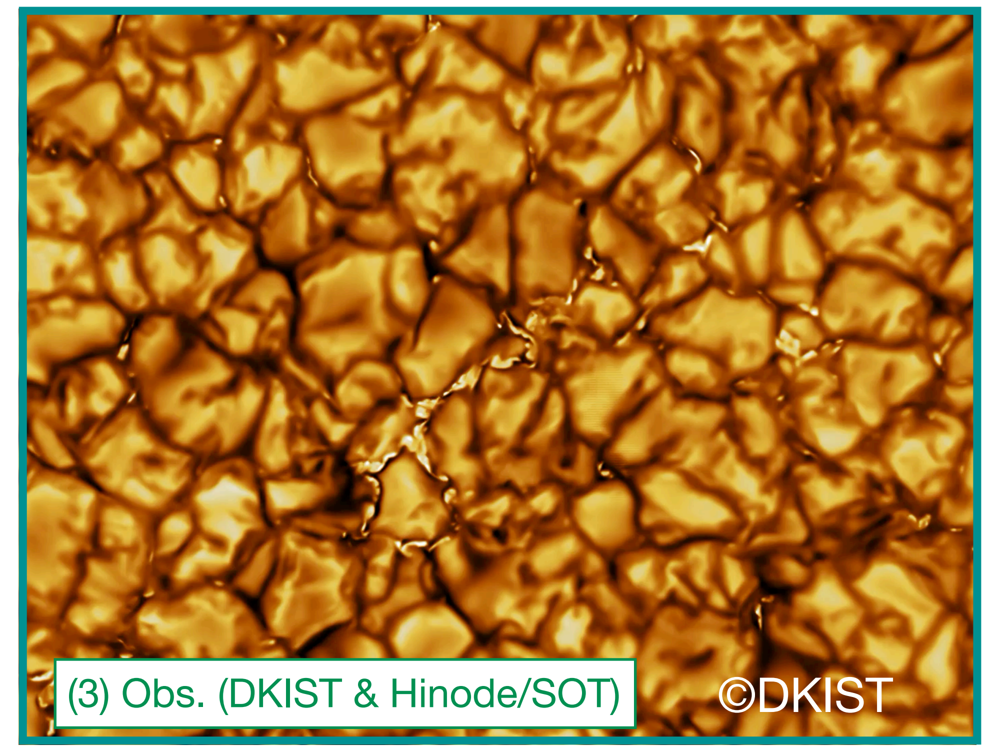

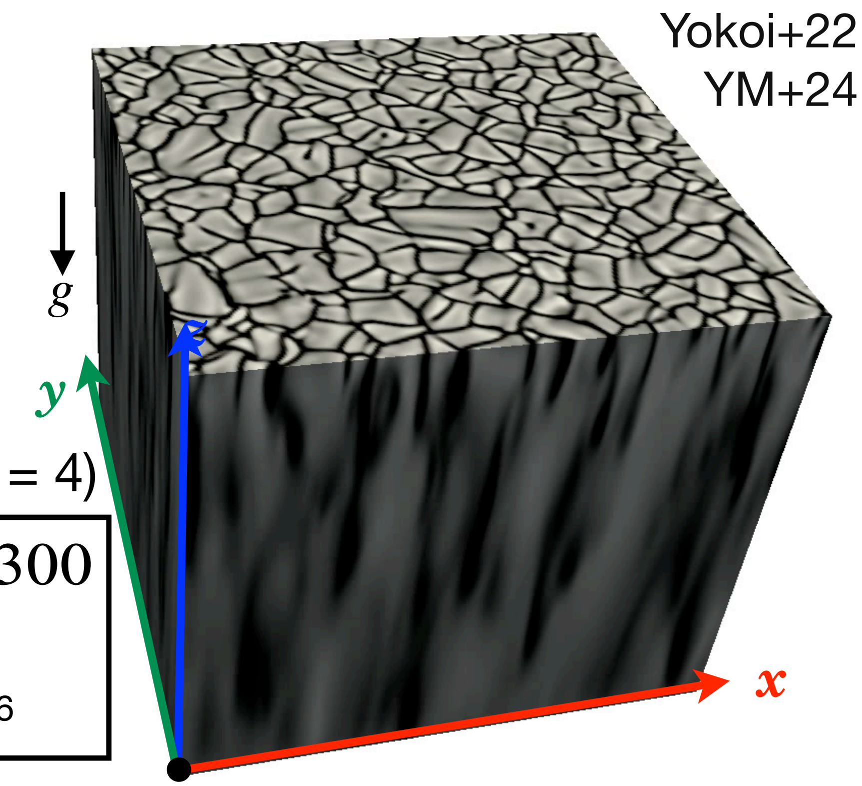

similar to Cossette & Rast (2016)

- Basic eqs：compressible HD eqs【Cartesian box】 ($L_x/L_z = L_y/L_z = 4$)
- polytropic atmosphere with an index m【CZ only】:
  - (1) S-grad-driven : m = 1.495 (whole CZ)
  - (2) Cooling-driven : m = 1.495 (upper 5%) + 1.5 (95%)
  - (Newtonian cooling is imposed on the upper 5% of CZ in the CD)
  - (There is 0.2% difference in the input energy between models)

$\rho_{\mathrm{bottom}}/\rho_{\mathrm{top}} = 300$
Pr = 1.0
Ra = 4.2×10^6

NO rotation

観測データから太陽熱対流の特徴量を抽出する

（エントロピー勾配駆動型と冷却駆動型、太陽の熱対流モデルとしてどちらが相応しいか）

Method : トポロジカルデータ解析（Topological Data Analysis：TDA）

Basic properties of convective motion are common: upflow cells surrounded by downflow networks

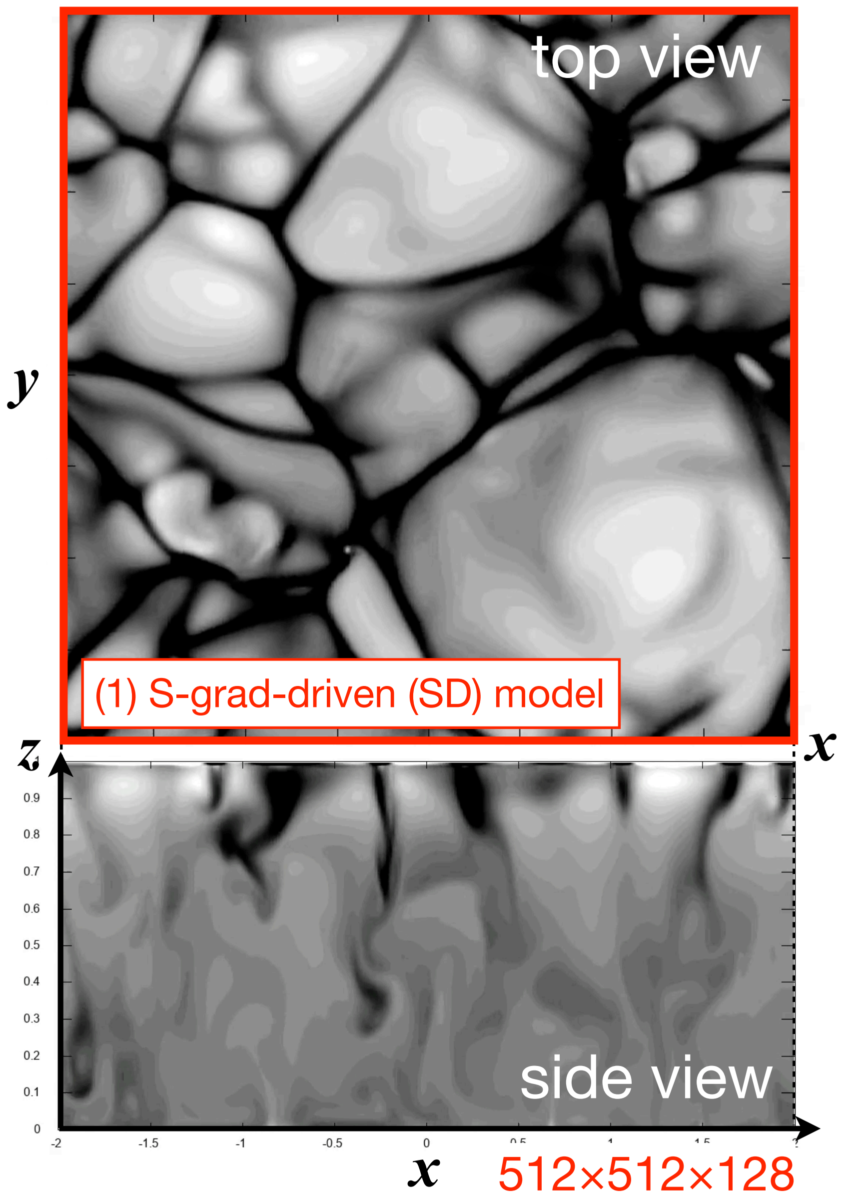

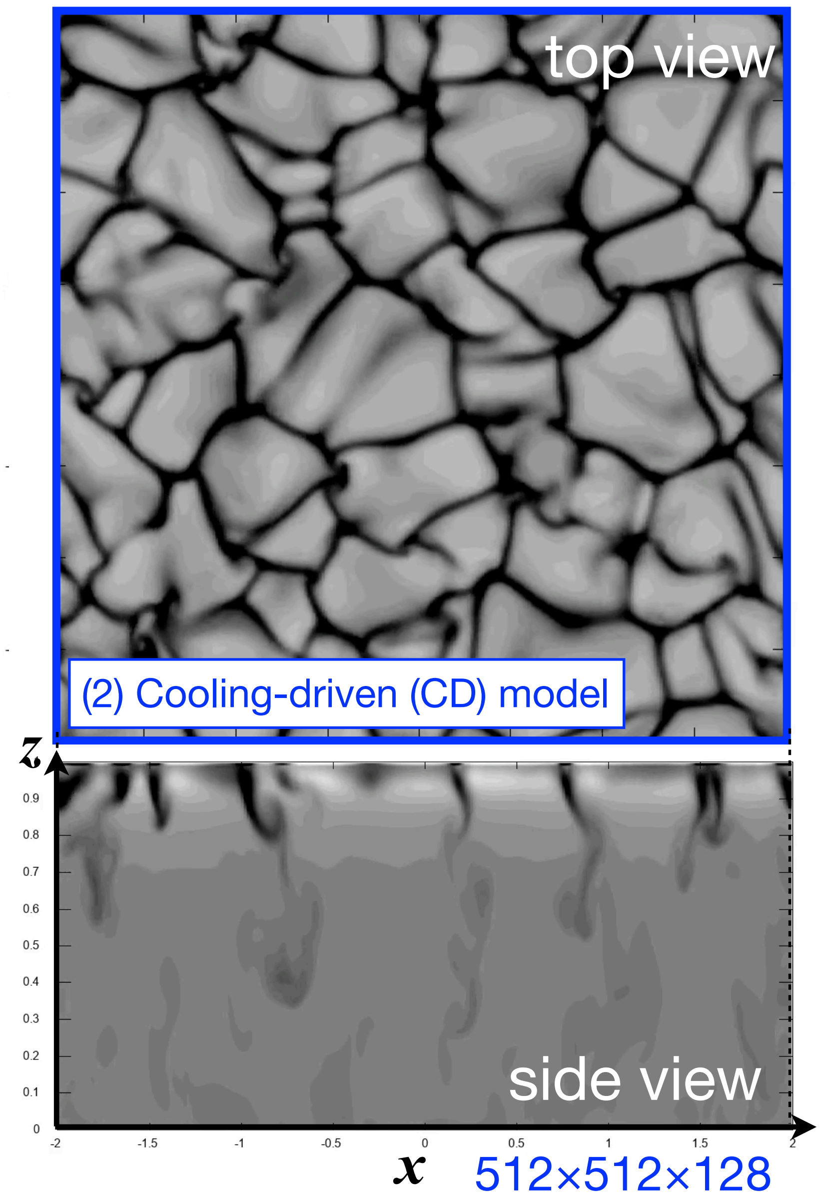

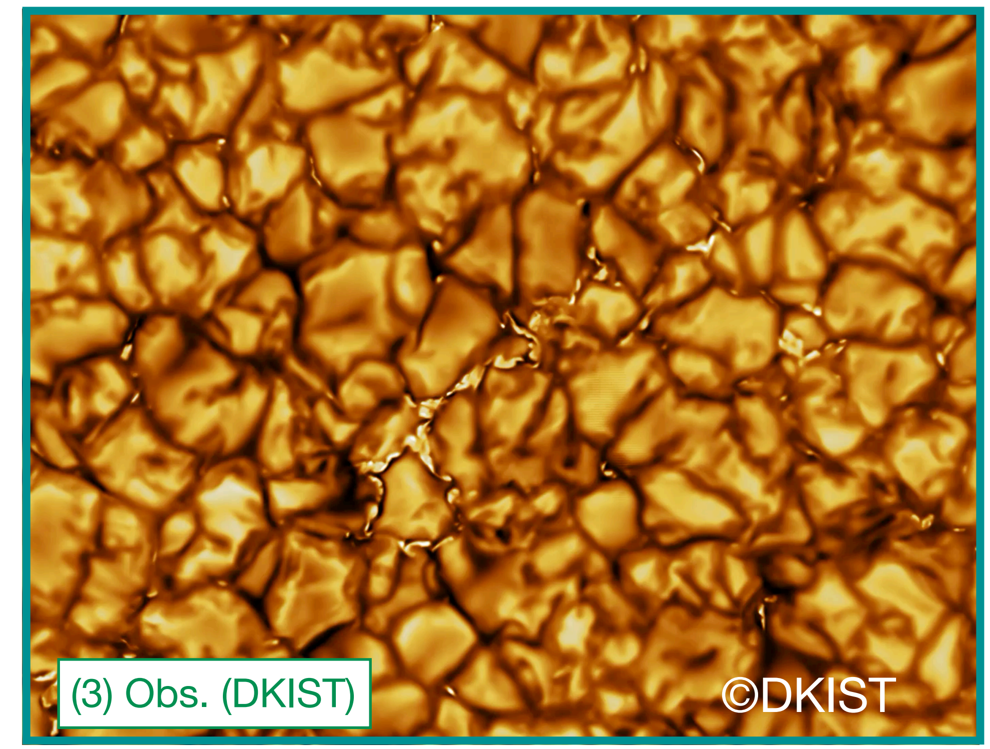

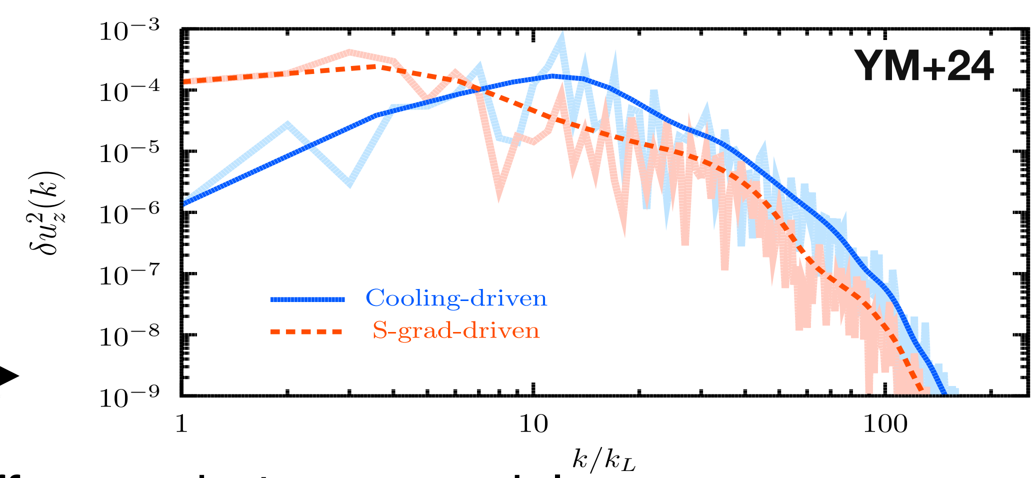

The small deference of the polytropic index cause the structural difference between models.

CD model has a spectrum in which the power is suppressed at the smaller k, similar to sun's conv. spectrum.

- TDA is performed on each data set and compare the results.
  - The topological structures hidden in the varieties of convection data is studied.
  - QUESTION: although the convection patterns are similar between data at a first glance, is there a remarkable difference in the topological property between them ?

で、何をするのか？→データから「穴」の情報を抽出する

- トポロジー：もののつながりを記述する数学の概念

（Topology studies how spaces are connected and how their structure remains unchanged through continuous deformations, focusing on the relationships and connections between points, shapes, and surfaces.）

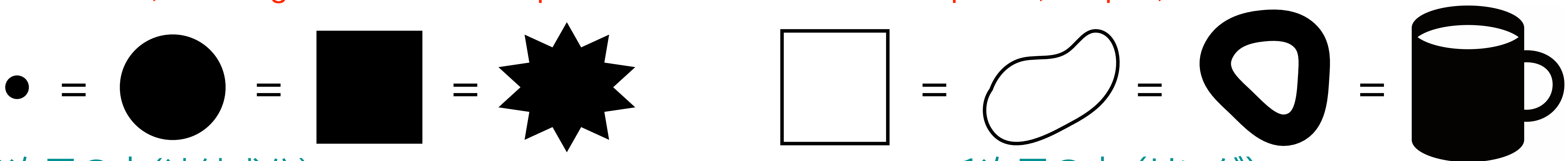

0次元の穴（連結成分）　　1次元の穴（リング）

「穴」（連結成分、リング、空洞）の数を，数学的に計算科学的にどうカウントするか？

- ホモロジー：「穴」の数を数える数学的技法（since Poincaré）

穴は何個見えますか？（ポイントクラウドデータ）？

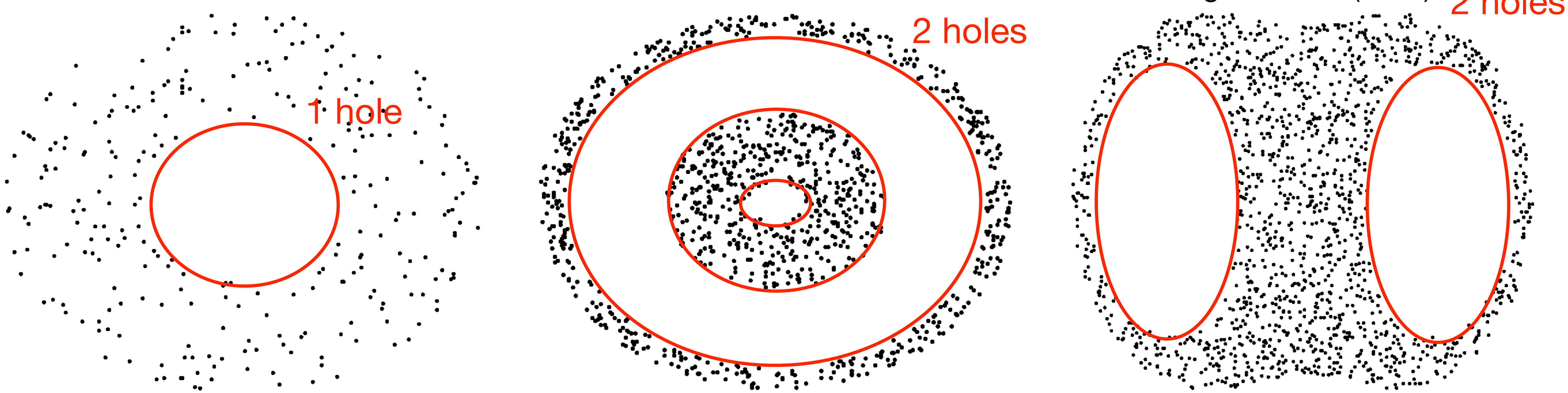

我々は無意識にデータを粗視化して「穴」の存在やそのサイズ、形状を認識できる。
では穴の情報（サイズや形）に関する情報を数学的にどう抜き出すか？

- パーシステントホモロジー (Persistent Homology : PH)（ノイジーなデータから穴の情報を抜き出す方法）

データからトポロジカルな情報を引き出し定量化する新しい手法

（originally proposed by Edelsbrunner et al. (2000), and further developed by many others, such as Carlsson (2005)）

パーシステントホモロジーとパーシステント図（PD）

パーシステントホモロジーでは「穴」をどう捉えるか？：その手法（ポイントクラウドデータの場合）

1. The point cloud data is supposed and given the sphere (radius r) centered around each data point.
2. You increase the radius of the sphere gradually (equivalent to the changing resolution) [~ filtration]
3. By calculating the homology with changing radius at multiple stages, we capture the shape.

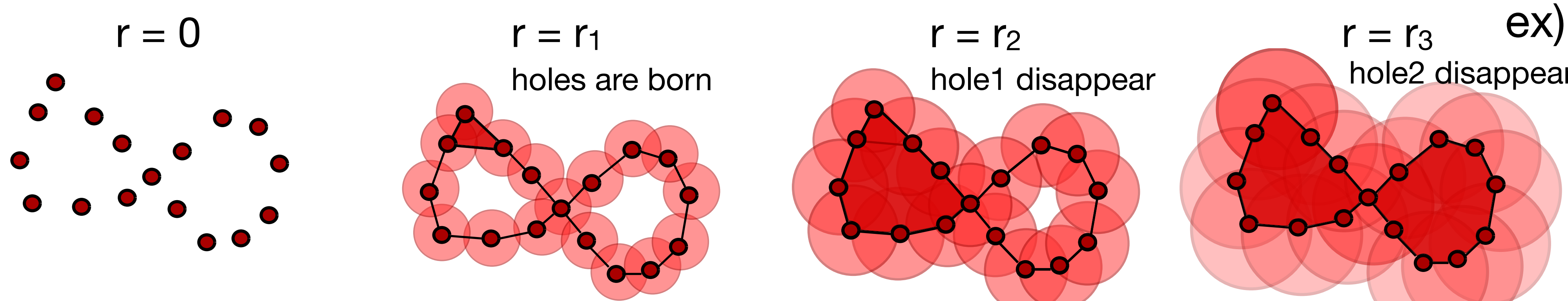

ex) point cloud

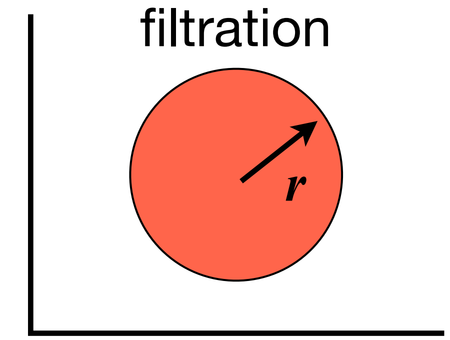

PH: $H_1 = 0$ $H_1 = 2$ $H_1 = 1$ $H_1 = 0$

See, Smith, A.D + 21

H_1 : 1D homology (ring) resolution of data being lower filtration →

(radius of (imaginary) sphere being increased)

「穴」の生成と消滅の半径（半径を次第に大きくする手続:フィルトレーション）がそれぞれの穴の形や構造を特徴づける

∴ The birth and death of the holes are represented as points in a persistence diagram (PD), with *x*=birth_radius and *y*=death_radius and persistence defined as (y – x).

r = 0

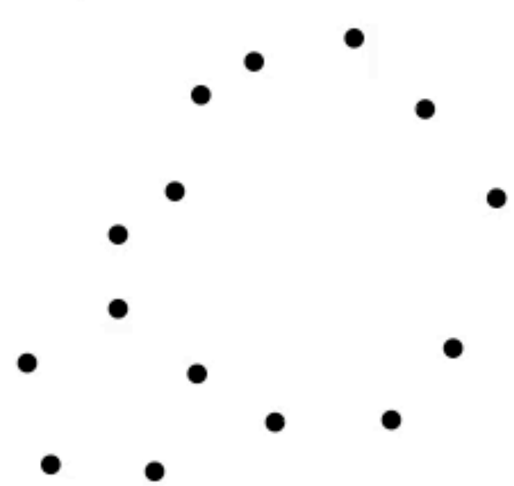

Imagine the sphere centered around each point.
Then, gradually increase the radius of the sphere.

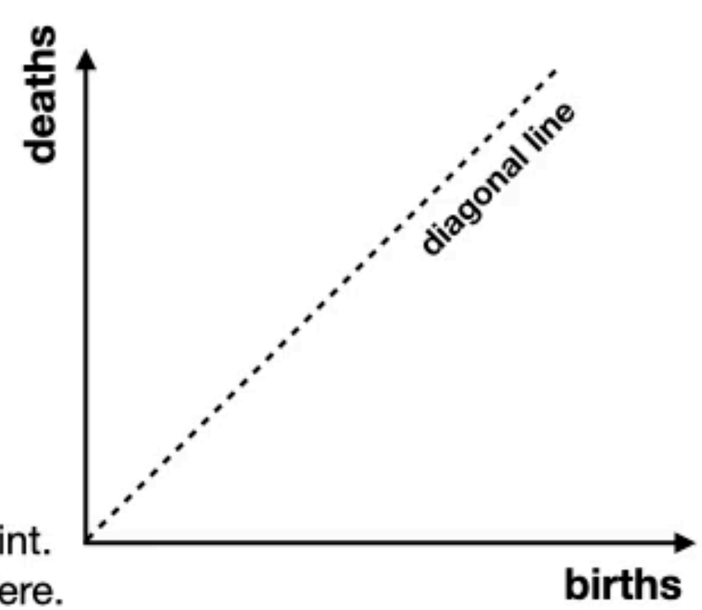

The points around the diagonal line on PD	= noise (short lifetime)

(they don't have important meanings)

The points with longer lifetime (far from DL)	= hole

→ characterizing the shape and structure of data

★ Procedure of TDA:

data → filtration → PD

場の量（グレイスケールイメージ）の場合のパーシステント図

ex) grayscale image (field data such as velocity and temperature)

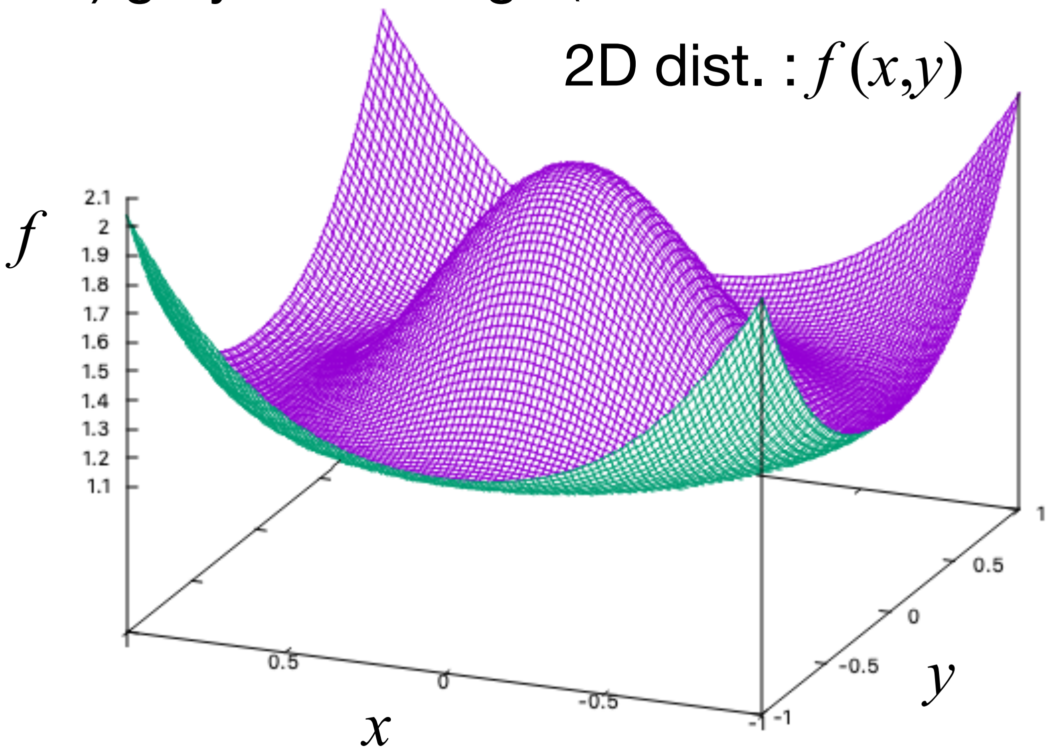

How can we study the topological structure of the field data ?

(What type of filtration is used to extract the topology information?)

→ Level-set method

Instead of changing the radius of a virtual sphere in the case point cloud, we set a threshold value and perform filtration on the image by changing it.

iteration

1. set (change) the threshold value $t = t_i$
2. the region with the value of $f < t_i$ is filled by black
3. calculate the homology and extract the information of hole

   (in this demonstration, "hole" is corresponding to "hill" in data)

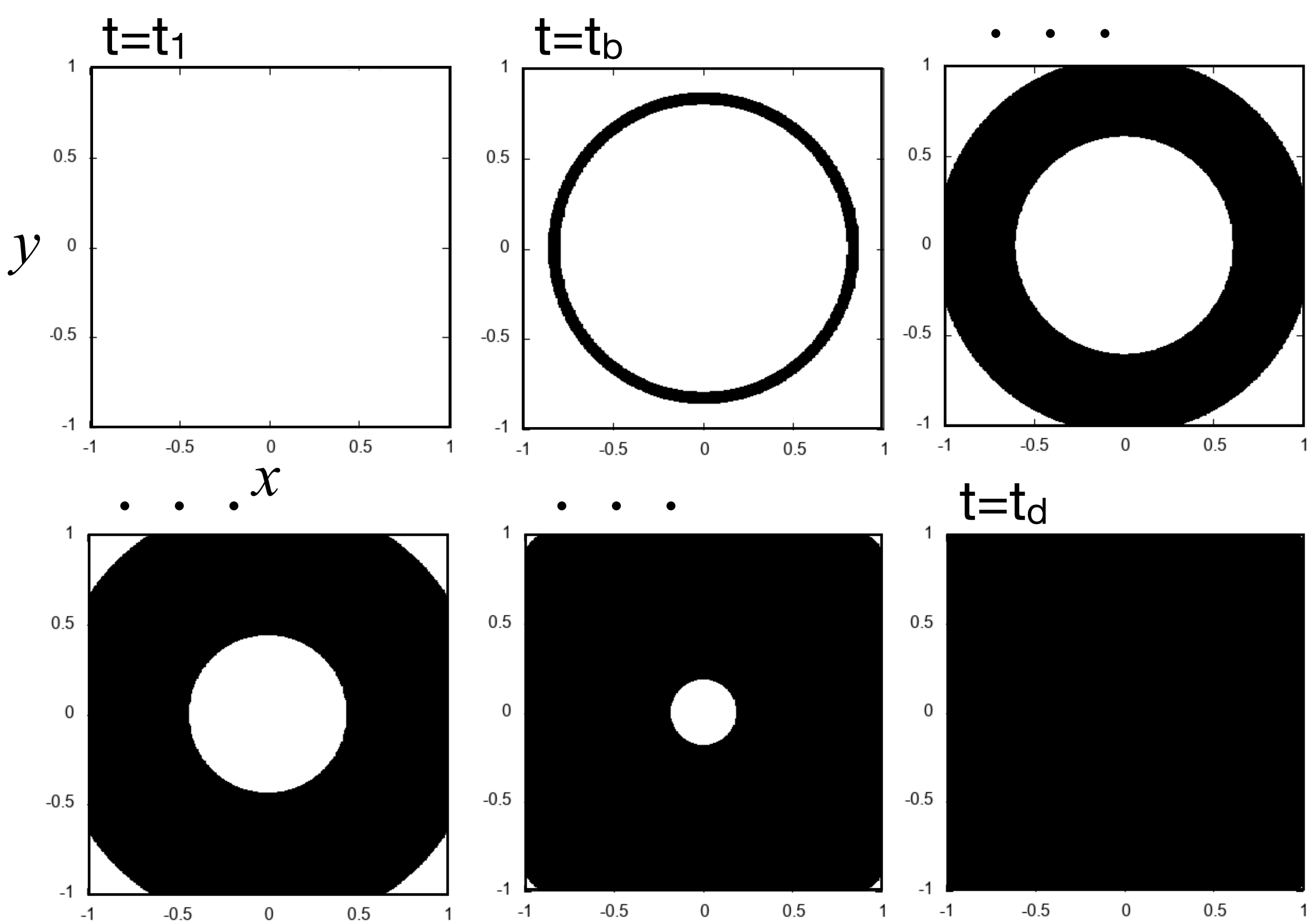

・threshold value when the birth of hole : $t = t_b$

・threshold value when the death of hole : $t = t_d$

birth-death pair, (t_b, t_d), for each hole

→ making PD

(lifetime = t_d - t_b)

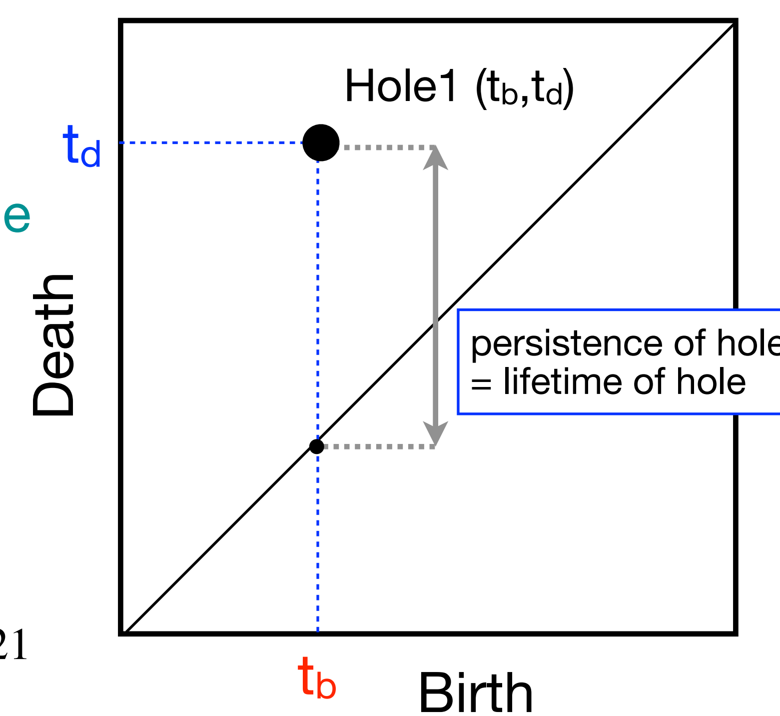

See, e.g., Smith, A.D + 21 for more details

With the TDA, we study the topological structure of the solar convection (focusing of H_1 : ring).

Topological Data Analysis

: application to the solar convection (model and observation)

with GUDHI and Homcloud (python libraries)

https://gudhi.inria.fr/index.html
https://homcloud.dev/index.en.html

Persistent Diagrams for Two Numerical Models

with the data of velocity field (U_z)

We can construct one persistent diagram (PD) from one snapshot data of the velocity distribution at the surface.

①S-grad-driven model (SD) :

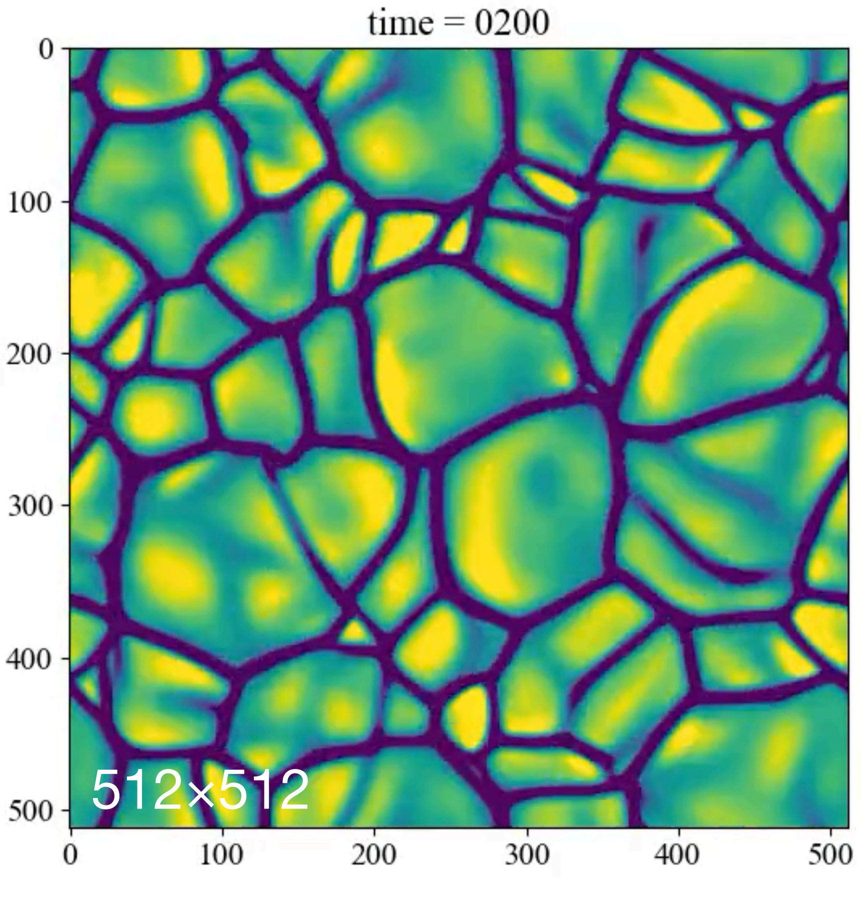

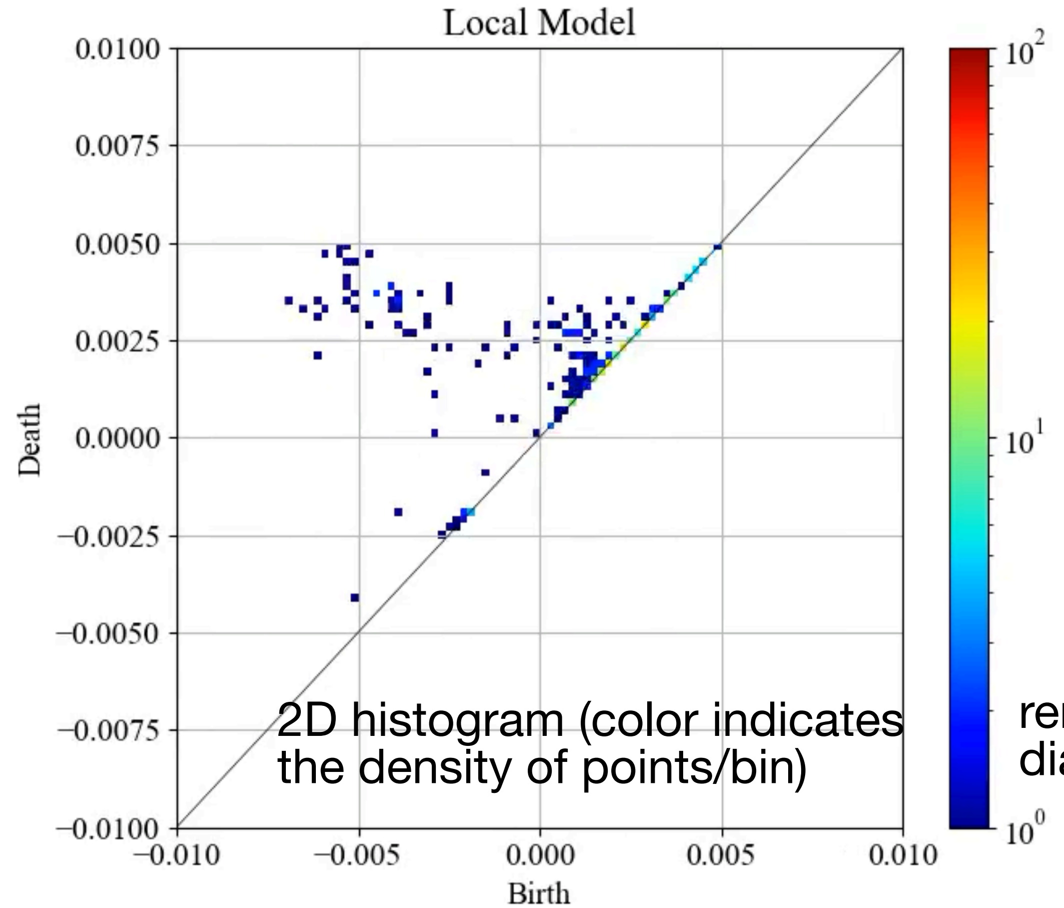

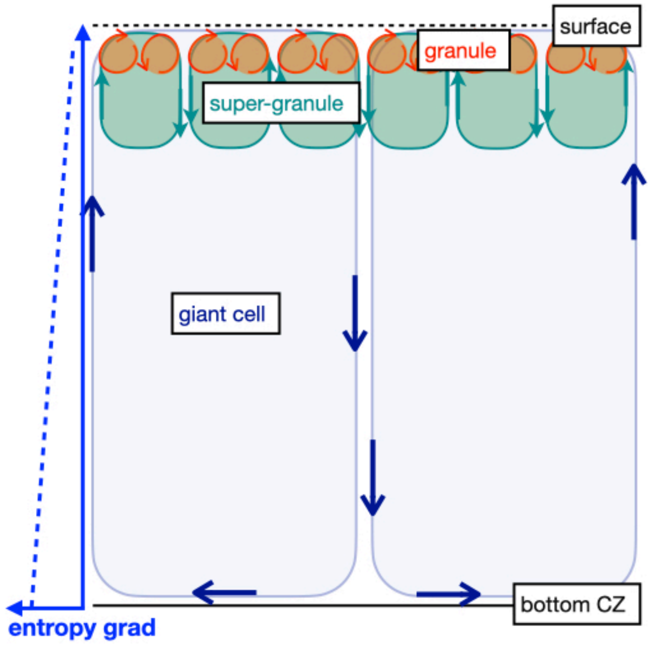

remember that points around the diagonal line are a kind of noise

②Cooling-driven model (CD) :

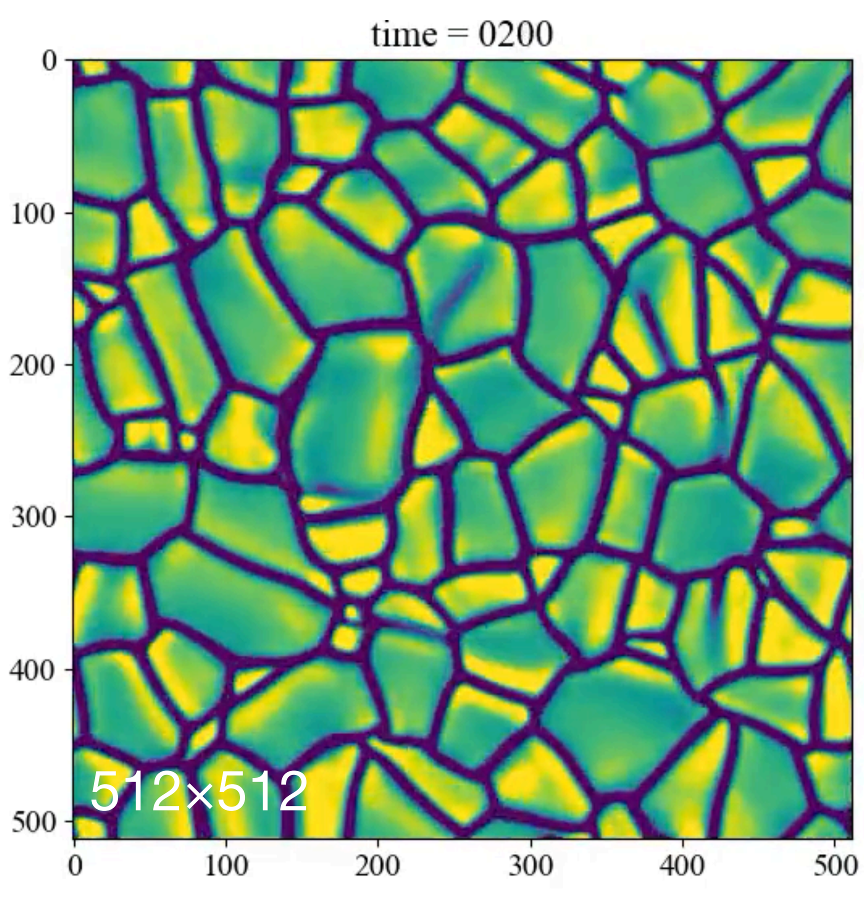

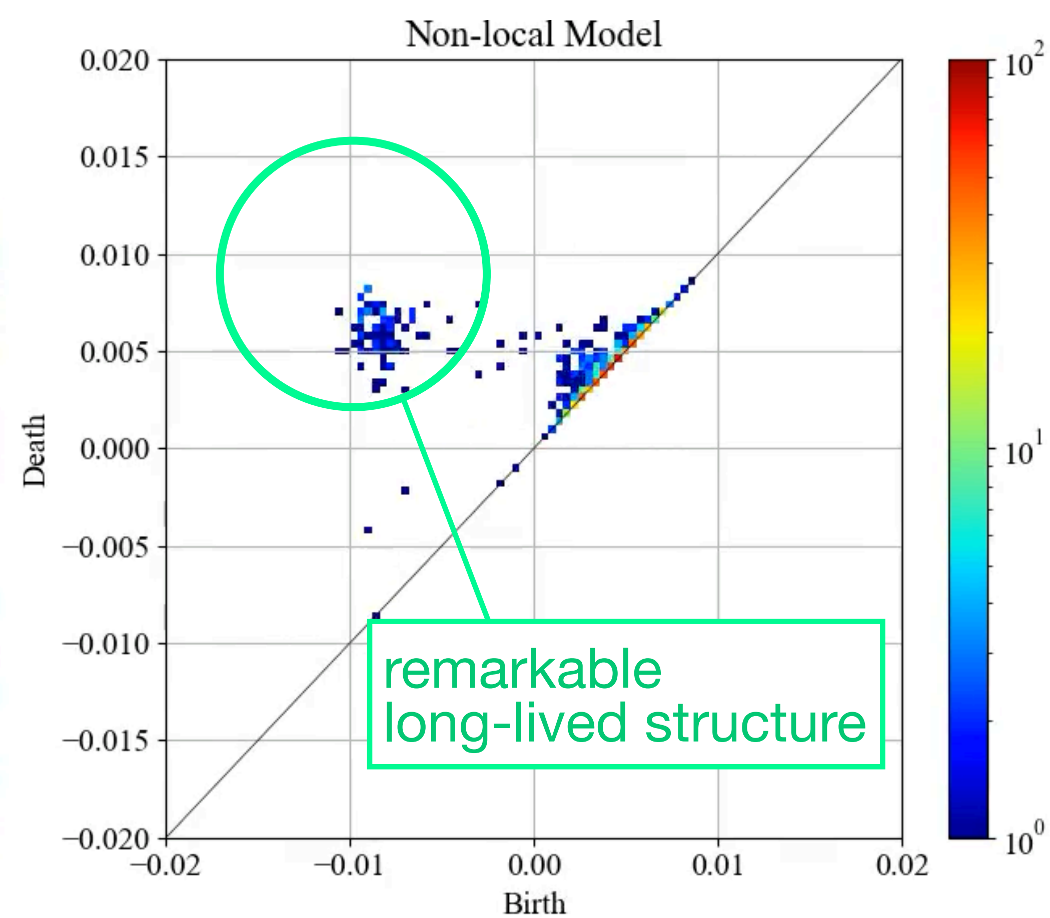

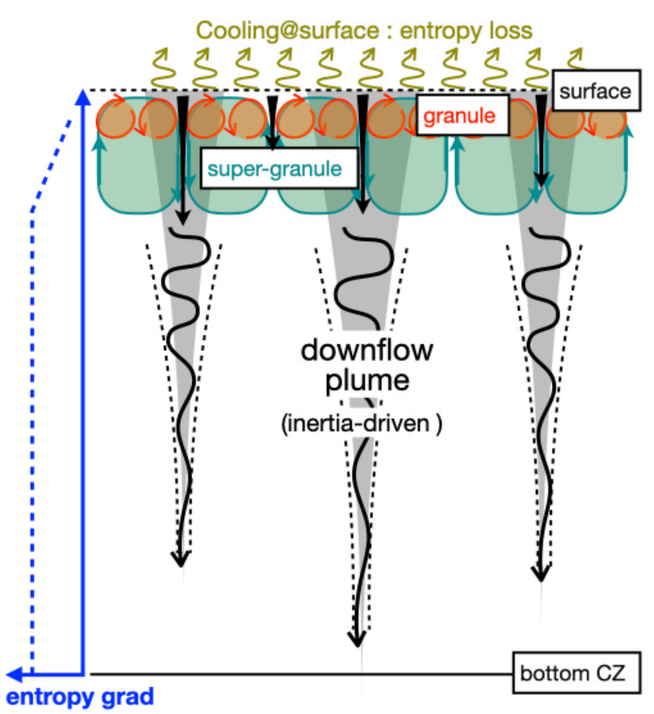

This is a type of "dimensionality reduction" : the distribution in PD = "feature" of thermal convection

Persistent Diagrams for Two Numerical Models

all the sequential data are gathered

Additionally to the PD with Uz, PDs with δT (temperature fluctuation) are also generated :

①S-grad-driven model (SD) :

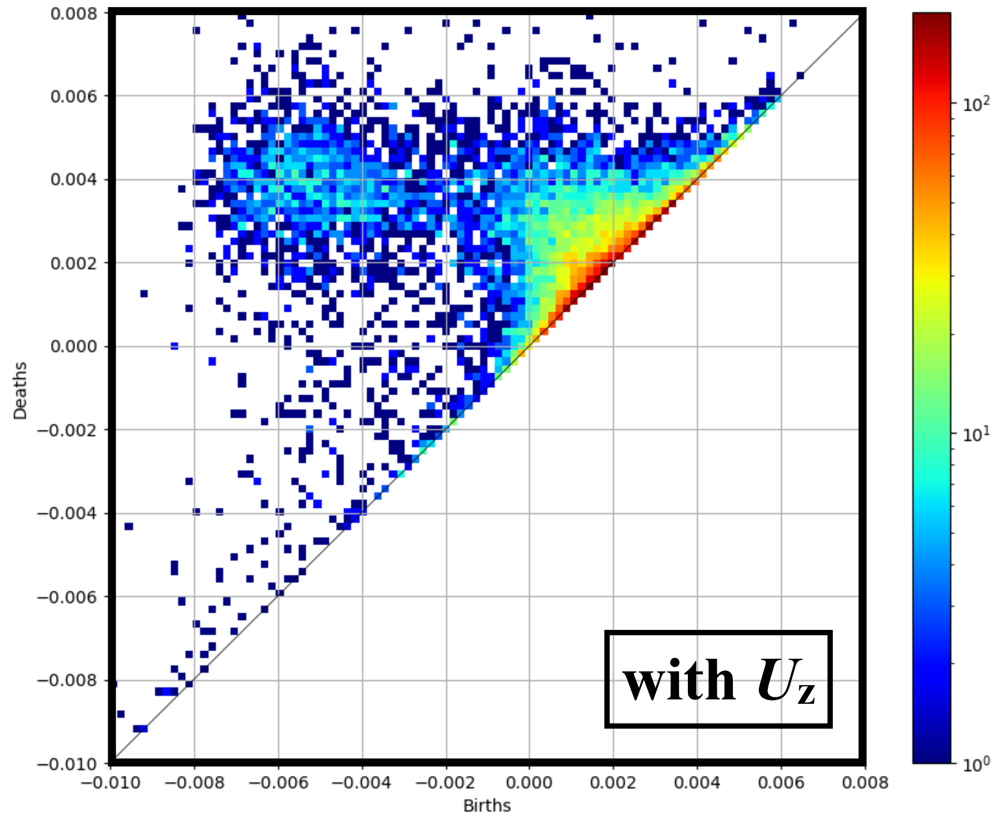

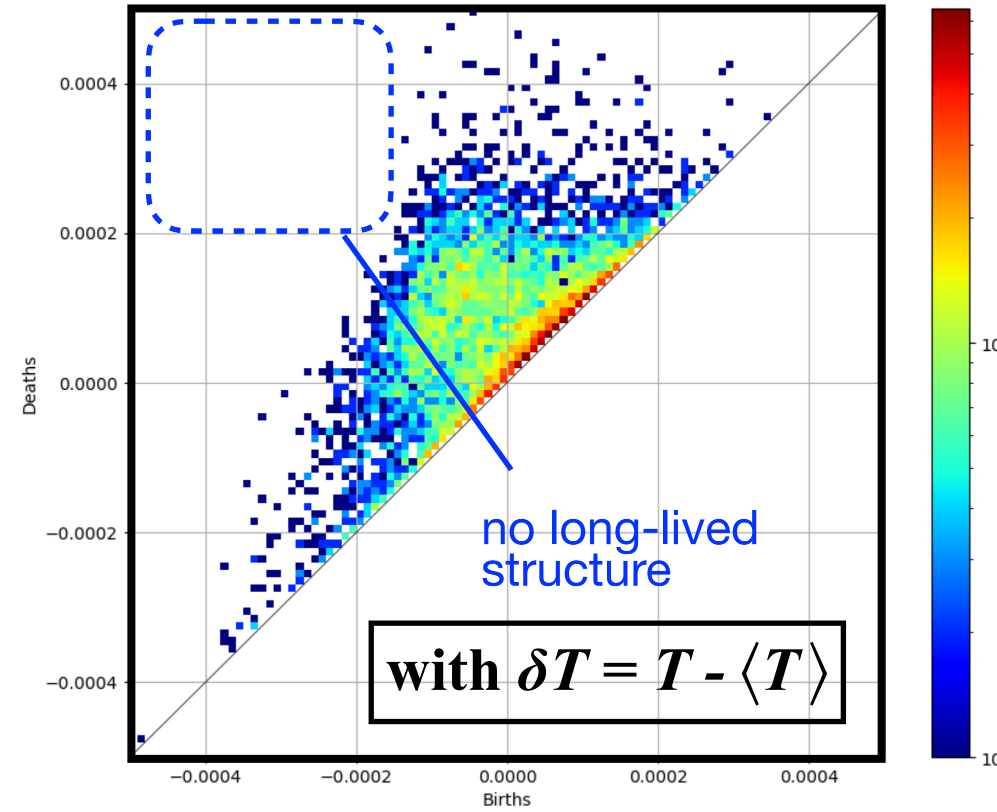

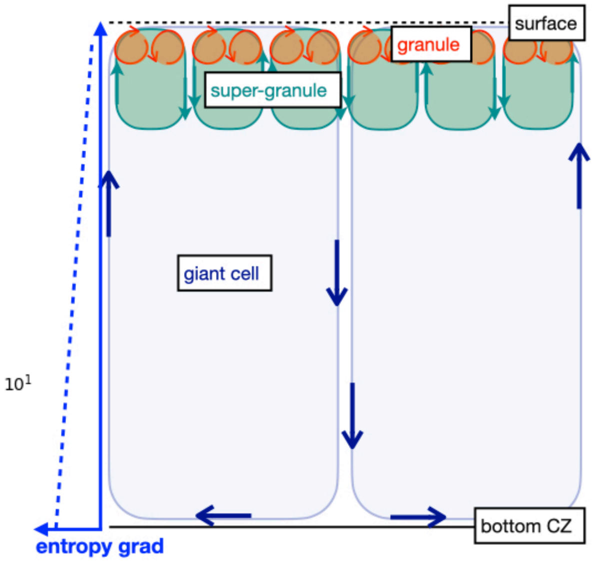

The "peninsula" structure is not remarkable especially on the PD with δT.

②Cooling-driven model (CD) :

"peninsula" structure is remarkable.

"peninsula" is more pronounced

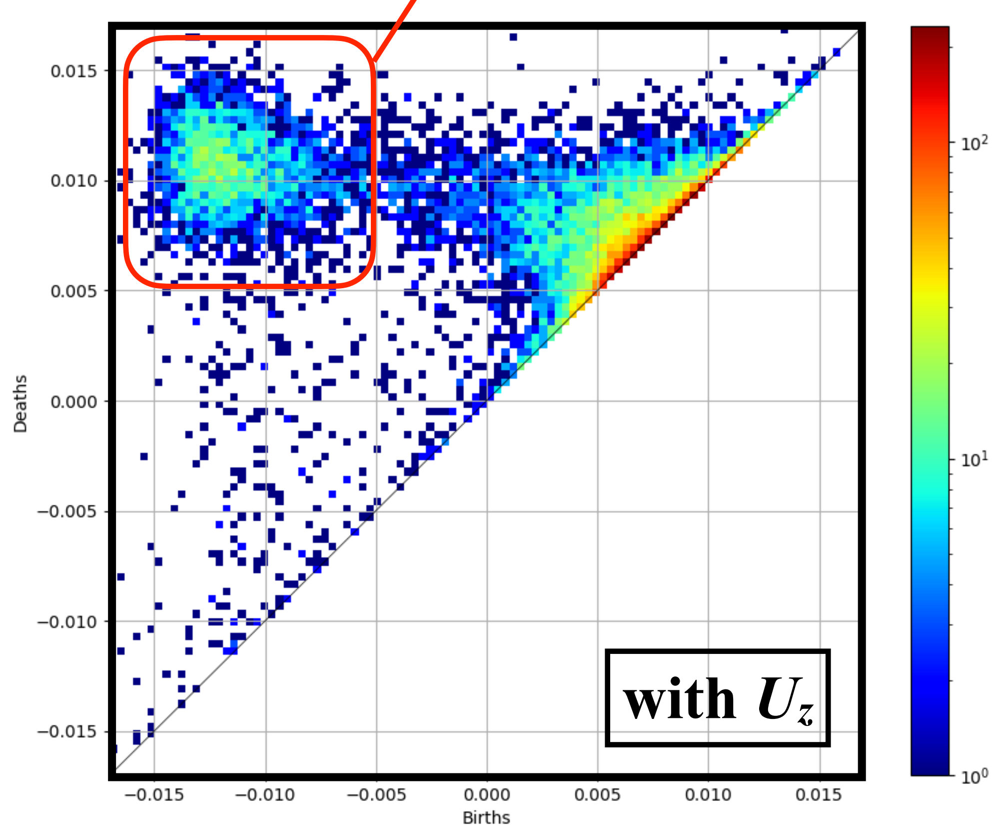

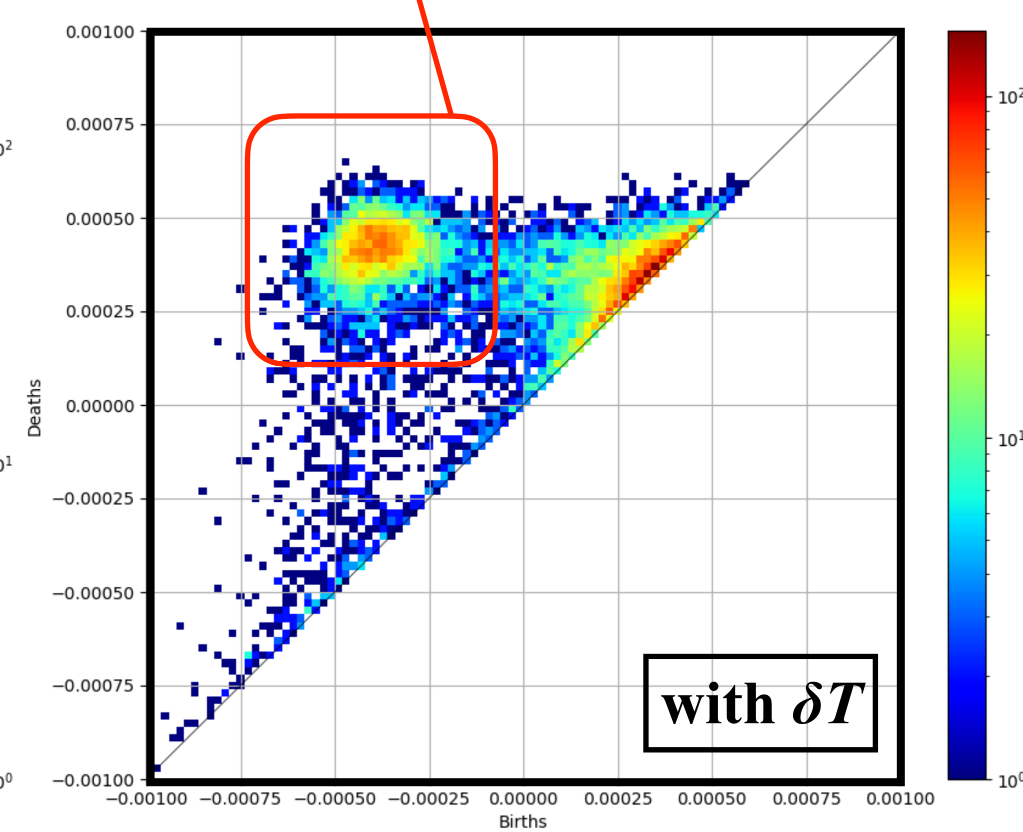

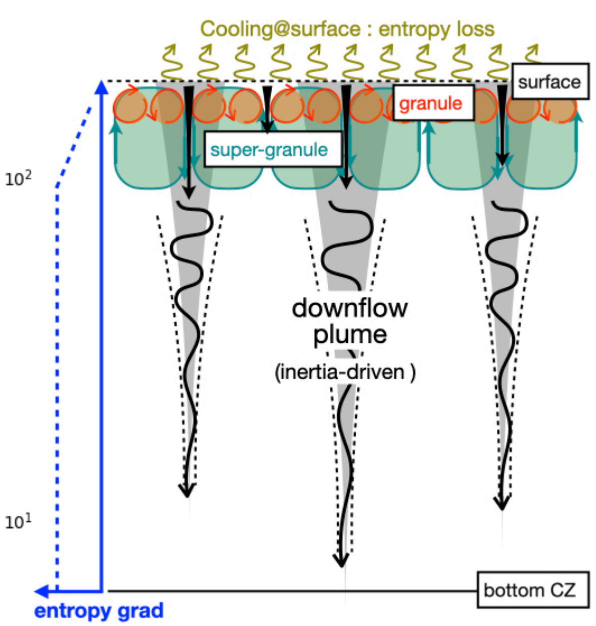

The "peninsula structure" with a long-lived properties characterizes the PD of CD

PD with obs. data : DKIST / Hinode SOT

- narrow field and high resolution obs.
  → **peninsula-like structure (DKIST)**
- wide field and low resolution obs.
  → vertical horn-like structure (SOT)

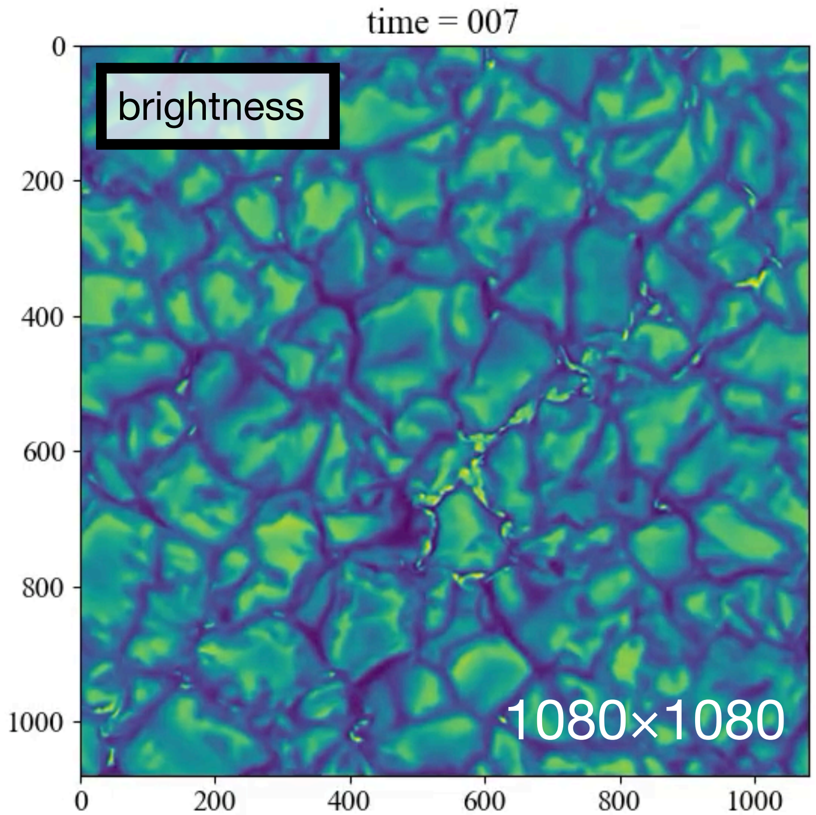

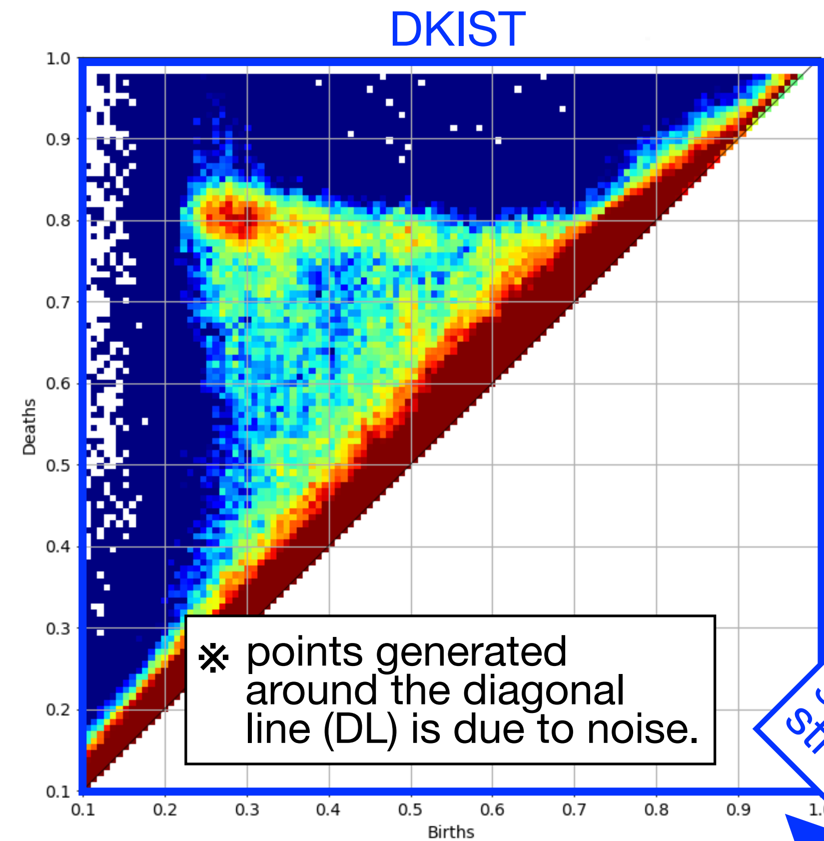

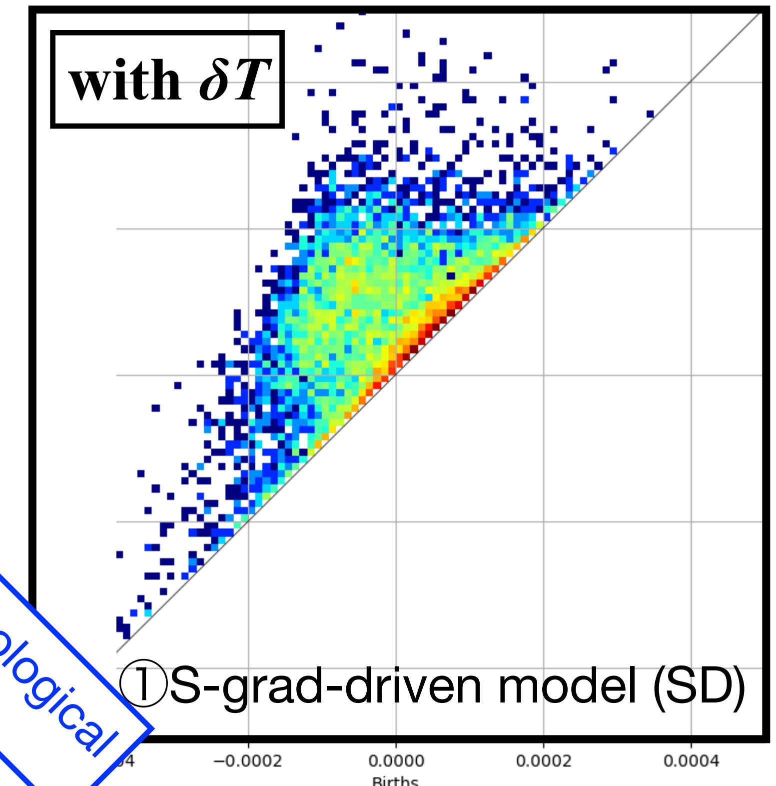

similar topological structure

Why the properties of PD different btw observations ?

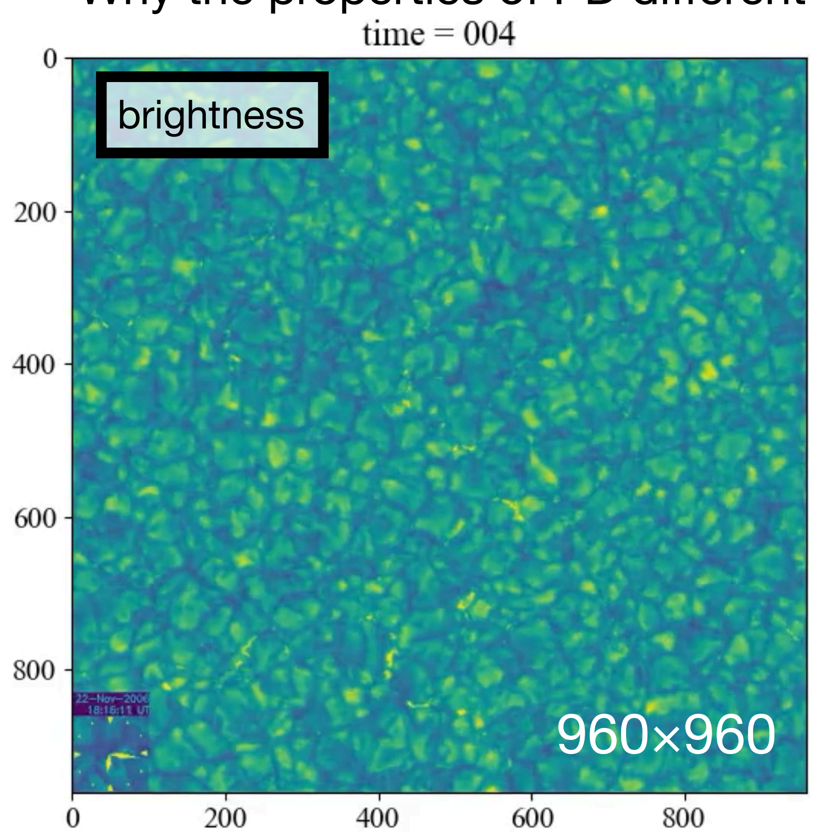

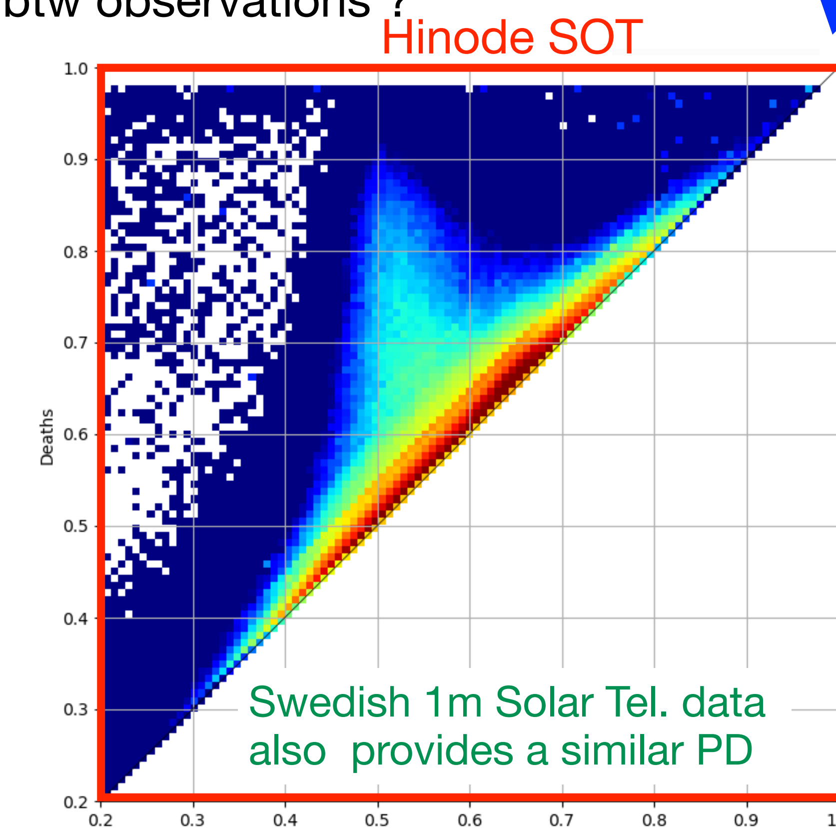

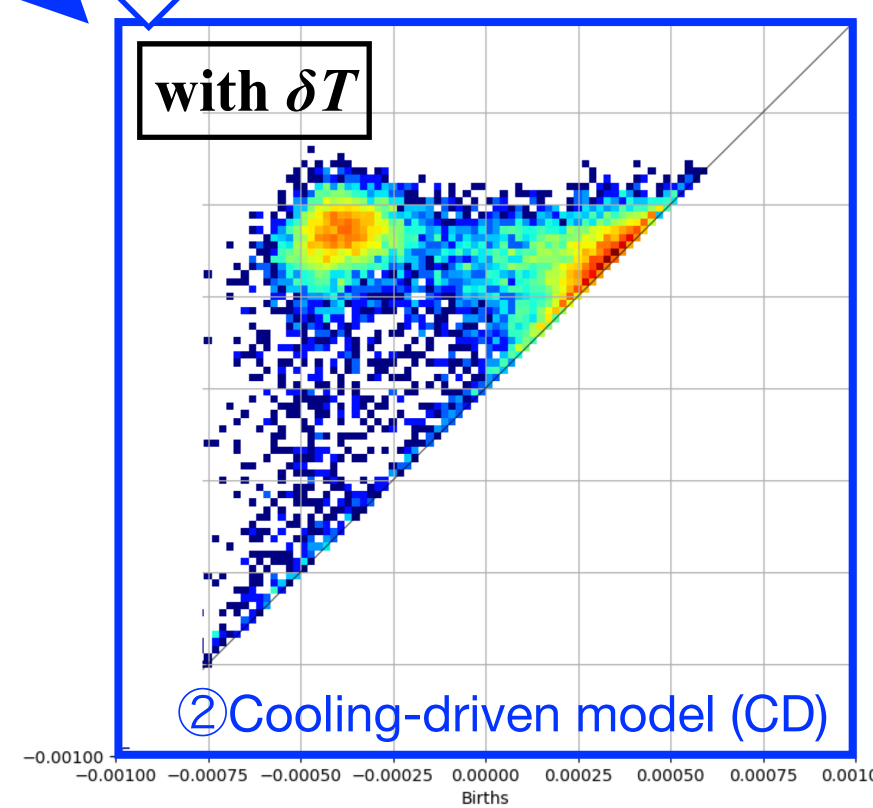

PD from DKIST (high-reso) data is similar to that of the CD model.

Inverse Analysis (i-TDA) (understanding Physics)

: Where does the "peninsula" on PD come from in the real space ?

Where does the peninsula on PD come from ? - inverse analysis -

- advantage of TDA : inverse analysis is possible (data ⇄ PD)

(we can see the correspondence between the feature structure on PD and the original spatial structure).

corresponding structure in the real space

from the specific data on PD

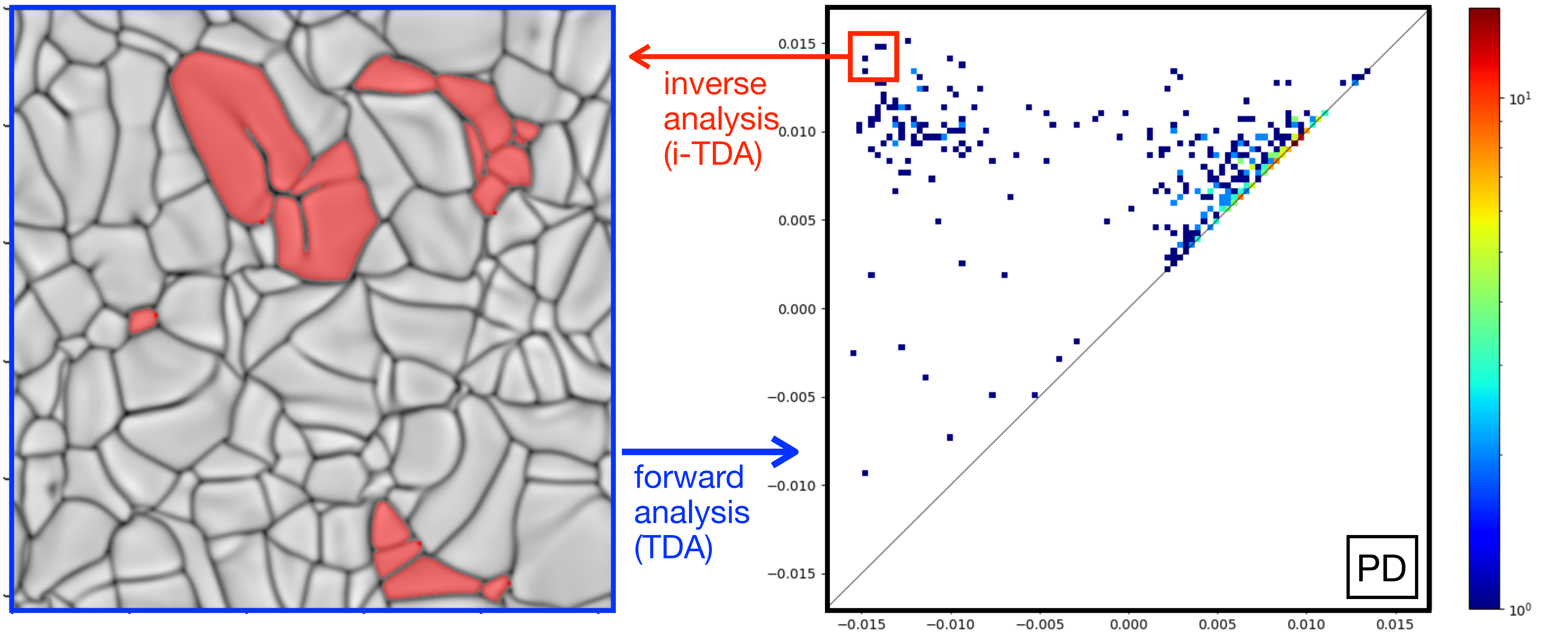

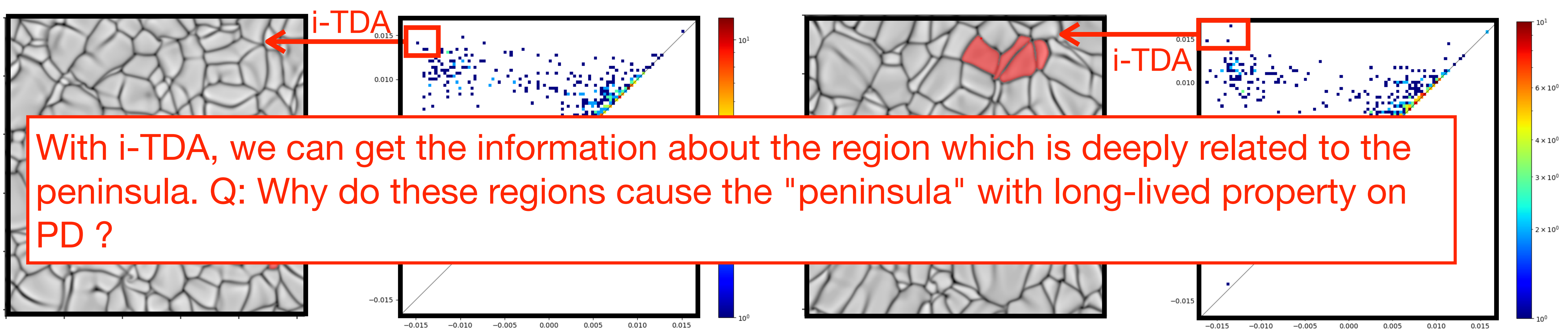

With i-TDA, we can get the information about the region which is deeply related to the peninsula. Q: Why do these regions cause the "peninsula" with long-lived property on PD ?

Where does the peninsula on PD come from ? - inverse analysis -

● filtration with level-set method (change threshold value by hand for demonstration) :

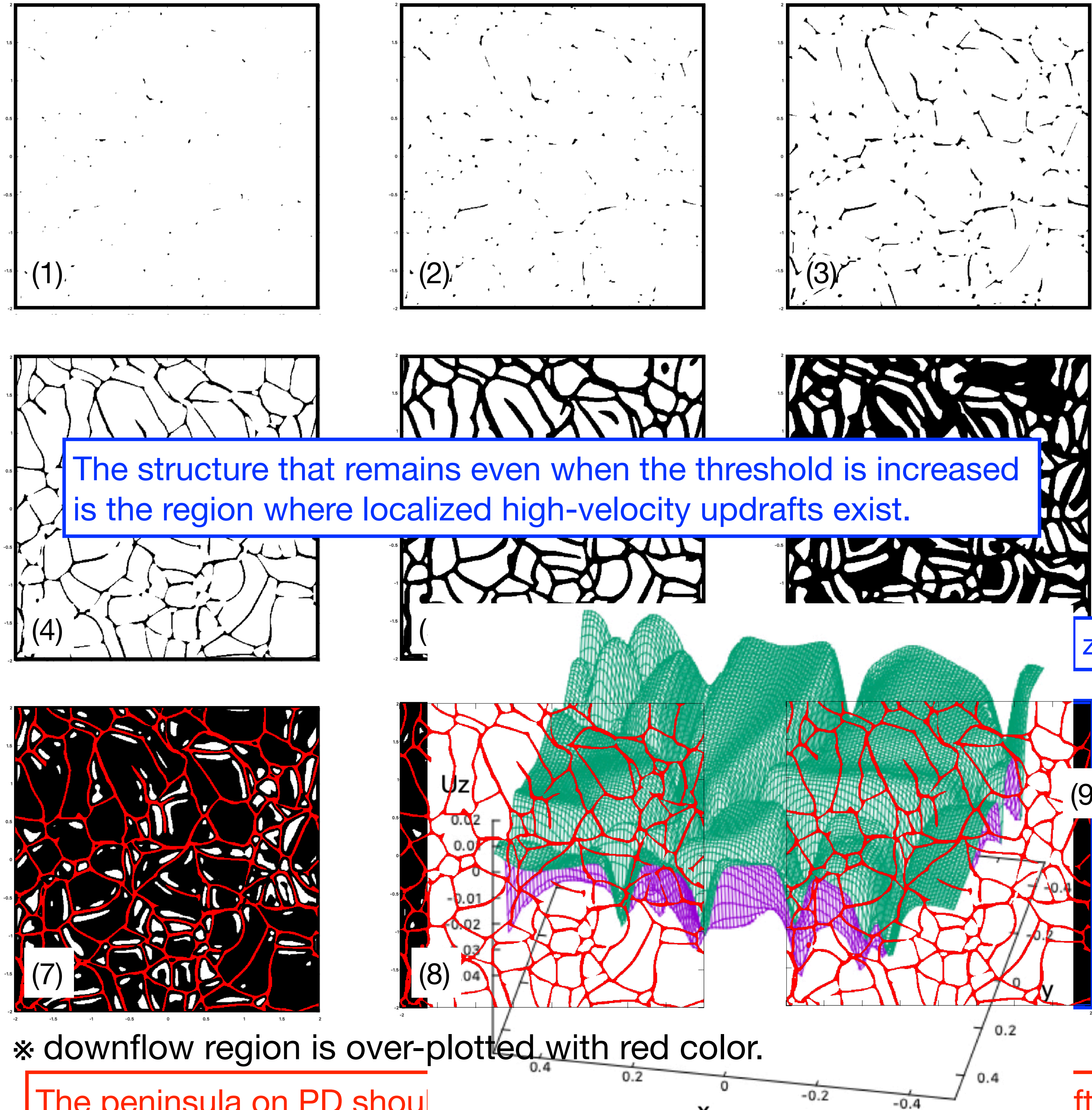

The structure that remains even when the threshold is increased is the region where localized high-velocity updrafts exist.

※ downflow region is over-plotted with red color.

The peninsula on PD shoul ... fts !

result of i-TDA

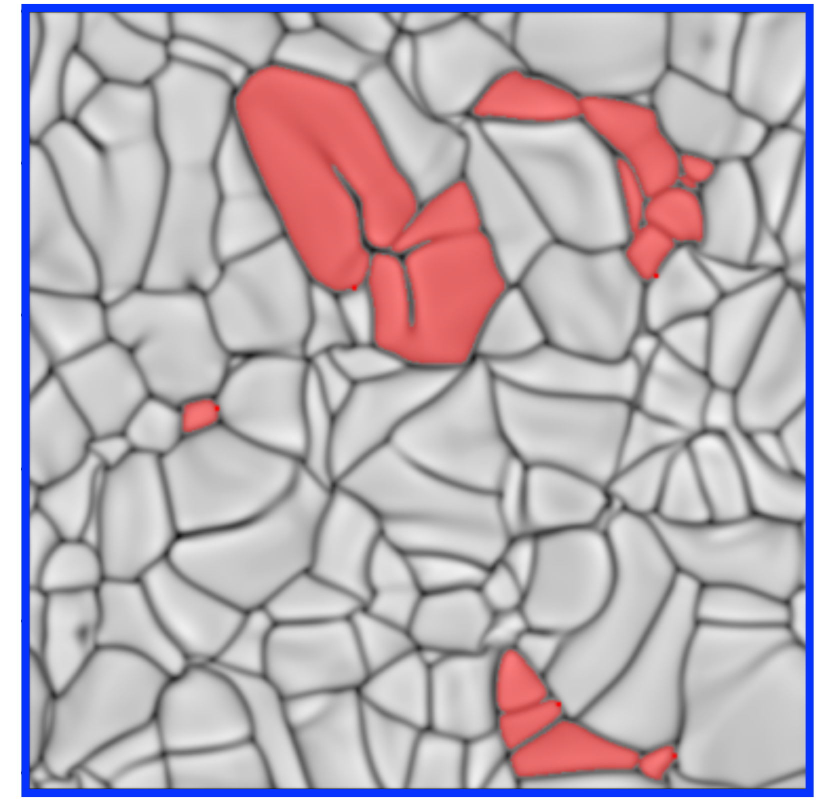

⇅ compare

zoom up

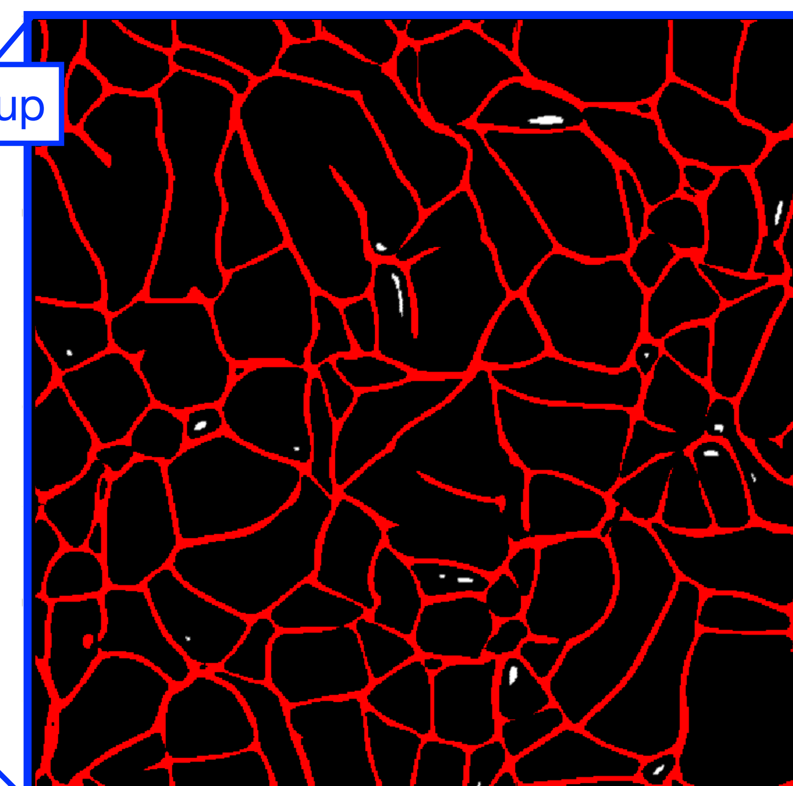

@final filtration stage

Then, what is the localized high-V updrafts ?

The formation mechanism of localized high-V updrafts is studied.

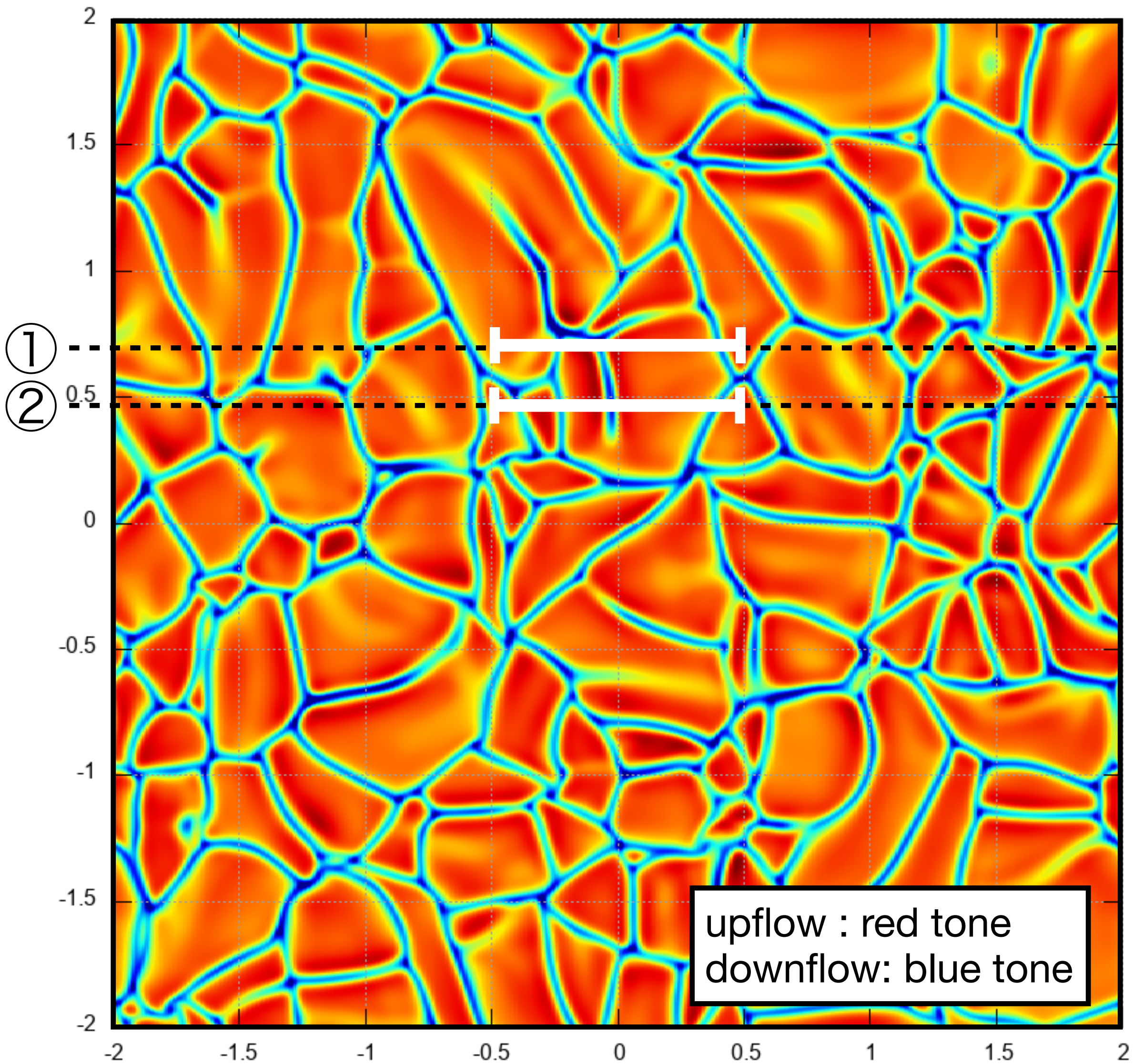

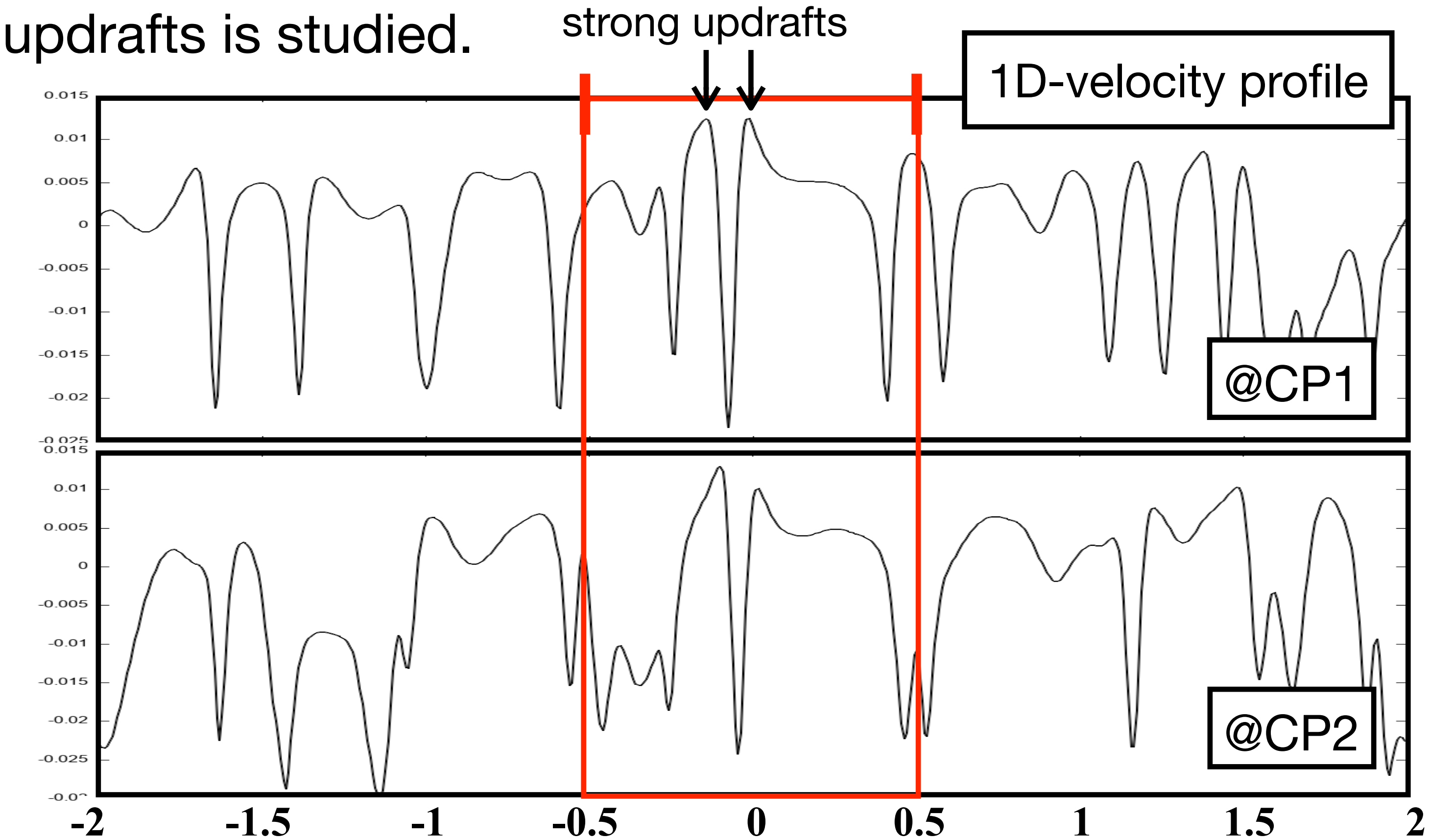

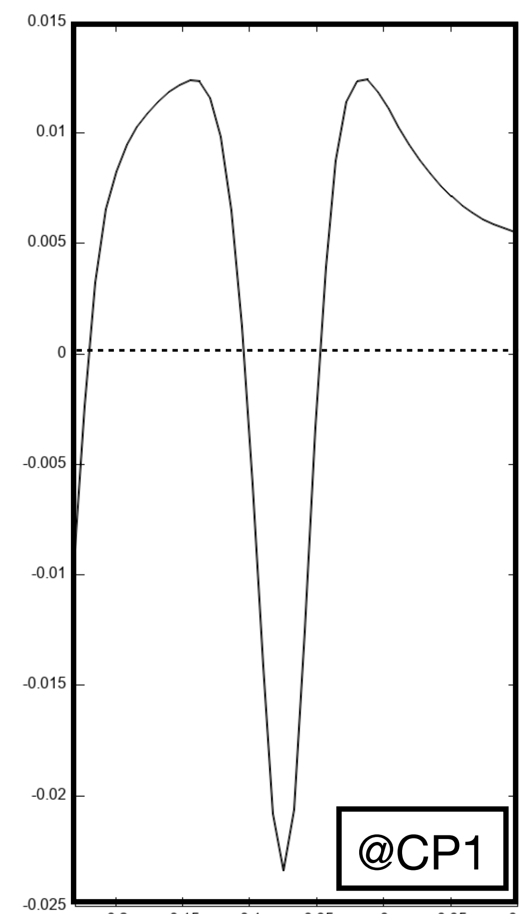

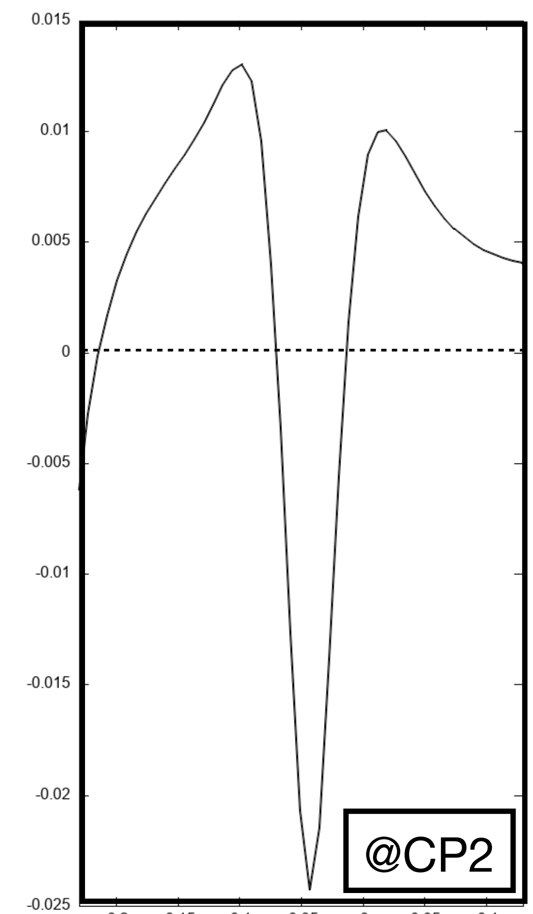

- almost all of localized high-V updrafts are accompanied with stronger downflows and are formed as the wing of them !
- Q: Then, what is the <u>physical origin</u> of this structure ?

  A: That seems to be the downflow plume !!!

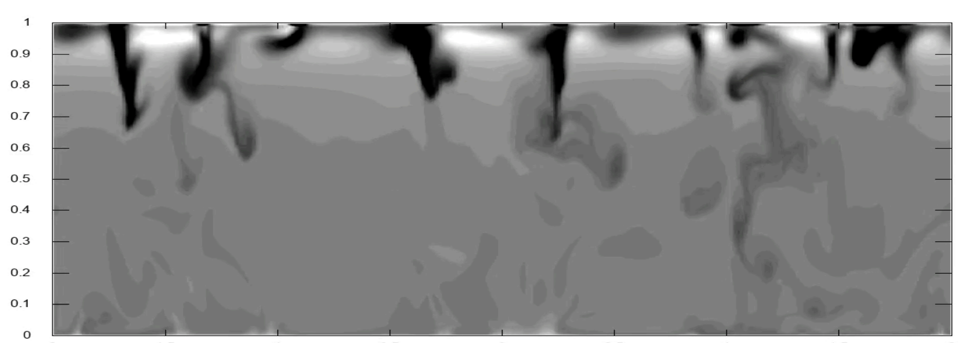

THE ASTROPHYSICAL JOURNAL, 443:863–868, 1995 April 20

Simulation study of the formation of donwflow plume (cooling-driven)

ON THE NATURE OF "EXPLODING" GRANULES AND GRANULE FRAGMENTATION

DKIST

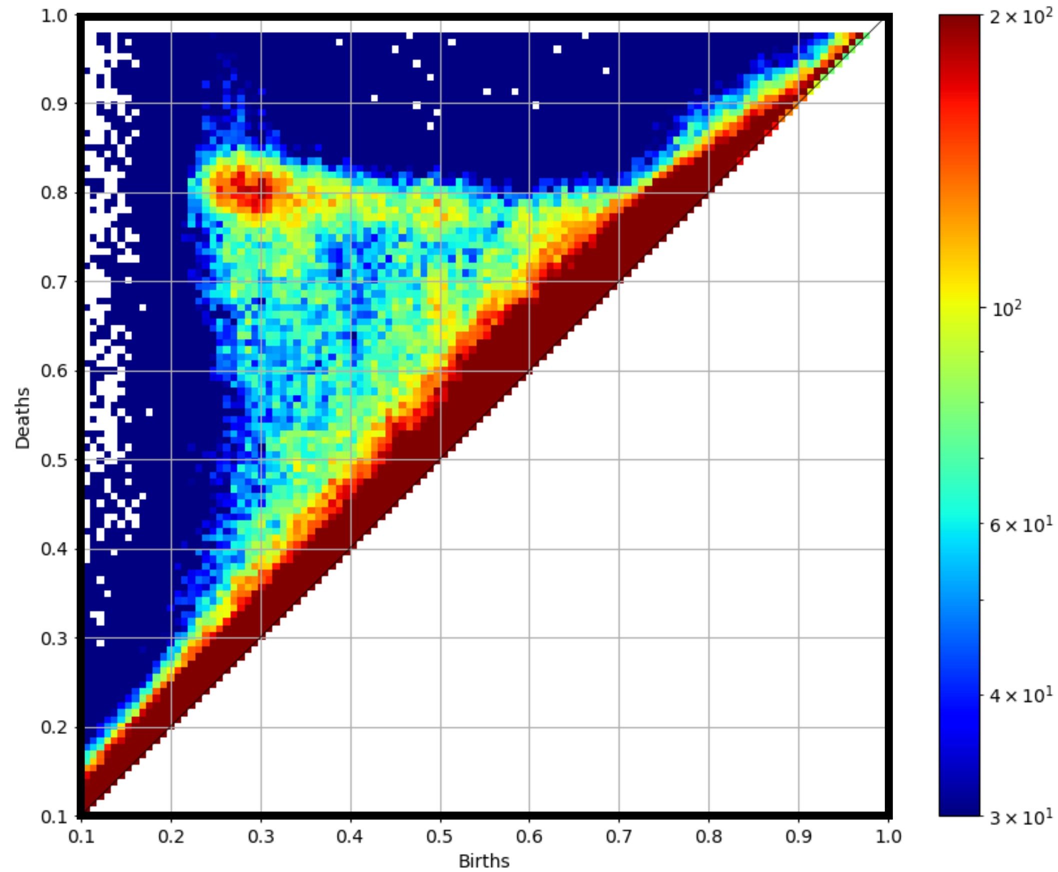

Cooling-driven model

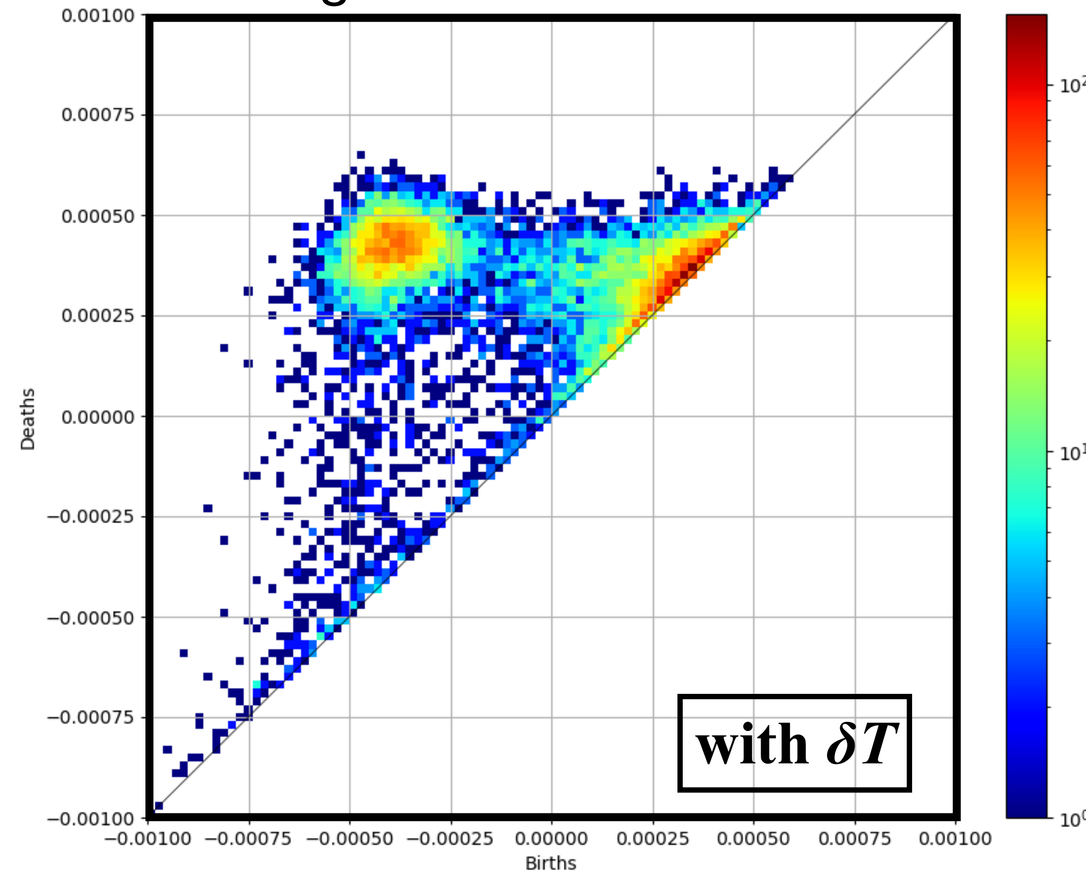

DKIST data seems to provide the "peninsula" with relatively longer lifetime than our CD model, implying the existence of stronger "thread-like" downflows with higher up-down asymmetry there, similar to Rast 95, than that seen in our simulation.

What is suggested :

(accompanied with strong updrafts)

① The "peninsula" on PD is the sign of the existence of a lot of downflow plumes in CD model.

② DKIST data suggests that there are a lot of "hidden" localized structure due to downflow plume.

(In contrast, such structure could not be resolved in the SOT data, thus no peninsula there)

☑ Compared with the plume's profile shown in Rast 95, that seen in our CD model seems to be broader (up-down asymmetry is weaker), suggesting the resolution in our simulation is still not enough.

ON THE NATURE OF "EXPLODING" GRANULES AND GRANULE FRAGMENTATION

MARK PETER RAST
Advanced Study Program, National Center for Atmospheric Research,[1] PO Box 3000, Boulder, CO 80307-3000

Received 1994 August 22; accepted 1994 October 26

ABSTRACT

The morphological evolution of solar granulation is dominated by granule expansion and fragmentation. "Exploding" granules undergo these processes in a particularly vigorous manner, rapidly expanding to a large size, darkening in the center, and splitting by the formation of dark interior radially directed lanes. We argue that such events can be better understood if granulation is viewed as downflow-dominated surface-driven convection rather than as a collection of more deeply driven upflowing thermal plumes.

Regions of maximum granular upflow lie not in the centers of the granules but along their sides, immediately adjacent to the intergranular downflow lanes. These upflows occur primarily in response to the buoyancy and pressure gradient forces induced in proximity to the strongly driven downflow plumes. The upflows are thus dynamically linked to the downflow sites, and granular expansion results in a weakening to the central flow. Radiative losses can then exceed the advected heat supply in the granule center, with the fluid cooling until buoyancy forces becomes sufficient to trigger the formation of a new downflow plume there. Lateral propagation proceeds as neighboring flows are disturbed, with propagation preferentially occurring in directions predisposed to weak upflow by the strength and shape of the downflows defining the granule boundary. Thus the radially oriented structures seen in observations of some fragmenting granules may be formed.

Finally, the strong downflow plumes initiated in the solar photosphere entrain surrounding material as they descend. With depth this more weakly downflowing material establishes a connectivity which is strikingly of mesogranular scale. This may help to explain the observed correlation between the spatial distribution of exploding granules and mesogranular flows, and suggests that both mesogranulation and supergranulation are secondary manifestations of granulation itself.

Subject headings: convection — Sun: granulation

The regions of high-V upflow, which is suggested by Rast 95,
is compatible with the regions fo high-V updrafts found in our study.

注)恐らくDKISTのデータは論文化する時に使えない.

PD with original data

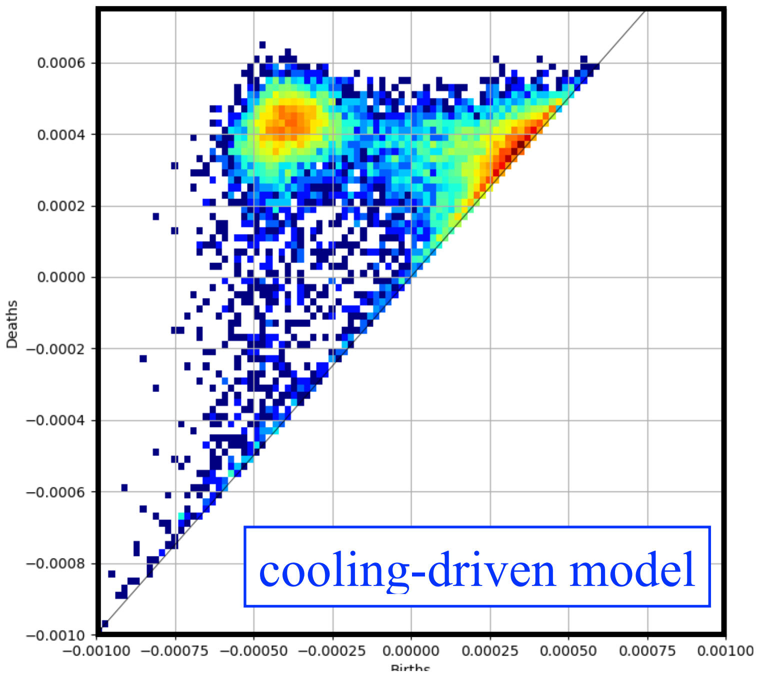

original data

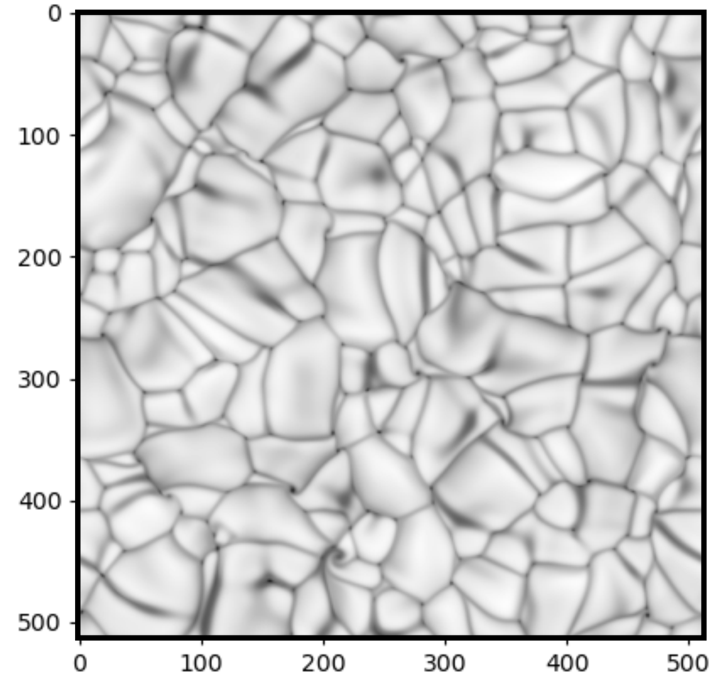

Gaussian kernel

$$f(x, y) = \frac{1}{2\pi\sigma^2} \exp\left(-\frac{x^2 + y^2}{2\sigma^2} \right)$$

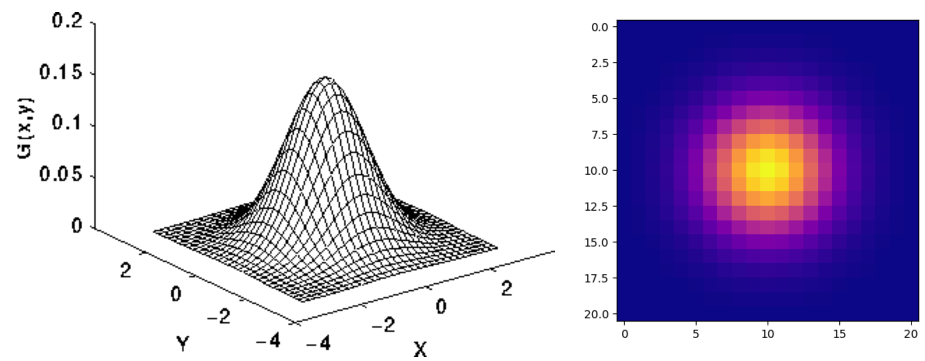

Convolution with a Gaussian kernel of 32×32 when assuming different dispersion σ :

$\sigma = 4.0$

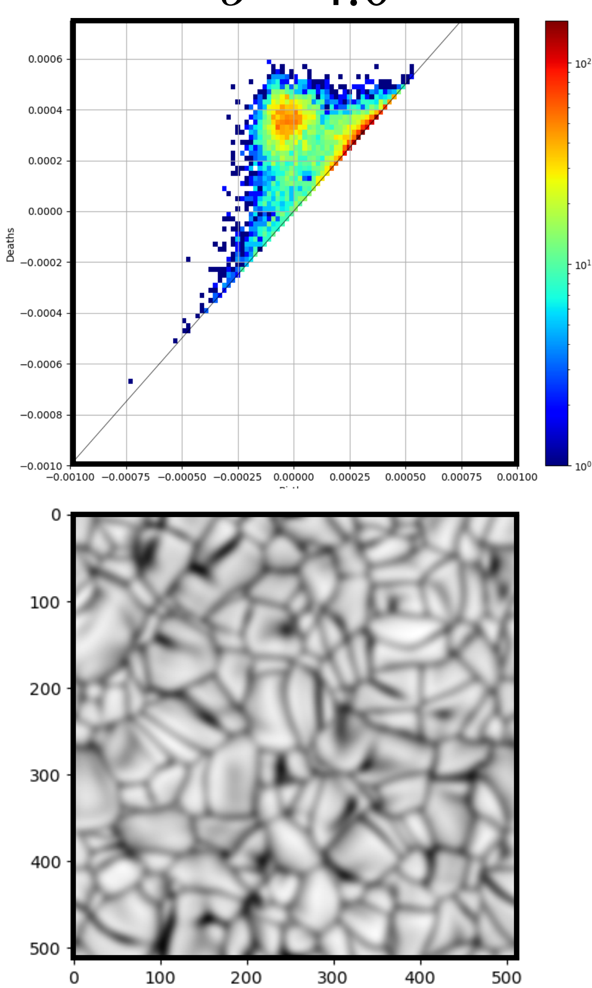

$\sigma = 8.0$

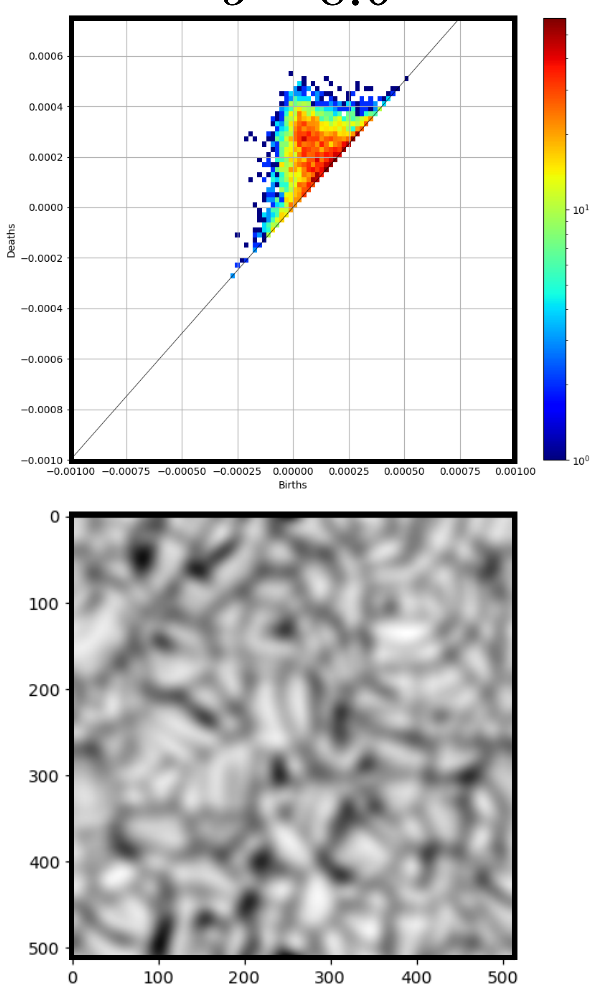

$\sigma = 12.0$

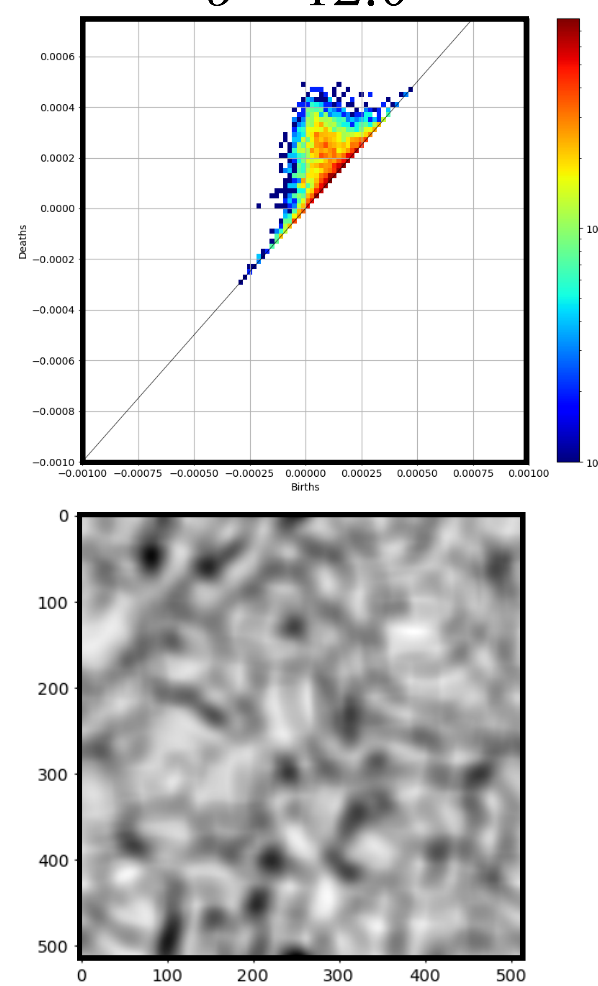

$\sigma = 16.0$

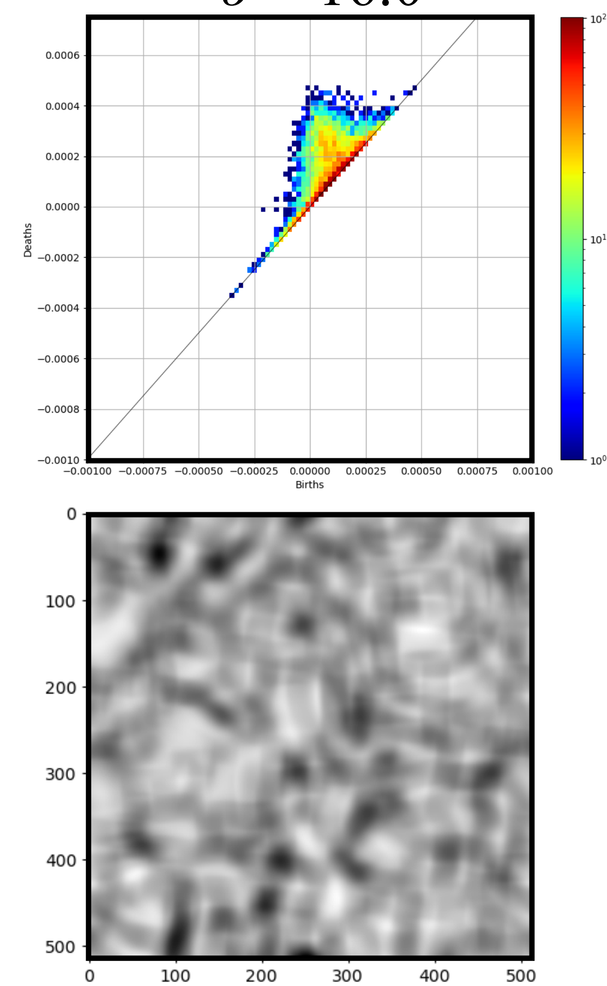

CDモデル模擬観測
（低解像度）

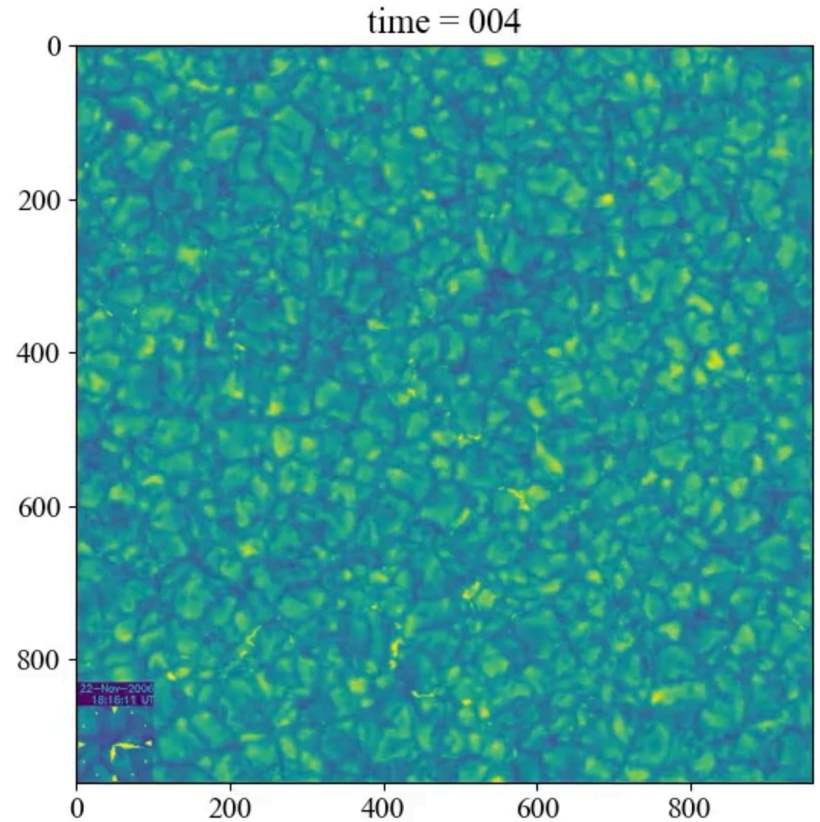

observation by Hinode SOT

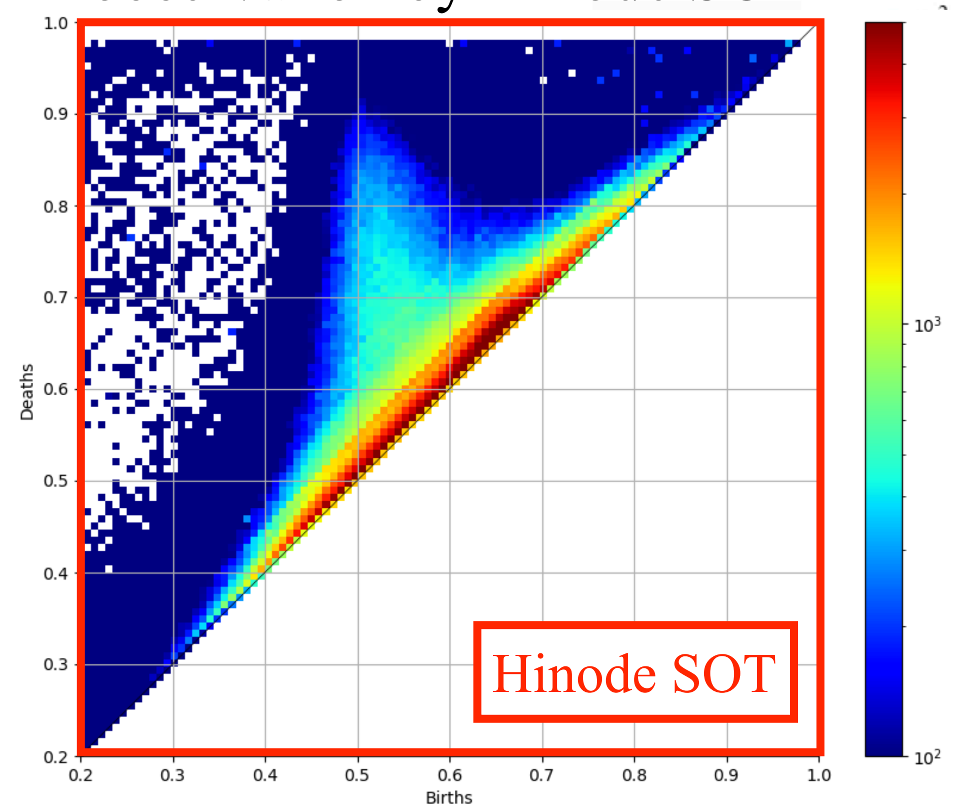

Changing the bin width and bin number for visualization of PD obtained from cooling-driven conv. data:

$\sigma = 8.0$

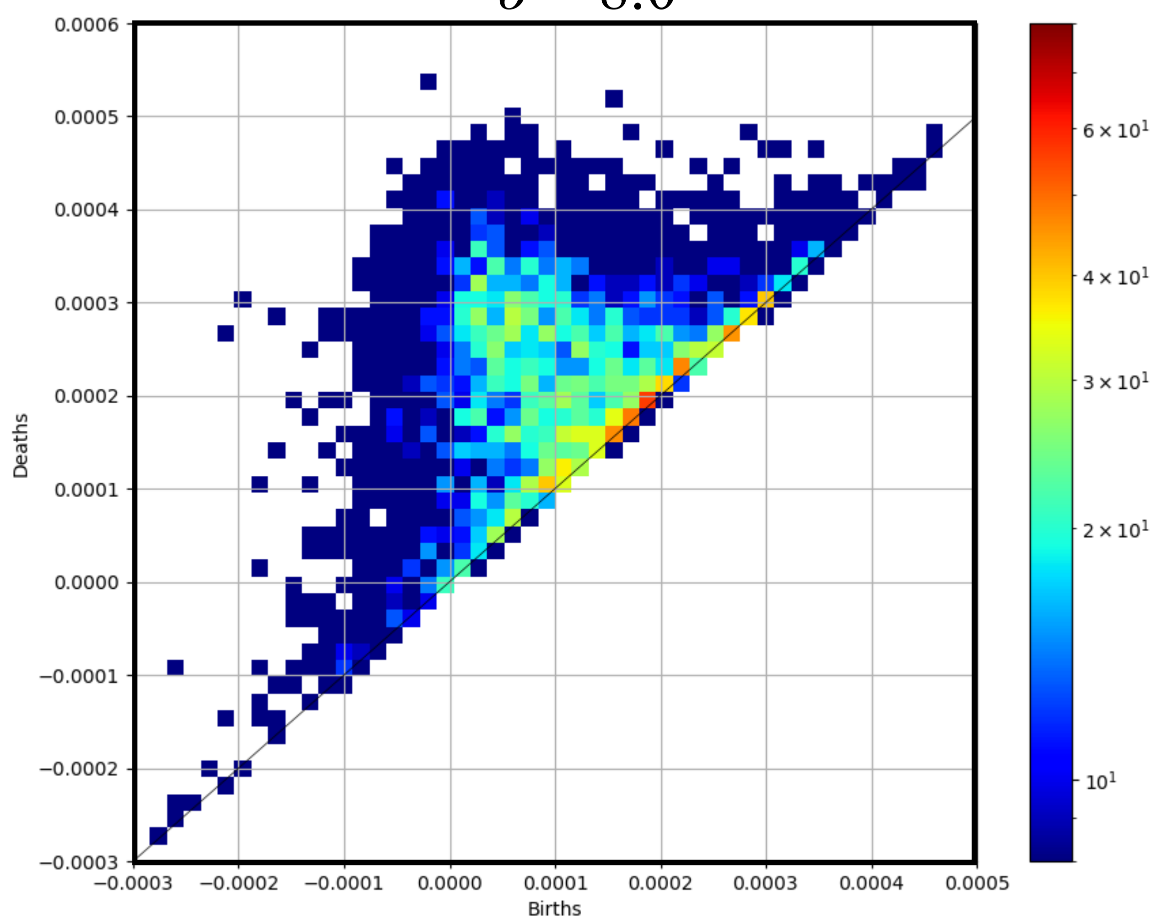

$\sigma = 12.0$

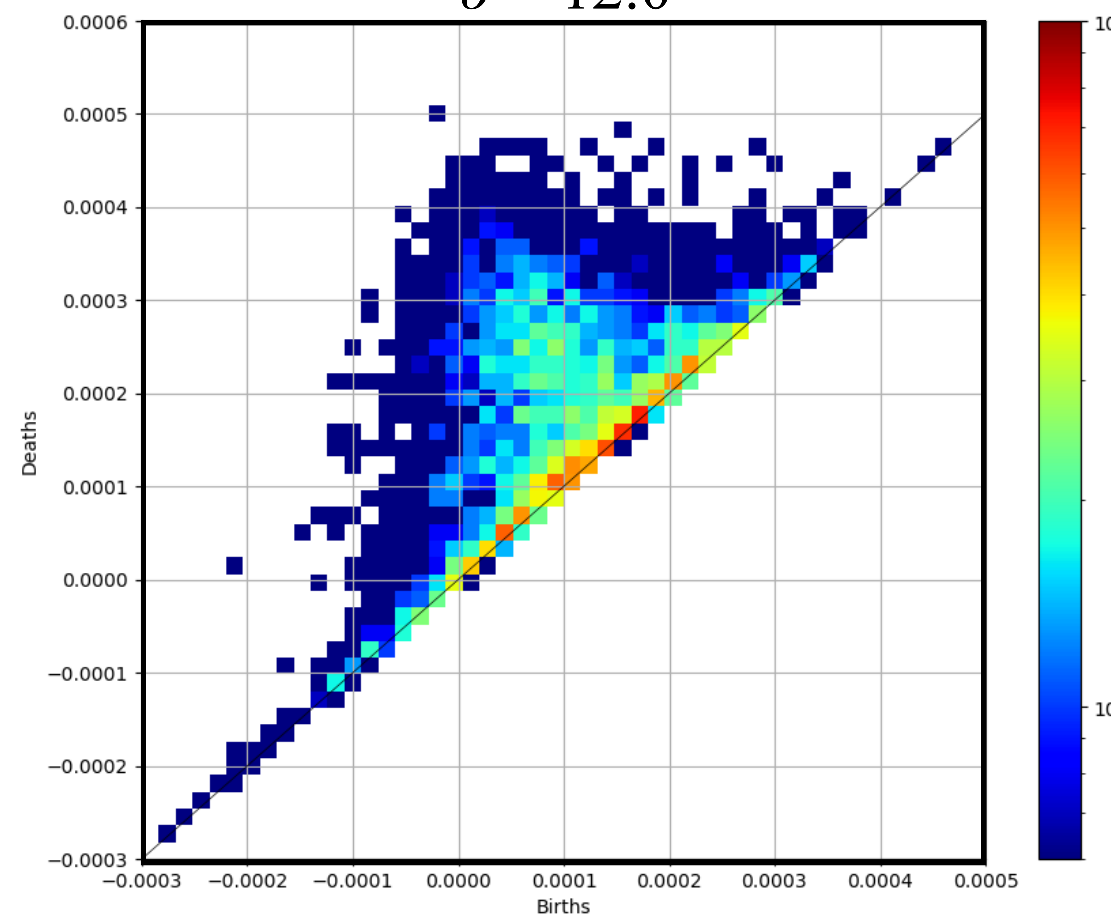

Similar structure of PD to that in obs. can be reproduced by corse graining of cooling-driven conv. data.

Driving mechanism of the solar convection deduced from TDA

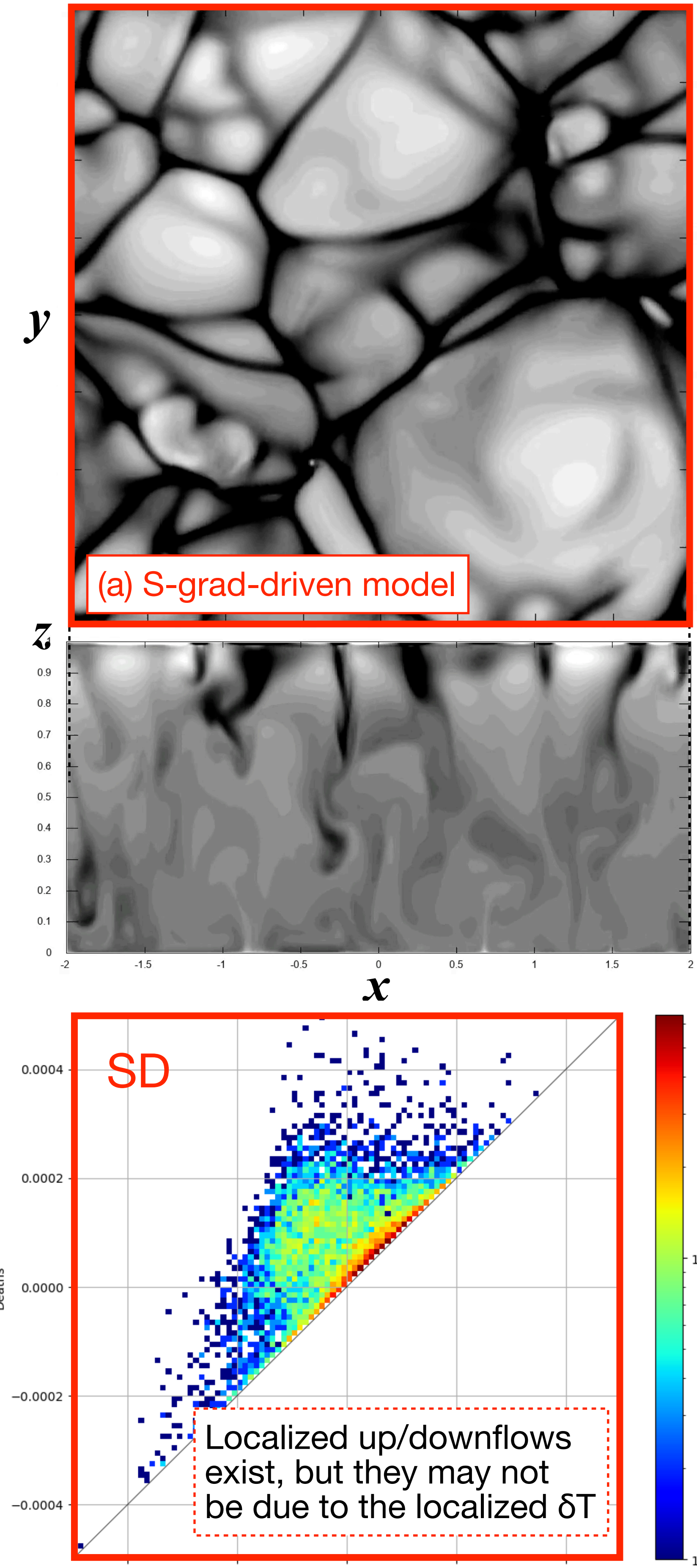

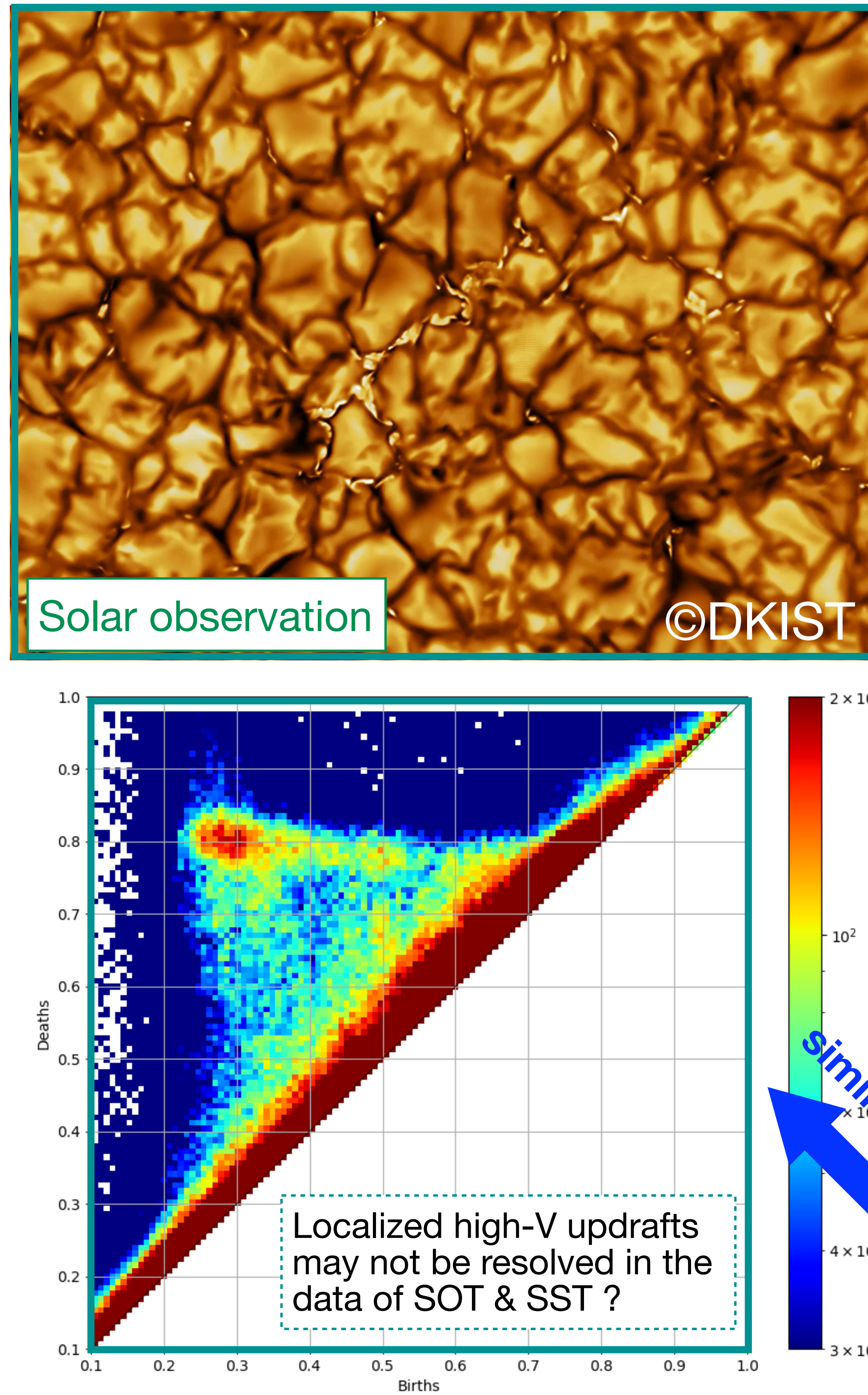

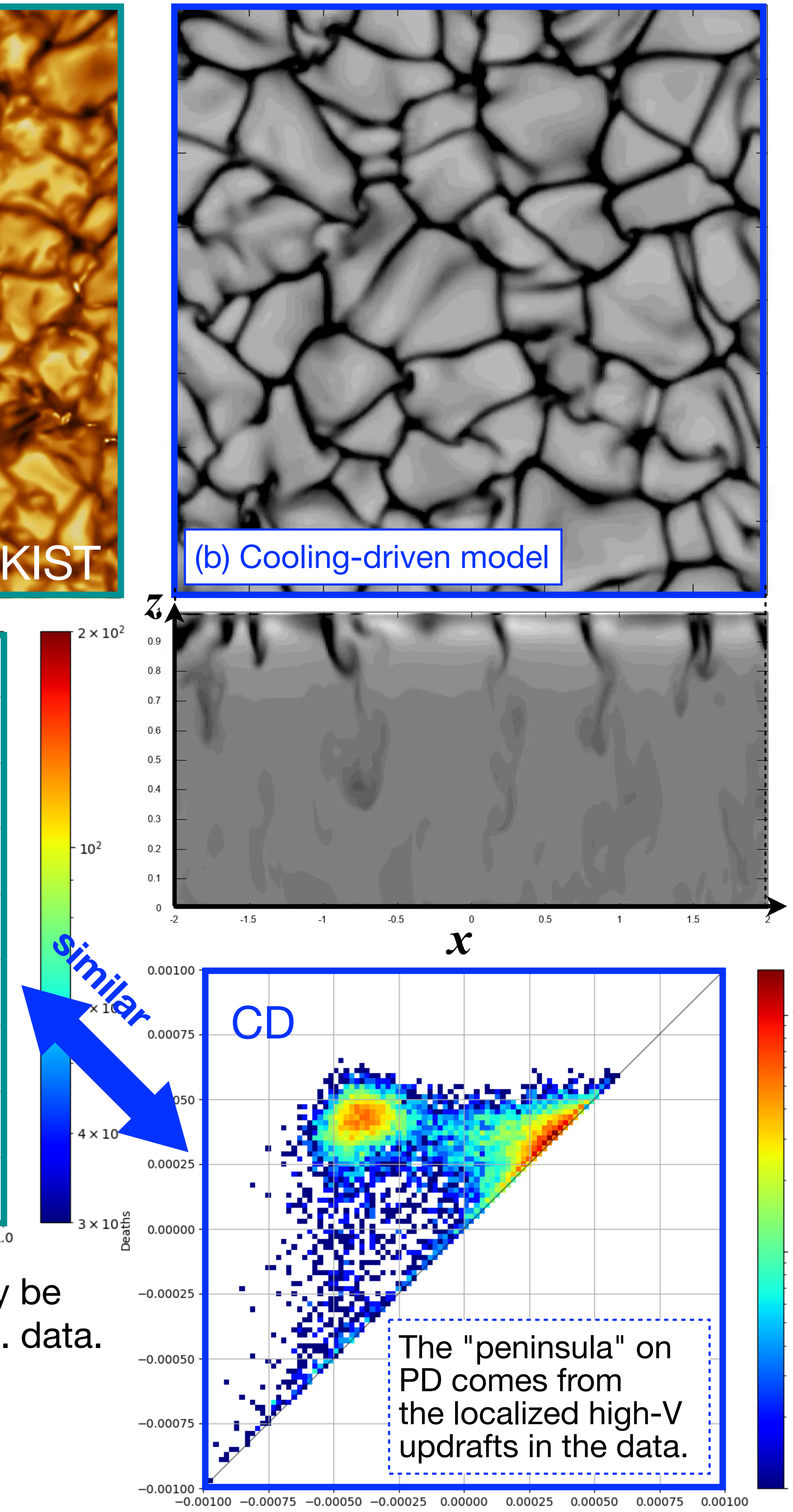

- A key for solving "conv. conundrum" may be hidden in the topological structure of obs. data.
- High-resolution observation ＋ TDA
  → new aspect of the solar convection

まとめ：太陽の熱対流の駆動機構は？

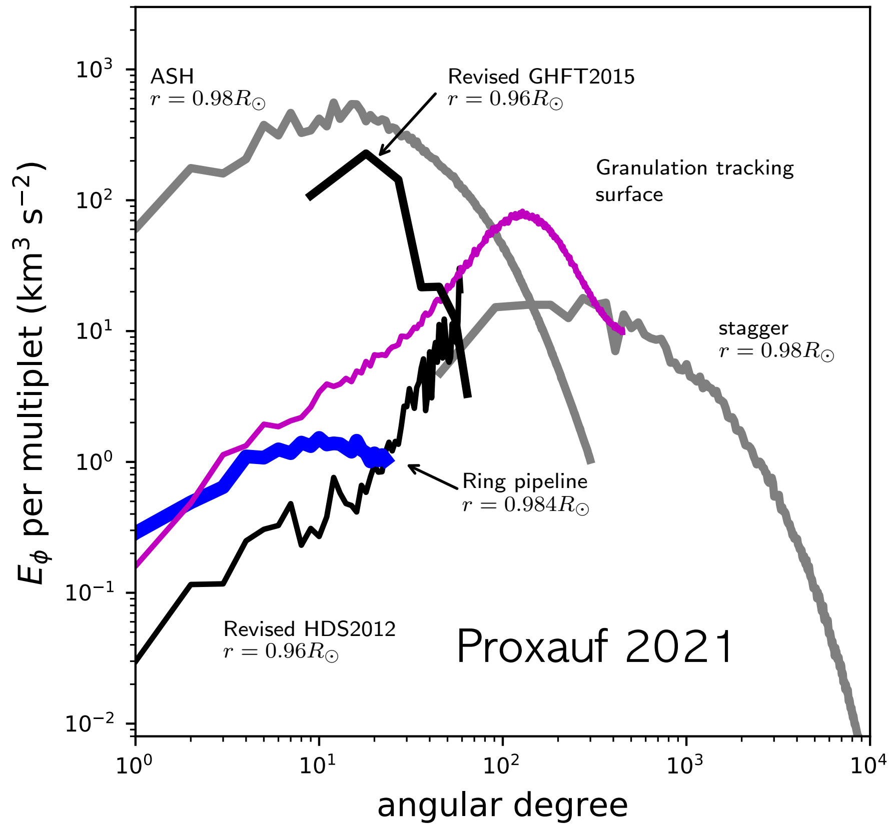

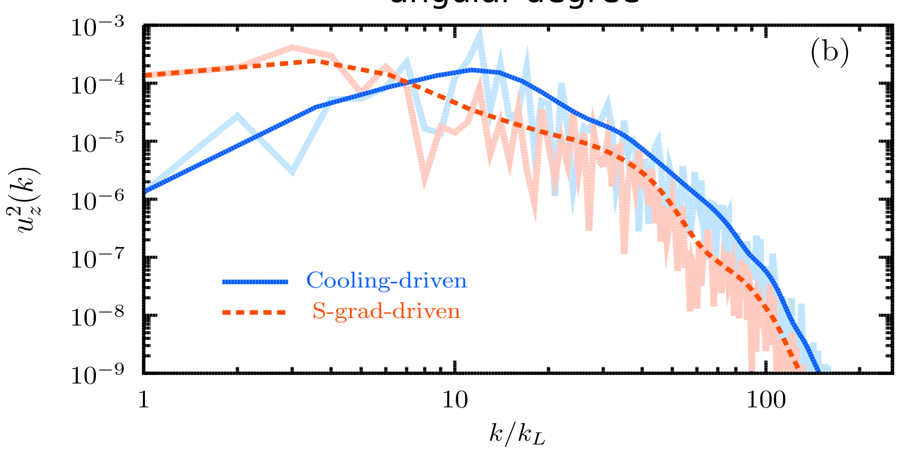

エネルギー輸送の性質が変わる

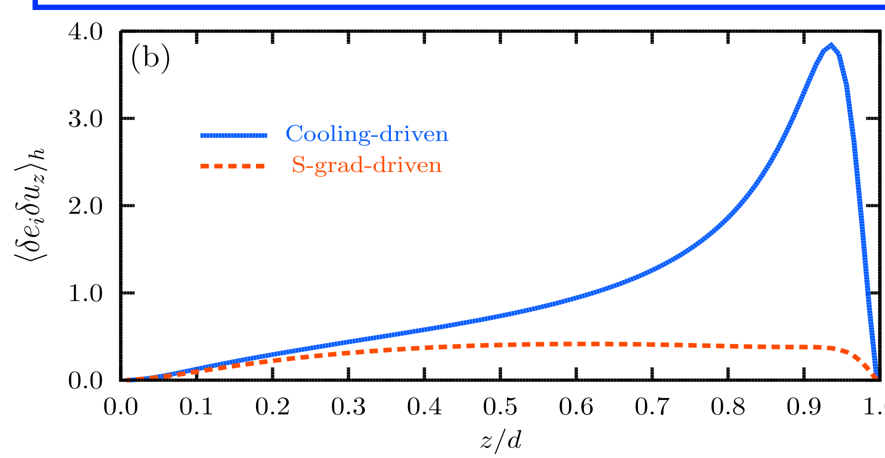

Convection conundrum 太陽ではどうやって
エネルギーを輸送しているのか？

- 巨大胞スケールの構造が観測されない
- シミュレーションの対流速度は観測より3桁大きい

数値モデル： 冷却駆動型 v.s., エントロピー勾配駆動型

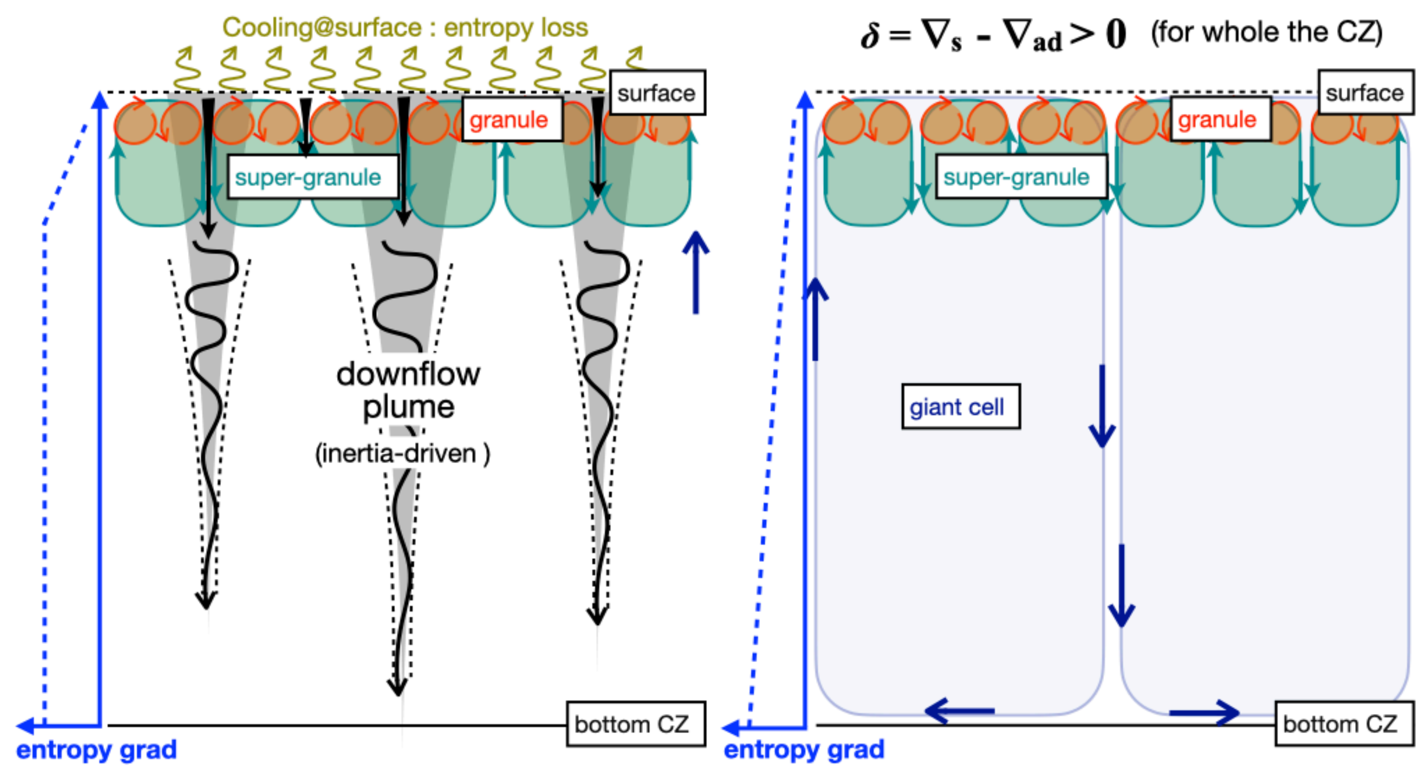

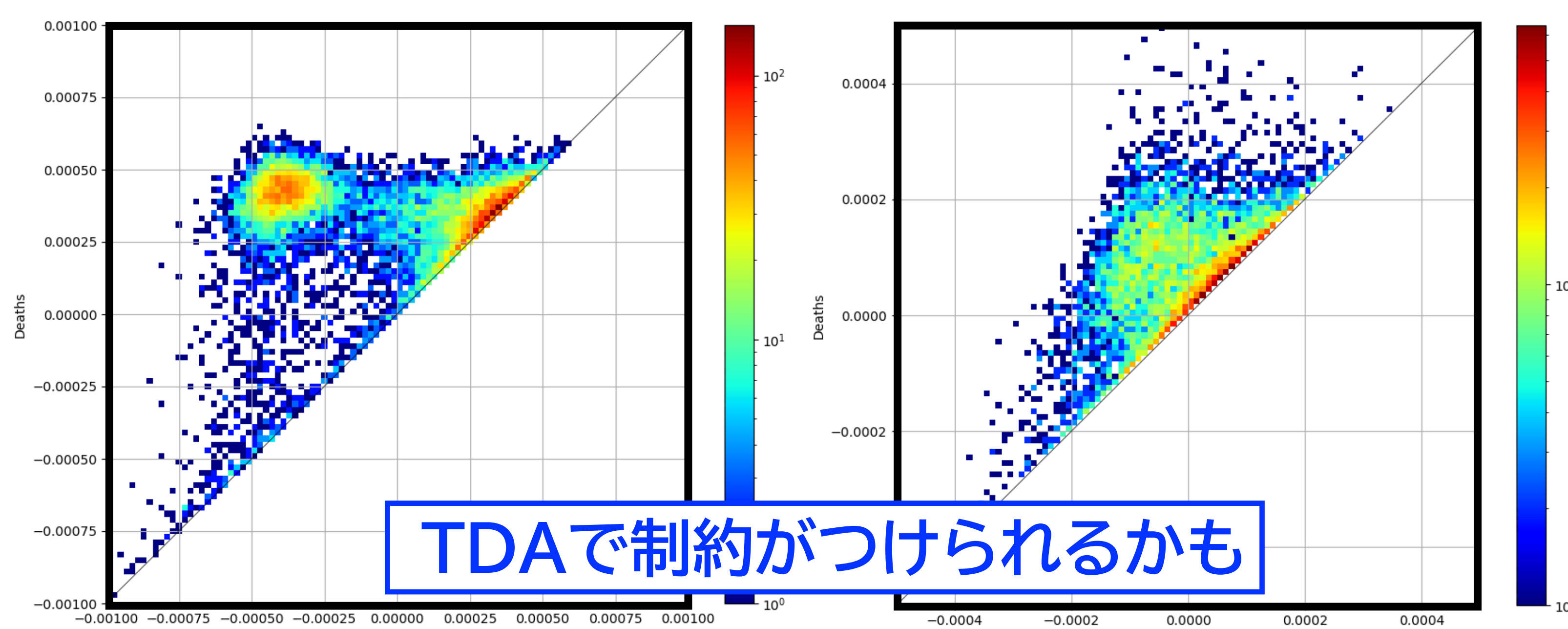

TDAで制約がつけられるかも

参考文献

1. “Effects of Penetrative Convection on Solar Dynamo”,
   Masada, Y., Yamada, K., and Kageyama, A. (2013), ApJ, Volume 778, Issue 1, article id. 11, 14 pp.

2 “Long-term Evolution of Large-scale Magnetic Fields in Rotating Stratified Convection”,
   Masada, Y, and Sano, T. (2014), PASJ, Volume 66, Issue SP1, id.S27 pp.

3. “Mean-Field Modeling of an α^2 Dynamo Coupled
   with Direct Numerical Simulations of Rigidly Rotating Convection”,
   Masada, Y, and Sano, T. (2014), ApJ Letters, Volume 794, Issue 1, article id. L6, 5 pp

4. “Differential Rotation in Magnetized and Non-magnetized Stars”,
   Mabuchi, J., **Masada, Y**, & Kageyama, A. (2015), ApJ, Volume 806, Issue 1, article id. 10, 16 pp.

5. “Spontaneous Formation of of Surface Magnetic Structure from Large-scale Dynamo in Strongly-stratified Convection”,
   Masada, Y, & Sano, T. (2016), ApJ Letters, Volume 822, Issue 2, article id. L22, 7pp.

6. “Large-scale Dynamos in Rapidly-rotating Plane-layer Convection”,
   Bushby, P., Kapyla, P., **Masada, Y**, Brandenburg, A., et al. (2018), A&A, Vol.612, id.A97, 16pp

7. ”Multi-scale deep learning for estimating horizontal velocity fields on the solar surface”,
   Ishikawa, R.T., Nakata, M., Katsukawa, Y., **Masada, Y**, & Riethmuller, T.L.,
   A&A, Volume 658, id.A142, 9pp

8. ”Modeling stellar convective transport with plumes:
   I. Non-equilibrium turbulence effect in double-averaging formulation”,
   Yokoi, N., **Masada, Y**, & Takiwaki, T., MNRAS, Vol.516, Issue 2, pp.2718-2735

9. ”Rotational Dependence of Large-scale Dynamo in Strongly-stratified Convection: What Causes It?”,
   Masada, Y, & Sano, T., ArXiv 2206.06566

10. ”Turbulent Processes and Mean-Field Dynamo”,
   Brandenburg, A. ; Elstner, D.; Masada, Y.; Pipin, V., Space Science Reviews, Volume 219, Issue 7, article id.55